SOLAR CELLS BASED ON DYE-SENSITIZED NANOCRYSTALLINE TiO_2 ELECTRODES

THÈSE N° 1214 (1994)

PRÉSENTÉE AU DÉPARTEMENT DE CHIMIE

ÉCOLE POLYTECHNIQUE FÉDÉRALE DE LAUSANNE

POUR L'OBTENTION DU GRADE DE DOCTEUR ÈS SCIENCES

PAR

ANDREAS KAY

Biologiste diplômé de l'Université de Cologne
de nationalité allemande

acceptée sur proposition du jury:

Prof. M. Grätzel, rapporteur
Prof. H. Girault, corapporteur
Dr W. Gissler, corapporteur
Prof. F. Willig, corapporteur

Lausanne, EPFL
1994

Contents

Abstract

This thesis presents a new type of photovoltaic solar cell based on dye-sensitized nanocrystalline titanium dioxide electrodes. In contrast to conventional solar cells, where light absorption is due to band gap excitation of the semiconductor itself, TiO_2 with its wide band gap is transparent in the visible spectrum. The light is rather absorbed by a dye, e.g. a ruthenium polypyridine complex or a chlorophyll derivative, attached to the semiconductor surface.

Charge separation occurs by electron injection from the excited dye molecule into the conduction band of TiO_2, followed by rapid reduction of the oxidized dye by a redox electrolyte. Such a purely kinetic charge separation mechanism is also found in the reaction centers of natural photosynthetic systems. The analogy goes even further: Just as the chlorophyll containing thylakoid membranes of the chloroplast are folded to grana stacks for efficient light harvesting, a thin film of nanocrystalline TiO_2 particles results in a several hundred times enlarged surface area for dye adsorption.

While the efficiency of conventional polycrystalline solar cells is limited by charge carrier recombination at grain boundaries as well as bulk defects and impurities, the TiO_2 serves only as conductor for majority carriers (injected electrons), so that recombination in the semiconductor is absent in this device. Thus high charge separation efficiencies are obtained even with thin film electrodes made from cheap TiO_2 powder.

We have investigated the theoretical principles, preparation and performance of the different components constituting the dye-sensitized nanocrystalline TiO_2 solar cell.

In the first chapter the current status of photovoltaics is briefly reviewed, followed by an introduction into the basic concepts of photoelectrochemical cells and dye sensitization.

The second chapter deals with the nanocrystalline thin film photoelectrode. First the choice of the substrate and its pretreatment by deposition of an underlayer are discussed. Then different methods for the preparation of nanoporous TiO_2 films are investigated. Three procedures were found to be suitable: *in situ* hydrolysis of titanium alkoxides, coating with a colloidal TiO_2 dispersion and

chemical vapor deposition of mixed TiO_2 / B_2O_3 films. The colloid route is the most versatile, since the particle size distribution can be influenced during colloid preparation, e.g. by precipitation, peptization and hydrothermal treatment or by dispersion of a TiO_2 powder made by flame hydrolysis or plasma oxygenolysis of $TiCl_4$. Moreover, the colloid can be applied to the substrate by many different techniques, such as with a doctor blade, screen printing, spraying or electrodeposition. Finally the after-treatment of the photoelectrode by deposition of a TiO_2 overlayer and the firing and handling before dye adsorption are addressed. The thus achieved improvements in electrode performance are rationalized by modeling the dye adsorption on the mostly exposed, dehydroxylated surface planes of the nanocrystalline anatase particles.

In chapter three we investigate the sensitization by dyes, beginning with a list of the general requirements that have to be met by the sensitizer. An experimental set-up for the acquisition of photocurrent action spectra is described and the results for some of the most successful ruthenium polypyridine complexes are reported. The sensitization by chlorophyll derivatives and related natural porphyrins is investigated in some detail and the effect of different coadsorbates, such as cholanic acids and sugars, compared and rationalized by molecular modeling. The mechanism of photosensitization by chlorophyll derivatives is deduced from static and time resolved fluorescence quenching as well as laser flash photolysis and photocurrent/voltage transients in combination with cyclic voltammetry and spectroelectrochemistry. The importance of surface states on the nanocrystalline TiO_2 particles in trapping of the injected electrons becomes obvious from these studies. Finally we present the results obtained with some other sensitizers, such as carotenoate and a merocyanine.

Chapter four treats the redox-electrolyte, which serves to transfer the electron arriving from the external circuit at the counter electrode back to the oxidized dye. We list the general requirements for the redox couple and discuss the peculiarities of the iodide/triiodide couple. The current status of solid electrolytes and their application in the dye-sensitized nanocrystalline TiO_2 solar cell are reviewed.

In chapter five we briefly report on the preparation and properties of the counter electrode, which should reduce the redox couple at low overvoltage and may at the same time serve a mirror on the backside of the solar cell.

In chapter six we draw some conclusions with regards to the further development of this new type of solar cell.

Zusammenfassung

Diese Dissertation beschreibt eine neuartige photovoltaische Solarzelle auf der Basis Farbstoff-sensibilisierter nanokristalliner Titandioxidelektroden. Im Gegensatz zu herkömmlichen Solarzellen, in denen das Licht von einem Halbleiter mit kleiner Bandlücke absorbiert wird, ist TiO_2 aufgrund seiner weiten Bandlücke im sichtbaren Spektralbereich durchlässig. Das Licht wird vielmehr von einem an die Halbleiteroberfläche gebundenen Farbstoff absorbiert, z. B. einem Ruthenium-Polypyridinkomplex oder einem Chlorophyllderivat.

Die Ladungstrennung erfolgt durch Elektroneninjektion vom angeregten Farbstoff in das Leitungsband von TiO_2, gefolgt von der raschen Reduktion des oxydierten Farbstoffes durch einen Redoxelektrolyten. Ein solch rein kinetischer Mechanismus der Ladungstrennung ist auch in den Reaktionszentren natürlicher Photosynthesesysteme anzutreffen. Der Vergleich läßt sich weiterführen: Ebenso wie die Chlorophyll enthaltenden Thylakoidmembranen des Chloroplasten zu Granastapeln gefaltet sind um das Sonnenlicht effizient zu nutzen, stellt ein dünner Film nanokristalliner TiO_2-Teilchen eine mehrere hundertfach vergrößerte Oberfläche zur Farbstoffadsorption bereit.

Während der Wirkungsgrad herkömmlicher polykristalliner Solarzellen durch Ladungsträgerrekombination an Korngrenzen und Gitterdefekten oder Verunreinigungen beeinträchtigt wird, dient das TiO_2 bloß als Leiter für Majoritätsträger (injizierte Elektronen), so daß bei dieser Solarzelle keine Rekombination im Halbleiter selbst auftritt. Daher läßt sich selbst mit dünnen, aus preiswertem TiO_2-Pulver hergestellten Elektroden eine effiziente Ladungstrennung erzielen.

Wir haben die theoretischen Grundlagen, Herstellung und Eigenschaften der verschiedenen Bestandteile der Farbstoff-sensibilisierten nanokristallinen TiO_2-Solarzelle studiert.

Das erste Kapitel gibt einen kurzen Überblick des gegenwärtigen Standes der Photovoltaik und eine Einführung in die Grundlagen von photoelektrischen Zellen und Farbstoff-Sensibilisierung.

Das zweite Kapitel behandelt die nanokristalline Dünnschicht-Photoelektrode. Zunächst wird die Wahl des Substrates sowie seine Vorbehandlung durch Abscheidung einer Unterschicht diskutiert. Anschließend werden verschiedene Methoden zur Herstellung nanoporöser TiO_2-Filme untersucht. Drei Prozeduren wurden als geeignet befunden: *in situ* Hydrolyse von Titanalkoxiden, Beschichtung mit einer kolloidalen TiO_2-Dispersion und chemische Abscheidung aus der Gasphase (CVD) von gemischten TiO_2 / B_2O_3-Filmen. Das Kolloidverfahren ist am vielseitigsten, weil sich die Teilchengrößenverteilung während der Kolloidherstellung beeinflussen läßt, z. B. durch Fällen, Peptisieren und hydrothermale

Behandlung oder durch Dispergierung eines durch Flammenhydrolyse oder Plasmaoxygenolyse hergestellten TiO_2-Pulvers. Zudem läßt sich das Kolloid mittels verschiedener Techniken auf das Substrat aufbringen, so zum Beispiel mit einer Doktorblade, durch Siebdruck, Sprühen oder Elektrodeposition. Schließlich kommen wir auf die Nachbehandlung der Photoelektrode durch Abscheidung einer TiO_2-Oberschicht und Ausheizen sowie die Handhabung bis zur Farbstoffadsorption zu sprechen. Um die hierdurch erzielte Verbesserung der Elektrodeneigenschaften zu deuten, wird die Adsorption des Farbstoffes an den meist exponierten, dehydroxylierten Oberflächenebenen der nanokristallinen Anatasteilchen modelliert.

In Kapitel drei wenden wir uns der Sensibilisierung mit Farbstoffen zu, beginnend mit einer Liste der allgemeinen Bedingungen, welche ein Sensibilisator erfüllen muß. Ein Versuchsaufbau zu Aufnahme von Photostrom-Aktionsspektren wird beschrieben und die Ergebnisse für einige der erfolgreichsten Ruthenium-Polypyridinkomplexe berichtet. Die Sensibilisierung mit Chlorophyllderivaten und verwandten natürlichen Porphyrinen wird ausführlich untersucht und der Einfluß verschiedener Koadsorbate, wie Cholansäuren und Zuckern, verglichen und mit Hilfe von Molekülmodellen gedeutet. Der Mechanismus der Photosensibilisierung mit Chlorophyllderivaten wird aus der statischen und zeitaufgelösten Fluoreszenzlöschung sowie Laser-Blitzphotolyse und Photostrom/spannungs Transienten in Verbindung mit zyklischer Voltammetrie und Spektroelektrochemie abgeleitet. Aus diesen Experimenten wird die Bedeutung von Oberflächenzuständen auf den nanokristallinen TiO_2-Teilchen für das Einfangen der injizierten Elektronen deutlich. Schließlich stellen wir die mit einigen anderen Sensibilisatoren erzielten Ergebnisse vor, unter anderem für Carotenoat und ein Merocyanin.

Kapitel vier behandelt den Redoxelektrolyten, der dazu dient das über den äußeren Stromkreis an der Gegenelektrode eintreffende Elektron zurück auf den oxydierten Farbstoff zu übertragen. Wir zählen die allgemeinen Anforderungen für das Redoxpaar auf und diskutieren die Besonderheiten des Jodid/Trijodid Paares. Der gegenwärtige Stand auf dem Gebiet fester Elektrolyten und ihre Anwendung in der Farbstoff-sensibilisierten nanokristallinen TiO_2-Solarzelle werden besprochen.

Im fünften Kapitel beschreiben wir kurz die Herstellung und Eigenschaften der Gegenelektrode, welche das Redoxpaar bei kleiner Überspannung reduzieren soll und gleichzeitig als Spiegel auf der Rückseite der Solarzelle dienen kann.

Kapitel sechs enthält einigen Schlußfolgerungen für die weitere Entwicklung dieser neuartigen Solarzelle.

Résumé

Cette thèse décrit un nouveau type de cellule solaire photovoltaïque ayant comme base une électrode nanocrystalline de dioxyde de titane sensibilisée par un colorant. Contrairement aux cellules solaires traditionnelles dans lesquelles la lumière est absorbée par un semi-conducteur de bande interdite étroite, le TiO_2 est transparent dans la partie visible du spectre en raison de sa bande interdite large. Dans notre cas, la lumière est absorbée par un colorant attaché à la surface du semi-conducteur, par exemple par un complexe polypyridyl du ruthénium ou un dérivé de la chlorophylle.

La séparation des charges est la conséquence de l'injection d'un électron par le colorant excité dans la bande de conduction du TiO_2, suivi par la réduction rapide du colorant oxydé par un électrolyte rédox. Un tel mécanisme purement cinétique de séparation des charges se trouve aussi dans les centres de réaction des systèmes naturels de photosynthèse. La comparaison va plus loin: de même que les membranes thylacoïdes des chloroplastes contenant la chlorophylle sont pliées en piles de grana pour bien capter la lumière, une couche mince de particules nanocrystallines de TiO_2 met à la disposition de l'adsorption du colorant une surface qui est élargie plusieurs centaines de fois.

Alors que l'efficacité des cellules solaires polycrystallines traditionnelles est restreinte par la recombinaison des porteurs de charge aux limites des grains et à cause des défauts ou des impuretés du réseau, le TiO_2 sert seulement comme conducteur des porteurs de majorité (électrons injectés), de sorte qu'une recombinaison dans le semi-conducteur même n'a pas lieu dans ce type de cellule solaire. Pour cette raison une séparation efficace des charges peut être obtenue même avec une électrode mince fabriquée à partir d'une poudre de TiO_2 bon marché.

Nous avons étudié les principes théoriques, la fabrication et les propriétés de différents éléments de la cellule solaire de TiO_2 nanocrystalline sensibilisée par un colorant.

Le premier chapitre donne un bref résumé de l'état actuel de la photovoltaïque et de la sensibilisation par des colorants. Le deuxième chapitre traite de la photoélectrode à couche mince polycrystalline. On discute d'abord du choix du substrat ainsi que de son prétraitement par déposition d'une sous-couche. Ensuite on examine différentes méthodes pour la fabrication des couches nanoporeuses de TiO_2. Trois procédures sont convenables: l'hydrolyse *in situ* d'un alcoxide de titane, l'application d'une dispersion colloïdale de TiO_2 et la déposition chimique à partir de la phase gazeuse (CVD) d'une couche mixte de TiO_2 et B_2O_3. Le procédé colloïdal est le plus universel, parce que la

distribution de la taille des particules peut être influencée pendant la préparation du colloïde, par exemple par précipitation, peptisation et traitement hydrothermique, ou par dispersion d'une poudre de TiO_2 préparée par hydrolyse dans une flamme ou oxygénolyse dans un plasma. De plus, le colloïde peut être appliqué par différentes techniques sur le substrat: avec un Doctor blade, par sérigraphie, par sprayage ou électrodéposition. Enfin, nous discutons le post-traitement de la photoélectrode par déposition d'une sur-couche de TiO_2 et par chauffage de même que sa manipulation jusqu'à l'adsorption du colorant. Afin d'interpréter l'amélioration des propriétés de l'électrode obtenue par ce procédé, l'adsorption du colorant sur les surfaces déshydroxylées les plus exposées des particules nanocrystalline d'anatase est modélisée.

Dans le troisième chapitre, nous passons à la sensibilisation avec des colorants, commençant avec une liste de conditions générales qui doivent être remplies par le sensibilisateur. On décrit une installation expérimentale pour enregistrer le spectre d'action du photocourant et on rapporte les résultats pour quelques-uns des complexes polypyridine du ruthénium les plus efficaces. La sensibilisation avec des dérivés de la chlorophylle et des porphyrines naturelles apparentées est examinée en détail. L'influence de différents coadsorbats, comme des acides cholanics et des sucres, est comparée et interprétée à l'aide des modèles moléculaires. Le mécanisme de la photosensibilisation avec des dérivés de la chlorophylle est déduit de l'extinction de la fluorescence statique et dynamique ainsi que par photolyse par éclair laser et transients du photocourant/tension en liaison avec la voltamétrie cyclique et la spectroélectrochimie. Ces expériences montrent l'importance des états de surface sur les particule nanocrystallines de TiO_2 pour capter les électrons injectés. Enfin nous présentons les résultats obtenus avec quelques autres sensibilisateurs, entre autres le carotenoate et une merocyanine.

Le quatrième chapitre traite de l'électrolyte rédox, qui sert à transmettre l'électron arrivant depuis le circuit externe à la contre-électrode sur le colorant oxydé. Nous énumérons les exigences générales pour le couple rédox et discutons les particularités du couple iodure/triiodure. On discute de l'état actuel des conaissances dans le domaine des électrolytes solides et leur application dans la cellule solaire de TiO_2 nanocrystalline sensibilisée par un colorant.

Au cinquième chapitre nous décrivons brièvement la fabrication et les propriétés de la contre-électrode, qui doit réduire le couple rédox à un sur-potentiel faible et qui en même temps peut servir de miroir au revers de la cellule solaire.

Le sixième chapitre contient quelques perspectives concernant le futur développement de ce nouveau type de cellule solaire.

1. Photovoltaic solar cells

1.1. Sunlight as ultimate source of energy

The economic growth and prosperity of the industrialized nations has largely been dependent on the availability of cheap sources of energy, mainly fossil fuels. The oil crisis made us aware of this dependency, but soon the oil wells gushed again and 20 years later a liter of gasoline is still as cheap as a liter of mineral water. As a consequence the energy consumption keeps growing and will continue to do so, as the developing countries also want to profit from the wealth of industrialization and individual mobility. Meanwhile we are not only concerned that the stock of cheap energy will soon be used up, but also that our wasteful use of fossil fuels and nuclear power causes irreversible damage to the environment, changes the climate and in one way or the other threatens ourselves.

Some people believe that fusion reactors will once and forever relieve us from energy problems. Unfortunately the peaceful exploitation of nuclear fusion remains confronted with enormous technical problems, although more money is spent for fusion research than for solar cells and other renewable energies. Even if fusion became practical one day, it would produce large amounts of radioactive waste, due to activation of the reactor walls by the strong, high energetic neutron flux.[1]

But we have a fusion reactor that works reliably, free of charge and at save distance: the sun. The sun is in fact the primary source of energy for nearly all forms of life on earth. Also the fossil fuels, oil, coal and gas, which we are going to consume within just a few decades, are the result of solar energy conversion

by the photosynthesis of plants several hundred million years ago. At the present rate of energy consumption ($5 \cdot 10^{13}$ kWh/year) we would consume the total non-renewable energy stored on earth (potential supply of fossil fuels: 10^{16} kWh) within only 200 years.[2] In comparison the earth receives over a year 7000 times more energy from the sun than we consume ($3.5 \cdot 10^{17}$ kWh/year). Other renewable energies, such as wind, hydroelectric, geothermal and tidal energy add up to less than one permille of the energy of solar radiation.[2] Hence there is plenty of energy coming from the sun that could be used without producing any exhaust gases or radioactive waste.

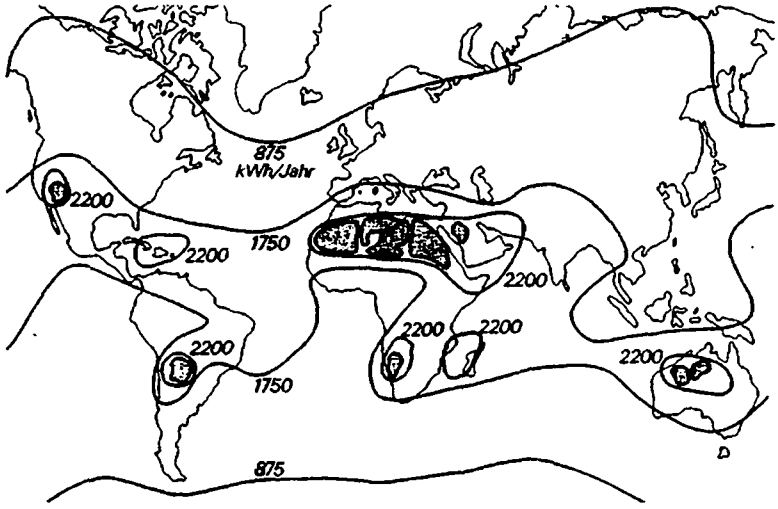

Figure 1: World sunshine map,[3] giving the annual solar radiation in kWh/m^2

The world sunshine map (Figure 1) indicates that in some regions, like the Sahara, more than 2200 kWh of solar radiation reach the earth per square meter and year. But even in Europe some 1000 kWh/m^2·year of sunlight are available. From these data we may estimate the land area demand of a photovoltaic power plant. For example solar cells of 10% efficiency would produce 220 kWh/m^2·year of electricity in the Sahara. To cover the world-wide energy consumption of $5 \cdot 10^{13}$ kWh/year a surface area of some 250 000 km^2 (500 x 500 km^2) would be needed, which corresponds to only 3% of the Sahara.

Of course this example is not very practical, since most of the energy is used in thermal applications, e.g. for heating of buildings and water, which do not

require the inefficient conversion of solar energy into electricity. It is more realistic to compare the land demand of a photovoltaic system with that of a coal-fired or nuclear power plant.[4,p.23] A typical plant of 1 GW electric power produces about $6 \cdot 10^9$ kWh/year. A photovoltaic system of 10% efficiency would require a surface of 60 km^2 in a place like Europe, with 1000 kWh/m^2 sunshine per year. This surface corresponds to a circle of 9 km in diameter, which is certainly much larger than a conventional power plant. However, if the land for mining of coal is included the land demand is in fact very similar.[4,p.24] After all, photovoltaics are ideal for non centralized applications, like on the roof of a house, which would not require any additional land at all.

The problem of photovoltaic energy is not its high land requirement, but rather its high cost. The photovoltaic power plant of the above example would have to produce 2,4 GW peak power to replace a conventional plant of 1 GW.[4,p.25] At present a peak watt of installed solar electricity costs at least \$6. Hence the photovoltaic plant would cost $\$14.4 \cdot 10^9$ without storage, such as in the form of hydrogen. If the plant is financed by a loan over 30 years with an interest rate of 10% the costs would be $\$1.44 \cdot 10^9$ per year for $6 \cdot 10^9$ kWh of electricity.[4,p.42] This corresponds to \$0.42/kWh, compared to the usual price of \$0.06-0.10/kWh.

We conclude that, although a photovoltaic power plant has no subsequent fuel cost and negligible operation and maintenance costs, the interest payments for such an investment render solar electricity still too expensive. However, the price we pay for electricity today does not take into account the secondary costs caused by burning of fossil fuels or by nuclear fission, e.g. as a consequence of damage to the environment, change of the climate or injure to the health of human beings. If these negative side-effects of conventional energy sources were taken into consideration, solar energy might already be competitive today.

The costs of a photovoltaic system can be split into two main parts: the solar modules themselves and the so-called balance of systems (BOS), which takes into account all other costs, e.g. for land area, installation, support structures, power conditioning like DC/AC conversion for connection to the utility grid, operation and maintenance, interest expenses for capital and possibly storage of the energy.[4,p.37] At present the module cost are by far the most important factor with about $\$500/m^2$ for a conversion efficiency of 10-15%.[4,p.51] This is why research aiming at a reduction of the module costs and an increase of their efficiency remains crucial for making photovoltaic systems economically practical on a large scale.

1.2. Solid state photovoltaic cells

1.2.1. Principles of operation

Conventional solar cells are diodes with p-n-junction between differently doped regions of the same semiconductor (homojunction) or two different semiconductors (heterojunction).[5,6] Diffusion of electrons from the electron rich n-side into the p-region results in a depletion or space-charge region and the built-up of an electric field within the p-n-junction (Figure 2). Light is absorbed by band gap excitation of the semiconductor, creating a free hole (defect electron) in the valence band and a free electron in the conduction band. The minority carriers (electrons on the p-type side, holes on the n-type side) diffuse to the p-n-junction, where charge separation by the built-in electric field occurs. Thus illumination creates a photovoltage that can drive a photocurrent through an external load.

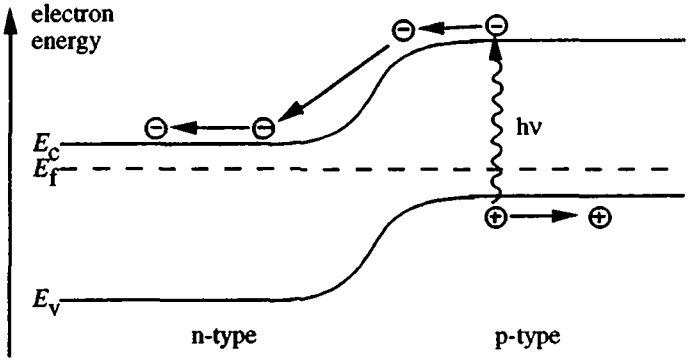

Figure 2: Charge carrier separation in a semiconductor p-n-junction (E_c, E_v = conduction and valence band edge, E_f = Fermi level)

One important factor for the choice of the semiconductor is its band gap, which determines the long wavelength limit of light absorption. Semiconductors of narrow band gap like germanium (Figure 3: E_g = 0.7 eV) absorb far into the infrared (in this case up to λ_g = 1770 nm) and thus use most of the solar spectrum yielding a high photocurrent. However, the excess energy of shorter wavelength photons is lost and the low band gap results in a low photovoltage.

In the other extreme semiconductors with wide band gap like CdS (E_g = 2,3 eV) give a high photovoltage, but low photocurrents, since they use the blue part of the solar spectrum only. The efficiency of a solar cell, given by the produced electrical power (photovoltage times current) in relation to the power of the incident light, reaches a broad maximum for a band gap around E_g = 1.4 eV (Figure 3). Semiconductors like crystalline and amorphous silicon, gallium arsenide (GaAs), copper sulfide (Cu_2S), cadmium telluride (CdTe) and copper indium selenide (CIS) fall into this region of highest theoretical efficiency.

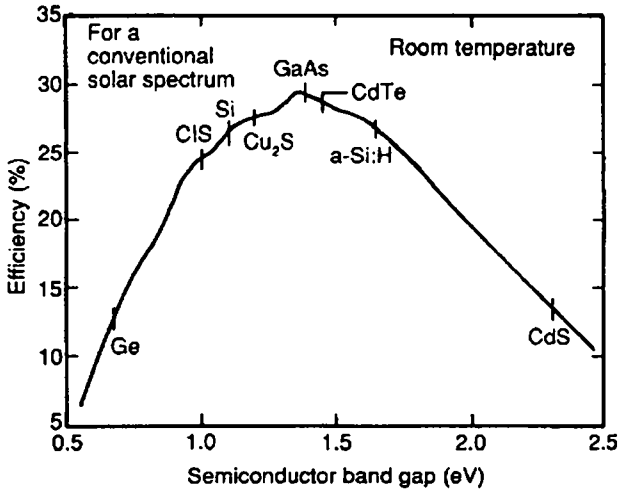

Figure 3: Theoretical efficiencies of photovoltaic cells as function of the semiconductor band gap [4,p.68]

1.2.2. Crystalline silicon solar cells

Photovoltaic cells made from crystalline silicon were the first to find an important application in supplying satellites with energy, and due to the extensive research related to the space program are still the most developed type of solar cells. The choice of silicon was originally motivated by its general use in the semiconductor industry. Silicon remains an attractive material, since it is one of the most abundant elements on earth (20% of the earth's crust), mainly in the form of sand (SiO_2). For solar cells quartz, which has a higher purity than ordinary sand is reduced in carbon arc furnaces to metallurgical-grade silicon (impurity content 2%, price \$1/kg).[7] The high level of impurities would result in rapid recombination of the photogenerated charge carriers in the semiconductor. Only after distillation as trichlorsilane and reduction with hydrogen semiconductor-grade silicon is obtained (impurity level in the ppb range, \$20/kg).

At present about half of the silicon solar cells are made from single-crystals. In the Czochralski-process a cylindrical silicon crystal (about ∅ 10 cm x 1 m) is slowly drawn from a melt (2,5 cm/hour). The crystal is cut into wafers of 0.3 mm thickness, whereby 50% of the material is lost as saw dust. Since over 1 kg of silicon is required per m^2 of solar cells the material itself contributes more than \$20/m^2 to the total price.

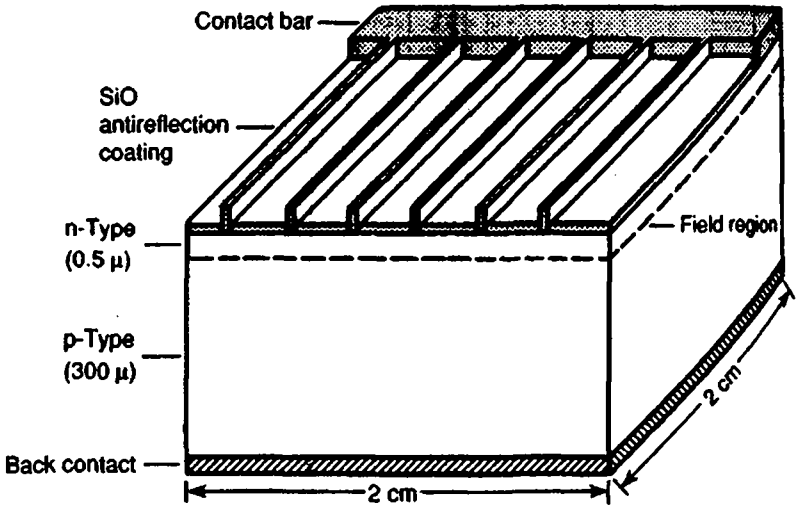

Figure 4: Design of a conventional single-crystal silicon solar cell[4,p.122]

During crystal growth the silicon has already been doped with boron, that has one valence electron less than silicon and causes an electron deficiency (p-doping). The p-n-junction is formed by doping the surface of the silicon wafer with phosphorus, having one valence electron more than silicon. The solar cell is completed by metal contacts on front and back side and an antireflection coating (Figure 4), since otherwise 40% of the incident light would be lost by reflection from the high refractive index silicon.

Several improvements of this scheme, such as buried contacts, surface passivation and pyramidal surface structures for light trapping have led to efficiencies up to 23% (at 1 sun, AM 1.5),[8,9] not far from the theoretical limit of 26% (Figure 3). However, such sophisticated cells are too expensive for large scale applications, and typical modules made from single-crystal silicon have rather efficiencies below 15%, in part due to the poor packing of cells made from circular wafers. Although their price dropped drastically during the last 20 years it will be difficult to get below $\$400/m^2$ for 16% efficient modules, which translates into AC electricity costs of \$0.16/kWh in the best case.[4,p.110] This is still too expensive to compete with conventional energy sources and explains the need for alternatives to single-crystal silicon.

The expensive Czochralski process of single-crystal growth can be avoided by simply casting the molten silicon into a mold. Solidification under well controlled conditions results in a rectangular polycrystalline or even single-crystal block of silicon.[4,7] This is cut into quadratic wafers that can be packed more tightly than circular cells, so that large modules reach efficiencies of 12% even for polycrystalline silicon, which exhibits higher charge carrier losses due to grain boundary recombination. However, more than 50% of the silicon is still lost by wafering.

Thin ribbons or sheets of silicon can be produced directly by different growth techniques.[4,6,7] At low growth rates single-crystal silicon may be obtained, while faster growth yields polycrystalline material. This leads to a trade-off between cost and efficiency: either cells of high efficiency are produced at low rate and therefore high cost, or vice versa.

All techniques mentioned so far have the disadvantage to require silicon of very high purity, which constitutes an important cost factor in itself. A completely different solar cell technology based on cheap metallurgical-grade silicon has been developed by the Texas Instruments company.[10] In the so called "Spheral solar cell" process granulated silicon is molten in the presence of oxygen and forms spherical balls under the influence of the surface tension.

Upon slow cooling crystallization starts from the center and the impurities enriched in the molten phase are carried to the periphery, as in zone refining. The impurity enriched surface layer is than removed mechanically. Multiple repetition of this process results in spheres of about 0.75 mm in diameter of much higher purity than the starting material. The residual impurities are gettered or complexed by a chemical treatment, while the remaining boron renders the silicon p-type. Doping of the surface layer with phosphorus makes it n-type and creates the p-n-junction.

To contact these spherical solar cells the spheres are pressed into the holes of a perforated aluminum foil, thus contacting the outer n-layer. The part of the n-layer that protrudes through the holes of the aluminum foil is etched away to expose the p-type core of the spheres. After application of an insulating plastic foil the p-zone is contacted by a second aluminum foil. The resulting array of 170 silicon spheres per cm^2 attached to a flexible aluminum foil substrate is completed by an antireflecting coating (Figure 5), resulting in solar cells with an efficiency around 10%. Due to the use of metallurgical-grade silicon and the absence of expensive vacuum processes the fabrication costs are estimated at \$1.5/W, which is much below the present price of \$8-15/W for conventional solar cells. Whether these optimistic expectations are realizable has to be proven by the mass production of the spherical solar cell, planned to start in 1994/95.

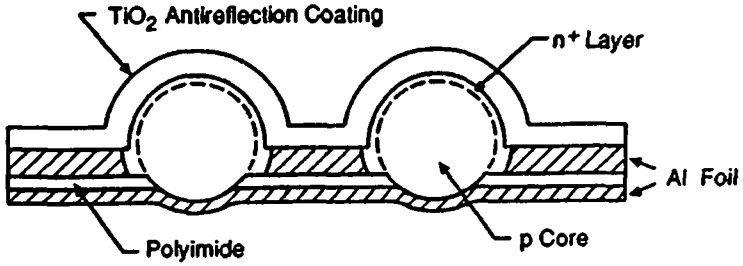

Figure 5: Spheral solar cells connected by aluminum foils [10b]

1.2.3. Thin-film solar cells

Conventional crystalline silicon modules require at least 1 kg of high purity silicon per m^2, which contributes more than \$20/m^2 to the total costs. Since the 1.1 eV band gap of crystalline silicon is an indirect one a minimum thickness of 100 μm is needed to absorb most sunlight. By contrast, amorphous silicon has a direct band gap of 1.7 eV and already a thin film of only 1 μm is sufficient for strong light absorption.[4,11] Although the free charge carrier diffusion length in amorphous silicon is reduced by orders of magnitude it is still large enough for efficient charge separation in an only 1 μm thick film. Dangling bonds and impurities create a high density of defect states in the band gap of amorphous silicon. These pin the Fermi level and made doping impossible until it was found that incorporation of hydrogen neutralizes the defects by saturating the dangling bonds. A layer of hydrogenated amorphous silicon (a-Si:H) can be deposited from silane (SiH_4) in a radio frequency glow-discharge onto a conducting substrate at relatively low temperatures (200-400°C). A p-i-n diode structure (Figure 6) is built up by deposition of a thin phosphorus doped, n-type layer, followed by a 0.4 - 2 μm thick undoped, intrinsic region, and finally a thin boron doped, p-type layer. A transparent conducting oxide film, such as fluorine doped tin oxide, serves as top contact. The p-i-n structure gives rise to an electric field that spans the whole intrinsic region guaranteeing efficient separation of the photogenerated charge carriers.

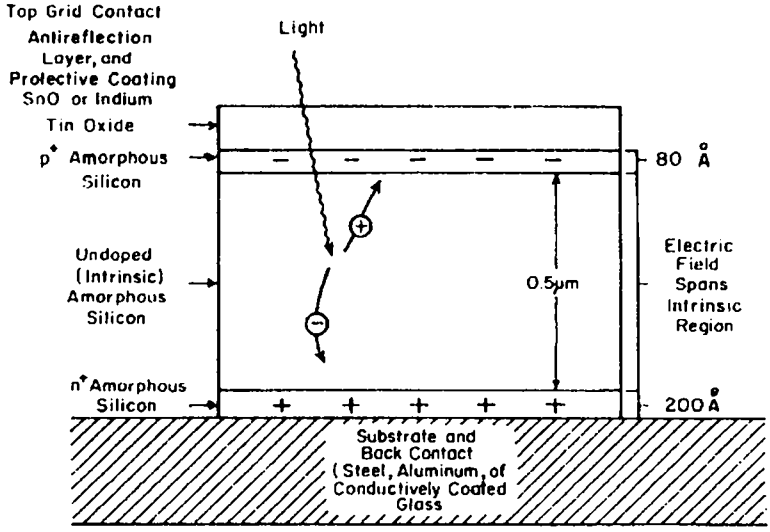

Figure 6: Amorphous silicon solar cell with p-i-n structure.[7,p.55]

Energy conversion efficiencies up to 13% have been reached with this design, however, the efficiency decreases during the first months under illumination and stabilizes at 8% for the best cells, and only 5% for typical modules. This so-called Stabler-Wronski effect has been the main impediment for the application of amorphous silicon cells in the power sector, in spite of their attractive price. The instability can in part be overcome by a multijunction of two or more thinner cells of different band gap. Unfortunately, the more complex design renders multijunction cells also more expensive.

Other materials for thin-film solar cells are Cu_2S, CdTe, $CuInSe_2$ and GaAs. Heterojunction photovoltaic cells formed by a thin layer of copper sulfide (Cu_2S) on cadmium sulfide (CdS) were already developed in the 1950s.[4,p.135] Such cells can be fabricated on a large scale by very simple nonvacuum processes, such as spray coating. While efficiencies up to 10% were attained, typical modules give only 5%. But the main problem of the Cu_2S/CdS cell is its instability, originating from the electromigration of copper creating short circuits.

Cadmium Telluride (CdTe) thin films can also be made by very cheap processes, such as electrodeposition or screen printing.[4,p.181] Efficiencies exceeding 14% have been obtained with CdTe/CdS cells, but again long term stability is a problem, although not as severe as in the case of Cu_2S. Moreover, the toxicity of cadmium is a matter of concern, and used cells would have to be recycled. Yet, even without recycling the cadmium consumption per kWh of produced electricity would in fact be comparable to the inadvertent release of cadmium through the fly ash of coal plants, which not only produce cadmium but many other pollutants as well.[4,p.197]

Still another material under investigation for thin-film solar cells is copper indium selenide ($CuInSe_2$).[4,ch.10] This ternary compound semiconductor is characterized by a narrow band gap (Eg = 1.0 eV) and very strong light absorption. $CuInSe_2$ is usually deposited by sputtering and stable efficiencies above 14% for small cells and 10% for modules of 0.4 m^2 have been reported. This makes $CuInSe_2$ a very promising candidate for thin-film photovoltaic cells and work is under way to replace the rather costly sputtering deposition by a nonvacuum process, such as spraying, screen printing or electrodeposition.[9]

1.3. Photoelectrochemical solar cells (PEC)

1.3.1. Regenerative PECs and photoelectrolysis cells

The photovoltaic effect was in fact not discovered with solid state junctions, but with a semiconductor dipped into an electrolyte. In 1839 C. Becquerel, the grandfather of the discoverer of radioactivity, found that a platinum electrode covered with a thin layer of silver chloride and immersed into an electrolyte solution developed upon illumination a voltage with respect to a counter electrode in the same solution.[12,13]

A theory of the semiconductor / liquid junction has been formulated by Gerischer and others.[14-17] According to this concept equilibration of the Fermi potentials (electrochemical potentials) of semiconductor and redox electrolyte by electron exchange creates a space charge layer in the semiconductor, in analogy to the Schottky barrier of a semiconductor / metal junction (Figure 7).

Charge carriers generated by band gap excitation of the semiconductor are rapidly separated by the electric field in the space charge region. The majority carriers drift to the bulk, while the minority carriers are expelled to the surface, where they react with the redox couple. Hence a photovoltage is built up that may drive an electrical current through an external load. The circuit is closed by a counter electrode where regeneration of the redox electrolyte takes place.

Such a photoelectrochemical cell (PEC) has the big advantage that the junction for charge carrier separation is formed by simple immersion of the semiconductor into an electrolyte solution. Even polycrystalline semiconductors with rough surface can be used since the liquid electrolyte follows any surface irregularities.[18] Examples for regenerative PECs are n-CdSe / (S^{2-}/S_n^{2-}), n-GaAs / (Se^{2-}/Se_n^{2-}), n-Si / (Fc^+/Fc), n-WSe / (I^-/I_3^-), n-InP / (V^{3+}/V^{2+})[17-22] and FeS_2 / (I^-/I_3^-).[23] Energy conversion efficiencies up to 16.4% have been attained with n-CdSe / $([KFe(CN)_6]^{2-/3-})_{aq}$.[24]

The main problem of most PECs has been their lack of long term stability. Especially with n-type semiconductors the valence band hole created by band gap excitation is strongly oxidizing and may attack the semiconductor itself, before being filled up by the redox electrolyte. This anodic decomposition or photocorrosion of the semiconductor electrode can at least to some extent be suppressed by high concentrations of fast redox couples and nonaqueous solvents.[20]

Contrary to regenerative PECs, where anodic and cathodic reactions compensate each other, photoelectrolysis cells contain two different redox couples resul-

ting in a net chemical change and the storage of light energy as chemical energy. Especially the light induced splitting of water into hydrogen and oxygen, which occurs in natural photosynthesis, has attracted widespread interest.[19,25] However, only oxide semiconductors such as TiO_2, $SrTiO_3$, SnO_2 and Fe_2O_3 are stable under the conditions of oxygen evolution. Since these oxides have in general a rather wide band gap ($E_g > 3$ eV, with the exception of Fe_2O_3: E_g = 2.3 eV) only short wavelength light is absorbed, which is responsible for the very small sunlight conversion efficiencies (around 1%). Moreover, cathodic and anodic reactions have to be spatially separated in order to avoid mixing and recombination of the generated chemical fuels, e.g. H_2 and O_2. This complicates appreciably the technical design of large area solar cells and is another reason, why separate photovoltaic modules and water electrolyzers are favored in practice.

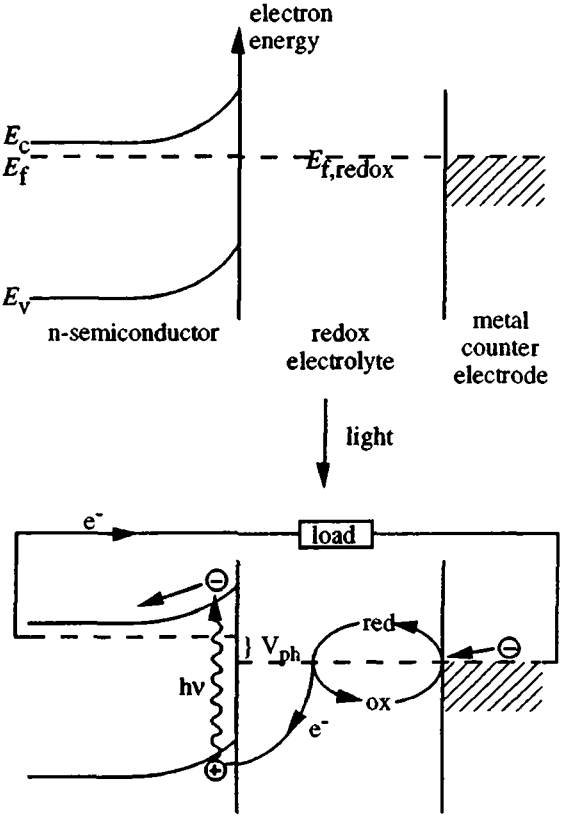

Figure 7: Semiconductor/electrolyte junction in the dark and under illumination

1.3.2. Dye-sensitized photoelectrochemical solar cells

The spectral response of stable wide band gap semiconductors like TiO_2 can be extended to visible light by sensitization with a dye. In this case free charge carriers are not generated by band gap excitation of the semiconductor, but by electron or hole injection from the excited dye. A well known application is the sensitization of silver halides for green and red light with organic dyes, which has become the basis of modern photography.

The general principles of spectral sensitization have been formulated by Gerischer and others.[26] In the case of a n-type semiconductor like TiO_2 the excited dye may inject an electron into the conduction band, if it is in close contact with the surface during the excited state lifetime and if it lies energetically above the conduction band edge (Figure 8). As in the case of an unsensitized PEC (Figure 7) immersion of the semiconductor into a suitable redox electrolyte creates a depletion layer at the surface. The electric field in this layer removes the injected electron rapidly from the interface and thus prevents its recombination with the oxidized dye. The sensitizer is regenerated by the redox electrolyte (sometimes called supersensitizer), which for its part receives the electron back from the counter electrode.

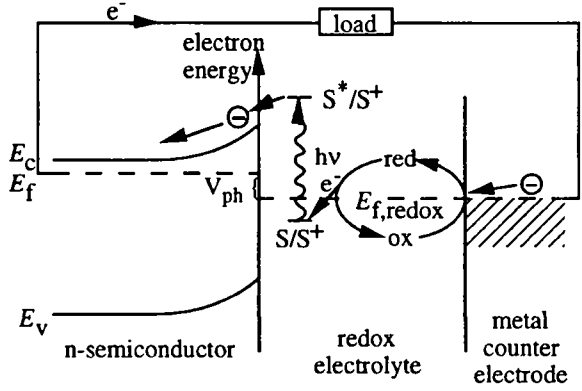

Figure 8: Operation scheme of a dye-sensitized photoelectrochemical cell

The short excited state lifetime of most dyes (several nanoseconds) requires direct attachment to the semiconductor surface to guarantee efficient electron injection. However, a monolayer of a dye absorbs at most a few percent of the incident light in its absorption maximum and an even smaller portion of the complete spectrum. This explains why flat semiconductor electrodes covered

with a monolayer of sensitizer show extremely low sunlight conversion efficiencies. A multilayer dye coverage does in most cases not improve the situation, since the electron injection efficiency decreases rapidly with distance and the excitation energy is quickly trapped and dissipated within the layer of aggregated dye molecules. In other words, the internal filter effect and concentration quenching usually preclude the use of thick dye coatings for light absorption enhancement.

Practical light harvesting and conversion efficiencies were first obtained with the advent of semiconductor electrodes of very high surface area.[27,28] Porous films of sintered nanometer-sized semiconductor particles having a 1000-fold enhanced surface area make light absorption efficient even with only a dye monolayer on each particle (Figure 9). Nature, in fact, uses a similar means of absorption enhancement by stacking the chlorophyll containing thylakoid membranes of the chloroplast to form the grana structures. Also the photoreceptor cells in the retina of the eye contain stacks of folded membranes with a monolayer of the light absorbing rhodopsin.

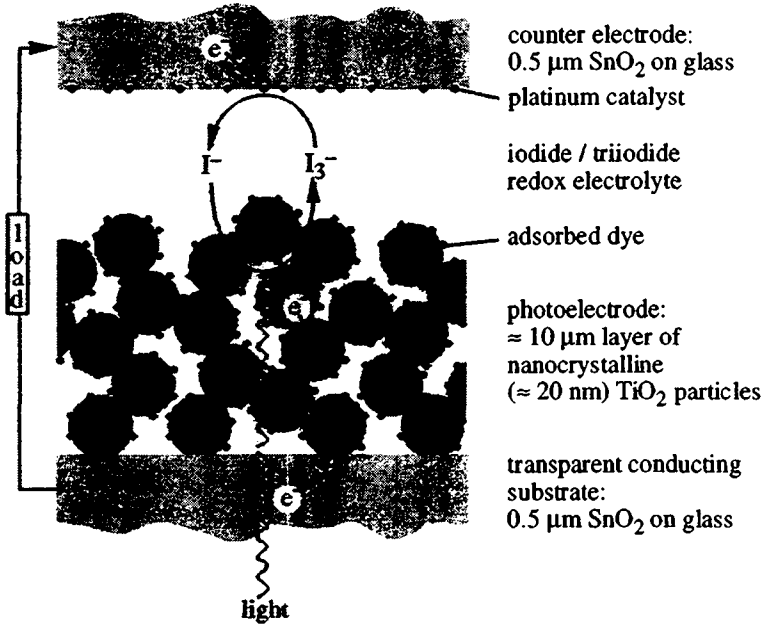

Figure 9: Structure and operation principle of the dye-sensitized solar cell

The charge separation mechanism in a dye-sensitized colloidal electrode is somewhat different from that for a bulk semiconductor (Figure 8), since a space charge region with an electric field cannot build up in the nanometer-sized particles. Efficient charge separation is nevertheless achieved due to rapid reduction of the oxidized dye by the redox couple in solution, before recombination with the injected electron can occur. This purely kinetic mechanism is comparable to that of natural photosynthesis, where an electron is rapidly transferred from the excited reaction center chlorophyll to a distant acceptor of lower energy, thereby preventing recombination before reduction of the chlorophyll cation by an electron donor has taken place. In view of the similarities in the primary charge separation mechanism the dye sensitized nanocrystalline photoelectrochemical cell may be called an artificial photosynthetic system.

The great advantage of this new type of solar cell is its ease of fabrication from cheap materials and the consequently low price. The nanocrystalline semiconductor, e.g. titanium dioxide, which is already widely used as pigment in white paints and in toothpaste, is applied as a thin layer ($\approx$ 10 μm) onto a conducting substrate, such as SnO_2 coated glass (Figure 9). Firing at moderately high temperature (300-500°C) in air results in a porous TiO_2 film of high surface area, which is coated with the sensitizer by immersion into a dye solution. The cell is completed by a thin layer of redox electrolyte filling the pores of the TiO_2 film and a counter electrode on top, activated by a small deposit of platinum. Sunlight conversion efficiencies up to 10% and promising long term stability have already been attained with this simple set-up.[29] Still, several technical problems remain to be solved and the practical applicability of this new photovoltaic device has to be proven by future developments.

In the experimental part of this thesis we have studied the different components of the dye-sensitized solar cell. In particular new methods for the preparation of porous, nanocrystalline TiO_2 films were developed. We also investigated the mechanism of photosensitization and charge carrier separation, focusing on chlorophyll derivatives as sensitizers. Our current knowledge with regard to the fabrication and function of the dye-sensitized nanocrystalline solar cell shall be presented in the following chapters.

References to chapter 1

1. **J. P. Holdren:** Safety and environmental aspects of fusion energy *Ann. Rev. Energy Environ.* 16 (1991) 235
2. **Ch.C. Swan:** *Suncell*, San Francisco 1986, p.5
3. Bild der Wissenschaft extra:*Energie aus Sonne und Wind*, Stuttgart 1986, p.12
4. **K. Zweibel:** *Harnessing Solar Power*, Plenum Press, New York 1990
5. **C. Hu, R.M. White:** *Solar Cells*, New York, 1983
6. **R.J. Van Overstraeten, R.P. Mertens:** *Physics, Technology and Use of Photovoltaics*, Bristol 1986
7. **F. Lasnier, T.G. Ang:** *Photovoltaic Engineering Handbook*, Bristol 1990
8. **M.A. Green:** High-efficiency silicon solar cell, in *Proc. 10th European Photovoltaic Solar Energy Conference*, Lisbon 1991, Kluwer Acad. Press, Amsterdam 1991, p.250
9. *11th European Photovoltaics Solar Energy Conference*, Montreux 1992, Book of Abstracts
10. a) **J. Fricke:** Solarzellen aus Silizium-Kügelchen, *Physik in unserer Zeit* 23 (1992) 42

    b) **J.D. Levine, G.D. Hotchkiss, M.D. Hammerbacher:** Basic properties of the Spheral Solar Cell, *22nd IEEE Photovoltaic Specialists Conference*, Nov. 1991, Las Vegas
11. **K. Takahashi, M. Konajai:** *Amorphous Silicon Solar Cells*, London 1986
12. **E. Becquerel:** *Compt. rend. Hebd. Seances Acad. Sci.* 9 (1839) 561
13. **R. Williams:** Becquerel photovoltaic effect in binary compounds *J. Chem. Phys.* 32 (1960) 1505
14. a) **H. Gerischer**: Electrochemical photo and solar cells, *Electroanal. Chem. Interf. Electrochem.* 58 (1975) 263

    b) **H. Gerischer:** Power generation by photoelectrolysis, in *Solar Power and Fuels*, J.R. Bolton, ed., New York 1977, p.77

    c) **H. Gerischer:** Solar photoelectrolysis with semiconductor electrodes, in *Solar Energy Conversion*, B. Seraphin, ed., Berlin 1979, p.115
15. a) **A.J. Nozik:** Photochemical diodes *Appl. Phys. Lett.* 30 (1977) 567

    b) **F. Williams, A.J. Nozik:** Solid-state perspectives of the photoelectrochemistry of semiconductor-electrolyte junctions *Nature* 312 (1984) 21
16. **S. Chandra:** *Photoelectrochemical Solar Cells*, New York 1985
17. **R. Memming:** Photoelectrochemical solar energy conversion, in *Topics in Current Chemistry*, E. Steckhan, ed., Berlin 1988, Vol. 143, p.79
18. **G. Hodes, S.J. Fonash, A. Heller, B. Miller:** Photoelectrochemical cells based on polycrystalline semiconductors, *Adv. Electrochem. Electrochem. Eng.*, H. Gerischer, ed., New York 1984, Vol. 13, p.113
19. **M.S. Wrighton:** Photoelectrochemical conversion of optical energy to electricity and fuels *Acc. Chem. Res.* 12 (1979) 303

20. **N.S. Lewis:** Photoeffects at the semiconductor / liquid interface *Ann. Rev. Mater. Sci.* 14 (1984) 95

21. a) **A. Heller:** Conversion of sunlight into electrical power and photoassisted electrolysis of water in photoelectrochemical cells *Acc. Chem. Res.* 14 (1981) 154

    b) **A. Heller:** Hydrogen-evolving solar cells *Science* 223 (1984) 1141

22. **B. Parkinson:** On the efficiency and stability of photoelectrochemical devices *Acc. Chem. Res.* 17 (1984) 431

23. **A. Ennaoui, S. Fiechter, C.H. Pettenkofer, N. Alonso-Vante, K. Büker, M. Bronold, Ch. Höpfner, H. Tributsch:** Iron disulfide for solar energy conversion *Sol. Energy Mat. Sol. Cells* 29 (1993) 289

24. **S. Licht, D. Peramunage:** Efficient photoelectrochemical solar cells from electrolyte modification *Nature* 345 (1990) 330

25. a) **A. Fujishima, K. Honda:** Electrochemical evidence for the mechanism of the primary stage of photosynthesis *Bull.Chem.Soc.Japan* 44 (1971) 1148

    b) **A. Fujishima, K. Honda:** Electrochemical photolysis of water at a semiconductor electrode *Nature* 238 (1972) 37

26. a) **H. Gerischer, F. Willig:** Reactions of excited dye molecules at electrodes, in *Topics in Current Chemistry* 61, Berlin 1976, p. 31

    b) **H. Gerischer, M.T. Spitler, F. Willig:** Electrode reactions of excited molecules, in *Proc. 3rd Symp. Electr. Proc.* (Boston 1979), S. Bruckenstein, ed., Princeton 1980

27. a) **H. Tsubomura, M. Matsumura, Y. Nomura, T. Amamiya:** Dye sensitized zinc oxide: aqueous electrolyte: platinum photocell *Nature* 261 (1976) 402

    b) **M. Matsumura, S. Matsudaira, H. Tsubomura, M. Takata, H. Yanagida:** Dye sensitization and surface structures of semconductor electrodes *Ind. Eng. Chem. Prod. Res. Dev.* 19 (1980) 415

28. a) **N. Vlachopoulos, P. Liska, A.J. McEvoy, M. Grätzel:** Efficient spectral sensitization of polycrystalline titanium dioxide photoelectrodes *Surf. Sci.* 189/190 (1987) 823

    b) **N. Vlachopoulos, P. Liska, J. Augustynski, M. Grätzel:** Very efficient light energy harvesting and conversion by spectral sensitization of high surface area polycrystalline titanium dioxide films *J. Am. Chem. Soc.* 110 (1988) 1216

    c) **B. O'Regan, M. Grätzel:** A low-cost, high efficiency solar cell based on dye-sensitized colloidal TiO_2 films *Nature* 353 (1991) 737

29. **M.K. Nazeeruddin, A. Kay, I. Rodicio, R. Humphry-Baker, E. Müller, P. Liska, N. Vlachopoulos, M. Grätzel:** Conversion of light into electricity by *cis*-X_2Bis(2,2'-bipyridyl-4,4'-dicarboxylate)-ruthenium(II) charge transfer sensitzers (X = Cl^-, Br^-, I^-, CN^- and SCN^-) on nanocrystalline TiO_2 electrodes *J. Am. Chem. Soc.* 115 (1993) 6382

2. The photoelectrode

2.1. Substrates

2.1.1. Introduction

The substrate of the photoelectrode serves as collector for the photogenerated current and has therefore to be well conducting. Moreover it must form an ohmic contact with the dye sensitized semiconductor layer, but should show a large overvoltage for reduction of the redox electrolyte to minimize the dark current. In the case of front side illumination it acts also as window for the incident light and should therefore be highly transparent in the visible region, while blocking of UV light may be desired to prevent photodecomposition of the cell due to band gap excitation of the semiconductor. In the case of back side illumination through the counter electrode a reflecting photoelectrode substrate has the advantage to enhance light absorption by reflecting the transmitted light back into the dye layer. The substrate is also the mechanical support for the very thin semiconductor coating, which should strongly adhere to it. It must withstand the high temperature during sintering of the photoelectrode (> 300°C, cf. chapter 2.4.4) as well as the often highly corrosive electrolyte.

2.1.2. Metallic substrates

Originally titanium sheet metal was used as substrate for "fractal" anatase films.[1] Although titanium is a rather poor metallic conductor (ρ_{Ti} = 42 μΩ·cm compared to ρ_{Cu} = 1.7 μΩ·cm), even a foil of only 10 μm thickness has a sheet resistance of merely 0.042 Ω/□, which is negligible for our purposes. The resistance of the surface oxide layer, which growths further on firing in air to sinter the porous TiO_2 coating, is much more important. This nonporous oxide layer has to be rendered conducting by a final firing in inert gas atmosphere, where doping through reduction from the metallic titanium occurs (see chapter 2.3.2). On the other hand, this oxide layer provides an ohmic contact with the porous TiO_2 coating and protects the underlying metal from corrosion. Thin titanium foil can serve as flexible substrate for the photoelectrode, but it is neither transparent nor well reflecting for visible light.

Higher reflectivity would be obtained with aluminum foil, which is also protected against corrosion by its oxide layer. However, the insulating Al_2O_3 film would block the electron transfer from the TiO_2 coating. Even a reduced, oxide free aluminum surface would be reoxidized by reaction with the TiO_2 coating:

$$2\,Al + 3/2\,O_2 \rightarrow Al_2O_3 \qquad \Delta H = -96\ kJ/mol$$
$$Ti + O_2 \rightarrow TiO_2 \qquad \Delta H = -50\ kJ/mol$$
$$4\,Al + 3\,TiO_2 \rightarrow Al_2O_3 + 3\,Ti \qquad \Delta H = -42\ kJ/mol$$

Other passivated metals like chromium and molybdenum, having a semiconducting oxide layer, may be more promising. More noble metals, such as nickel, copper, silver and gold are excluded with the present iodide / triiodide redox electrolyte, due to corrosion (e.g. a solution of KI / I_2 is widely employed to etch gold). Platinum metals, although stable in this electrolyte, catalyze the reduction of triiodide and would cause an internal short circuit of the solar cell.

A thin, nonporous layer of TiO_2 might in principle protect the underlying metal from corrosion and prevent electron transfer to the electrolyte. Yet, in practice an absolute pin hole free coating is difficult to achieve, especially in view of the widely different thermal expansion coefficients of TiO_2 and the metal substrate. While titanium is often used as an intermediate layer for silver contacts on silicon solar cells,[2] this combination would not present any advantage over a pure titanium foil in our case, since the reflectivity of silver is deteriorated by the titanium coating. The ultimate solution of the corrosion problem would probably be the replacement of the liquid I^-/I_3^- redox electrolyte by a solid electrolyte (chapter 4.4).

2.1.3. Transparent conducting oxides

Thin films of transparent conductors are widely used as front contacts for crystalline and amorphous silicon solar cells, but also for energy saving windows, due to their high reflectivity in the infrared.[3-10] The most successful materials are tin oxide, doped with fluorine (SnO_2:F) or antimony and indium oxide, doped with tin (ITO). For large scale fabrication of SnO_2:F, mainly employed for amorphous silicon cells, atmospheric pressure chemical vapor deposition is the method of choice,[11] while a heat reflecting ITO layer is applied to window panes of up to 3 x 4 m^2 by dip coating.[10] ITO has a higher specific conductivity than SnO_2:F, so that thinner layers suffice to reach a certain sheet resistance. However, the resistivity of ITO increases rapidly on firing above 350°C due to segregation of the SnO_2 dopent to the grain boundaries.[12,13] By contrast SnO_2:F remains stable at firing temperatures of up to 550°C used to sinter the TiO_2 film (a minimum of 300°C is required: cf. chapter 2.4.4).

The sheet resistance of a typical SnO_2:F layer of 0.6 µm thickness on glass is less than 10 Ω/□ and the optical transmission in the visible range around 80%.[14] Most of the light is lost by reflection at the air / glass (refractive index $n \approx 1.5$) interface ($R = (n_1-n_2)^2/(n_1+n_2)^2 \approx 4\%$), the glass / SnO_2 ($n \approx 2.0$) interface ($R \approx 2\%$) and the SnO_2 / air interface ($R \approx 11\%$). The last reflection is absent in the solar cell, since the porous TiO_2 layer has about the same refractive index as the SnO_2 substrate. Light reflection at the air / glass interface can be reduced by an antireflecting coating.

The SnO_2 coating is made with different degrees of haze, which is due to its rough surface.[15] This results in diffuse scattering of the incident light and increases the efficiency of amorphous silicon solar cells in the red region due to light trapping. Light scattering at the SnO_2 surface does not occur in presence of the TiO_2 layer with its refractive index matching that of SnO_2, but is not required, since the colloidal TiO_2 film itself scatters the light, if it contains some rather large ($d > 50$ nm) particles or aggregates. Still, a rough SnO_2 surface presents the advantage of a larger interfacial area with the TiO_2 coating, which improves adhesion and electrical contact (cf. chapter 2.2).

The corrosion resistance of SnO_2:F is excellent: It is only attacked by acids under reducing conditions. Also the blocking behavior with respect to the I^-/I_3^- redox couple meets the requirements: The dark current caused by the SnO_2 substrate is negligible compared to that of the high surface area, dye loaded TiO_2 coating (see chapter 2.2).

The only limiting factor is the sheet resistance of the transparent conducting oxide, which cannot be reduced much below 10 Ω/□ without an appreciable loss in optical transmission. With a spacing of 0.5 cm between front and back

contacts and a current density of 20 mA/cm^2 in full sunlight a sheet resistance of 10 Ω/□ causes a voltage drop of 100 mV, which is about the tolerable limit. Solar cells wider than about 0.5 cm therefore necessitate a well conducting finger grid to collect the current, as known from silicon solar cells.[2,16-18] Since only metals have the required conductivity we are again confronted with the problems discussed in chapter 2.1.2, namely corrosion by the electrolyte, formation of an insulating oxide layer or increased dark current due to triiodide reduction.

One can do without a finger grid by connecting cells of the limiting width (0.5 - 1 cm) in series, as commonly done with amorphous silicon cells. The possibility of illuminating the dye sensitized TiO_2 solar cell either from the front (TiO_2) or the back (transparent counter electrode) side leads to a very convenient manner of connecting alternating photo- and counterelectrodes on the same SnO_2 substrate in series (Figure 10). The disadvantage of this scheme is that the least efficient cell in the series connection limits the photocurrent of the whole module.

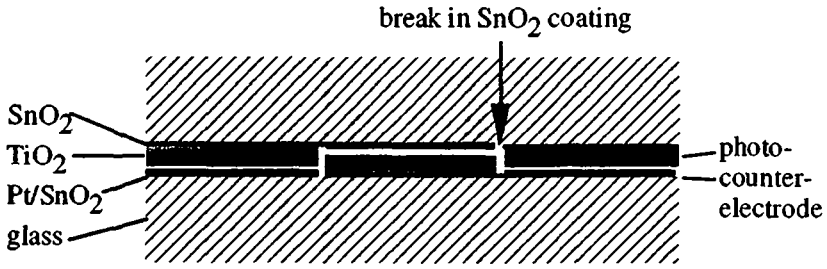

Figure 10: Series connection of TiO_2 solar cells

2.2. Underlayers

The surface of the SnO_2 conducting coating should make a good mechanical and above all electrical contact with the porous TiO_2 film, but is should block the back electron transfer to the redox electrolyte. For the iodide / triiodide couple the latter requirement is largely fulfilled, as shown by the dark current curve in Figure 11a. The characteristics were measured in the thin layer cell configuration with platinum counter electrode and a 40 µm thick spacer of porous paper to prevent short-circuiting. The untreated SnO_2 electrode shows a dark current of about 0.1 mA/cm^2 at 0.6 V, which is a typical operating voltage for the dye sensitized solar cell. Hence, the photocurrent would be reduced by 0.1 mA/cm^2 at this voltage due to reduction of triiodide at the SnO_2 substrate of the photoelectrode.

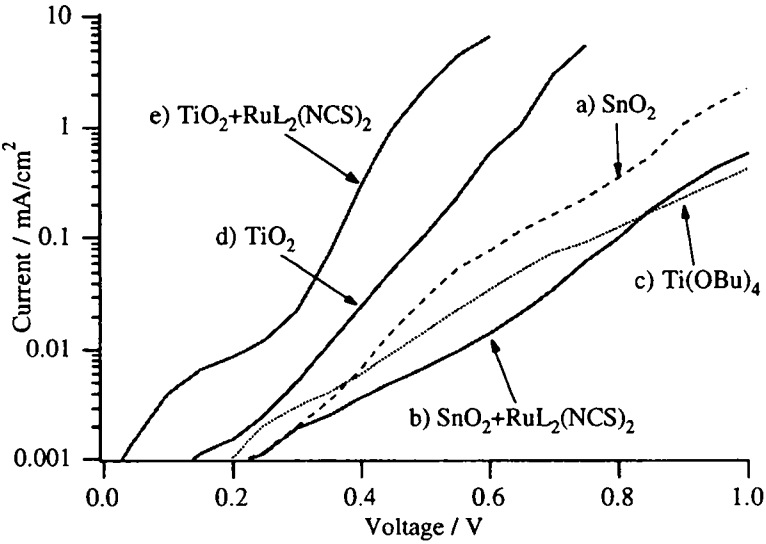

Figure 11: Cathodic dark current / voltage characteristics in 80 % ethylene carbonate / 20 % propylene carbonate / 0.5 M KI / 40 mM I_2 for **a)** bare SnO_2:F (10Ω/□, ≈ 2% haze of Glastron, France, after firing 10 min. in air at 550°C); **b)** SnO_2 with adsorbed dye ($RuL_2(NCS)_2$); **c)** SnO_2 with a 10 nm thick layer of TiO_2 prepared by application of 5 µl/cm^2 of 10 mM $Ti(OBu)_4$ in isopropanol and firing 10 min. in air at 550°C; **d)** SnO_2 coated with 12 µm thick nanocrystalline TiO_2 (P-25) layer, treated with $TiCl_4$ and fired 10 min. in air at 550°C; **e)** the same electrode with adsorbed dye

Adsorption of a ruthenium dye on SnO_2 (Figure 11b) decreases the dark current in the present case, although the opposite has been observed with other SnO_2 electrodes of higher haze and thus larger surface roughness. Also a thin layer of TiO_2 prepared by hydrolysis of titanium butoxide (Figure 11c) reduces somewhat the dark current. By contrast, it increases by about one order of magnitude after application of the porous TiO_2 layer (Figure 11d). This can be rationalized by the very high surface area (roughly 1000 times the geometrical area) of the nanocrystalline TiO_2 coating. The dark current increases by another order of magnitude after adsorption of the sensitizer (Figure 11e). Thus, at least the dye $RuL_2(NCS)_2$ (cf. chapter 3.3) catalyses the back electron transfer from TiO_2 to triiodide. We conclude, that the dark current due to the SnO_2 substrate is negligible compared to that of the dye coated TiO_2 film.

The situation is different for one electron redox couples such as $Fe^{2+/3+}$, $Fe(CN)_6^{3-/4-}$ and $Ce^{3+/4+}$ which are much more reversible on SnO_2 than the two electron couple I^-/I_3^-.[19] In this case a blocking underlayer below the porous TiO_2 film is required to prevent a short-circuit due to reduction of the redox couple on the SnO_2 substrate. Blocking underlayers of nonporous TiO_2 can be prepared by spray coating (chapter 2.3.9), e.g. from the acetyl acetone chelate $Ti(acac)_2(i\text{-}OPr)_2$ in isopropanol, by chemical vapor deposition (chapter 2.3.11), or by electrodeposition from $TiCl_3$ solution.[20]

Although a thin underlayer of TiO_2 does not reduce significantly the dark current with I^-/I_3^- as redox couple, it does improve the mechanical adhesion of the porous TiO_2 film on the SnO_2 substrate and also the photocurrent efficiency of the dye sensitized solar cell. With untreated SnO_2 the adhesion is sometimes so poor that the TiO_2 coating flakes off during firing. Since the surface of the fluorine doped SnO_2 is at least partially fluorinated it may be difficult to wet by the colloidal TiO_2 solution, even if a detergent has been added to decrease the surface tension. The adhesion is better with SnO_2 of high haze, due to its increased surface roughness and thus larger contact area. But even SnO_2 of low haze can be rendered more adhesive by applying a solution of titanium butoxide in isopropanol to the surface (Figure 11c) just before coating with the porous TiO_2 layer. The $Ti(OBu)_4$ hydrolyses quickly in humid air and forms a gelly hydrated TiO_2 layer of about 10 nm thickness. Titanium butoxide is in fact a well known adhesion promoting primer for polyethylene and fluorinated polymers like PTFE, which are otherwise difficult to bond. While the nanocrystalline TiO_2 particles of the porous coating make only point contacts with the SnO_2 substrate, the nonporous underlayer made by hydrolysis of $Ti(OBu)_4$ covers the whole surface. The nanocrystalline TiO_2 particles are embedded into

this soft gelly underlayer which provides an intimate mechanical and electrical contact with the substrate (Figure 12).

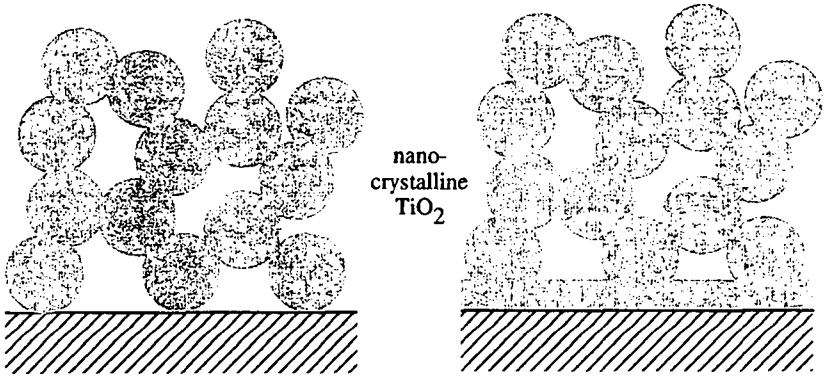

Figure 12: SnO_2/porous TiO_2 interface without and with a thin nonporous TiO_2 underlayer

2.3. Nanoporous TiO_2 films

2.3.1. Introduction

An appreciable part of this thesis has been devoted to the development of new methods for the preparation of nanoporous TiO_2 films for dye sensitized solar cells. The original method was a sol-gel process consisting in the application of a titanium-alkoxid solution to the substrate, followed by hydrolysis and firing in air. This process had to be repeated more than ten times to build up a sufficient thick "fractal" TiO_2 layer, rendering this procedure rather time and energy consuming. There is another kind of sol-gel process, which starts from preformed, colloidal particles and has turned out to be very versatile in the fabrication of TiO_2 electrodes. Thick films can now be made in one step and the pore size can be controlled by changing the particle size of the colloid. Still, the production of colloidal TiO_2 by precipitation and peptization followed by a hydrothermal treatment to increase the particle size is a rather complicated process. We made some effort to produce the colloid in situ, as in the original procedure, but to prevent cracking of thicker films by a polymer matrix, which at the same time determines the porosity of the film.
Since the SnO_2 conducting glass substrate for the dye-sensitized solar cell is made by chemical vapor deposition, we also investigated this technologically attractive, because continuous one step process for the deposition of porous TiO_2 films. We found that pores could be created by codeposition of B_2O_3, which afterwards is sublimed off, resulting in photoelectrodes of high efficiency. Another idea was to preform the TiO_2 particles in the gas phase, for example by flame hydrolysis of $TiCl_4$, and to deposit this "aerosol" on the substrate. Although the direct deposition of the aerosol always gave very loose, powdery layers, a commercial TiO_2 powder produced by the aerosol process proved to yield efficient electrodes if it was first dispersed in a liquid. This TiO_2 dispersion may be compared to a paint, which can be applied to the substrate by different techniques, such as spreading, spraying, painting or electrophoretic deposition.

2.3.2. Nanoporous TiO_2 films by polymerization of alkoxide precursors

The original method of making porous TiO_2 films for dye sensitized solar cells consists in the repeated application of an alcoholic solution of $TiCl_4$ to the substrate (titanium rods and sheets or SnO_2 coated glass), followed by hydrolysis in humid air and firing in air:[1]

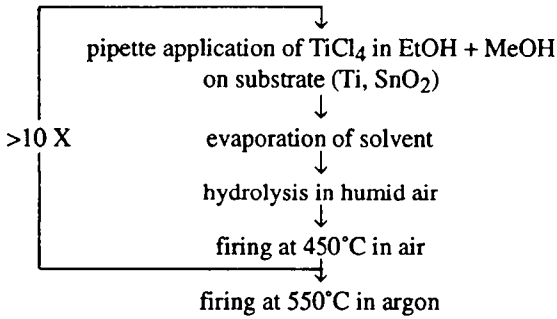

When $TiCl_4$ is dissolved in ethanol, an exothermic reaction takes place[21-23]

$$TiCl_4 + 2\ EtOH \rightarrow TiCl_2(OEt)_2 + 2\ HCl$$

Dilution with an excess of methanol, which is a stronger ligand than ethanol, gives $TiCl_2(OMe)_2$. This hydrolysis in humid air:

$$TiCl_2(OMe)_2 + 2\ H_2O \rightarrow TiO_2 + 2\ MeOH + 2\ HCl$$

At room temperature this reaction is far from being complete, due to the slowly hydrolyzing Cl-ligands. Thus, the product has rather the composition $TiO_x(OH)_yCl_{(4-2x-y)}$ and transforms to TiO_2 (anatase) only during firing. The hydrolysis conditions seem to be rather critical in determining the pore structure of the resulting gelatinous film, as expected from the very sensitive nucleation reactions involved in the condensation of the partially hydrolyzed precursors to a polymeric network. In fact, the comparison of different titanium precursors shows a strong dependence of the electrode morphology and its dye adsorption capacity on the hydrolysis rate.[24] Also the subsequent heat treatment, leading to drying of the gel and crystallization of the TiO_2, will have an influence on the final pore structure of the film.

During drying the gel shrinks as a result of the capillary forces produced by the evaporating liquid. For example a pore of 2 nm diameter filled with water produces a capillary pressure of

$$\Delta P = 2\gamma / r = 2{\cdot}73 \text{ mN m}^{-1} / 10^{-9} \text{ m} = 3000 \text{ bar}$$

Thin films on a substrate will only shrink in the vertical direction and stay intact, but films thicker than about 0.5 μm usually crack or peel off the substrate due to the high drying stress, as shown very schematically in Figure 13.

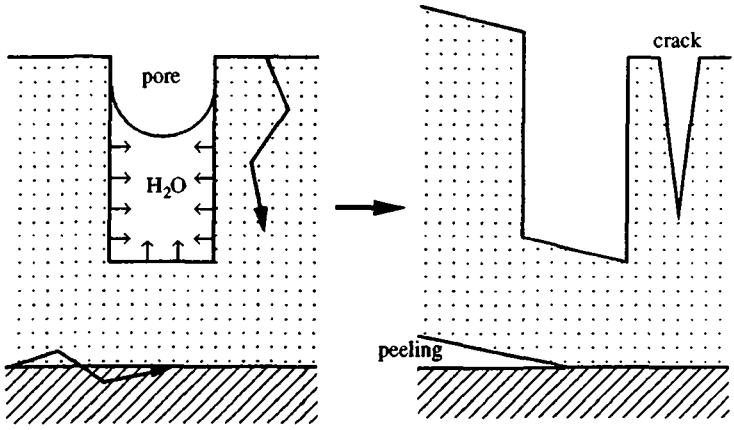

Figure 13: Cracking and peeling of a gel film during drying (the pore is largely oversized for clarity)

The repeated application and cracking of the TiO_2 film gives rise to the typical "fractal" appearance of these electrodes, as seen in scanning electron micrographs.[1] However, the micrometer large cracks are not sufficient to explain the high roughness factor (RF ≈ 200) of the 20 μm thick film. One can easily calculate that a quadratic pattern of cracks at an interval of 10 μm, which approximates the SEM pictures, gives only RF = 9. The observed value rather indicates a roughness on the submicrometer scale, and transmission electron micrographs have in fact revealed a colloidal fine structure of the film, with primary particles of 10 to 20 nm in diameter. Although not necessary for a high surface area of the TiO_2 electrode, the cracks may reduce the diffusion resistance of the film for the redox electrolyte, if the distance between the cracks is smaller than the thickness of the film.

The electrodes are finally fired in argon atmosphere, which was thought to dope the TiO_2 by partial reduction. We found that it is only important with titanium substrates, since a nonporous, insulating oxide layer forms on the titanium metal below the porous coating during firing in air. The oxide layer is rendered conductive by firing in argon, where it is partially reduced and thus doped by the metallic titanium substrate. For SnO_2 conducting glass substrate this treatment is not necessary: doping of the porous TiO_2 layer does not occur in absence of a reducing agent and is in fact not desired, since it becomes "photodoped" by electron injection from the adsorbed dye.

It should be mentioned that TiO_2 films have been made before from $TiCl_2(OEt)_2$ by dip coating at the Schott company for optical applications.[25] Crack free coatings of almost unlimited thickness can be deposited by repeated application of 0.1 μm layers. Similar films have also been obtained from partially hydrolyzed titanium alkoxides by Yoldas [26] for optical purposes and by Yoko et al.[27] for the photocleavage of water. The preparation of thin films from alkoxides is one kind of sol-gel process, and has found many new applications recently.[28,29]

2.3.3. The preparation of colloidal TiO_2 electrodes

There is another kind of sol-gel process, which employs preformed, dispersed colloidal particles (the sol), which form a gel on concentration and sinter together on firing. A method of producing porous transparent gels from colloidal particles has first been described by Yoldas for aluminum oxide.[30] He first precipitated alumina by hydrolyzing an aluminum alkoxide with an excess of water. This precipitate is then peptized by adding an acid, preferentially nitric acid, because it decomposes to volatile products upon firing. The peptization is due to protonation of the hydroxyl groups on the primary particles of the precipitate. The surface of the particles becomes highly positively charged, so that they repel each other and disperse to a clear colloidal sol. This sol can than be used to coat a substrate and results in a highly porous film of narrow pore size distribution.

The colloidal route has first been used by O'Regan [31] for the fabrication of nanoporous TiO_2 films for dye sensitized solar cells. In this case a titanium alkoxide is hydrolyzed with excess water and the resulting precipitate peptized by addition of acid:

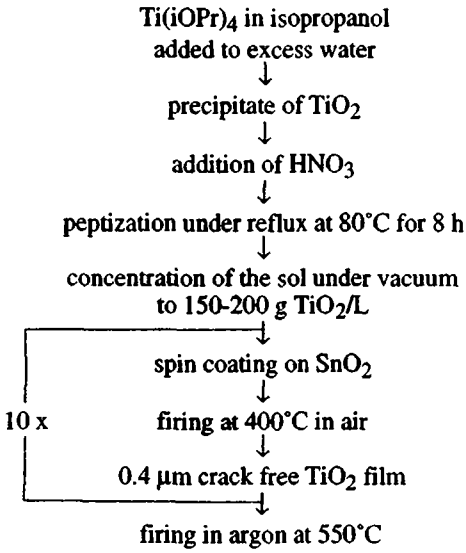

The thickness for crack free layers was limited to 0.5 µm, which required again multiple application and firing to build up a sufficient thick film. The last firing step in argon is actually not necessary, as already mentioned for the fractal electrodes. The main advantages of this colloid method are the better control of the hydrolysis process resulting in a reproducible particle and thus pore size distribution, as well as the transparency of the electrodes, making them ideal for optical, e.g. laser studies.

Independent of O'Regan we found that a literature method [32] for anti-reflective optical coatings is applicable to the dye sensitized solar cell. In this case titanium isopropoxide is hydrolyzed with excess water at 60°C and the precipitate peptized after addition of a strong base, like tetramethylammonium hydroxide, by refluxing at 100°C for 6h. The transmission electron micrograph indicates rectangular particles of 10-20 nm length and 5 nm width, while X-ray analysis shows them to be anatase.[32] The sol can be concentrated to more than 500 g TiO_2/L under vacuum without gelling and redisperses to a colloidal solution even after complete drying. We applied the colloid by dip coating [33] or spin coating [34] to SnO_2 coated glass and fired the film at 550°C in air. Again cracking occurred for layers thicker than 0.5 µm, and multiple application and firing was required for thicker films.

2.3.4. Crack free thick films in a single coating step

As discussed before (chapter 2.3.2) cracking arises from the capillary forces of the liquid evaporating from the pores. Many efforts have been undertaken to produce crack free monoliths from gels in the sol-gel process.[28,ch.8] Biologists were confronted with the problem of drying of histological samples long time ago and they found that the original structure can be preserved by slow exchange of the tissue water by a solvent of lower surface tension like ethanol. With the invention of electron microscopy freeze drying became fashionable, because it completely avoids capillary forces by sublimation of the solvent. This method was then also employed for the drying of gels in the sol-gel process, producing so called cryogels. Another method to bypass the surface tension is to work above the critical point of the solvent, were no liquid-gas phase boundary exists. Large gels can be dried in this manner without cracking and the product is called an aerogel.[35-38]

Freeze drying as well as critical point drying require rather extreme temperatures and pressures. We therefore preferred the classical solvent exchange method to obtain thicker crack free TiO_2 films. We had some success by adding ethylene glycol to the TiO_2 colloid, since it evaporates after the water and has a lower surface tension than this. But the crack free film thickness was still limited to 1 µm. The addition of water soluble polymers in order to hold the particles together during drying and thus prevent cracking led to the flocculation of the colloid. Finally we examined the effect of surfactants, which decrease the surface tension and thus reduce the drying stress. It turned out that the addition of nonionic surfactants of the Triton series did not destabilize the colloid and allowed crack free layers of up to 4 µm in thickness. The Triton surfactants contain a hydrophilic polyethylene glycol chain coupled to a hydrophobic alkylphenol group. Triton X-100 for example has an average of 9.5 ethylene glycol units and an octylphenol group:

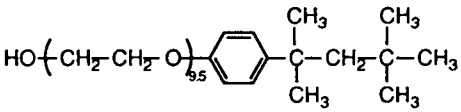

It is well established that the polyethylene glycol part binds strongly to the hydroxylated surface of metal oxide particles. Thus Triton X-100 forms a closely packed monolayer on TiO_2 particles.[39] The optimum concentration in a 500 g/L TiO_2 sol is 200 g/L Triton X-100 and hence more than enough to cover the colloid particles with a monolayer. The amount of surfactant is in fact

sufficient to fill out the pores in the TiO_2 film after evaporation of the water. Since Triton hardly evaporates but rather burns out at about 300°C in air, the pore filling liquid may be removed without the concomitant surface tension effects, similar to the method of supercritical drying, but without need for an autoclave. We found that the same effect can be obtained by addition of Carbowax 20M, which is a moderately long chain polyethylene glycol with a short hydrophobic middle segment. It is now routinely used at a concentration of about 40% by weight of the TiO_2 also for colloids peptized with nitric acid to make thick and crack free films in a single application.[31b]

2.3.5. Doping of the TiO_2 to increase its conductivity

The colloid route results in rather pure, stoichiometric TiO_2 since neither doping impurities are introduced intentionally nor reducing firing conditions are employed to create oxygen vacancies. The free carrier density and thus the dark conductivity of the film are therefore expected to be very low. In fact, we were unable to measure the sheet resistance between two silver paste electrodes in darkness under vacuum at room temperature ($R > 10^{12}\ \Omega/\square$ at $\Delta V = 200$ V). The conductivity measured in air was found to arise from the adsorption of water vapor in the pores of the film. The specific conductivity is given by

$\sigma = n \cdot \mu \cdot e$ with n = electron concentration, μ = electron mobility

and the resistance is

$R = l / A \cdot \sigma$ with l = distance of contacts, A = cross section of conductor

which for two electrodes at opposite edges of a square reduces to

$R = 1 / d \cdot \sigma$ with d = thickness of the film

Hence the free electron density can be calculated from

$n = \sigma / \mu \cdot e = 1 / R \cdot d \cdot \mu \cdot e$

With $R > 10^{12}\ \Omega\square$, $d = 5\ \mu m$ and $\mu = 0.2\ cm^2V^{-1}s^{-1}$ for TiO_2 [40] we get $n < 6 \cdot 10^{10}\ cm^{-3}$. This value is unrealistically low even for an intrinsic semiconductor and indicates that either most electrons are trapped in surface states of the high surface area TiO_2 film, or their mobility is reduced due to the grain boundaries between the colloidal TiO_2 particles. Both effects are usually observed in conductivity studies on polycrystalline films.[41-42] Nevertheless, it

was thought that doping of the TiO_2 colloid might improve the current/voltage characteristics of the dye sensitized solar cell and we shall briefly summarize our relevant experiments:

The doping method most often used for single crystal TiO_2 electrodes in photoelectrochemical studies is heat treatment in reducing atmosphere to create oxygen vacancies.[43-45] The treatment of colloidal TiO_2 electrodes on conducting glass in hydrogen at 500°C resulted in the reduction of the SnO_2 substrate and loss of its transparency. The electrochemical hydrogen loading by cathodic polarization of the electrode in acid [46-48] led to only temporary blue coloration of the TiO_2 film, but not to stable doping. We therefore investigated the possibility of substitutional doping by introduction of impurities already during the colloid preparation.

The addition of HF or NH_4F during the hydrolysis of titanium isopropoxide in order to substitute fluorine for oxygen in TiO_2[49-51] gave a precipitate which could not be peptized any longer. It is known that fluoride replaces the surface hydroxyl groups on the TiO_2 particles [52] which are protonized or deprotonized by the peptizing acid or base and thus are necessary for electrostatic stabilization of the colloid. Fluorine doping of the finished colloid layer may be possible, but would again create a fluorinated TiO_2 surface that could no longer adsorb the dye.

We further carried out experiments on antimony doping of the colloid,[53] but encountered difficulties due to the slower hydrolysis of the $SbCl_3$ used as compared to titanium isopropoxide, apparently resulting in TiO_2 particles coated with a layer of Sb_2O_3. Other precursors of antimony or niobium [54-56] with appropriate hydrolysis rates have to be used to achieve homogenous doping of TiO_2.

However, it has in fact turned out that an increase of the free electron concentration in the dark is not necessary and may even be detrimental for the photoelectrochemical behavior of the dye sensitized semiconductor. We now know that the TiO_2 becomes "photodoped" by electron injection from the adsorbed dye. For example one electron injected into a colloid particle of 10 nm diameter results in a carrier density of $2 \cdot 10^{18} cm^{-3}$, which is by far sufficient for good conductivity. Electron trapping in surface states and grain boundaries seem to be much more important factors in determining the ohmic resistance of the colloidal film (see chapter 3.5.6). In particular the electrical contact between the TiO_2 particles resulting from sintering at a maximum temperature of 550°C, as limited by the glass substrate, seemed insufficient to us and let us search for methods to improve it.

2.3.6. Improvement of the electrical contact between the colloid particles

In the original fractal TiO_2 electrodes the necks between the primary particles of the film are reinforced by the repeated application of the titanium precursor. In colloidal electrodes interparticle contacts are only formed by sintering during firing in air. Due to the high melting point of TiO_2 (1840°C) very limited sintering occurs at 550°C even for the small colloidal particles employed here.[57-59] This is also indicated by the rather poor resistance of the layer against mechanical abrasion. Since the photocurrent in a several micrometer thick film has to pass through hundreds of interparticle contacts, which are "bottlenecks" of may be 1 nm diameter, we hoped to improve the electrode performance by enlarging these necks.

Simple application of a hydrolizable titanium compound, such as $Ti(iOPr)_4$ or $TiO(acac)_2$ to the colloid film in order to deposit additional TiO_2 gave no improvement. We therefore investigated possibilities to accelerate the sintering process at moderate high temperatures by fluxing agents, which slightly dissolve TiO_2. Sintering is like Ostwald ripening driven by differences in surface energy between areas of different curvature.[28(ch.11),60] Material is transported from convex areas of higher surface energy and thus higher solubility to the concave neck regions between particles:

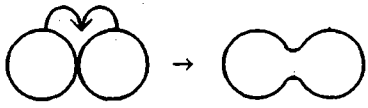

In gaseous atmosphere the transport occurs by surface diffusion, which is very slow at temperatures far below the melting point. Sintering as well as Ostwald ripening can therefore be enhanced by a liquid phase, that dissolves the solid to some extent.[61-64] We first tried the hydrothermal method by heating colloidal electrodes in an autoclave together with water at 140-180°C. Electrodes which had been in contact with the liquid phase did not adsorb the dye $(RuL_2(H_2O)_2$ or $RuL_2[\mu\text{-}(CN)Ru(CN)L'_2]_2$ (L = 2,2'-bipyridine-4,4'-dicarboxylic acid, L' = 2,2'-bipyridine) in water, pH 4) any longer, indicating excessive densification of the film or blocking of the pores by reprecipitated TiO_2. Electrodes treated in the water vapor phase showed undiminished dye adsorption, but yielded only 1/10 of the initial photocurrent. We found that the original efficiency can be restored by short firing in air at 550°C. This led us to the conclusion that the hydroxylation or hydration state of the TiO_2 surface is crucial for dye sensitization (see 2.4.4). However, an improvement due to the hydrothermal treatment was not observed.

The autoclave risks to introduce impurities, especially iron, into the TiO_2 film. We therefore studied high boiling compounds as sintering aids under atmospheric pressure, in particular such that form titanium complexes and slightly dissolve TiO_2. For example polyhydroxy compounds combine high boiling point with the property to complex titanium. We wetted the porous TiO_2 film with ethylene glycol (b.p. 198°C), glycerol (b.p. 290°C), sorbitol (m.p. 110°C) or triethanolamine (b.p. 335°C) and placed it on a hot plate of 100-150°C. In spite of their high boiling point these solvents evaporated within minutes without having improved the abrasion resistance of the film. Only sulfuric acid (b.p. 338°C), which is known to dissolve TiO_2 under formation of $TiOSO_4$, although evaporating rather quickly as well, somewhat enhanced sintering, but unfortunately attacked the SnO_2 substrate.

Molten NaOH (m.p. 318°C) and KOH (m.p. 360°C) evaporate much slower and dissolve TiO_2 to titanates, but also attack the SnO_2 conducting glass during firing at 550°C in argon (to prevent carbonate formation with atmospheric CO_2). Molten B_2O_3 (m.p. 450°C) seems to be more promising, also because it can easily be removed in the presence of water vapor by sublimation as HBO_2. It may be worth-while to reinvestigate its application as sintering aid with the present, more advanced TiO_2 electrodes, since the grain boundaries between the colloid particles may well contribute to the series resistance of the solar cell. We shall come back to the use of B_2O_3 in chapter 2.3.11.

2.3.7. Increase of the colloid particle size

Transmission electron microscopy of the TiO_2 colloid prepared according to Thomas[32] (cf. chapter 2.3.3) shows primary particles with the following size distribution:

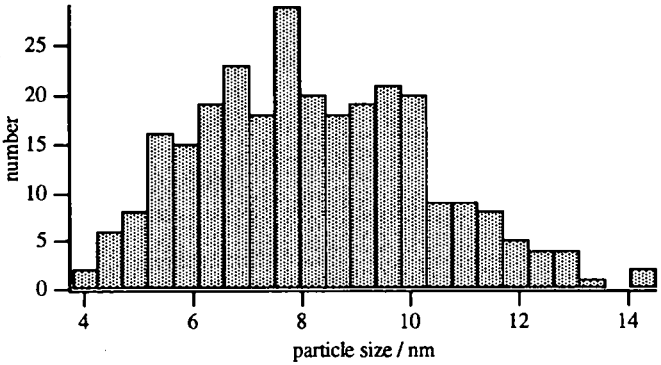

Quasi elastic light scattering,[65] measuring the stokes radius of the particles, indicates a bimodal particle size distribution, due to much stronger scattering caused by the presence of even less than one percent of larger aggregates. Taking into the account the dependence of the scattering intensity on the sixth power of the particle diameter, we got a primary particle size in the order of 15 nm, the exact size distribution depending on the mathematical model used for data analysis.

The electrodes made from colloids of such small particle size often showed a sublinear increase of photocurrent with light intensity and photocurrent transients at high light intensity, due to diffusion limitation of the triiodide transport in the nanometer sized pores of the TiO_2 film. We therefore attempted to make TiO_2 sols of larger primary particle size to increase the pore size of the electrode.

It has been reported that the particle size of TiO_2 powders prepared by hydrolysis of titanium alkoxides depends on the hydrolysis rate of the alkoxide.[57,66,67] In our experiments the replacement of titanium isopropoxide by the slower hydrolyzing titanium ethoxide or butoxide, as well as cooling during the hydrolysis process to slow down the reaction gave precipitates, which were difficult to peptize with tetramethylammonium hydroxide. The hydrolysis of titanium isopropoxide occurs almost instantaneously, resulting in homogenous nucleation and growth of separate TiO_2 particles, which then aggregate to form an easily peptizable precipitate. With more slowly hydrolyzing precursors the particle growth continues after aggregation, which provokes strengthening of the interparticle contacts and leads to a precipitate, that is difficult to peptize. Still, the primary particle size measured by quasi elastic light scattering was significantly larger with titanium ethoxide or butoxide, and it may be worth-while to repeat these experiments with nitric acid as peptizing agent.

Another method to make larger particles is Ostwald ripening of the sol by hydrothermal treatment in an autoclave.[60(p.239),62-64] In this case the smallest particles are preferentially dissolved, due to their higher surface energy, while the larger particles grow. We did some hydrothermal treatments of the tetramethylammonium hydroxide stabilized sol, which was sealed into glass ampoules, to avoid contact with the steel autoclave. It was found that rather high temperatures (at least 200°C) are required to obtain particle growth. The method has been investigated in more detail by B. O'Regan in our laboratory. He used a corrosion resistant titanium autoclave for the nitric acid stabilized sol and succeeded in making colloidal TiO_2 electrode with better high photocurrent performance due to enlarged particle and pore sizes.[31b]

2.3.8. *In situ* formation of the colloid in a polymer matrix

In the original method of making "fractal" TiO_2 electrodes (chapter 2.3.2) a film of colloidal particles is formed by hydrolysis of a titanium alkoxy halide *in situ* on the substrate. It has been reported, that the fine structure of the film depends on the hydrolysis rate of the employed titanium precursor.[24] Fast hydrolysis leads to small particles of high surface area, but poor electrical contact between them. Slow hydrolysis results in particle growth and reinforcement of the interparticle contacts, but lower surface area of the electrode. We have tested further titanium precursors and the addition of polymers as binder to prevent cracking of the layer. At the same time the polymer may increase the porosity of the obtained films.[68]

The following table lists some of the investigated systems:

polymer	solvent	titanium precursor
polyethylene glycol	isopropanol, ethanol	$Ti(iOPr)_4$
= PEG (m.p. 66°C)	ethylene glycol = EG	$TiCl_2(EG)$
	H_2O	$TiCl_3$, $TiCl_4$
polyvinyl alcohol	ethylene glycol	$TiCl_2(EG)$
= PVA (m.p. 230°C)	H_2O	$TiOSO_4$
polyvinyl acetate	ethanol	$TiCl_2(OEt)_2$
paraffin (m.p. 46°C)	petrolether	$Ti(iOPr)_4$

The solutions were spreaded on a glass substrate and either fired immediately or after hydrolysis in humid air. In all cases the film cracked or peeled off the glass for thicknesses above ca. 0.5 µm. We attributed this to the high volume fraction of the polymer matrix, resulting in a film containing separated TiO_2 particles. In order to get films consisting of interconnected TiO_2 particles with pores filled by a polymeric binder polymerizable titanium precursors were investigated. For example $TiCl_4$ reacts with polyvinyl alcohol (PVA) to form a polymeric titanium complex,[69,70] which decomposes on heating:

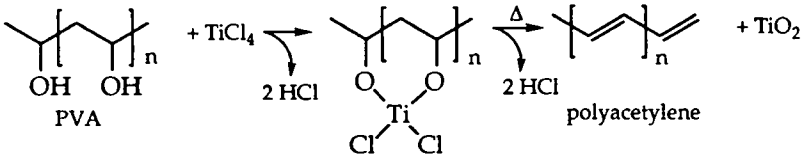

It has been reported that PVA splits off water on heating to form polyacetylene, a semiconducting and light absorbing polymer.[71] One might speculate about a p-n-junction between TiO_2 and polyacetylene, acting as sensitizer and conducting polymer at the same time (cf. chapter 3.1). However, in the practical realization of these ideas we encountered difficulties due to the crosslinking of PVA by $TiCl_4$, resulting in an insoluble, resinous polymer, which was not suitable for making thin films. This could be avoided by a modified reaction scheme:

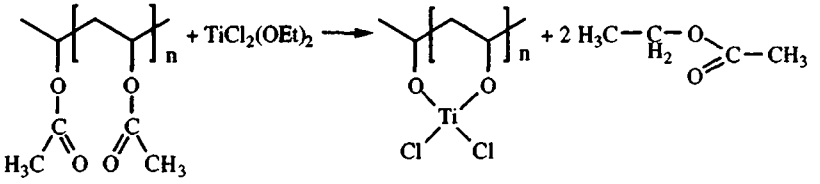

PVAcetat

A solution of polyvinylacetate in ethanol was mixed with $TiCl_2(OEt)_2$ and gave a clear solution, which was spreaded on a glass substrate. Firing in air yielded a rather thick crack free TiO_2 film ($\approx$ 1 µm), but dipping in an ethanolic solution of $RuL_2[\mu\text{-}(CN)Ru(CN)L'_2]_2$ (L = 2,2'-bipyridine-4,4'-dicarboxylic acid, L' = 2,2'-bipyridine) gave hardly any coloration, indicating too small pores. Firing under argon or vacuum produced black films at 300-450°C, possibly due to formation of polyacetylene. However no conductivity or photosensitivity could be detected.

Another approach to get high TiO_2 loading in a polymeric binder matrix for thick crack free films is to start with a monomeric titanium precursor having a polymerizable ligand. For example the ethylene glycol complex of titanium[72,73] should decompose to TiO_2 in a polyethylene glycol matrix:

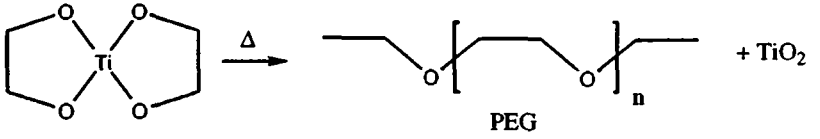

PEG

Similarly a titanium complex with an α-hydroxy carboxylic acid ligand would result in a polyester matrix, and titanium complexes are in fact uses as catalysts in the manufacture of polyesters (ref. 69, p. 225):

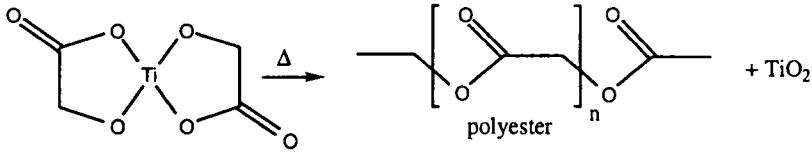

Chelates of polyhydroxy alcohols and α-hydroxy carboxylic acids with titanium and lead or alkali earth metals are also used in the fabrication of titanates by the so called Pechini method, in order to avoid the segregation of the components.[74-76] However, even with ethylene glycol as the smallest possible ligand one ends up with a polymer content of more than 80 % by volume which has to be burned out. Since the resulting pure TiO_2 film should have a porosity of about 50 % excessive shrinkage will occur and give rise to cracks in the film. This is born out by our numerous experiments with ethylene glycol, glycerol, glycolic, lactic, succinic, citric and terephthalic acid chelates of titanium, which gave either powdery layers or cracked films.

There are few titanium compounds which have a density comparable to that of the porous TiO_2 film and thus can be converted into TiO_2 without appreciable shrinkage. One of them is $TiOSO_4$, which decomposes to TiO_2 and SO_3 above 500°C.[23(p.348),69(p.169),77] But now the problem is to make a crack free $TiOSO_4$ film of sufficient thickness: slow evaporation of an aqueous solution led to crystallization while flash evaporation on a hot substrate gave cracked, not adherent films. Nevertheless, thinner layers up to about 1 μm could be prepared from an aqueous solution of $TiOSO_4$ and showed good adsorption of the dye $(RuL_2[\mu\text{-}(CN)Ru(CN)L'_2]_2$ (L = 2,2'-bipyridine-4,4'-dicarboxylic acid, L' = 2,2'-bipyridine) in ethanol). The electrode had an incident photon to current efficiency (IPCE, cf. chapter 3.2) of 20% at 520 nm and an open circuit voltage of 500 mV with 0.5 M LiI, 3 mM I_2 in ethanol as redox electrolyte. We conclude that this method is suitable for the preparation of thin, transparent porous TiO_2 films.

Finally we pursued the idea to make a microemulsion of TiO_2 particles by starting from a long chain titanium alkoxide:

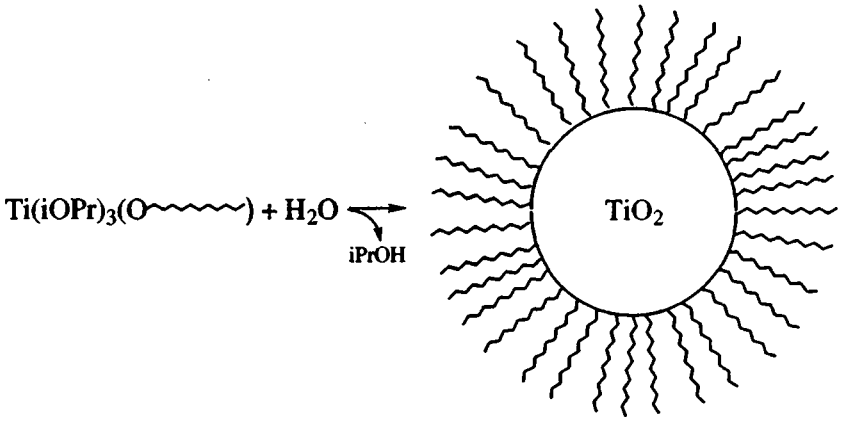

The long chain alkoxid is simply obtained by addition of the required amount of long chain alcohol to titanium isopropoxide.[69(p.176)] Hydrolysis in humid air should lead to a dense microemulsion of TiO_2 particles stabilized by a monolayer of the more slowly hydrolyzing long chain alcohol on the particle surface. For example 1-dodecanol was dissolved in the equivalent amount of $Ti(iOPr)_4$ and spin coated on a glass substrate. Unfortunately hydrolysis in air and firing yielded again crack free films of less than 1 μm only.

We have to conclude that the in situ preparation of TiO_2 always results in a rather weak, low density gel, which cracks on firing due to excessive shrinkage. This may be prevented by film deposition at high temperature, so that the film immediately densifies while it is built up. This approach shall be discussed in the following chapter.

2.3.9. Film deposition by spray-coating

In spray-coating a solution of a precursor of the compound to be deposited is sprayed onto the hot substrate, where it decomposes by hydrolysis or pyrolysis. Due to the simplicity of the process spray-coating has widely been used especially for transparent conducting oxide films. The deposition mechanism depends on the droplet size in the spray and the substrate temperature.[78,79] In the ideal case the droplets evaporate just above the hot substrate and the gaseous precursor decomposes on the surface due to heterogeneous catalysis. The mechanism then corresponds to chemical vapor deposition. For example, fluorine doped SnO_2 as conducting coating on glass is easily made by spraying an alcoholic solution of $SnCl_4$ and NH_4F, containing a certain amount of water, onto the glass heated to about 500°C.[80] Hydrolysis of $SnCl_4$ on the hot surface yields a clear, transparent SnO_2 film rendered conductive by the partial substitution of fluorine for oxygen.

By spraying a solution of $TiCl_4$ in ethanol, isopropanol or toluene on glass at 500°C we obtained nicely transparent and abrasion resistant but nonporous coatings of TiO_2. In general spray coating yields relatively dense, nonporous films, since the gaseous reactant diffuses rapidly into any pores and fills them with its decomposition product. Addition of water to the alcoholic $TiCl_4$ solution gave white, powdery coatings, which were easily wiped off. In this case TiO_2 is already formed in the gas phase by homogenous nucleation. The particles then aggregate and deposit as a very loose, nonadherent layer. Other titanium precursors ($Ti(iOPr)_4$, $Ti(OEt)_4$, $Ti(OBu)_4$, $TiOSO_4$, $(NH_4)_2TiO(oxalate)_2$ [81]) in different solvents (isopropanol, ethanol, toluene, petrolether, water) at substrate temperatures of 300-550°C gave similar results.

We therefore investigated the possibility of creating pores by pyrolysis of a titanium compound in inert gas atmosphere in order to fill the film with soot or a polymer, that is afterwards burnt out to leave a porous TiO_2 coating. Spray coating of titanium alkoxides in alcohol with argon as carrier gas did not result in the codeposition of organic material. Titanium isopropoxide for example is known to decompose to TiO_2 and volatile propene and water:[82]

$$Ti(OC_3H_7) \rightarrow TiO_2 + 4\ C_3H_6 + 2\ H_2O$$

Also benzene or kerosene as solvents or addition of naphthalene gave no pyrolytic carbon. Titanium acetylacetonate in isopropanol was expected to yield polyacene as a conducting polymer in the pores of the TiO_2 film:[83]

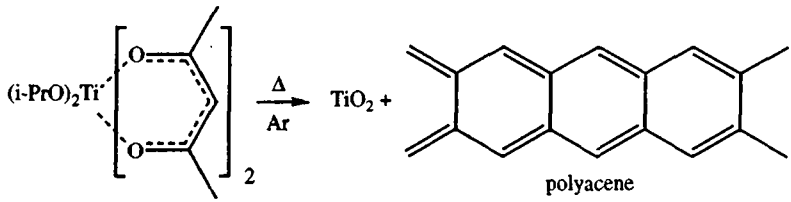

However, it produced rather a nonporous film of pure TiO_2, which turned out to be useful as blocking layer on the SnO_2 substrate (chapter 2.2). Similarly, titanium phenoxide should decompose to the highly heat resistant conducting polymer polyphenylene:

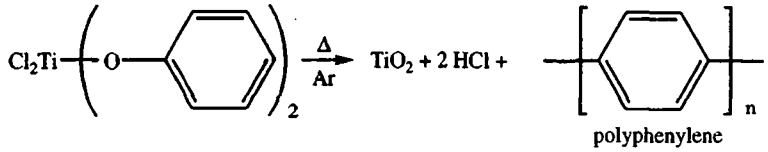

The red reaction products of $TiCl_4$ or $Ti(iOPr)_4$ with phenol or catechol in toluene or acetone gave indeed black films on spraying with argon, but the films were either nonadherent or cracked on firing in air.

2.3.10. Spray-coating of leachable mixed oxide layers

A porous TiO_2 film may be formed with spray coating by codeposition of a second, soluble oxide, which is leached out to leave a skeleton of pure TiO_2. This principle is widely used in the fabrication of "thirsty" glass by the Vycor process.[84,85] In this process borosilicate glass is phase separated by heat treatment into a nearly pure SiO_2 phase and an alkali-borate phase, which can be leached out by acid, resulting in a nanoporous silica glass. Porous films with a gradient refractive index as antireflecting coating have been obtained in a similar way.[86,87] For the fabrication of nanoporous TiO_2 electrodes we have taken into consideration the following systems:

$TiO_2 + Al_2O_3$ We first investigated the codeposition of Al_2O_3 by spray coating with $TiCl_4 + AlCl_3$ in ethanol and $Ti(iOPr)_4 + Al(iOPr)_3$ in isopropanol. After leaching in 1 M HCl and firing at 500°C in air no dye adsorption was observed. The preparation of composite Al_2O_3-TiO_2 particles has been

described before.[88,89] Solid solutions in anatase are formed up to 20 mol% Al_2O_3.[90] This may explain our unsuccessful experiments with this system.

TiO_2 + SiO_2 Glasses and thin films of SiO_2-TiO_2 with a wide range of compositions have repeatedly been described in the literature.[28,91,92] However, phase separation of anatase occurs only at rather high temperature (700°C)[93] and leaching of SiO_2 would require HF, which attacks TiO_2 as well.

TiO_2 + K_2O Leaching of alkali silicate glass leaves a nanoporous silica skeleton, similar to the Vycor process.[94] With TiO_2 the alkali metal alkoxides form titanates of different stoichiometry.[23(p.383,393)] Especially $K_2Ti_4O_9$ has found wide application in highly selective cation exchange columns, due to its layered lattice structure and fibrous morphology.[95,96] The alkali metal can be leached out with acid and the obtained hydrous titania dehydrated by heating to a pure TiO_2 (B) with bronze structure, which transforms to anatase above 550°C.[97] The bronze TiO_2 (B) is a fourth modification of TiO_2, beside rutile, anatase and brookite. It has been proposed as cathodic material in lithium batteries, due to its cation insertion capability. Since $K_2Ti_4O_9$ forms fibers or whiskers of for example 0.1 µm diameter and 10 µm length, which can be leached and dehydrated to anatase fibers [CA 96: 23720, 104: 191718 / 191738] it may be interesting to make dye sensitized electrodes from this material. A perpendicular alignment of these fibers on the substrate would result in large surface area combined with high electrical conductivity, due to the absence of grain boundaries. The preparation of $K_2Ti_4O_9$ from metal alkoxides has been reported [CA 110: 164906].

In our experiments on spray coating we employed solutions of KOH and $Ti(iOPr)_4$ in methanol, which are expected to react according the following scheme:[98]

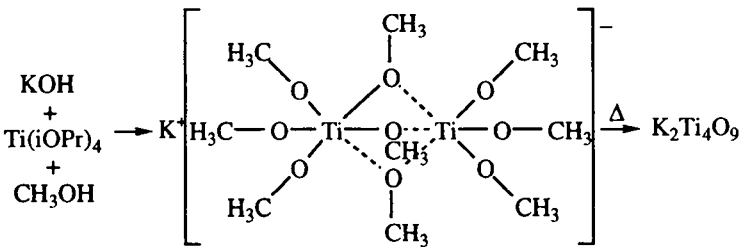

Spraying at a substrate temperature above 200°C gave non adherent films or no deposit at all, probably due to gas phase decomposition of the complex. Deposition at 100-200°C, followed by firing at 550°C, leaching with 1 M HCl and again firing gave adherent white films of about 5 μm thickness, which adsorbed well the dye ($RuL_2[\mu\text{-}(CN)Ru(CN)L'_2]_2$ (L = 2,2'-bipyridine-4,4'-dicarboxylic acid, L' = 2,2'-bipyridine) in ethanol). Similar coatings were obtained from KOH and $Ti(OEt)_4$ in ethanol. However, the photocurrent efficiency (cf. chapter 3.2) of these electrodes was IPCE < 10%. The comparably high photovoltage indicates that residual potassium, rendering the TiO_2 surface basic, may be responsible for the low injection yield.

$TiO_2 + B_2O_3$ In the Vycor process boron oxide constitutes the leachable phase, as mentioned in the introduction. Titanium dioxide can be dissolved in alkali borosilicate glasses to more than 20 wt% at the melting temperature of 1400°C. However, it crystallizes in the form of fine anatase and, to less extent, rutile particles on firing at 800°C, rendering the glass opace and highly reflecting. This is the basis for TiO_2 opacified porcelain enamels, which are widely used as protective coatings for example on steel.[99] Nanoporous TiO_2-SiO_2 glass-ceramics of high titania content and very high surface area (100 to 300 m^2/g) have been produced by acid leaching of phase separated borosilicate glasses containing dissolved TiO_2.[100] Also the formation of $SrTiO_3$ and $BaTiO_3$ by phase separation from B_2O_3 has been reported.[101,102] Interestingly, the addition of some boron in the vapor-phase production of TiO_2 from $TiCl_4$ promotes the formation of the anatase form [CA 68 (1986) 23214], which is preferred for dye-sensitized solar cell applications, since it has a wider band gap than rutil and is not so easily excited by UV light under generation of highly oxidizing valence band holes..

Since B_2O_3 is liquid above 450°C and dissolves TiO_2 to some extent it is expected to improve sintering between the TiO_2 particles (see chapter 2.3.6). Besides leaching with acid B_2O_3 can also be removed in the presence of water vapor by sublimation as metaboric acid:[103]

$$B_2O_3 + H_2O \rightarrow 2\,HBO_2$$

In order to codeposit TiO_2 and B_2O_3 by spray coating we first tried a mixture of $B(OPr)_3$ and $Ti(iOPr)_4$, but observed only very slow film deposition at a substrate temperature of 500°C with air as carrier gas. Pure boron alkoxides gave no film at all, which may be ascribed to their high thermal stability.[104] They become much more reactive by exchange of one or two of the alkoxy

ligands with chlorine,[105] which is easily achieved by reaction with $TiCl_4$ [CA 99 (1983) 186343, 71 (1969) 71885]:

$$B(OR)_3 + TiCl_4 \rightarrow BCl(OR)_2 + TiCl_3(OR) \text{ and } BCl_2(OR) + TiCl_2(OR)_2$$

Formally these may react further to the pure oxides:

$$4\ B(OR)_3 + 3\ TiCl_4 \rightarrow 3\ TiO_2 + 2\ B_2O_3 + 12\ RCl$$

By spray coating of equimolar solutions of $TiCl_4$ and H_3BO_3 or boron alkoxides ($B(OMe)_3$, $B(OEt)_3$, $B(OPr)_3$, $B(OBu)_3$) in methanol, ethanol, isopropanol, butanol, methoxyethanol, acetyl acetone, petrolether or toluene we obtained clear transparent films of more than 1 μm thickness. They became turbid on exposure to humid air, indicating the hydration of B_2O_3 to H_3BO_3. The B_2O_3 content of these films can be determined by infrared spectroscopy, due to the B-O stretching vibration at 1265 cm^{-1} and the boroxol ring stretching shoulder at 1400 cm^{-1},[106,107] while TiO_2 absorbs at 850 cm^{-1}.[108]

The FTIR spectra of the mixed TiO_2 / B_2O_3 films were obtained in reflexion on SnO_2 conducting glass substrate, which is highly reflective in the infrared. As an example, we report the spectrum of a film sprayed with 1 mL of 0.5 M $B(OBu)_3$ + 0.5 M $TiCl_4$ in isopropanol on a 2.5 x 3 cm^2 SnO_2 substrate at 520°C before and after heat treatment (Figure 14).

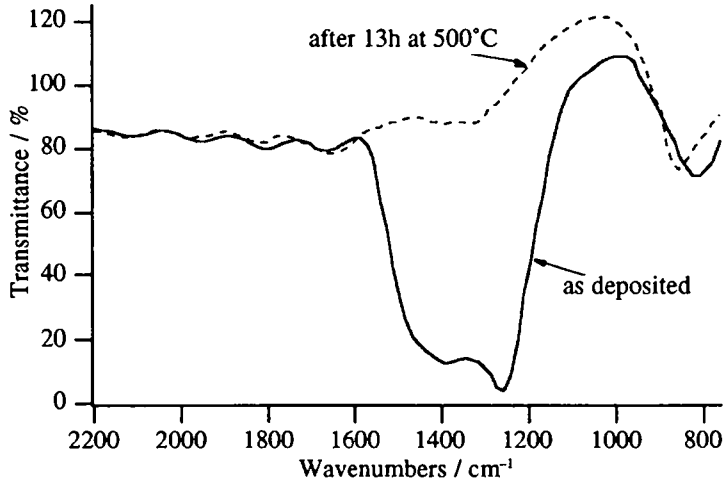

Figure 14: FTIR spectra of a spray deposited TiO_2 / B_2O_3 film before and after firing

The removal of B_2O_3 during heat treatment by sublimation as HBO_2 is clearly visible, while the TiO_2 band is undiminished. Unfortunately, the electrode did not adsorb any dye ($RuL_2[\mu\text{-}(CN)Ru(CN)L'_2]_2$ (L = 2,2'-bipyridine-4,4'-dicarboxylic acid, L' = 2,2'-bipyridine) in ethanol), indicating that the pores created by codeposition of B_2O_3 were still too small. Attempts to enhance the porosity by increasing the boron alkoxide concentration in the spraying solution resulted in drastically reduced film deposition rates. In addition, the $B(OR)_3$ / $TiCl_4$ mixtures changed their properties with time, due to continuing ligand exchange and polymerization reactions, rendering the experiments difficult to reproduce. In order to have a better control over the reaction conditions we therefore turned to chemical vapor deposition, which differs from spray coating by the use of gaseous reactants.

2.3.11. Chemical vapor deposition of mixed TiO_2 / B_2O_3 films

Chemical vapor deposition (CVD) is a widely employed method for the fabrication of thin films.[109] CVD is also the method of choice for SnO_2 transparent conducting coatings, as they are used in amorphous silicon cells and also in our dye sensitized photoelectrochemical cell (chapter 2.1.3). The deposition of multiple coatings in a single CVD apparatus is technical standard [11] and it would be highly advantageous to add the TiO_2 film right after SnO_2 deposition in the same production step.

The literature on the CVD of TiO_2 is extensive.[110-126] The following reactions were mostly employed:

Hydrolysis of titanium alkoxide: $Ti(OR)_4 + 2\,H_2O \xrightarrow{50\text{-}600^\circ C} TiO_2 + 4\,ROH$

Pyrolysis of titanium alkoxide: $Ti(OR)_4 \xrightarrow{200\text{-}750^\circ C} TiO_2 + 4\,R' + 2\,H_2O$

Hydrolysis of $TiCl_4$: $TiCl_4 + 2\,H_2O \xrightarrow{100\text{-}900^\circ C} TiO_2 + 4\,HCl$

Oxygenolysis of $TiCl_4$: $TiCl_4 + O_2 \xrightarrow{400\text{-}1050^\circ C} TiO_2 + 2\,Cl_2$

The reported deposition rates range from 1 nm/min up to 6 µm/min and film thicknesses up to 300 µm were obtained. Both the anatase and rutile modification of TiO_2 can be deposited, depending mainly on the substrate temperature. The most important application of CVD TiO_2 films are antireflecting coatings on silicon solar cells.

Although these films have a certain degree of porosity, as can be inferred from their refractive index, the void fraction is usually less than 20%,[127] while about 50% of interconnected pores are required for dye penetration and adsorption. This explains why none of the TiO_2 coatings we obtained according to the literature methods showed a significant dye uptake, even with a small dye like quinalizarin.

We investigated the possibility of creating pores by codeposition of NH_4Cl by the following reaction:

$$TiCl_4 + 4\,NH_3 + 2\,H_2O \rightarrow TiO_2 + 4\,NH_4Cl$$

Air dried over a column of molecular sieves and saturated with $TiCl_4$ in a gas wash bottle flowed through an inner glass tube onto the glass substrate, while air saturated with 1 M NH_3 solution flowed through a concentric outer tube. At a substrate temperature of 500°C we obtained opace white and yellow films of more than 1 µm thickness, however, only very poor dye adsorption was observed. Since NH_4Cl decomposes at 320°C into NH_3 and HCl it is obviously not suited as pore filler at 500°C. At lower substrate temperature (250°C) clear transparent films were produced. However, they cracked on firing at higher temperature to remove the NH_4Cl, indicating that a mechanically stable TiO_2 matrix was not formed at this low deposition temperature.

In continuation of our experiments on spray-coating (chapter 2.3.10.) we applied the CVD technique to make mixed TiO_2 / B_2O_3 films. The deposition of SiO_2 / B_2O_3 films by CVD is used in the semiconductor industry,[128] but employs highly toxic silane (SiH_4) and diborane (B_2H_6) gases. More recently these were replaced by the alkoxides $Si(OEt)_4$ and $B(OMe)_3$ [129] or the unique precursor $B[OSi(CH_3)_3]_3$ [CA 109 (1988) 241901]. A volatile compound containing both titanium and boron is $Ti(BH_4)_3$, but it decomposes already at room temperature.[130]

Following our positive experiences with $TiCl_4$ and boron alkoxides in spray coating we also started CVD with these rather stable and safe compounds. Argon carrier gas streams were bubbled through $TiCl_4$ ($p_{20°C}$ = 1.3 kPa) and $B(OEt)_4$ ($p_{20°C}$ = 2.0 kPa) or $B(OPr)_4$ and flowed through a glass tube or a slot nozzle (0.5 mm x 10 cm) onto the heated substrate (SnO_2 conducting glass). Upon mixing of the gas streams we observed fogging even at room temperature, indicating homogenous reaction of $TiCl_4$ with $B(OR)_3$, which interfered with the heterogeneous deposition on the substrate. This could be prevented by a nozzle having three parallel slots, build from titanium sheets by P. Liska in our

lab, which separated an interior $TiCl_4$ stream from two exterior $B(OR)_3$ streams. The deposition rate was determined from the weight increase of the substrate for different gas flow rates ($TiCl_4$: 0.5...1 L/min, $B(OR)_3$: 1...2 L/min). Although some film deposition occurred, the B_2O_3 content was very low, as judged from the weight loss on heat treatment to remove B_2O_3 as HBO_2. Accordingly the dye adsorption by these films was very poor. We conclude that the reaction

$$3\ TiCl_4 + 4\ B(OR)_3 \rightarrow 3\ TiO_2 + 2\ B_2O_3 + 12\ RCl$$

is not complete under the present reaction conditions, probably due to its complicated multistep mechanism.

Replacement of $B(OR)_3$ by the more reactive BBr_3, which, contrary to BCl_3, is still liquid at room temperature, necessitates a third gas stream carrying water vapor for hydrolysis:

$$TiCl_4 + BBr_3 + 7/2\ H_2O \rightarrow TiO_2 + 1/2\ B_2O_3 + 4\ HCl + 3\ HBr$$
($p_{20°C}$ = 1.3 7.2 2.4 kPa)

With equimolar amounts of $TiCl_4$ and BBr_3 the reaction would yield 80 g / 3.8 g/cm^3 = 21 cm^3 TiO_2 and 35 g / 1.8 g/cm^3 = 19.4 cm^3 B_2O_3. Thus, after removal of the B_2O_3 a TiO_2 film of about 50% porosity is expected. Chemical vapor deposition was carried out according to Figure 15.

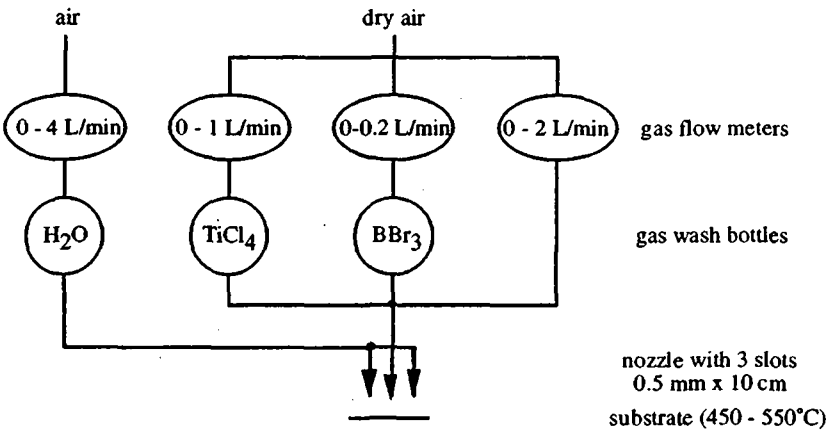

Figure 15: Gas flow diagram for the CVD of mixed TiO_2 / B_2O_3 films.

While rapid film deposition occurred with $TiCl_4$ alone, addition of BBr_3 resulted in much slower growth rates. Only with a small proportion of BBr_3 (e.g. 0.5 L/min $TiCl_4$ + 0.02 L/min BBr_3 + 4 L/ min H_2O + 1 L/min air) we obtained rapidly growing films which adsorbed quinalizarin from ethanol. After a series of experiments we found that $TiBr_4$, a solid formed by reaction of $TiCl_4$ with BBr_3, had deposited in the nozzle. In order to avoid this complication BCl_3 was produced by bubbling an air stream saturated with BBr_3 at 0...–17°C through $TiCl_4$ at 20 °C. The $TiBr_4$ formed precipitates, while the $TiCl_4$ enriches in BCl_3 until the steady state is attained, where the BCl_3 stream carried away by the carrier gas equals that of the BBr_3 influx. The partial pressure of BCl_3 in the $TiCl_4$ saturated gas is then given by the vapor pressure of BBr_3 at the temperature chosen. For example, the carrier gas will contain equal concentrations of $TiCl_4$ and BCl_3 at a BBr_3 temperature of –11°C ($p^{-11°C}_{BBr_3} = p^{20°C}_{TiCl_4}$ = 1.3 kPa). The experiments with this gas mixture gave very promising results, however, a change of the BCl_3 / $TiCl_4$ ratio required adjustment of the BBr_3 temperature with subsequent establishment of the steady state in the $TiCl_4$ bubbler and was therefore rather time consuming. Since the BCl_3 / $TiCl_4$ ratio was found to be very critical for deposition rate and porosity of the films we finally turned to BCl_3 itself as boron source.

The gas mixture $TiCl_4$ + BCl_3 + H_2 is widely used in the CVD of TiB_2,[131] but requires temperatures in excess of 1000°C, in contrast to the hydrolysis to TiO_2 + B_2O_3, which we are interested in. In order to measure the flow of the highly humidity sensitive and corrosive BCl_3 gas ($p^{20°C}_{BBr_3}$ = 133 kPa) at a rate of a few mL/min a thermal mass flowmeter was build (Figure 16).[132,133]

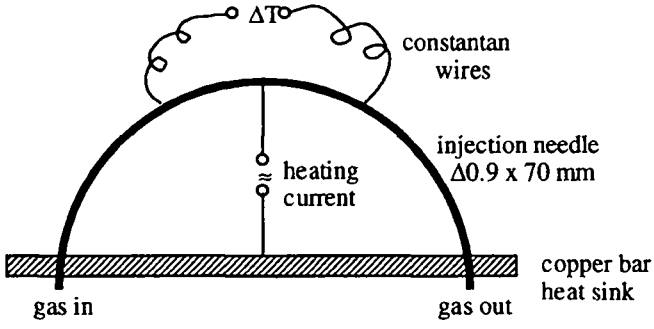

Figure 16: Thermal mass flowmeter to measure the flow of BCl_3 gas

The BCl_3 gas flows through a stainless steel injection needle, which is electrically heated by an alternating current. The gas flow creates a temperature gradient along the needle, which is measured as thermovoltage between two constantan wires, forming thermoelements with the stainless steel needle. The DC thermovoltage of several μV is amplified by a chopper stabilized operational amplifier, while the AC voltage due to the heating current is mostly nullified by a symmetrical attachment of the wires and completely suppressed by an RC filter.

The thermal mass flowmeter was calibrated with air and a soap film gas flowmeter, consisting of a 10 mL burette containing soap solution at the outlet through which the air was bubbled. The thermovoltage output of the mass flowmeter was linear from 0 to 20 mL air per minute. Since the output depends on the heat transported by the gas, a flow of 1 mL air / min corresponds to

$$\frac{\rho(BCl_3)}{\rho(air)} \cdot \frac{c_p(air)}{c_p(BCl_3)} = 3.96 \cdot \frac{0.24\ kcal/kg \cdot K}{0.127\ kcal/kg \cdot K} = 0.477\ mL\ BCl_3 / min.$$

The gas wash bottles with $TiCl_4$ and H_2O as well as the ampoule containing liquid BCl_3 were placed in a thermostated waterbath (20°C) in order to keep the vapor pressure constant.

We also build a new injector nozzle with five slots of 0.5 mm x 10 cm,[11,134] in order to separate the central $TiCl_4$ + BCl_3 stream from the outer H_2O vapor stream by a dry air stream, and thus prevent the deposition of hydrolysis products on the slots. The injector was completed by two peripheral "vacuum cleaners" which remove the gaseous reaction products (mainly HCl). The nozzle was made from glass sheets of 0.5 mm thickness, glued together with silicon rubber. For all other components coming into contact with $TiCl_4$ or BCl_3 glass or Teflon were used. The SnO_2 conducting glass substrate was continuously transported below the nozzle by two turning rollers, pressing it against a glass ceramic plate (Ceran from Schott), which was heated by stainless steel tapes connected to a high current power supply (Figure 17).

For optimization of the deposition parameters stationary glass substrates of 2.5 x 1 cm^2 were positioned transversely below the nozzle and coated for one minute. The homogeneity of the film was judged visually, while the deposition efficiency was obtained from the weight increase of the substrate. The flow rate of dry air for the $TiCl_4$ bubbler was usually kept at 0.5 L/min, corresponding to 4.9 μmol $TiCl_4$/s. The BCl_3 gas was mixed with the $TiCl_4$ loaded air stream before entering the nozzle. It contributed only a few mL/min to the total flow rate and thus could be varied without modifying the flow pattern below the slots. A water saturated air stream of 4 L/min, or 2 L/min through each of the

outer slots, provided excess H_2O (70 µmol/s) for hydrolysis. A separating dry air stream of 0.5 L/min prevented deposition on the nozzle, but allowed mixing of the reactant gases at a distance of about 3 mm below the slots, as indicated by the formation of fog. The optimum distance of the nozzle from the substrate was 5 mm under these conditions. A larger distance decreased the deposition efficiency, due to loss of reactants by homogeneous reaction. At shorter distance the deposit consisted of two parallel stripes with an uncoated area between them, since the reactants did not mix in the center.

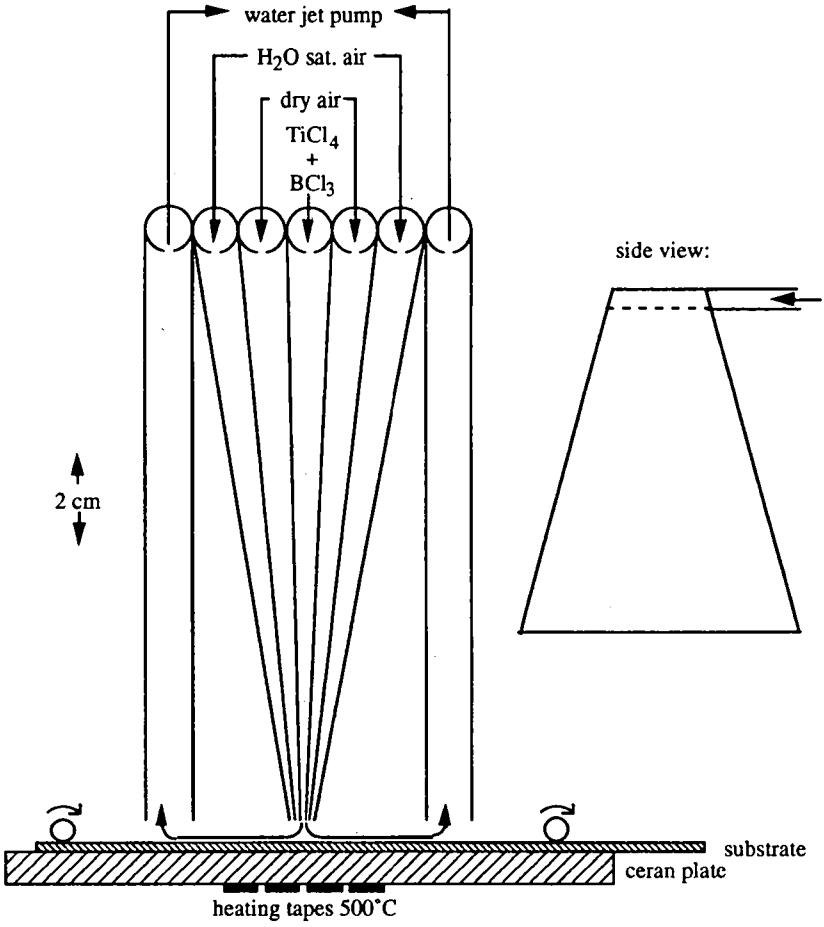

Figure 17: Multislot nozzle and substrate heating/transport mechanism for the CVD of mixed TiO_2 / B_2O_3 films.

The dye uptake by the film was tested after additional firing at 550°C in a flow of humid air, to remove B_2O_3 as HBO_2. It was found to be crucial not to expose the freshly deposited film to water vapor at room temperature, since it swells by formation of H_3BO_3 and then shrinks on firing, which leads to cracking and peeling of the film or even the SnO_2 coating of the substrate. However, the freshly made film can also be dipped directly into the ethanolic dye solution without firing, since the B_2O_3 is leached out by ethanol as $B(OEt)_3$. As expected the dye uptake (tested with different Ru-complexes) improved with increasing BCl_3 flow rate. However, the deposition rate decreased above an optimal BCl_3 flow rate, which depends on the substrate temperature (under the conditions given above: 4 µmol/s at 430°C and 3 µmol/s at 500°C). Supposedly, the glassy B_2O_3 phase inhibits the nucleation of TiO_2, so that the heterogeneously catalyzed deposition ceases, as soon as the B_2O_3 phase spreads over the entire surface. With flow rates of 4.9 µmol $TiCl_4$/s and 4 µmol BCl_3/s the resulting film should contain 40 vol% B_2O_3 ($\rho(TiO_2)$ = 3.8 g/cm^3, $\rho(B_2O_3)$ = 1.8 g/cm^3), assuming equal reactivity of $TiCl_4$ and BCl_3. In fact, the films loose about 30% of their weight on removal of B_2O_3 by firing in humid air, corresponding to a volume fraction of 48 vol%, which provides a reasonable porosity for dye sensitized electrodes.

The deposition rate for the cited gas flow rates and a substrate temperature of 430°C was 14 mg/min, while the complete conversion of the reactants would have yield 44 mg TiO_2 + B_2O_3. The deposition efficiency of 32% is rather poor in comparison with industrial CVD processes, but can certainly be improved with a different nozzle design and a larger heating zone, in order to keep the gases near the substrate and give them more time to react.

For large electrodes we transported the SnO_2 coated substrate at a speed of 1 cm/min below the nozzle and obtained relatively uniform, transparent films of 7...8 µm thickness. The transmission electron micrograph of material which was scratched from the film shows TiO_2 particles with a diameter of 10...20 nm, similar to films prepared from colloidal TiO_2 (Figure 18). Also the dye adsorption is comparable to colloidal TiO_2 electrodes and photocurrent efficiencies up to IPCE = 80% were obtained with $RuL_2(NCS)_2$ (L = 2,2'-bipyridine-4,4'-dicarboxylic acid).

Although the CVD process gives electrodes which are competitive with those made by the sol-gel process we did not investigate it further in view of its rather high complexity on the laboratory scale. However, the feasibility of atmospheric pressure chemical vapor deposition of porous TiO_2 films has been shown and it would be very economical to combine this step with the SnO_2 deposition, which is done in the same way, but with $SnCl_4$ + dopant instead of $TiCl_4$ + BCl_3.[11]

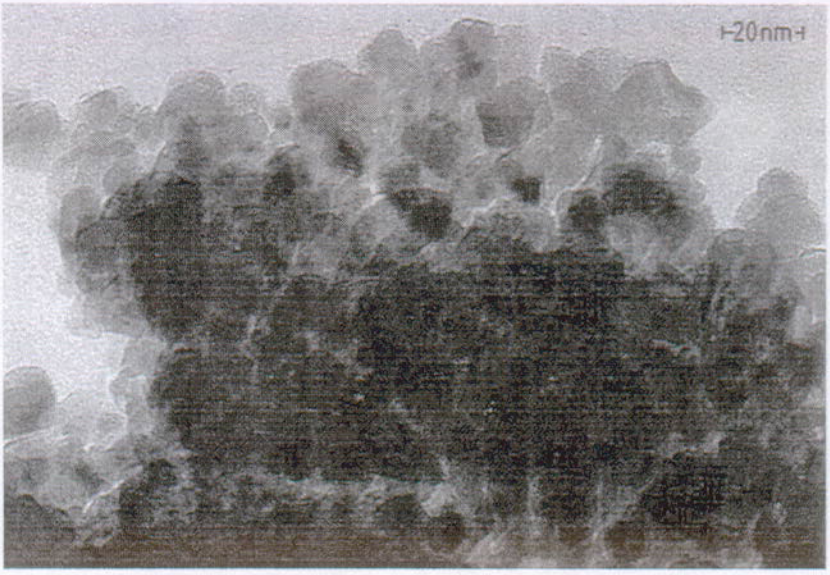

Figure 18: Transmission electron micrograph of a porous TiO_2 CVD layer

2.3.12. Porous TiO_2 films from aerosols

Industrially TiO_2 and other oxide powders of small, controlled particle size are produced on a large scale by flame hydrolysis in the aerosol process.[28(p.284),135-138] For the production of TiO_2 gaseous $TiCl_4$ is oxidized in a flame (usually $H_2 + O_2$):

$$TiCl_4 + O_2 \rightarrow TiO_2 + 2\,Cl_2$$

The size of the resulting particles can be controlled in a wide range by variation of reactant concentration, flame temperature and residence time in the hot zone. Instead of coating the substrate with an aqueous sol of TiO_2 particles it would be interesting to deposit them directly from such an aerosol. In fact, glass fibers for optical communications are made by deposition of a silica aerosol from a flame, yielding a glass of extreme purity.[139-141] In this case $SiCl_4$ and some dopant like BCl_3 or $GeCl_4$ to adjust the refractive index are oxidized in a hydrogen / oxygen torch, which is directed onto the rotating substrate. A porous preform consisting of submicron sized SiO_2 particles is deposited, which is sintered at higher temperature and than drawn out to a fiber.

Following this rather simple recipe we saturated part of the oxygen supply for a propane gas burner with $TiCl_4$, resulting in a bright flame due to the formation of a TiO_2 aerosol. The particles were readily deposited on a glass substrate held into the flame, since the thermophoretic force acting on the particles in a temperature gradient drives them towards the colder surface.[142] The white, opace layers adsorbed a lot of dye, however, they showed very poor adherence and were easily wiped off with the finger. Since the particles aggregate already in the flame [136,143] and further in the boundary layer above the substrate, the obtained deposits are rather loosely packed.[144] This results in few interparticle contacts and, especially in the absence of significant sintering of TiO_2 at temperatures up to 550°C, as limited by the glass substrate, in low mechanical stability of the film.

Scratch resistant, transparent coatings were obtained at very low $TiCl_4$ concentration in the flame, however, they adsorbed no dye. In this case no particles are formed by homogenous nucleation in the flame, but the reaction is heterogeneously catalyzed by the substrate and hence corresponds to CVD, yielding a nonporous film. An intermediate regime would be required to form some particles by homogenous nucleation in the gas phase, which are deposited on the substrate and then consolidated by heterogeneous reaction of the residual reactant (Figure 19).

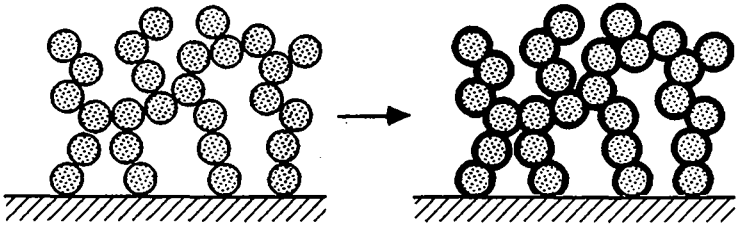

Figure 19: Porous film formation by precipitation aided chemical vapor deposition (PP-CVD)

This method has only recently been described in the literature and is called particle precipitation aided chemical vapor deposition (PP-CVD).[145] The preparation of porous TiO_2 films (thickness 50-100 µm, surface area 20-50 m^2/g) by such a process has in fact been reported.[146a] Helium gas loaded with $Ti(iOPr)_4$ was fed into a reactor containing a central tube, heated to 350°C, which was surrounded by a concentric outer tube held at 190-270°C. While nonporous TiO_2 films deposited at the inlet of the reactor, porous layers were formed further downstream on the outer tube by thermophoretic deposition of

homogeneously nucleated TiO_2 particles. Due to the low reaction temperature these films were amorphous according to X-ray analysis. They are expected to shrink on firing at higher temperature, which is required for crystallization to anatase, and would then crack and peel off the substrate. The anatase phase has therefore to be formed already in the gas phase by increasing the reaction temperature.

In order to prepare porous anatase films by PP-CVD we used the experimental set-up shown in Figure 20. The argon carrier gas transports the $Ti(iOPr)_4$ ($p^{100°C}$ = 2.8 kPa) through the flat channel between micro slide and heating plate. A transparent and well adherent, but nonporous TiO_2 film formed on both surfaces in front of the heating zone by normal CVD. A powdery, non adherent layer formed on the micro slide above the heating zone at T > 400°C by thermophoretic deposition of homogeneously nucleated TiO_2 particles. At these high temperatures the gas phase reaction is complete and leaves no reactant for consolidation of the particle layer. Only at 390°C an adherent film of aerosol particles was deposited in a small area above the heating zone. However, the experiment was difficult to reproduce, since the TiO_2 deposited in the colder parts of the heating plate catalyzed the $Ti(iOPr)_4$ decomposition [146b] and rapidly changed the behavior of the system. This problem could perhaps be overcome by laser heating of the reaction gas,[147,148] which, however, was beyond our technical possibilities.

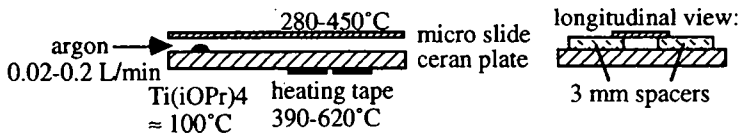

Figure 20: A simple set-up for the preparation of porous anatase films by PP-CVD

In order to have better control over the reaction parameters, we turned to tubular flow reactors (Figure 21), as they are used for the production of ultrafine TiO_2 particles.[146,149] Due to the high reactivity of $Ti(iOPr)_4$ its only partial conversion to TiO_2 is not possible at reaction temperatures above 400°C, as required for the formation of anatase particles. We therefore employed the oxygenolysis of $TiCl_4$, which is complete above 750°C only and leads to anatase powders with submicron particle size.[150,151]

An oxygen stream saturated with $TiCl_4$ at 20°C flowed through an electrically heated quartz tube onto the likewise heated substrate. Only at very high reactor temperature (1000°C) an aerosol was formed and thermophoretically deposited on the substrate. For a $TiCl_4$ / O_2 flow below 0.3 L/min the deposit was powdery and non adherent, but became scratch resistant at higher flow rates. Under these conditions the reactant is only partially consumed due to the shorter residence time in the reactor and remains available for consolidation of the deposited particles by CVD. Unfortunately, these films were limited to a circular zone below the quartz tube, and a more sophisticated reactor design would be needed for homogeneous coatings of large area. Also, the opacity of these films indicated the presence of large, open aggregates, as expected from the stochastic coagulation and deposition mechanism.[144] For electrode applications more closely packed particles with many electrical contacts between them are preferred.

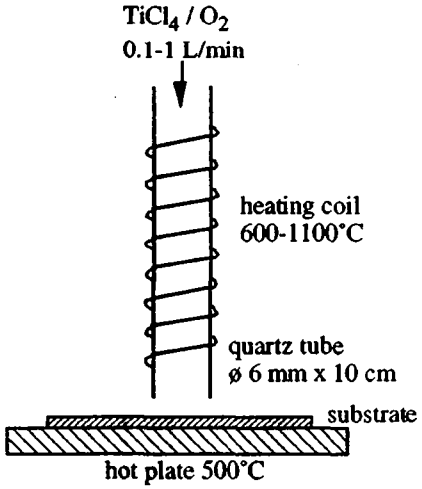

Figure 21: Tubular flow reactor for the PP-CVD of anatase by oxygenolysis of $TiCl_4$

Coagulation may be prevented by electrical charging of the aerosol particles,[152,153] in analogy to the electrostatic stabilization of aqueous colloids by excess surface charges. The aerosol is homopolar charged in a corona discharge, which at the same time may accelerate the chemical reaction (oxygenolysis of $TiCl_4$), by creating highly reactive radicals at low temperature,[154] as in plasma enhanced chemical vapor deposition (PECVD). In

addition, the electrically charged particles are attracted by the counter electrode and may be deposited with high efficiency.[155] This principle is employed in electrostatic dust precipitators but also in corona spraying of SnO_2 transparent conducting coatings.[156,157]

We investigated this technique for the deposition of TiO_2 films by injecting a $TiCl_4$ saturated O_2 stream through a needle connected to a high voltage power supply onto the grounded substrate (Figure 22). In the absence of an electric field a cloud formed by reaction of $TiCl_4$ with humidity in the air but no deposition occurred on the substrate at room temperature. Connecting the injection needle to a high positive voltage (several kV) resulted in a silent discharge and disappearance of the fog, while a transparent, semisolid film deposited rapidly on the substrate even at room temperature. The film cracked on firing due to shrinkage (cf. chapter 2.3.2.). On heated substrates (500°C) only powdery, non adherent films were formed.

Systematic investigations with more refined apparatus would be required to find suitable conditions for the deposition of porous TiO_2 films from aerosols. However, in view of the high complexity in comparison to other coating technologies we did not pursue this approach any further. Nevertheless, TiO_2 made by the aerosol process proved to be an interesting alternative source for the preparation of aqueous colloids, as described in the following chapter.

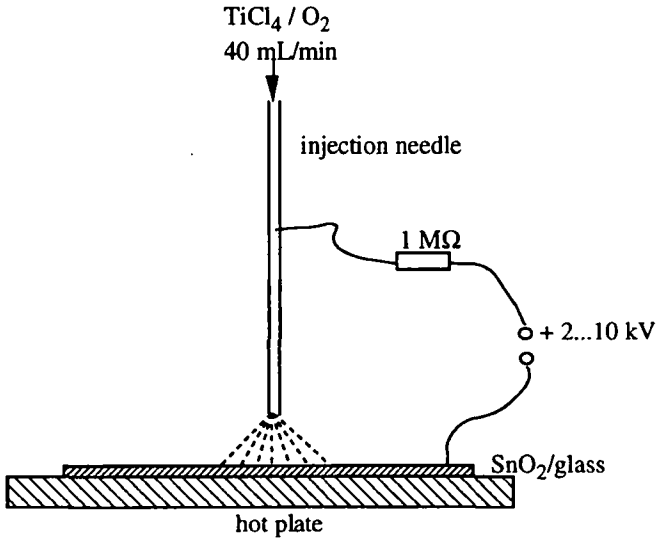

Figure 22: Deposition of an electrostatically charged aerosol of TiO_2 particles

2.3.13. Colloidal TiO_2 electrodes from aerosol powder dispersions

Titanium dioxide powders with a primary particle size between 5 and 20 nm and BET surface areas from 50 to 300 m^2/g are produced in large quantity by solution precipitation from $TiOSO_4$ and $TiCl_4$, mainly for the manufacture of white pigments.[158,159] The freshly precipitated TiO_2 can be peptized after removal of the excess sulfuric or hydrochloric acid to a highly concentrated sol (up to 640 g TiO_2 / L).[160] However, on drying the precipitate densifies to a rather compact powder with numerous interparticle contacts. This explains why we did not succeed in re dispersing such TiO_2 powders to the colloidal state. They rather formed white opace suspensions which sediment rapidly. TiO_2 powder made by the aerosol process (chapter 2.3.12) is much less aggregated and exhibits few interparticle contacts, rendering it much more suitable for the preparation of colloidal dispersions. We employed P 25 of Degauss, which is made by flame hydrolysis of $TiCl_4$, has a BET surface area of 55 m^2/g and consists mainly of anatase particles (> 70 %).[161] This powder exhibits only 2% of the density of bulk TiO_2, due to its low degree of aggregation.

We had repeatedly attempted to peptize P 25 by refluxing with acid or base (as in chapter 2.3.3.) or by ultrasonication. However, the obtained dispersions were always white opace and sediment rapidly, indicating the presence of large aggregates. Films prepared from such dispersion were only moderately adherent and showed photocurrent efficiencies in the order of 40 %. Since these films were deeply colored by the sensitizer the poor efficiency must be due to insufficient electrical contact between the loosely packed aggregates.

In yet another screening of peptizing agents we found that a colloidal dispersion of P 25 can be achieved by grinding the powder with a very small amount of solvent in a mortar, followed by stepwise dilution under continued grinding. For example 12 g of P 25, which corresponds to a volume of 150 mL, due to the very low powder density, are ground with 4 mL water and 0.4 mL acetyl acetone in a porcelain mortar. Within 5 minutes the voluminous powder is reduced to 8 mL of a paste containing 45 vol% TiO_2, resulting in a very high viscosity. This is diluted stepwise with four times 4 mL water by grinding. The thus obtained, rather fluid dispersion of 500g TiO_2/L does not settle during months. Only after centrifugation a much more compact sediment is formed, indicating the absence of bulky aggregates, while a poorly dispersed powder forms a very voluminous sediment under the same conditions.

Films made from this colloid are bluish white if seen from above and translucent with a red tint if held against the light, due to Rayleigh scattering by particles much smaller than the wavelength of the light. The surface of the dried films is shiny, in accordance with a flatness on the submicron scale. According to quasi elastic light scattering the hydrodynamic diameter of the particles in the dispersion lies between 40 and 80 nm, with a few particles up to 200 nm.

The break-up of larger aggregates occurs during the first grinding step due to the extreme shear forces in the highly viscous paste. The importance of this mechanism is well known in the paint industry, were pigment powders (mainly TiO_2) have to be dispersed in a solvent.[162,163] In the manufacture of paint continuously working three-roll mills are widely used (Figure 23). The powder, premixed with a small amount of solvent, is introduced into the feed bank and forced under tremendously high shear through the narrow space between the rotating rolls. Part of it turns back to the feed bank, while the rest is transported by the center roll to the second, still narrower gap, where it undergoes even more intense shearing action. A part is again returned to the feed bank, while the rest is taken off by a knife from the apron roll.

A small three-roll mill with porcelain rolls has also proven effective in the preparation of colloidal TiO_2 from P 25 powder. Again, a very high solid content in the first milling step is crucial in order to obtain a high viscosity and hence strong shearing action for the brake-up of aggregates. Ball mills, which are also widely use in paint industry, did not yield a satisfactory dispersion of P 25 powder. In this case dispersion occurs mainly by impact of the balls, which is most effective at low viscosity, but does not break up aggregates which are already less than 1 μm in size.

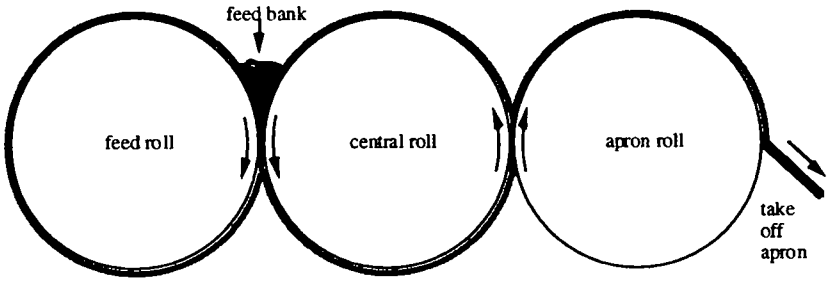

Figure 23: Three-roll mill for the dispersion of powders in liquids

The addition of acetyl acetone facilitates and improves the dispersion process considerably by its adsorption to the TiO_2 surface:

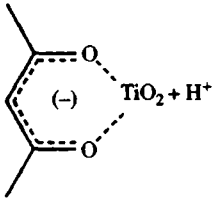

The chelation of a surface Ti^{4+} atom by acetyl acetone is accompanied by loss of a proton. Hence, the TiO_2 particles acquire a negative surface charge, although the solution becomes acidic, which usually results in positive TiO_2 particles due to protonation of surface hydroxy groups (charge inversion). Other titanium chelating agents like α-hydroxy carboxylic acids (e.g. glycolic, lactic, citric, tartratic acid), which also inverse the charge of the sol,[164] or triethanolamine and even H_2O_2 are effective as well. Peptization is also achieved by addition of mineral acids (HCl, HNO_3) or bases (NaOH, NH_3, $(CH_3)_4NOH$) due to simple electrostatic stabilization of the colloid. Another class of useful additives are polymers with a high affinity to the TiO_2 surface, such as polyvinyl alcohol, polyacrylate, polyethylene glycol, polyphosphate or polyethylene imine, resulting in steric or electrostatic stabilization of the sol. The additive is usually burned out after film formation and should leave no residues, which limits its choice and excludes compounds like NaOH and polyphosphate, but also the very slowly decomposing polyethylene imine.

The great versatility of the colloid preparation from aerosol powder allows even the use of organic solvents instead of water, such as alcohols and polyalcohols (ethylene glycol, glycerol), ethers (methoxyethanol), carboxylic acids (lactic acid) and amines (triethanolamine) which, due to their titanium chelating capability, can often be employed without further additives. Other, less polar solvents, like terpinol, require the adsorption of an amphiphile (e.g. salicylic acid, catechol, fatty acids and other surfactants) onto the TiO_2 surface, to improve its wettability.

The addition of a binder or pore filler in order to prevent cracking of the film (chapter 2.3.4.) is not necessary with P 25. The low shrinkage during firing due to the relatively large particle size and their high crystallinity resulting from the high fabrication temperature allows the preparation of crack free films of 20 µm thickness in a single application. Nevertheless, the kind and amount of stabilizing agent in the colloid influences the rearrangement of the particles

when the film dries and consequently their packing before firing.[165] For nanometer sized particles the electric double layer or the surface adsorbed molecules contribute significantly to the effective diameter. While this surface layer prevents the aggregation of the particles in the sol it also leads to their mutual repulsion in the film. During the first drying stage this repulsion has a lubricating effect and allows rearrangement of the particles into a more densely packed configuration. However, on continued drying a phase transition from the liquid sol to a solid gel takes place, preventing further restructuring. Only during firing the film shrinks again by removal of the surface adsorbed molecules and partial sintering of the TiO_2 particles. The packing density in the gel state, which also determines the density of the sintered film, depends on the extent of repulsion between the particles. A well stabilized sol with highly repulsive particles will result in a low packing density and cracking of the film during firing due to excessive shrinkage. On the other hand, a poorly stabilized sol will still contain aggregates which cannot be closely packed, or the weakly repulsive particles form ramified structures of low density in the early states of drying. Either extreme must be avoided to achieve dense packing as required for crack free films with many interparticle contacts for electrical conductivity.

Another important factor is the mechanical adhesion and electrical contact of the porous TiO_2 film on the conducting substrate. Besides pretreatment of the substrate (chapter 2.2) these can be improved by addition of a surfactant to the colloid to help wetting of the surface. Nonionic detergents like Triton X-100 are generally suited, since they do not destabilize the sol, but may in fact contribute to its steric stabilization by adsorption with the hydrophilic polyethylene glycol chain.[166-168] However, anionic surfactants like fatty acid salts (soaps) or cationic surfactants like alkyl trimethyl ammonium salts can be suitable as well. The surfactant not only decreases the surface tension of the colloid and thus facilitates wetting and uniform spreading on the substrate, but it may also act as a lubricant between the particles during drying and improve their packing.[165] We usually add 1% Triton X-100 to the acetyl acetone stabilized sol containing 500 g TiO_2/L.

The application of the colloid onto the substrate can be carried out in many different ways. Films of well defined thickness are easily made with a doctor blade, a wire-wound rod or a rod sliding over the scotch tape covered edges of the substrate, providing at the same time noncoated areas for electrical contact. For an applicator of circular cross section the resulting thickness of the wet film is 2/3 of the spacer thickness.[162(p.583)] In order to obtain very thin films after drying a colloid of low TiO_2 content can be used, however, a certain viscosity

has to be maintained by addition of a polymer to prevent contraction of the film due to the surface tension. Other application methods like spin coating and dip coating are suited as well. For large scale film fabrication screen printing and spraying are more economical and have proven to give efficient electrodes.[169,170] The versatility of the colloid preparation from aerosol powder is of great advantage here, since it permits the free choice of solvent and additives, in order to adjust the rheological, leveling, drying and other properties of the colloid. The use of organic solvents with low electric conductivity like methoxyethanol also renders electrodeposition possible, which is interesting for very thin films or nonplanar substrates.

While P 25 was found satisfactory for the preparation of dye sensitized nanoporous TiO_2 electrodes, it has the disadvantage of containing some rutil (up to 30%), exhibiting a smaller band gap than anatase (3.0 compared to 3.2 eV), and resulting in a light adsorption edge at 415 nm instead of 390 nm. Since band gap excitation of TiO_2 creates highly oxidizing holes in the valence band, which may destroy the adsorbed dye or the redox electrolyte, UV filters are required to guarantee stability of the solar cell. Also, P 25 has a rather broad particle size distribution and contains an appreciable portion of large particles (> 30 nm), which contribute much to the volume, but not to the surface area of the film.

The TiO_2 preparation by the aerosol process, whether in a flame or a tubular flow reactor (chapter 2.3.12.) permits easy control of the powder properties, such as particle size distribution, crystal structure and extent of aggregation. However, due to the limited availability only a few other TiO_2 powders have been tested up today. A P 25 analog of increased surface area (75 instead of 55 m^2/g) turned out to be much more difficult to disperse and gave opace films that cracked on firing, indicating the presence of large aggregates. Accordingly these films showed a lower photocurrent efficiency.

A TiO_2 powder of 55 m^2/g (80% anatase, 20% rutile) prepared by oxygenolysis of $TiCl_4$ in a radio frequency plasma (Ultram, Moscow) dispersed much more readily than P 25 and gave a liquid dispersion containing 1 g TiO_2/L, which corresponds to about 30% TiO_2 by volume. This indicates a very low degree of aggregation of the primary particles. Films made from this dispersion are more transparent than the strongly light scattering P 25 films. Scanning electron microscopy shows them to be more densely packed, a consequence of the lower degree of aggregation. The dye sensitized films exhibited similar photocurrent / voltage characteristics as P 25 electrodes, but the white light efficiency was somewhat lower, probably due to the weaker light scattering in the film, which enhances light absorption especially in the red spectral region. A

higher degree of aggregation and thus more light scattering may of course be obtained by a less perfect dispersion of the powder, which presents an advantage for large scale applications. The main concern is again the rutile content of this powder, which can presumably be reduced by addition of anatase stabilizing dopants, such as boron [CA 68 (1986) 23214].

A nanophase TiO_2 powder prepared by inert gas condensation of ultrafine titanium particles and in situ oxidation (Nanophase technology corporation, USA) [171,172] was found difficult to disperse, as expected from the agglomeration of the particles during the oxidation process.[171] In addition, this powder contains 95 % rutile and is thus of less interest for dye sensitized solar cells.

Powders prepared by precipitation from $TiCl_4$ or $TiOSO_4$ could in general not be dispersed to the colloidal state by grinding. This is due to their strong aggregation, as reflected in the high density of these powders. Other aerosol oxides prepared by flame hydrolysis, such as SiO_2, Al_2O_3 and ZrO_2,[161] disperse very easily and usually yield even clear transparent films, which have proven useful reference adsorbents in luminescence and laser flash photolysis studies (chapter 3.5).

2.3.14. Porous TiO_2 formed by anodization of titanium

Metallic titanium owes its chemical resistivity to a passivating oxide layer which forms spontaneously on its surface. As for aluminum the thickness of the oxide film can be enhanced by anodic oxidation. Aluminum has the peculiarity of forming a columnar oxide film on anodization, with hexagonally arranged pores of about 0.1 μm diameter extending through the whole thickness of the film (e.g. 20 μm).[173] These pores are very useful for the adsorption of inorganic and organic pigments and dyes which impart a decorating color to the surface.

On titanium the anodic oxide film is usually pore free and only under certain conditions thick layers of several μm can be obtained.[174,175] However, the formation of a porous TiO_2 film can be provoked by very high anodization voltages, giving rise to sparking due to electrical breakdown of the oxide layer.[176-179] We prepared such films by anodization of titanium sheets (2 x 2 cm^2) in saturated Na_2SO_4 solution for 30 minutes at up to 75 V.[176] The scanning electron micrograph shows in fact a highly porous surface with pores of about 0.2 μm in diameter (Figure 24).

Unfortunately, the dye uptake by these electrodes was very poor. This is not unexpected, since pores with a diameter of 200 nm are nearly two orders of magnitude larger than in the colloidal films, resulting in an even larger difference in surface area. The same problem of an insufficient roughness factor may arise with porous TiO_2 films made by the replication of porous anodic alumina.[180] However, these films have not been tested yet, and it may well be that their TiO_2 columns of 0.1 μm diameter and 3 μm length have a rough surface in their own, since they are formed by a sol-gel process. With respect to the current flow in the semiconductor on one side and the electrolyte on the other side, such a columnar arrangement may offer distinct advantages over a particulate layer with hundreds of narrow interparticle necks and tortuous pores.

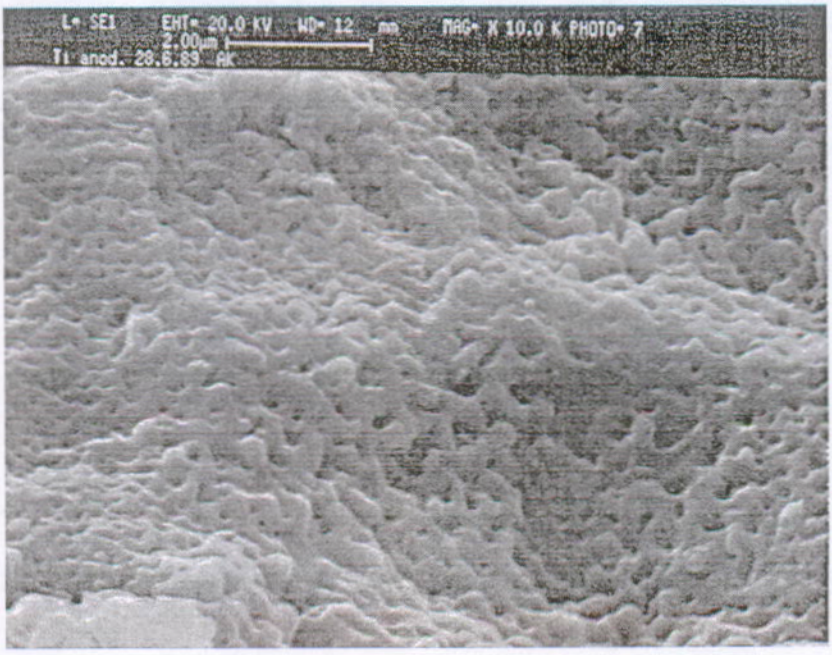

Figure 24: Scanning electron micrograph of a TiO_2 film prepared by spark anodization of titanium

2.4. After-treatments

2.4.1. Introduction

Following deposition of the colloidal TiO_2 film the electrode is usually fired to burn out any additives, such as polyethylene glycol, acetyl acetone and Triton X-100, as well as to sinter the particles to provide better mechanical and electrical contact between them. It has been found that the photoelectrical properties of the electrode can often be improved by an additional after-treatment of the porous TiO_2 layer before adsorption of the dye. For example further TiO_2 can be deposited on the film with intent to reinforce the interparticle necks, enhance the purity of the surface layer or increase the active surface area. We shall describe several methods to deposit such an overlayer, namely CVD, hydrolysis of $TiCl_4$ and electrodeposition from $TiCl_3$.

The efficiency of the electrode is in most cases improved by firing just before dye adsorption. We have varied the firing conditions, in particular temperature and oven atmosphere, and came to the conclusion that adsorbed water and surface hydroxyl groups influence strongly the electron injection efficiency of many dyes.

All these after-treatments modify the surface of the TiO_2 electrode on an atomic level. Since this is where dye adsorption and electron injection take place the strong influence of surface modification is not unexpected. After having presented the experimental results we shall discuss several possible mechanisms responsible for the observed effects.

2.4.2. Chemical vapor deposition of a TiO_2 overlayer

It has already been mentioned (chapter 2.3.6.) that we attempted to improve the interparticle contacts in the colloidal film by deposition of additional TiO_2 from hydrolyzable compounds like $Ti(iOPr)_4$ or $TiO(acac)_2$. Deposition is expected to occur preferentially in the concave neck regions due to their lower surface energy. No positive effects were observed at that time, but later we investigated again the possibility of reinforcing the necks, this time by chemical vapor deposition. The colloidal TiO_2 film was placed in a quartz tube of

quadratic cross section (2 x 2 cm^2) and heated from below to 550°C. After an oxygen flow of 1 L/min during 10 minutes the oxygen was bubbled for 10 to 30 seconds through $TiCl_4$ at 20°C, followed by again 10 minutes in pure oxygen. Since the temperature of 550°C is rather low for oxygenolysis of $TiCl_4$ the deposition of TiO_2 on clean glass or SnO_2 surfaces is negligible within the short reaction time.[112] By contrast, on the high surface area TiO_2 film a significant amount of TiO_2 is deposited, as indicated by the weight increase Δm of the electrode (Table 1).

Table 1: Effect of CVD treatment on the weight (Δm), absorbance at 520 nm (A_{520nm}) and the photoelectrical properties of TiO_2 electrodes (9 μm P 25, ≈ 2 mg TiO_2/cm^2), sensitized with $RuL_2[\mu\text{-}(CN)Ru(CN)L'_2]_2$ (L = 2,2'-bipyridine-4,4'-dicarboxylic acid, L' = 2,2'-bipyridine, in ethanol), electrolyte: 84% ethylene carbonate, 16% propylene carbonate, 0.5 M KI, 10 mM I_2

elec-trode	CVD-treatment	Δm mg	A 520nm	IPCE %	U_{oc} mV
A	none, 30 min firing at 550°C	–	0.90	58	520
B	10 s 1 L/min $TiCl_4/O_2$ at 550°C	0.25	1.12	65	520
C	20 s " "	0.39	1.41	72	520
D	30 s " "	0.58	1.55	74	520
E	10 s " at 20°C	0.04	0.42	48	420
F	" " " 10 min O_2 at 520°C	0.09	1.06	63	520
G	20 s " at 450°C	0.05	0.88	63	520
H	60 s " "	0.15	1.34	67	520
I	10 x (59 s 1 L/min O_2 + 1 s $TiCl_4$ at 550°C)	0.33	1.21	66	530
K	10 s 1 L/min $TiCl_4$/He at 550°C	0.18	0.98	69	540

Quite unexpectedly the CVD treated electrodes adsorbed more dye than the non treated reference, as indicated by the increase in absorbance at 520 nm (measured with an Ulbricht integrating sphere) from 0.90 to 1.55 (electrodes A to D). The monochromatic photocurrent efficiency in the absorption maximum at 520 nm increased from IPCE = 58% to 74%, while the open circuit voltage remained U_{oc} = 520 mV. This improvement cannot be due to the higher dye coverage alone, since the non treated electrode absorbs already 87% of the light at 520 nm and even more, if the reflective counter electrode is taken into account. The higher coverage is more important in spectral regions where the extinction coefficient of the dye is smaller. In fact the white light efficiency is even more enhanced by CVD treatment than the monochromatic efficiency in the absorption maximum.

Treatment with $TiCl_4/O_2$ at room temperature without subsequent firing decreases dye uptake, photocurrent and voltage (electrode E). With subsequent firing the electrode (F) is significantly more efficient than the untreated reference, although the amount of deposited TiO_2 is small (0.09 mg). At 450°C (electrodes G and H) the deposition takes longer than at 550°C, yet has the same positive effect. Intermittent treatment in oxygen (59 seconds) and $TiCl_4$ saturated O_2 (1 second) for 10 cycles gives similar results (electrode I).

Surprisingly, helium instead of oxygen as carrier gas for $TiCl_4$ improves the efficiency as well (electrode K). The electrode was cooled down in a stream of helium and transferred to the dye solution without further firing. Although the dye adsorption is not much increased, both photocurrent and voltage are higher than for the reference. Due to the absence of oxygen the $TiCl_4$ can only have reacted with the oxygen and hydroxyl groups on the TiO_2 surface in this case. The weight gain of the electrode (0.18 mg) was determined after dye adsorption, since it was immediately transferred under a helium stream to the dye solution. From the optical density of the electrode ($A_{520} = 0.98$), the extinction coefficient of the dye ($\varepsilon_{520} = 1.8 \times 10^4\ M^{-1}cm^{-1}$) and its molecular mass (1700 g/mol) a dye loading of 0.09 mg/cm^2 is calculated. This leaves about 0.09 mg for the amount of TiO_2 deposited. In comparison, a monolayer of TiO_2 (10^{19} titanium atoms/m^2) on a 1 cm^2 electrode of roughness factor 1000 has a mass of 0.12 mg. We conclude that, as expected, less than a monolayer of TiO_2 has been deposited.

The CVD treatment with $TiCl_4/O_2$ was found to be also effective with colloidal electrodes made from precipitated and peptized TiO_2 (chapter 2.3.3.) and with a monomeric ruthenium complex as sensitizer ($RuLL'(H_2O)$, L = 2,2'-bipyridine-4,4'-dicarboxylic acid, L' = N,N'-dimethyl-2,6-benzimidazolpyridine, in ethanol). Possible mechanisms responsible for this effect shall be discussed in chapter 2.4.5.

2.4.3. Solution-deposition of a TiO_2 overlayer

Considering the positive influence of CVD treatment on the electrode efficiency we investigated other possibilities for the deposition of a TiO_2 overlayer. The most simple method is application of the desired quantity of a pyrolizable titanium compound to the colloidal TiO_2 film. To prevent uncontrolled hydrolysis by water adsorbed in the film or by atmospheric humidity the electrodes were first fired at 550°C and cooled down in a stream of dry air. Application of 5 μL/cm^2 of a 1 M alcoholic solution of the Ti-precursor

under dry air gave a more or less homogenous impregnation of the porous TiO_2 film with the Ti-precursor, equivalent to 0.4 mg TiO_2. Pyrolysis was carried out at 530°C in a stream of dry air. All treated electrodes were significantly more colored and showed higher photocurrent efficiencies and voltages. (Table 2).

Table 2: Deposition of a TiO_2 overlayer by pyrolysis of titanium complexes (9 µm P 25, sensitized with $RuL_2[\mu\text{-}(CN)Ru(CN)L'_2]_2$ (L = 2,2'-bipyridine-4,4'-dicarboxylic acid, L' = 2,2'-bipyridine), electrolyte: 80% ethylene carbonate, 20 % propylene carbonate, 0,5 M KI, 40 mM I_2)

electrode	treatment	A_{520nm}	$IPCE_{520}$/%	U_{oc}/mV
A	none	0.86	60	530
B	5 µL/cm² $TiCl_4$ in ethanol	1.08	72	570
C	" $Ti(iOPr)_4$ in isopropanol	1.50	71	560
D	" $Ti(acac)_2$ "	1.26	73	560

A method for electrodeposition of TiO_2 from aqueous $TiCl_3$ solution has been developed by B. O'Regan in our lab.[181] He found that the colloidal TiO_2 electrode dipped into a 50 mM $TiCl_3$ solution, adjusted to pH ≈ 2, develops a negative voltage with respect to a platinum electrode in the same solution. A current flows on connecting the electrodes via a resistor and TiO_2 is deposited on the colloidal film, while hydrogen evolves at the counter electrode. This observation can be rationalized by electron injection from the highly reducing $Ti^{3+}(aq)$ species into the conduction band of TiO_2. The resulting $Ti^{4+}(aq)$ species is unstable at pH 2 and forms hydrated TiO_2. Deposition of 0.1-0.5 mg TiO_2 / cm² by this method improves both dye coverage and photocurrent efficiency of ruthenium dye sensitized TiO_2 electrodes, although the higher dye loading alone is, as for the CVD treated electrodes (chapter 2.4.2.), not sufficient to explain the improvement.[181]

Electrodeposition from $TiCl_3$ requires accurate pH-adjustment, electrical connections and exclusion of oxygen, rendering these treatment rather painstaking. We found that the same improvement in electrode performance can be achieved much easier by exposing the TiO_2 film directly to an aqueous $TiCl_4$ solution, instead of forming Ti^{4+} first by oxidation of $TiCl_3$. In highly acidic solution at low temperature Ti^{4+} is metastable, due to the very slow hydrolysis and polymerization reaction.[182,183] In fact, a 2 M solution of $TiCl_4$ in water, prepared by careful addition of $TiCl_4$ (Aldrich, 99.9%) to frozen water, remained clear after over one year of storage at −18°C. Even after twenty fold dilution and at room temperature no precipitation occurs within one day on a

clean glass substrate. However, the deposition is catalyzed by the presence of TiO_2 acting as nucleation center. Thus the weight of a 1 cm^2 TiO_2 electrode covered with 50 µL of 0.2 M $TiCl_4$ and stored in an airtight box to prevent evaporation, had increased by 0.52 mg in 22 hours, after rinsing with water and firing of the electrode. The amount of deposited TiO_2 depends on the initial quantity of $TiCl_4$ and the exposure time, but not on the $TiCl_4$-concentration (Table 3).

Table 3: Weight increase of TiO_2 electrodes (1 cm^2, 10 µm P 25) after treatment with aqueous $TiCl_4$ solution

electrode	$TiCl_4$-concentration	volume	exposure time	Δm (mg)
A	0.1 M	0.1 mL/cm^2	0.5 h	0.00
B	"	"	1.2 h	0.05
C	"	"	3 h	0.11
D	"	"	22 h	0.54
E	0.05 M	0.2 mL/cm^2	"	0.51
F	0.2 M	0.05 "	"	0.52
G	0.1 M	0.05 "	25 h	0.32
H	"	0.1 "	"	0.66
I	"	0.2 "	"	1.00

The $TiCl_4$ treatment results in a similar enhancement of dye uptake and photocurrent efficiency as electrodeposition from $TiCl_3$ (Table 4). The equivalence of electrodeposition and $TiCl_4$ treatment has been confirmed by the independent studies of Y. Athanassov in our lab. Possible explanations for the improved electrode performance shall be discussed in chapter 2.4.5.

Table 4: Comparison of electrodeposition of TiO_2 from $TiCl_3$ and deposition from aqueous $TiCl_4$ solution (10 µm P 25, sensitized with $RuL_2(NCS)_2$ (L = 2,2'-bipyridine-4,4'-dicarboxylic acid), electrolyte: 80% ethylene carbonate, 20 % propylene carbonate, 0,5 M KI, 40 mM I_2)

electrode	treatment	$IPCE_{520}$/%	U_{oc}/mV
A	none	61	430
B	18 h 0.1 mL/cm^2 0.1 M $TiCl_4$	71	430
C	1 h 50 mM $TiCl_3$, pH 2.0, 0.73 C/cm^2	71	410

2.4.4. Firing and further handling of the TiO_2 electrode

Firing of the TiO_2 electrode not only serves to remove the organic additives in the colloid and sinter the particles to a mechanically adhering and electrically conducting film. It also provides a partially dehydroxylated, highly reactive surface for dye adsorption. The sensitivity of the electrode performance to changes in the weather had been known for a long time, but was not really understood. Only when the photocurrent efficiencies dropped systematically during a period of high air moisture (relative humidity RH = 80%) we suspected that water adsorption during handling of the electrode was the responsible factor. The nanoporous TiO_2 film with its very high internal surface area resembles in fact a drying agent, such as silica gel. Water may not only adsorb to the hydrophilic oxide surface, but even condense in the narrow pores between the colloidal particles.[184] Under the assumption of complete wetting of the surface the capillary condensation follows the Kelvin equation:

$$\ln \frac{p}{p_0} = -\frac{2 V_m \sigma}{r R T} \qquad \text{with} \qquad V_m = 18 \cdot 10^{-6}\ \text{m}^3\ \text{mol}^{-1}$$

$$\sigma = 7 \cdot 10^{-2}\ \text{N m}^{-1}$$

$$\frac{p}{p_0} = \text{RH (relative humidity)}$$

Thus, at a relative humidity of RH = 80% pores up to 9 nm in diameter (r = 4.5 nm) will be filled with water. Capillary condensation becomes even more important if the electrode is cooled, as happens when it is taken out of the dye solution and the ethanol evaporates from its surface. The temperature dependence of the vapor pressure is given by the Clausius-Clapeyron equation:

$$\ln \frac{p}{p_0} = -\frac{\Delta H_{mV}}{R}\left(\frac{1}{T_0} - \frac{1}{T}\right) \qquad \text{with} \qquad \Delta H_{mV} = 4.4 \cdot 10^4\ \text{J mol}^{-1}$$

If, for example, the electrode surface is cooled from 20°C to 15°C by evaporation of the ethanolic dye solution, the vapor pressure decreases by a factor of 0.74, which means that water would condense at a relative humidity of RH = 74% even on a flat surface. This can actually be observed by the formation of tiny droplets on the uncoated glass side of the electrode.

In order to prevent condensation of atmospheric humidity in the pores of the TiO_2 film we now remove the electrode from the dye solution under a stream of dry air (compressed air at 6 bar contains less than 1/6 ≈ 17% humidity and was found satisfactory). After evaporation of the ethanol the electrode is immediately wetted with electrolyte and pressed against the counter electrode,

all this under a stream of dry air. With these precautions the sensitization efficiency is independent of the atmospheric humidity during cell assemblage. However, the heat treatment of the electrode before dipping into the dye solution is important as well and shall be discussed now.

As follows from the preceding paragraph a TiO_2 electrode which had been exposed to atmospheric humidity will contain adsorbed and even capillary condensed water, which is easily removed by firing. To prevent readsorption of water the electrode has either to be cooled down in a dry atmosphere or dipped still hot into the dye solution. For example, at 80°C the vapor pressure of water increases according to the Clausius-Clapeyron equation by a factor of 22 with respect to 20°C. Thus, even under an atmospheric humidity of RH = 100% the relative humidity in the pores of an 80°C hot TiO_2 film corresponds to less than 5%. This certainly prevents capillary condensation in the pores, however, some rehydroxylation may still occur.

In addition to the physisorbed water the TiO_2 surface also contains chemisorbed water in the form of hydroxyl groups. The surface hydroxylation of TiO_2 has been the subject of numerous publications.[185-192] Hydroxylation occurs by chemisorption of water on coordinatively unsaturated surface Ti^{4+} ions, followed by proton transfer to a nearby O_2^- ion. This creates equal numbers of singly coordinated, basic and doubly coordinated, acidic OH groups. They exhibit different stretching frequencies in the IR spectrum and can be determined quantitatively by different titration methods. For the mainly anatase powder P 25 a hydroxyl density of 5-6.5 OH/nm^2 has been found after removal of the physisorbed water at 150-250°C.[185b,187b] Theoretically the most likely (001) and (111) cleavage planes of anatase could accommodate 7.1 and 15.2 OH/nm^2, respectively. However, for electrostatic reasons half of the hydroxyl groups on the (111) surface are unstable.[190] Nearly complete dehydroxylation of P 25 can be achieved by outgassing at 350-400°C.[185b,187b] A mechanism for the dehydroxylation of the (001) and (111) surfaces of anatase involving the surface migration of protons has been proposed.[190] Dehydroxylation of the TiO_2 surface creates coordinatively unsaturated Ti^{4+} ions, which act as electron-acceptor sites and are supposed to be important for dye adsorption (chapter 2.4.5.).

The minimum firing temperature for the TiO_2 electrode is of great practical interest, since it limits the choice of the substrate (e.g. flexible plastic foils withstand only up to 300°C and ITO conducting glass looses some of its conductivity above 350°C), but also because the heat treatment is one of the most energy consuming steps in the fabrication of the solar cell. We have compared the efficiency of P 25 electrodes after firing at different temperatures (Table 5).

Table 5: Influence of the firing temperature on the efficiency of TiO_2 electrodes made from P 25 colloid (2% acetyl acetone, 1% Triton X-100), sensitizer: $RuL_2(NCS)_2$ (L = 2,2'-bipyridine-4,4'-dicarboxylic acid), electrolyte: 80% ethylene carbonate, 20 % propylene carbonate, 0,5 M KI, 40 mM I_2)

electrode	heat treatment	$IPCE_{520}$/%	U_{oc}/mV
A	30 min air (350 L/min) 255°C	13	320
B	" 300°C	22	330
C	60 min " "	44	400
D	30 min O_2 (1 L/min) "	54	390
E	20 min air (350 L/min) 350°C	62	400
F	" 400°C	66	440
G	" 450°C	66	430
H	" 500°C	67	440
I	" 550°C	73	420

After firing at 255°C the TiO_2 film was still brown, indicating incomplete combustion of the organic additives. This is confirmed by thermogravimetry of the P 25 colloid, which shows a weight loss at 270°C accompanied by an exothermic DSC peak. At 300°C in air the film is still pale brown after half an hour and becomes white after one hour only. Accordingly, photocurrent efficiency and voltage increase after longer firing at this temperature (electrode B and C). In pure oxygen the complete combustion takes less time (electrode D). However, the electrode performance improves further on increasing the firing temperature (electrodes E to I). This may be due to the formation of better interparticle contacts by sintering as well as to the advancing surface dehydroxylation. Hence, the minimum firing temperature is 300°C for the present colloid, but better efficiencies are obtained after firing at higher temperatures.

The influence of different firing atmospheres (air, dry air, humidified air, argon, hydrogen, vacuum) has only been studied with electrodes prepared from precipitated and base peptized TiO_2 colloid (chapter 2.3.3.). At that time we found that simple firing in air is at least as good as any other atmosphere. Only on titanium as substrate a final firing in argon is necessary to render the oxide layer, formed on firing in air, conductive by partial reduction from the titanium metal (cf. chapter 2.3.2.). Heat treatment in water vapor accelerates sintering of the particles due to enhanced surface diffusion.[193] However, even after

additional firing in air for dehydroxylation the dye uptake and the photocurrent efficiency were found to be diminished, in accordance with a reduction of the surface area by sintering. Dry air or vacuum appear not to be necessary to achieve dehydroxylation of the TiO_2 surface, since even the relative humidity of normal air becomes negligible at the high firing temperature.

It has been reported, that surface dehydroxylation of TiO_2 is facilitated by the presence of chloride impurities, which may migrate to the surface during firing and replace the hydroxyl groups.[186b,188] Since P 25, which is prepared by flame hydrolysis of $TiCl_4$, contains up to 0.3% Cl^-,[161] its comparatively easy dehydroxylation may be related to the chloride content.

Also during CVD treatment with $TiCl_4/O_2$ (chapter 2.4.2.) the surface is expected to be completely dehydroxylated by reaction of $TiCl_4$ with the OH groups. In order to decide whether dehydroxylation or deposition of additional TiO_2 is responsible for the observed improvements in electrode performance, we investigated alternative chemical dehydroxylation methods. A treatment with Cl_2 or CCl_4 is employed in the manufacture of fiber optics to remove OH groups from the glass, since they absorb strongly in the near infrared region and increase the fiber losses.[28(p.639)] The surface reactions of CCl_4 with TiO_2 (P 25) have already been studied.[194] Even at temperatures below 150°C superficial oxygen atoms and hydroxyl groups were found to be exchanged for chlorine. At higher temperature the lattice itself is attacked and $TiCl_4$ evolved. We have compared the efficiency of TiO_2 electrodes treated at different temperatures in a CCl_4 saturated helium stream ($p^{20°C}_{CCl_4}$ = 13 kPa, Table 6).

Table 6: Effect of CCl_4 treatment on the photoelectrical properties of TiO_2 (P 25) electrodes , sensitized with $RuL_2[\mu\text{-}(CN)Ru(CN)L'_2]_2$ (L = 2,2'-bipyridine-4,4'-dicarboxylic acid, L' = 2,2'-bipyridine, in ethanol), electrolyte: 80% ethylene carbonate, 20% propylene carbonate, 0.5 M KI, 40 mM I_2

electrode	treatment	IPCE$_{520}$/%	U_{oc}/mV
A	30 min air 550°C	65	450
B	" 1 min CCl_4 sat. He (1 L/min) 20°C	67	450
C	" " 120°C	62	430
D	" " 160°C	62	410
E	" " 220°C	61	340
F	" " 300°C	uncolored	–

The coloration of the electrodes was the same, with the exception of electrode F, which did not adsorb any dye. The photocurrent efficiency decreases slightly, the voltage more clearly with increasing reaction temperature. We conclude that exchange of the surface hydroxyl groups for chlorine does not improve the sensitization efficiency. The lower photovoltage is probably due to a flatband potential shift caused by the liberation of hydrochloric acid. At 300°C and higher temperatures the TiO_2 layer is etched by reaction with CCl_4 to form $TiCl_4$, which leads first to obstruction of the pores by chemical vapor transport (electrode F) and finally to disappearance of the TiO_2 film.

2.4.5. Rationalization of the improvements achieved by surface treatment

The experiments of the preceding chapters have shown that different methods for the deposition of a TiO_2 overlayer result in similar improvements in the photocurrent efficiency. The amount of TiO_2 deposited is several 0.1 mg on a 1 cm^2 P 25 electrode of roughness factor ≈ 1000, and corresponds to a few monolayers only. One possible explanation for the better electrode performance is a higher purity of the TiO_2 surface after treatment. Although flame hydrolysis of $TiCl_4$, which can be highly purified by distillation, gives a rather pure TiO_2 powder, the P 25 contains up to 0.3% Al_2O_3 , 0.2% SiO_2 and 100 ppm Fe_2O_3,[161] which for semiconductor standards is quite a lot. One also has to consider that the surface might be enriched in these impurities. Although surface segregation is not expected for Al_2O_3 and SiO_2, in view of their high solubility in TiO_2 (cf. chapter 2.3.10), they might form slower than the TiO_2 particles during flame hydrolysis, due to the absence of condensation nuclei, and would than deposit on the TiO_2 surface. The electron injection from the adsorbed dye would be affected by Al_2O_3 and SiO_2, which simply act as an insulating layer on the TiO_2 surface, while Fe^{3+} has been reported to act as trap for photogenerated electrons.[195,196] In fact, we found that deposition of Fe^{3+} by application of an aqueous $FeCl_3$ solution on the TiO_2 electrode quenches the dye sensitized photocurrent (Table 7). However, appreciable amounts of Fe_2O_3 are required for complete quenching and the less than 100 ppm Fe_2O_3 of P 25 would not have much influence, even if they were segregated onto the surface.

Table 7: Effect of Fe^{3+} impurities in the TiO_2 surface on the photosensitization efficiency (≈ 2 mg P 25/cm², sensitizer: $RuL_2[\mu\text{-}(CN)Ru(CN)L'_2]_2$ (L = 2,2'-bipyridine-4,4'-dicarboxylic acid, L' = 2,2'-bipyridine, in ethanol), electrolyte: 80% ethylene carbonate, 20% propylene carbonate, 0.5 M KI, 40 mM I_2)

electrode	treatment	IPCE$_{520}$/%	U_{oc}/mV
A	none	57	460
B	+ 10 µL 10^{-4} M $FeCl_3$ = 40ppm Fe_2O_3	58	450
C	" 10^{-3} M " 400 "	16	340
D	" 10^{-2} M " 4000 "	1	230

Another source of impurities are the solvent (usually water) and the additives (e.g. 2% acetyl acetone and 1% Triton X-100) employed in the preparation of the TiO_2 colloid. Since the solvent evaporates and the organic additives are burned off, any nonvolatile impurities will deposit on the TiO_2 surface. Yet, due to the high colloid concentration of about 0.5 g TiO_2/mL rather high impurity levels would be necessary to contribute significantly to the surface impurity content.

Some of the TiO_2 overlayer deposition techniques may improve the surface purity, e.g. the hydrolysis of $TiCl_3$ or $TiCl_4$ leads to a very low Fe_2O_3 content, because iron is not precipitated under reducing or acidic conditions, even if it is present in solution.[197] But since the TiO_2 surface should be reasonable pure already before overlayer deposition, we doubt that surface purity enhancement explains the improved electrode performance.

The deposition of a TiO_2 overlayer usually results in better dye adsorption and deeper coloration of the electrode. However, this is not sufficient to rationalize the higher monochromatic photocurrent efficiencies at a wavelength where the light is nearly completely absorbed even without after-treatment. The enhanced dye uptake may either be due to an increased surface area of the electrode or a higher activity of the already present surface. The roughness factor of a P 25 electrode, containing 2 mg TiO_2/cm² with a BET surface area of 55 m²/g [161] is RF = 1100, if the reduction in surface area by sintering is neglected. The saturation dye coverage of $RuL_2[\mu\text{-}(CN)Ru(CN)L'_2]_2$ (L = 2,2'-bipyridine-4,4'-dicarboxylic acid, L' = 2,2'-bipyridine) on P 25 in ethanol at pH 3 has been determined to Γ_{max} = 3.7 µmol m^{-2}, corresponding to 0.45 nm²/molecule.[198] Since the dye has a cross section of about 1 nm² this coverage probably indicates double layer formation, due to the hydrophobic

effect and base stacking of the bipyridine ligands. In fact, the symmetric dye analog $RuL_2[\mu\text{-}(CN)Ru(CN)L_2]_2$, having carboxyl groups on all bipyridine ligands, gives only $\Gamma_{max} = 1.7$ μmol m^{-2}, corresponding to 0.95 nm^2/molecule, as expected for a closely packed monolayer.[198] The absorbance of such a monolayer would be $A_{520} = \varepsilon_{520} \cdot \Gamma_{max} = 1.8 \cdot 10^4$ $M^{-1}cm^{-1} \cdot 1.7 \cdot 10^{-6} mol/m^2 = 3.06 \cdot 10^{-3}$. A P 25 electrode of roughness factor RF = 1100 should thus have an optical density of $A_{520} = 3.4$, if the surface was completely covered with dye. By contrast, the measured value is only $A_{520} = 0.9$ for an electrode without overlayer (Table 1 and 2). Hence, the active surface area is nearly four times smaller than expected. This seems only in part to be due to the decrease of the surface area during sintering, since most of the particle surface remains exposed after firing at 500°C, as shown by the scanning electron micrograph (Figure 25).

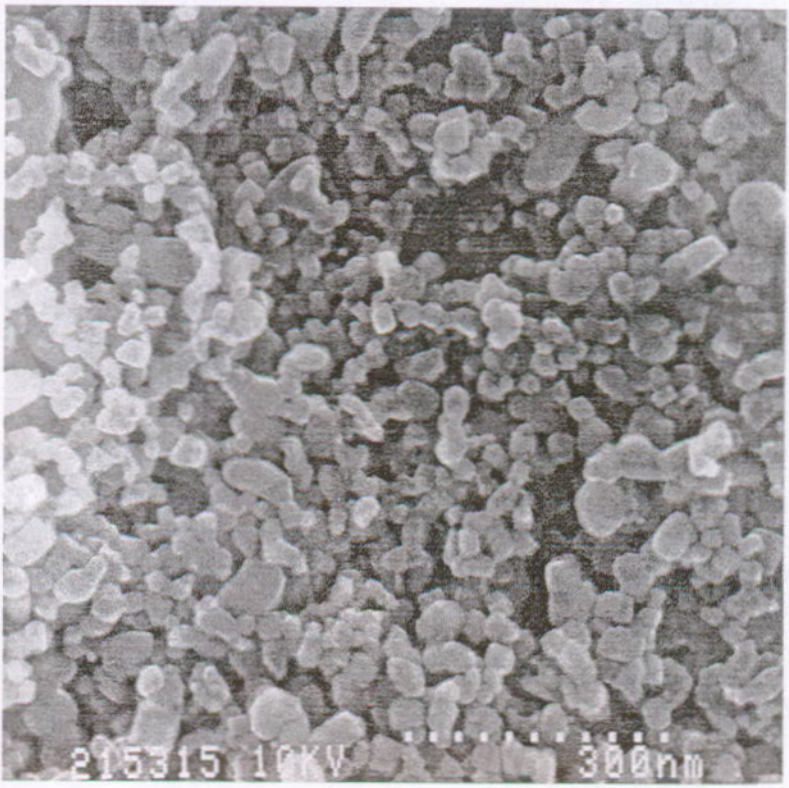

Figure 25: High resolution scanning electron micrograph of a fractured P 25 layer treated by electrodeposition from $TiCl_3$

Also the inaccessibility of the narrow interparticle neck regions and the smallest pores for the rather large dye molecule (∅ 1 nm compared to a particle size of about ∅ 20 nm) cannot explain the drastically diminished dye uptake, especially in view of the effect of overlayer deposition, which fills up the pores even more.

High resolution scanning and transmission electron micrographs of $TiCl_3$ or $TiCl_4$ treated TiO_2 electrodes often show very small (∅ 2-5 nm) particles on the colloid particles of the film. However, this secondary roughness is limited to the surface of the TiO_2 layer and is probably due to the deposition of very small particles formed in solution, but they are too large to penetrate through the pores into the interior of the film. Figure 25 shows in fact the interior of an electrode that has been treated by electrodeposition from $TiCl_3$. One cannot discern any overlayer, which is expected for a deposition of only a few monolayers of TiO_2.

The question is then, how to explain the low activity of the untreated surface and the increased dye adsorption and higher electron injection efficiency after overlayer deposition. To answer this question, we have to consider the mechanism of dye adsorption on the atomic scale.

It is well established, that the carboxyl groups of the dye are responsible for attachment on the TiO_2 surface. From aqueous solution the dye is best adsorbed under slightly acidic conditions (pH 3-4). Since the isoelectric point of anatase is IEP ≈ 6 the hydroxyl groups on TiO_2 are partially protonated at this pH, while the carboxyl groups of the dye are mostly deprotonated. This results in a purely electrostatic attachment of the dye.[199] However, higher electron injection yields are usually obtained by dehydroxylation of the TiO_2 surface (chapter 2.4.4) and dye adsorption from non aqueous solvents like ethanol.

The dehydroxylated TiO_2 surface is known to be very active in chemisorption, due to the presence of coordinatively unsaturated Ti^{4+} centers with Lewis acid character. For example, alcohols adsorb dissociatively on such a surface to produce alkoxy and hydroxyl groups.[200-202] Hence, ethoxy and hydroxyl groups will be formed on dipping the fired electrode into the ethanolic dye solution. Acetic acid also has been reported to adsorb dissociatively on Ti-O-Ti bridges of dehydroxylated TiO_2, forming an acetate and a hydroxyl group.[203] Formic acid was found to adsorb in a monodentate fashion on TiO_2, but can hydrogen bond with the neighboring hydroxyl group.[204] The ethoxy groups resulting from dipping into the ethanolic dye solution are expected to be replaced by the carboxyl groups of the dye, in analogy to the reaction of titanium alkoxides with carboxylic acids:[21(p.182)]

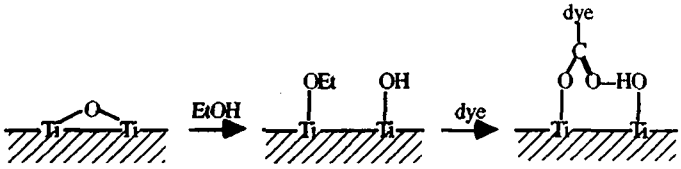

However, at least two carboxyl groups are necessary for strong adsorption of the dye on the TiO_2 electrode. This again requires two Ti^{4+} centers at a distance equal to the separation of the carboxyl groups of the sensitizer.

The structural, electronic and chemisorption properties of the different dehydroxylated surface planes of rutile have been extensively studied by techniques such as LEED (low-energy electron diffraction), AES (Auger electron spectroscopy), EELS (electron energy loss spectroscopy), UPS (ultraviolet photoemission spectroscopy), XPS (X-ray photoelectron spectroscopy), STM (scanning tunneling microscopy), STS (scanning tunneling spectro-scopy).[205-211] However, these studies were done on reduced, non-stoichiometric rutile, exhibiting an appreciable density of oxygen vacancies, which influence both the electronic and structural properties of the surface. Besides, for solar cell applications we are more interested in the wider band gap anatase modification of TiO_2, which is the predominant phase in the colloids used for electrode preparation. For example, P 25 contains more than 70% anatase, and it has been shown by HRTEM (high resolution transmission electron microscopy) in combination with EELS that this powder is composed of separate anatase and rutile particles.[212]

Experimental data on defined surface planes of anatase are more difficult to obtain, because natural anatase is contaminated with iron, while synthetic crystals have rarely been grown.[213,214] Natural as well as synthetic crystals of anatase expose the (001) and (111) surface planes [215] (the latter corresponds to the (101) face in another notation [216]), and these are also assumed to be predominant in polycrystalline samples, such as P 25 powder.[185a,187a,190] In fact, HRTEM of nanocrystalline Al_2O_3 particles (Ø 30 nm) has shown, that the (111) surface is predominant, even on the roughly spherical particles.[217] This is due to numerous steps, giving rise to a highly faceted surface. P 25 also shows well developed surface planes in HRTEM,[212] and a TiO_2 colloid prepared by hydrolysis of $Ti(iOPr)_4$, peptized with nitric acid and crystallized by autoclavation [31b] was indeed found to expose mainly the (111) surface of anatase.[218]

We have modeled the dye adsorption on both(001) and (111) surfaces with molecular models (Cochranes of Oxford) as well as with computer generated structures (CAChe molecule editor). The crystal lattice was calculated from the unit cell parameters of anatase.[216] The (001) surface exhibits only one type of 5-coordinated Ti^{4+} in a quadratic arrangement (Figure 26)

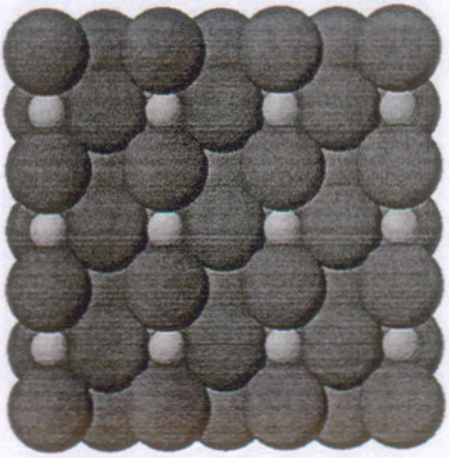

Figure 26: Ideal (001) cleavage plane of anatase

The most successful ruthenium dyes have 2,2'-bipyridine-4,4'-dicarboxylate ligands as attaching groups. The oxygen atoms presumed to be involved in adsorption have a distance of about 0.60 nm, if the carboxyl groups are kept in plane with the bipyridine to allow conjugation of the π-orbitals. Since two diagonal Ti^{4+} centers in the (001) surface have a separation of 0.535 nm and dangling bonds (d_{z2} orbitals [219,220]) perpendicular to the plane, the carboxyl groups of the dye may adsorb dissociatively on them and complete their coordination octahedron. However, in order to keep the bonding angle of the oxygen atoms close to 120° the whole ligand has to be tilted on the surface, which makes hydrogen bonding of a third carboxyl group with a surface oxygen atom or a surface hydroxyl group possible (Figure 27).

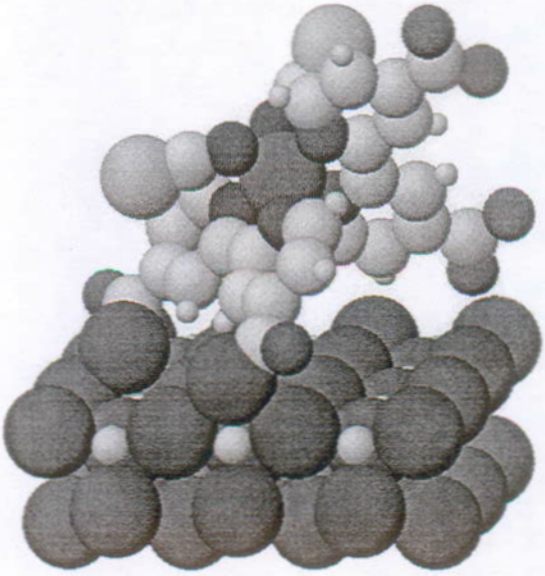

Figure 27: Adsorption of $RuL_2(NCS)_2$ (L = 2,2'-bipyridine-4,4'-dicarboxylic acid) on two diagonal Ti^{4+} centers of the (001) surface of anatase ($d_{Ti-O} \approx$ 0.20 nm, angle(C,O,Ti) $\approx 140°$).

The adsorption with one carboxyl group of each bipyridine ligand is also possible. However, since other dyes with only one carboxylated ligand (e.g. $RuL(bpy)(NCS)_2$) show similar adsorption and photosensitization behavior, we shall not further consider this possibility.

The situation is more complicated on the most frequent (111) surface of anatase, which exhibits a saw-tooth structure with two types of 5-coordinated and one type of 4-coordinated Ti^{4+} (Figure 28).[187a]

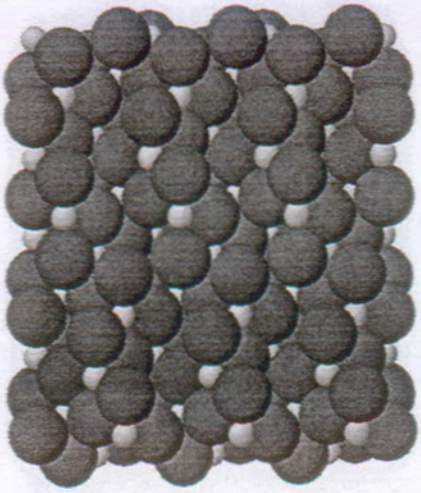

Figure 28: Ideal (111) cleavage plane of anatase

The distance of Ti^{4+} centers in the same row is again 0.535 nm, but the dangling bonds are $d_{x^2-y^2}$ orbitals with an angle of 45° to the plane.[219,220] Adsorption of the dye on two of these Ti^{4+} centers results in a stronger deviation from the optimal oxygen binding angle of 120° (Figure 29).

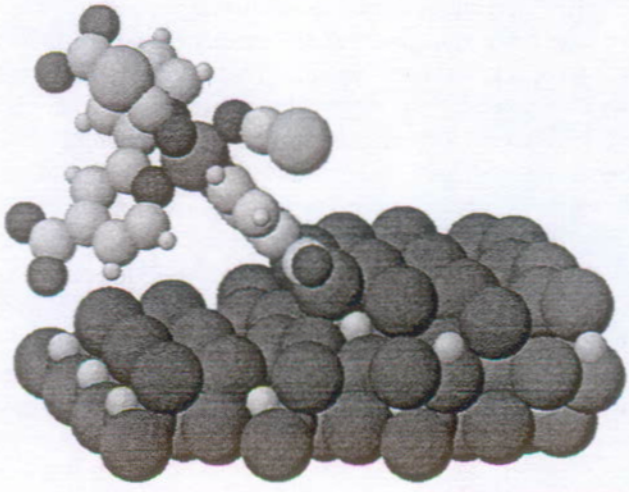

Figure 29: Adsorption of $RuL_2(NCS)_2$ (L = 2,2'-bipyridine-4,4'-dicarboxylic acid) on two Ti^{4+} centers (4-coordinated in this case) of the same row of the (111) surface of anatase ($d_{Ti-O} \approx 0.20$ nm, angle(C,O,Ti) ≈ 135° and 160°).

There are other pairs of Ti^{4+} centers with a separation of 0.549 nm, involving one 4- and one 5-coordinated Ti^{4+}. However, the latter are rather deeply buried below the O^{2-} ions, and the model shows steric hindrance by the second oxygen atom of the carboxyl group.

Another class of dyes, namely derivatives of natural porphyrins and chlorophylls (chapter 3.4) have more flexible propionic and acetic acid groups for attachment, which can accommodate different Ti^{4+} separations and binding angles. On the other hand, the electronic coupling of the dye π-orbitals with the conduction band of TiO_2, which arises from overlap of the t_{2g}-orbitals d_{xy}, d_{xz} and d_{yz} of titanium, is hampered by the flexible, but insulating σ-bonds in this case. A third type of dye forms a chelate with only one Ti^{4+} center, e.g. dyes with two neighboring oxygen functionalities like Coumarin 343.[221] These can only adsorb on well exposed 4-coordinated Ti^{4+} centers, as they are present on the (111) surface of anatase.

We conclude, that adsorption of the most important ruthenium dyes with 2,2'-bipyridine-4,4'-dicarboxylate ligand is possible on the perfect (001) and (111) surfaces of anatase. However, the coordinatively unsaturated Ti^{4+} centers representing the sites of attachment are rather well shielded by the surface O^{2-} ions, a situation that has already been described for rutile.[222] In addition, the formation of two Ti–O bonds involves appreciable strain in the ligand, due to deviations from the optimal bonding angles. This may explain the rather low dye coverage on TiO_2 electrodes without overlayer.

Deposition of a few monolayers of additional TiO_2 under conditions of high super-saturation, e.g. from an aqueous $TiCl_4$ solution already containing oligomeric Ti–O species,[183] is supposed to create an atomically rough surface with many defects, especially steps and kinks. It has in fact been observed, that high supersaturation favors the growth of surfaces with high electrostatic potential, which adsorb molecules much stronger than the usual equilibrium surfaces.[215] Although some surface diffusion and restructuring will occur on firing at 500°C, the surface is still expected to show less prefect crystal planes than the original powder, which has been prepared at high temperature in a flame. The less regular surface resulting from overlayer deposition will contain highly exposed, coordinatively unsaturated Ti^{4+} centers at varying distances, presenting more possibilities for dye adsorption. This would explain the better coloration of the after-treated electrodes. The greater choice of adsorption sites on a disordered surface may also allow more favorable binding angles of the carboxyl attaching groups and hence a stronger overlap of the dye π-system with the conduction band of TiO_2. This may be the reason for the higher electron injection efficiencies on electrodes with overlayer.

In this context it is interesting to note that the photosensitization quantum efficiency of ruthenium dyes with a 2,2'-bipyridine-4,4'-dicarboxylate ligand covalently attached to a defined cleavage plane of single crystal rutile electrodes was found to be much lower ($\approx 0.25\%$) than with the present colloidal electrodes.[223] One possible explanation is that the surface of a nanocrystalline particle, although exposing mainly the most stable planes, contains a lot of steps due to facetting,[217] which present better adsorption sites than an atomically flat crystal surface. Still, dye adsorption and electron injection efficiency can be enhanced further by overlayer deposition, creating an even less regular surface.

While this model explains both the higher dye uptake and the improved electrode performance achieved by surface treatment, other factors may be involved as well. For example, overlayer deposition followed by firing will result in stronger necking between the particles and hence a better electrical contact. Also the contact with the SnO_2 substrate should be improved and this may be another reason for the increased photocurrent efficiencies. On the other hand, the better electrode coloration could be merely a consequence of the increased surface area due to deposition of very small (2-5 nm) TiO_2 particles on the layer surface, as mentioned above. However, this would not account for the poor dye coverage without overlayer, which we found to be nearly four times lower than expected.

Up to now we have mainly discussed geometric constraints for adsorption and mostly neglected the electronic structure of the semiconductor surface. For rutile it has been derived theoretically [220] and confirmed experimentally [205-209] that defects in the surface create surface states, that is electronic states with an energy different from the bulk crystal. These were found to be the active sites for chemisorption and charge transfer. Since these studies were carried out on reduced rutile, the Fermi level lies at or even above the conduction band edge. This implies filling of the surface states, equivalent to reduction of the surface Ti^{4+} sites to Ti^{3+}. In our case, by contrast, the TiO_2 is insulating in absence of electron injection from the dye, indicating a Fermi level well below the conduction band edge. Therefore the surface states arising from coordinatively unsaturated Ti^{4+} centers remain unfilled and may act as electron acceptors for the photoexcited dye. Since the electron transfer rate depends on the energetic position of the acceptor levels, the distribution of surface states will influence the photosensitization efficiency (chapter 3.5.6). In addition, the photocurrent conduction mechanism may involve electron hopping between surface states below the conduction band edge of bulk TiO_2. In view of the high surface to volume ratio in a colloidal TiO_2 electrode these surface electronic properties will be extremely important. This may be another reason, why deposition of a TiO_2 overlayer improves the performance of the solar cell.

References to chapter 2

1. **N. Vlachopoulos, P. Liska, J. Augustynski, M. Grätzel:** Very efficient visible light energy harvesting and conversion by spectral sensitization of high surface area polycrystalline titanium dioxide films, *J. Am. Chem. Soc.* 110 (1988) 1216
2. **M. Sittig:** *Solar cells for photovoltaic generation of electricity*, Park Ridge 1979, p. 190-225
3. **G. Haacke:** Transparent conducting coatings *Ann. Rev. Mater. Sci.* 7 (1977) 73
4. **C.M. Lampert:** Heat mirror coatings for energy conserving windows *Sol. Energy Mater.* 6 (1981) 1
5. **J.C. Manifacier:** Thin metallic oxides as transparent conductors *Thin Solid Films* 90 (1982) 297
6. **K.L. Chopra, S. Major, D.K. Pandya:** Transparent conductors *Thin Solid Films* 102 (1983) 1
7. **A.L. Dawar, J.C. Joshi:** Semiconducting transparent thin films *J. Mater. Sci.* 19 (1984) 1
8. **H. Haitjema, J.J.Ph. Elich, C.J. Hoogendoorn:** The optical, electrical and structural properties of fluorine-doped, pyrolytically sprayed tinoxide coatings *Sol. Energy Mater.* 19 (1989) 283
9. **G. Frank, H. Köstlin:** Electrical properties and defect model of tin-doped indium oxide layers *Appl. Phys.* A 27 (1982) 197
10. **N.J. Arfsten:** Sol-gel derived transparent IR-reflecting ITO semiconductor coatings and future applications *J. Non-Cryst. Sol.* 63 (1984) 243
11. **N.M. Gralenski:** Optical coatings by conveyorized atmospheric chemical vapor deposition, in *Transparent heat-mirror materials and deposition technology*, C.M. Lampert, S. Selkowitz, eds., Berkeley 1982, p. 79
12. **F.T.J. Smith, S.L. Lyn:** Effects of heat-treatment on indium-tinoxide films *J. Electrochem. Soc.* 128 (1981) 2388
13. **J.-G. Na, Y.-R. Cho, Y.-H. Kim, T.-D. Lee, S.-J. Park:** Effects of annealing temperature on microstructure and electrical and optical properties of radio-frequency sputtered tin-doped indium oxide films *J. Am. Ceram. Soc.* 72 (1989) 698
14. **Glastron:** *Transparent electroconductive glass* (technical data sheet), Courbevoie (France) 1991
15. **R.G. Gordon, J. Proscia, F.B. Ellis, A.E. Delahoy:** Textured tin oxide films produced by atmospheric pressure chemical vapor deposition from tetramethyltin and their usefulness in producing light trapping in thin film amorphous silicon solar cells *Sol. Energy Mater.* 19 (1989) 263
16. **I. Chambouleyron:** Solar cell sheet resistance analysis, in *First European Community Photovoltaic Energy Conference*, Luxemburg 1977, p. 987
17. **S. Bobbio, F.P. Califano, E. Ciccarone:** Non-linear analysis of solar-cell-series resistance, in *First European Community Photovoltaic Energy Conference*, Luxemburg 1977, p. 1006

18. **A. Flat, A.G. Milnes:** Theoretical performance of multi-layer grid patterns for solar cells, in *Second European Community Photovoltaic Energy Conference*, Berlin 1979, p. 654

19. **F. Möllers, R. Memming:** Electrochemical studies of semiconducting SnO_2-electrodes *Ber. Bunsenges. Phys. Chem.* 76 (1972) 469, 475

20. **L. Kavan, B. O'Regan, A. Kay, M. Grätzel:** Preparation of TiO_2 (anatase) films on electrodes by anodic oxidative hydrolysis of $TiCl_3$ *J. Electroanal. Chem.* 346 (1993) 291

21. **Kirk-Othmer:** *Encyclopedia of Chemical Technology*, 3rd edition, Wiley, New York 1983, Vol. 23, p. 176

22. **D.C. Bradley, R.C. Mehrotra, D.P. Gaur:** *Metal Alkoxides*, Acad. Pr., London 1978

23. **Gmelins** *Handbuch der anorganischen Chemie*, Titan, Weinheim 1951, Vol.41, p. 309

24. **C. Mailhe-Randolph, A.J. McEvoy, M. Grätzel:** Influence of precursors on the morophology and performance of TiO_2 photoanodes, *J. Mater. Sci.* 26 (1991) 3305

25. **H. Schroeder:** Oxide layers deposited from organic solutions, in *Physics of Thin Films*, G. Hass, R.E. Thun, eds., New York 1969, Vol. 5, p. 87

26. a) **B.E. Yoldas:** Deposition and properties of optical oxide coatings from polymerized solutions, *Appl. Opt.* 12 (1982) 2960

    b) **B.E. Yoldas, T. O'Keeffe:** Deposition of optically transparent IR reflective coatings on glass, *Appl. Opt.* 23 (1984) 3638

27. a) **T. Yoko, K. Kamiya, S. Sakka:** Preparation of TiO_2 film by the sol-gel method and its application to photoelectrochemical electrodes, *Denki Kagaku* 54 (1986) 6

    b) **T. Yoko, K. Kamiya, S. Sakka:** Photoelectrochemical properties of TiO_2 films prepared by the sol-gel method, *Yogyo-Kyokai-Shi* 95 (1987) 150

    c) **T. Yoko, A. Yuasa, K. Kamiya, S. Sakka:** Sol-gel-derived TiO_2 film semiconductor electrode for photocleavage of water, *J. Electrochem. Soc.* 138 (1991) 2279

28. **C.F. Brinker, G.W. Scherer:** *Sol-Gel Science*, Acad. Pr., San Diego 1990

29. **H.D. Gesser, P.C. Goswami:** Aerogels and related porous materials, *Chem. Rev.* 89 (1989) 765

30. a) **B.E. Yoldas:** Alumina gels that form porous transparent Al_2O_3, *J. Mater. Sci.* 10 (1975) 1856

    b) **B.E. Yoldas:** A transparent porous alumina, *Am. Ceram. Soc. Bull.* 54 (1975) 286

    c) **B.E. Yoldas:** Investigation of porous oxides as an antireflective coating for glass surfaces, *Appl. Opt.* 19 (1980) 1425

    d) **B.E. Yoldas:** Molecular and microstructural effects of condensation reactions in alkoxide based alumina systems, in *Ultrastructure Processing of Advanced Ceramics*, J.D. Mackenzie, D.R. Ulrich, eds., 1988, p. 333

31. a) **B. O'Regan, J. Moser, M. Anderson, M. Grätzel:** Vectorial electron injection into transparent semiconductor membranes and electric field effects on the dynamics of light-induced charge separation, *J. Phys. Chem.* 94 (1990) 8720

b) **B. O'Regan, M. Grätzel:** A low-cost, high efficiency solar cell based on dye-sensitized colloidal TiO_2 films, *Nature* 353 (1991) 737

32. a) **I.M. Thomas:** Single-layer TiO_2 and multilayer TiO_2-SiO_2 optical coatings prepared from colloidal suspensions, *Appl. Opt.* 26 (1987) 4688

b) **H.G. Floch, J.J. Priotton, I.M. Thomas:** Optical coatings prepared from colloidal media, *Thin Solid Films* 17 (1989) 173

33. **L.E. Scriven:** Physics and application of dip coating and spin coating, in *Mat. Res. Soc. Symp. Proc. Vol.* 121 (1988) p. 717

34. **B.D. Washo:** Rheology and modeling of the spin coating process, *IBM J. Res. Develop.* (1977) 1909

35. **H.D. Gesser, P.C. Goswami:** Aerogels and related porous materials, *Chem. Rev.* 89 (1989) 765

36. **S.S. Kistler:** Coherent expanded aerogels, *J. Phys. Chem.* 36 (1932) 52

37. **J. Zarzycki, M. Prassas, J. Phalippon:** Synthesis of glasses from gels: the problem of monolithic gels, *J. Mater. Sci.* 17 (1982) 3371

38. **S.P. Mukherjee:** Supercritical drying and structural and microstructural evolution of gels, in *Ultrastructure Processing of Advanced Ceramics*, J.D. Mackenzie, D.R. Ulrich, eds., 1988, p. 747

39. **J.S. Clunie, B.T. Ingram:** Adsorption of nonionic surfactants, in *Adsorption from solution at the solid/liquid interface*, G.D. Parfitt, C.H. Rochester, eds., Acad. Press 1983, p. 105

40. **J.M. Warman, M.P. de Haas, P. Pichat, N. Serpone:** Effect of isopropyl alcohol on the surface localization and recombination of conduction-band electrons in Degussa P 25 TiO_2. A pulse-radiolysis time-resolved microwave study *J. Phys. Chem.* 95 (1991) 8858

41. a) **J.W. Orton, M.J. Powell:** The Hall effect in polycrystalline and powdered semiconductors, *Rep. Prog. Phys.* 43 (1980) 1263

b) **J.W. Orton. B.J. Goldsmith, J.A. Chapman, M.J. Powell:** The mechanism of photoconductivity in polycrystalline cadmium sulphide layers, *J. Appl. Phys.* 53 (1982) 1602

42. **J.Y.W. Seto:** The electrical properties of polycrystalline silicon films, *J. Appl. Phys.* 46 (1975) 5247

43. **D.C. Cronemeyer:** Infrared absorption of reduced rutile TiO_2 single crystals, *Phys. Rev.* 113 (1959) 1222

44. **J. Gautron, P. Lemasson, J.-F. Marucco:** Correlation between the non-stoichiometry of titanium dioxide and its photoelectrochemical behaviour, *Faraday Trans. Chem. Soc.* 70 (1980) 81

45. **K.H.Yoon, J.S. Kim:** Photoelectric behaviour of sintered TiO_2 electrodes, *J. Phys. Chem.* 90 (86) 6488

46. **L.A. Harris, M.E. Gerstner, R.H. Wilson:** Room temperature diffusion in a single crystal rutile electrode, *J. Electrochem. Soc.* 126 (79) 850

47. **J.P. Frayret, A. Caprani, F. Charru, G. Momplot:** Influence of cathodic reduction on the photoelectrochemical behaviour of titanium dioxide, *Electrochim. Acta* 27 (1982) 1525

48. **S.-E. Lindquist, A. Lindgren, C. Leygraf:** Effects of electrochemical reduction of polycrystalline TiO_2 photoelectrodes in acidic solutions, *Sol. Energy Mater.* 15 (1987) 367

49. **S.N. Subbarao, Y.H. Yun, R. Kershaw, K. Dwight, A. Wold:** Electrical and optical properties of the system $TiO_{2-x}F_x$, *Inorg. Chem.* 18 (1979) 488

50. **T. Hepel, M. Hepel, R.A. Osteryoung:** Thermodynamic and photoelectrochemical behaviour of the n-TiO_2 electrode in fluoride-containing solutions, *J. Electrochem. Soc.* 129 (1982) 2132

51. **C.M. Wang, T.E. Mallouk:** Photoelectrochemistry and interfacial energetics of titanium dioxide photoelectrodes in fluoride-containing solutions, *J. Phys. Chem.* 94 (1990) 423

52. **M. Hermann, U. Kaluza, H.P. Boehm:** Über die Chemie der Oberfläche des Titandioxids. Austausch von Hydroxidionen gegen Fluoridionen, *Zeitschr. anorg. allg. Chem.* 372 (1970) 308

53. **K.H. Yoon, D.H. Kang, K.H. Kim, J.S. Choi:** Photoeffects due to thickness and dopant (Sb_2O_3) in polycrystalline TiO_2 electrodes, *Ind. Eng. Chem. Prod. Res. Dev.* 25 (1986) 93

54. **P. Salvador:** The influence of niobium doping on the efficiency of n-TiO_2 electrode in water photoelectrolysis, *Sol. Energy Mater.* 2 (1980) 413

55. **A. Tsuzuki, H. Murakami, K. Kani, S. Kawakami, Y. Torii:** Preparation of Nb-doped TiO_2 films by the sol-gel method, *J. Mater. Sci. Lett.* 9 (1990) 624

56. **S.R. Kurtz, R.G. Gordon:** Chemical vapour deposition of doped TiO_2 thin films, *Thin Solid Films* 147 (1987) 167

57. **L. Springer, M.F. Yan:** Sintering of TiO_2 from organometallic precursors, in *Ultrastructure processing of ceramics, glasses and composites*, L.L. Hench, D.R. Ulrich, eds., 1984, p. 465

58. **L.E. Edelson, A.M. Glaeser:** Role of particle substructure in the sintering of monosized titania, *J. Am. Ceram. Soc.* 71 (1988) 225

59. **H. Hahn, J. Logas, R.S. Averback:** Sintering characteristics of nanocrystalline TiO_2, *J. Mater. Res.* 5 (1990) 609

60. **R.K. Iler:** *The Chemistry of Silica*, Wiley, New York 1979, p. 227

61. **J.-L. Hébrard, P. Nortier, M. Pijolat, M. Soustelle:** Initial sintering of submicrometer titania anatase powder, *J. Am. Ceram. Soc.* 73 (1990) 79

62. **Y. Oguri, R.E. Riman, H.K. Bowen:** Processing of anatase from hydrothermally treated alkoxy-derived hydrous titania, *J. Mater. Sci. 23* (1988) 2897

63. **S. Komarneni, R. Roy, E. Breval, M. Ollinen, Y. Suwa:** Hydrothermal route to ultrafine powders utilizing single and diphasic gels, *Adv. Ceram. Mater.* 1 (1980) 87

64. **T.R.N. Kutty, R. Vivekanandan, P. Murugaraj:** Preparation of rutile and anatase (TiO_2) fine powders and their conversion to $MTiO_3$ (M = Ba, Sr, Ca) by the hydrothermal method, *Mater. Chem. Phys.* 19 (1988) 533

65. **B.E. Dahneke**, ed.: *Measurement of suspended particles by quasi-elastic light scattering*, Wiley, New York 1983

66. **M.T. Harris, C.H. Byers:** Effect of solvent on the homogenous precipitation of titania by titanium ethoxide hydrolysis, *J. Non-Cryst. Sol.* 103 (1988) 49

67. **V.W. Day, T.A. Eberspacher, W.G. Klemperer, L.W. Park:** Dodecatitanates: A new family of stable polyoxotitanates *J. Am. Chem. Soc.* 115 (1993) 8469

68. **A. Matsuda, Y. Matsuuo, S. Katayama, T. Tsumo, N. Tohge, T. Minami:** Physical and chemical properties of titania-silica films derived from polyethylene glycol-containing gels *J. Am. Ceram. Soc.* 73 (1990) 2217

69. **Kirk-Othmer:** *Encyclopedia of Chemical Technology*, 3rd edition, Wiley, New York 1983, Vol. 23, p. 228

70. *Encyclopedia of Polymer Science and Engineering*, Wiley, New York 1989, Vol. 17, p. 178

71. **L. Drechsel, P. Görlich:** Über die lichtelektrischen Eigenschaften von Polyvinylenfolien, Jenaer Jahrbuch 1963, p. 165

72. **R.E. Reeves, L.W. Mazzeno:** The composition of some tetra-t-butyl titanate-glycol reaction products *J. Am. Chem. Soc.* 76 (1954) 2533

73. **D.M. Puri, R.C. Mehrotra:** Ethylene glycol derivatives of titanium *Indian J. Chem.* 5 (1967) 448

74. **K.D. Budd, D.A. Payne:** Preparation of strontium titanate ceramics and internal boundary layer capacitors by the Pechini method *Mat. Res. Soc. Symp. Proc.* Vol. 32 (1984) 239

75. **C.P. Scherer, C.C. Pantano:** Titania-silica glasses using a colloidal sol-gel process *J. Non-Cryst. Sol.* 82 (1986) 246

76. **H. Salze, P. Odier, B. Cales:** Elaboration of fine micropowders from organometallic polymers precursors *J. Non-Cryst. Sol.* 82 (1986) 314

77. **M.R. Udupa:** Thermal decomposition of Cerium (IV), Cerium (III), Chromium (III) and Titanium (IV) sulphates *Thermochim. Acta* 57 (1982) 377

78. **J.C. Vignié, J. Spitz:** Chemical vapour deposition at low temperatures *J. Electrochem. Soc.* 122 (1975) 585

79. **G. Blandenet, M. Court, Y. Lagarde:** Thin layers deposited by the pyrosol process *Thin Solid Films* 77 (1981) 81

80. **K.L. Chopra, S. Major, D.K. Pandya:** Transparent conductors *Thin Solid Films* 102 (1983) 1

81. **W. Piekarczyk:** Herstellung von reinem Titandioxid, in *Reinstoffprobleme*, E. Rexer, ed., Berlin 1966, Vol. 1, p. 213

82. **H. Komiyama, T. Kanai, H. Inoue:** Preparation of porous, amorphous, and ultrafine TiO_2 particles by chemical vapour deposition *Chem. Lett.* 1984, 1283

83. **H. Meier:** *Organic Semiconductors*, Weinheim 1974, p. 235

84. **T.H. Elmer, M.E. Nordberg, G.B. Carrier, E.J. Korda:** Phase separation in borosilicate glasses as seen by electron microscopy *J. Am. Ceram. Soc.* 53 (1970) 171

85. **N. Ford, R. Todhunter:** Applications of microporous glasses, in *Glasses and Glass-Ceramics*, M.H. Lewis, ed., London 1989, p. 203

86. **M.J. Minot:** Single-layer, gradient refractive index antireflection films effective from 0.35 to 2.5 μ *J. Opt. Soc. Am.* 66 (1976) 515

87. **S.P. Mukherjee, W.H. Lowdermilk:** Gel-derived single layer antireflection films *J. Non-Cryst. Sol.* 48 (1982) 177

88. **P.A.Brugger, A. Mocellin:** Preparation of composite Al_2O_3-TiO_2 particles from organometallic precursors and transformations during heating *J. Mater. Sci.* 21 (1986) 4431

89. **T. Woignier, P. Lespade, J. Phalippou, R. Rogier:** Al_2O_3-TiO_2 and Al_2TiO_5 ceramic materials by the sol-gel process *J. Non-Cryst. Sol.*100 (1988) 325

90. **O. Yamaguchi, Y. Mukaida:** Formation and transformation of TiO_2 (anatase) solid solution in the system TiO_2-Al_2O_3 *J. Am. Ceram. Soc.* 72 (1989) 330

91. **B.E. Yoldas, T.W. O'Keeffe:** Antireflective coatings applied from metal-organic derived liquid precursors *Appl. Opt.* 18 (1979) 3133

92. **C.J. Brinker, M.S. Harrington:** Sol-gel derived antireflective coatings for silicon *Sol. Energy. Mat.* 5 (1981) 159

93. **M.F. Best, R.A. Condrate:** A Raman study of TiO_2-SiO_2 glasses prepared by sol-gel processes *J. Mater. Sci. Lett.* 4 (1985) 994

94. **B.C. Bunker, T.J. Headley, S.C. Douglas:** Gel structures in leached alkali silicate glass *Mater. Res. Soc. Symp. Proc.* Vol. 32 (1984) 41

95. **H. Izawa, S Kikkawa, M. Koizumi:** Ion exchange and dehydration of layered titanates, $Na_2Ti_3O_7$ and $K_2Ti_4O_9$ *J. Phys. Chem.* 86 (1982) 5023

96. **T.Sasaki, M. Watanabe, Y. Komatsu, Y. Fujiki:** Layered hydrous titanium dioxide *Inorg. Chem.* 24 (1985) 2265

97. **M. Tournoux, R. Marchand, L. Brohan:** Layered $K_2Ti_4O_9$ and the open metastable TiO_2 (B) structure *Progr. Sol. St. Chem.* 17 (1986) 33

98. **R.C. Mehrotra, M.M. Agrawal:** Double alkoxides of some quadrivalent metals *J. Chem. Soc.* (A) 1967, 1026

99. a) **R.A. Eppler:** Glazes and Enamels, in *Glass: Science and Technology*, D.R. Uhlmann, N.J. Kreidl, eds., Acad. Press, New York 1983, Vol. 1, p. 301

    b) **R.A. Eppler:** Crystallisation and phase transformation in TiO_2 opacified porcelain enamels *J. Am. Ceram. Soc.* 52 (1969) 89, 94

    c) **R.A. Eppler:** Microstructure of titania-opacified porcelain enamels *J. Am. Ceram. Soc.* 54 (1971) 595

100. **T. Kokubu, M. Yamane:** Preparation of porous glass-ceramics of the TiO_2 -SiO_2 system *J. Mater. Sci.* 20 (1985) 4309

101. **M. Kirsch, U. Banach:** Untersuchungen der dielektrischen Eigenschaften an Gläsern und Glaskeramiken im System $SrO-TiO_2-B_2O_3$, 28. Intern. Wiss. Koll. TH Ilmenau 1983, p. 171

102. **A. Bhargava, R.L. Snyder, R.A. Condrate:** Preparation of $BaTiO_3$ glass-ceramics in the system Ba-Ti-B-O *Mater. Lett.* 7 (1988) 185, 190

103. **Kirk-Othmer:** *Encyclopedia of Chemical Technology*, 3rd edition, Wiley, New York 1978, Vol. 4, p. 69

104. **Gmelin** *Handbuch der anorganischen Chemie*, Borverbindungen Teil 13, Springer, Berlin 1977, p. 71

105. **Gmelin** *Handbuch der anorganischen Chemie*, Borverbindungen Teil 9, Springer, Berlin 1976, p. 67, 78

106. a) **A.S. Tenney:** Nondestructive determination of the composition and thickness of thin films of pyrolytically deposited borosilicate glass by infrared absorption *J. Electrochem. Soc.* 118 (1971) 1658

b) **A.S. Tenney, J. Wong:** Vibrational sprectra of vapor-deposited binary borosilicate glasses *J. Chem. Phys.* 56 (1972) 5516

107. **E.A. Taft:** Infrared absorption of chemical vapor deposited borosilicate glass films *J. Electrochem. Soc.* 118 (1971) 1985

108. **G. Durinck, H. Poelman, P. Clauws, L. Fiermans, J. Vennik, G. Dalmai:** Observation of surface phonons on the (001) and (100) surfaces of anatase minerals *Sol. St. Com.* 80 (1991) 579

109. **H.O. Pierson:** *Handbook of chemical vapor deposition*, New Jersey 1992

110. **M. Yokozawa, H. Iwasa, I. Teramoto:** Vapor deposition of TiO_2 *Japan. J. Appl. Phys.* 7 (1968) 96

111. **C.C. Wang, K.H. Zaininger, M.T. Duffy:** Vapor deposition and characterization of metal oxide thin films for electronic applications *RCA Review* 31 (1970) 728

112. a) **R.N. Ghoshtagore:** Mechanism of heterogenous deposition of thin film rutil *J. Electrochem. Soc.* 117 (1970) 529

b) **R.N. Ghoshtagore, A.J. Noreika:** Growth characteristics of rutile film by chemical vapor deposition *J. Electrochem. Soc.* 117 (1970) 1310

113. **E.T. Fitzgibbons, K.J. Sladek, W.H. Hartwig:** TiO_2 film properties as a function of processing temperature *J. Electrochem. Soc.* 119 (1972) 735

114. **K.J. Sladek, H.M. Herron:** Titanium dioxide coatings. Room temperature deposition *Ind. Eng. Chem Prod. Res. Develop.* 11 (1972) 92

115. **M. Balog, M. Schieber, S. Patai, M. Michman:** Thin films of metal oxides on silicon by chemical vapor deposition with organometallic compounds *J. Cryst. Growth* 17 (1972) 298

116. **K.L. Hardee, A.J. Bard:** Semiconductor electrodes. The chemical vapor deposition and application of polycrystalline n-type titanium dioxide electrodes to the photosensitized electrolysis of water *J. Electrochem. Soc.*122 (1975) 739

117. a) **S. Hayashi, T. Hirai:** Chemical vapor deposition of rutile films *J. Cryst. Growth* 36 (1976) 157

b) **S. Hayashi, T. Hirai:** Intermittent chemical vapor deposition of anatase films *J. Cryst. Growth* 41 (1977) 41

c) **S. Hayashi, T. Hirai:** Effect of codeposition of Nb metal oxides on the polymorphism of chemically vapor-deposited TiO_2 *J. Cryst. Growth* 52 (1981) 269

118. **H.J. Hovel:** TiO_2 antireflection coatings by a low temperature spray process *J. Electrochem. Soc.*125 (1978) 983

119. a) **Y. Takahashi, K. Tsuda, K. Sugiyama, H. Minoura, D. Makino, M. Tsuiki:** Chemical vapor deposition of TiO_2 film using an organometallic process and its photoelectrochemical behaviour *J. Chem. Soc., Faraday Trans.* 1, 77 (1981) 1051

b) **Y. Takahashi, A. Ogiso, R. Tomoda, K. Sugiyama, H. Minoura, M. Tsuiki:** Electrical and electrochemical properties of TiO_2 films grown by organometallic chemical vapor deposition *J. Chem. Soc., Faraday Trans.* 1, 78 (1982) 2563

c) **Y. Takahashi, H. Suzuki, M. Nasu:** Rutile growth at the surface of TiO_2 films deposited by vapor-phase decomposition of isopropyl titanate *J. Chem. Soc., Faraday Trans.* 1, 81 (1985) 3117

d) **H. Minoura, M. Nasu, Y. Takahashi:** Comparative studies of photoelectrochemical behaviours of rutile and anatase electrodes prepared by OMCVD technique *Ber. Bunsenges. Phys. Chem.* 89 (1985) 1064

120. **K.S. Yeung, Y.W. Lam:** A simple chemical vapor deposition method for depositing thin TiO_2 films *Thin Solid Films* 109 (1983) 169

121. a) **L.M. Williams, D.W. Hess:** Structural properties of titanium dioxide films deposited in an rf glow discharge *J. Vac. Sci. Technol.* A 1 (1983) 1810

b) **L.M. Williams, D.W. Hess:** Photoelectrochemical properties of plasma-deposited TiO_2 thin films *Thin Solid Films* 115 (1984) 13

122. a) **T. Fuyuki, H. Matsunami:** Electronic properties of the interface between Si and TiO_2 deposited at very low temperature *Jap. J. Appl. Phys.* 25 (1986) 1288

b) **T. Fuyuki, T. Kobayashi, H. Matsunami:** Effects of small amount of water on physical and electrical properties of TiO_2 films deposited by CVD method *J. Electrochem. Soc.*135 (1988) 248

123. **S.R. Kurtz, R.G. Gordon:** Chemical vapor deposition of doped TiO_2 thin films *Thin Solid Films* 147 (1987) 167

124. **K. Kamata, K. Maruyama, S. Amano, H. Fukazawa:** Rapid formation of TiO_2 films by a conventional CVD method *J. Mater. Sci. Lett.* 9 (1990) 316

125. a) **K.L. Siefering, G.L. Griffin:** Kinetics of low-pressure chemical vapor deposition of TiO_2 from titanium tetraisopropoxide *J. Electrochem. Soc.*137 (1990) 814

b) **K.L. Siefering, G.L. Griffin:** Growth kinetics of low-pressure chemical vapor deposition of CVD TiO_2: Influence of carrier gas *J. Electrochem. Soc.*137 (1990) 1206

126. **E. Frederiksson:** *CVD of titanium oxides and aluminium oxides,* Dissertation, Uppsala 1993

127. **F. Mitschke:** Fiber-optic sensor for humidity, *Opt. Lett.* 14 (1989) 967

128. a) **W. Kern, R.C. Heim:** Chemical vapor deposition of silicate glasses for use with silicon devices *J. Electrochem. Soc.*117 (1970) 562, 568

b) **W. Kern, G.L. Schnable:** Chemically vapor deposited borophosphosilicate glasses for silicon device applications *RCA Review* 43 (1982) 423

129. **F.S. Becker, D. Pawlik, H. Schäfer, G. Standigl:** Process and film characterization of low pressure tetraethylorthosilicate-borophosphosilicate glasses *J. Vac. Sci. Technol.* B 4 (1986) 732

130. a) **Gmelin** *Handbuch der anorganischen Chemie:* Borverbindungen Teil 8, Berlin 1976, p. 34,

b) **Gmelin** *Handbuch der anorganischen Chemie:* Boron compounds 1 st Supplement Vol.1, Berlin 1980, p. 50

131. **T.M. Besmann, K.E. Spear:** Analysis of the chemical vapor deposition of titanium diboride *J. Electrochem. Soc.*124 (1977) 786, 790

132. **J.M. Benson, W.C. Baker, E. Easter:** Thermal mass flowmeter *Instruments and Control Systems* 43 (1970) 85

133. **K. Komiya, F. Higuchi, K. Ohtani:** Characteristics of a thermal gas flowmeter *Rev. Sci. Instrum.* 59 (1988) 477

134. **L.W. Winkle, C.W. Nelson:** Improved atmospheric-pressure chemical-vapor-deposition system for depositing silica and phosphosilicate glass films *Sol. St. Techn.* 24 (1981) 123

135. **A.T. Lin. P. Kleinschmit:** Production of fumed oxides by flame hydrolysis *British Ceramic Proceedings* 38 (1986) 1

136. a) **G.D. Ulrich:** Theory of particle formation and growth in oxide synthesis flames *Combustion Science and Technology* 4 (1971) 47

b) **G.D. Ulrich, B.A. Mikes, N.S. Subramanian:** Particle growth in flames. II: Experimental results for silica particles *Combustion Science and Technology* 14 (1976) 243

c) **G.D. Ulrich, N.S. Subramanian:** Particle growth in flames. III: Coalescence as a rate-controlling process *Combustion Science and Technology* 17 (1977) 119

d) **G.D. Ulrich, J.W. Riehl:** Aggregation and growth of submicron oxide particles in flames *J. Coll. Interf. Sci.* 87 (1982) 257

137. **F. Juillet, F. Lecomte. H. Mozzanega, S.J. Teichner, A. Thevenet, P. Vergnon:** Inorganic oxide aerosols of controlled submicronic dimensions *Faraday Symp. Chem. Soc.* 7 (1973) 57

138. **A.P, George, R.D. Murley, E.R. Place:** Formation of TiO_2 aerosol from the combustion supported reaction of $TiCl_4$ and O_2 *Faraday Symp. Chem. Soc.* 7 (1973) 63

139. **R.D. Maurer:** Doped-deposited-silica fibers for communications *Proc. IEE* 123 (1976) 581

140. **P.C. Schultz:** Fabrication of optical waveguides by the outside vapor deposition process *Proc. IEEE* 68 (1980) 1187

141. **G.W Scherer; P.C. Schultz:** Unusual methods for producing glasses in *Glass: Science and Technology*, D.R. Uhlmann, N.J. Kreidl, eds., Acad. Press, New York 1983, Vol. 1, p. 49

142. **C.N. Davies:** *Aerosol Science*, Acad. Press, London 1966, p. 139

143. **K. Okayama, Y. Konsaka, K. Hayashi:** Change in size distribution of ultrafine aerosol particles undergoing Brownian coagulation *J. Coll. Interf. Sci.* 101 (1984) 98

144. a) **H.M. Park, D.E. Rosner:** Boundary layer coagulation effects on the size distribution of thermophoretically deposited particles *Chem. Eng. Sci.* 44 (1989) 2225

b) **M. Tassapoulos, J.A. O'Brien, D.E. Rosner:** Simulation of microstructure / mechanism relationship in particle deposition *AIChE Journal* 35 (1989)967

145. **J.P. Dekker, P.J. van der Put, H.J. Veringa, J. Schoonman:** Gas to particle conversion in the particle precipitation aided chemical vapor deposition process *Aerosol Science* in print

146. a) **Y. Shimogaki, H. Komiyama:** Preparation of amorphous TiO_2 films by thermophoresis-aided chemical vapor deposition *Chem. Lett.* 1986, 267

b) **H. Komiyama, T. Kanai, H. Inoue:** Preparation of porous, amorphous, and ultrafine TiO_2 particles by chemical vapor deposition *Chem. Lett.* 1984, 1283

c) **F. Kirkbir, H. Komiyama:** Effects of temperature and reactant concentration on porperties of fine TiO_2 particles prepared by vapor-phase hydrolysis of titanium tetraisopropoxide *Mat. Res. Soc. Symp. Proc.* Vol. 121 (1988) 263

d) **F. Kirkbir, H. Komiyama:** Low temperature synthesis of TiO_2 by vapor-phase hydrolysis of titanium tetraisopropoxide *Chem. Lett.* 1988, 791

e) **F. Kirkbir, H. Komiyama:** Continous production of fine TiO_2 powders by vapor-phase hydrolysis of titanium tetraisopropoxide *Adv. Ceram. Mat.* 3 (1988) 511

147. **J.S. Haggerty:** Growth of precisely controlled powders from laser heated gases, in *Ultrastructure processing of Ceramics, Glasses and Composites*, L.L. Hench, D.R. Ulrich, eds., New York 1984, p. 353

148. **G.R. Rice:** Laser driven pyrolysis: Synthesis of TiO_2 from titanium isopropoxide *J. Am. Ceram. Soc.* 70 (1987) C-117

149. a) **J.J. Wu, H.V. Nguyen, R.C. Flagan:** A method for the synthesis of submicron particles *Langmuir* 3 (1987) 266

b) **K. Okuyama, Y. Kousaka, N. Tohge, S. Yamamoto, J.J. Wu, R.C. Flagan, J.H. Seinfeld:** Production of ultrafine metal oxide aerosol particles by thermal decompostion of metal alkoxide vapors *AIChE Journal* 32 (1986) 2010

c) **J.J. Wu, H.V. Nguyen, R.C. Flagan, K. Okuyama, Y. Kousaka:** Evaluation and control of particle properties in aerosol reactors *AIChE Journal* 34 (1988) 1249

d) **K. Okuyama, J.-T. Jeung, Y. Kousaka, H.V. Nguyen, J.J. Wu, R.C. Flagan:** Experimental control of ultrafine TiO_2 particle generation from thermal decomposition of titanium tetraisopropoxide vapor *Chem. Eng. Sci.* 44 (1989) 1369

150. **Y. Suyama, A. Kato:** TiO_2 produced by vapor-phase oxygenolysis of $TiCl_4$ *J. Am. Ceram. Soc.* 59 (1976) 146
151. **S.E. Pratsinis, H. Bai, P. Biswas, M. Frenklach, S.V.R. Mastrangelo:** Kinetics of titanium (IV) chloride oxidation *J. Am. Ceram. Soc.* 73 (1990) 2158
152. **G. Kasper:** Electrostatic dispersion of homopolar charged aerosols *J. Coll. Interf. Sci.* 81 (1981) 32
153. **A. Oron, J.H. Seinfeld, K. Okuyama:** The dynamic behaviour of charged aerosols *J. Coll. Interf. Sci.* 133 (1989) 57, 66, 80
154. **R.F. Gould**, ed.: *Chemical Reactions in Electrical Discharges*, Adv. in Chem. Ser. 80, 1969
155. **M. Shimada, K. Okuyama, Y. Kousaka, Y. Okuyama, J.H. Seinfeld:** Enhancement of brownian and turbulent diffusive deposition of charged aerosol particles in the presence of an electric field *J. Coll. Interf. Sci.* 128 (1989) 157
156. **W. Seifert:** Corona spray pyrolysis: A new coating technique with an extremely enhanced deposition efficiency *Thin Solid Films* 120 (1984) 267, 275
157. **W.M. Sears, M.A. Gee:** Mechanics of film formation during the spray pyrolysis of tin oxide *Thin Solid Films* 165 (1988) 265
158. **Gmelin** *Handbuch der anorganischen Chemie* Titan, Weinheim 1951, p. 97-115
159. **Ullmanns** *Encyclopädie der technischen Chemie*, Pigmente, anorganische: Weißpigmente, Weinheim 1979, Band 18, p. 569
160. **H. Freundlich, W. Kross:** Untersuchungen über Titandioxidsole *Kolloid-Zeitschrift* 52 (1930) 37
161. **Degussa:** *Hochdisperse Metalloxide nach dem AEROSIL-Verfahren*, Schriftenreihe Pigmente Nr. 56, Frankfurt 1989
162. **T.C. Patton:** *Paint Flow and Pigment Dispersion*, Wiley, New York 1979
163. **G.D. Parfitt**, ed.: *Dispersion of Powders in Liquids*, London 1981
164. **Gmelin** *Handbuch der anorganischen Chemie* Titan, Weinheim 1951, p. 264-267
165. **A. Aksay, W.Y. Shih, M. Sarikaya:** Colloidal processing of ceramics with ultrafine particles, in *Ultrastructure Processing of Advanced Ceramics*, J.D. Mackenzie, D.R. Ulrich, eds., 1988, p. 393
166. **R.H. Ottewill:** Effect of nonionic surfactants on the stability of dispersions, in *Nonionic Surfactants*, M.J. Schick, ed., London 1967, p. 627

167. **S. Fukushima, S. Kumagai:** The adsorption of nonionic ethoxylated surfactants on titanium dioxide and their dispersion effect in water *J. Coll. Interf. Sci.* 42 (1973) 539, 56 (1976) 227

168. **J.S. Clunie, B.T. Ingram:** Adsorption of nonionic surfactants, in *Adsorption from Solution at the Solid/Liquid Interface*, G.D. Parfitt, C.H. Rochester, eds., Acad. Press, London 1983, p. 105

169. **A. Hagfeldt, B. Didriksson, T. Palmquist, H. Lindström, S. Södergren, H. Rensmo, S.-E. Lindquist:** *Sol. Energy Mater.* 31 (1994) 481

170. **R. Knödler, J. Sopka, F. Harbach, H.W. Grünling:** *Sol. Energy Mater.* 30 (1993) 277

171. **H. Hahn, J. Logas, R.S. Averback:** Sintering characteristics of nanocrystalline TiO_2 *J. Mater. Res.* 5 (1990) 609

172. **M. Uchic, H.J. Höfler, W.J. Flick, R. Tao, P. Kurath, R.S. Averback:** Sinter forging of nanophase TiO_2 *Scripta Metallurgica et Materialia* 26 (1992) 791

173. *Die Oberflächenbehandlung von Aluminium,* S.Wernick, ed. Saulgau 1977, p. 197-226

174. **P.C.S. Hayfield:** Anodic oxidation of titanium in aqueous solution, in *Titanium Science and Technology,* R.I. Jaffee, H.M. Burte, eds., New York 1973, Vol.4, p. 2405

175. **D.J. Blackwood, L.M. Peter:** The influence of growth rate on the properties of anodic oxide films on titnaium *Electrochim. Acta* 34 (1989) 1505

176. **Y. Matsumoto, T. Shimizu, A. Toyoda, E. Sato:** New preparation method for doped polycrystalline TiO_2 and Nb_2O_5 and their photoelectrochemical properties *J. Phys. Chem.* 86 (1982) 3581

177. **D. Miller, S. Mamiche-Afara, M.J. Dignam, M. Moskovits:** The photoactivity of porous TiO_2 anodized at a high voltage *Chem. Phys. Lett.* 100 (1983) 236

178. **E. Smotkin, A.J. Bard, A. Campion, M.A. Fox, T. Mallouk, S.E. Webber, J.M. White:** Bipolar TiO_2/Pt semiconductor photoelectrodes and multielectrode arrays for unassisted photolytic water splitting *J. Phys. Chem.* 90 (1986) 4604

179. **F. Climent, R. Capellades:** Anodic oxidation of titanium up to 100 V *Electrochim. Acta* 33 (1988) 433

180. **H. Masuda, K. Nishio, N. Baba:** Fabrication of porous TiO_2 films using two-step replication of microstructure of anodic alumina *Jpn. J. Appl. Phys.* 31 (1992) L 1775

181. **L. Kavan, B. O'Regan, A. Kay, M. Grätzel:** Preparation of TiO_2 (anatase) films on electrodes by anodic oxidative hydrolysis of $TiCl_3$ *J. Electroanal. Chem.* 346 (1993) 291

182. **E. Matijevic, M. Budnik, L. Meites:** Preparation and mechanism of formation of titanium dioxide hydrosols of narrow size distribution *J. Coll. Interf. Sci.* 61 (1977) 302

183. **P. Comba, A. Merbach:** The titanyl question revisited *Inorg. Chem.* 26 (1987) 1315

184. **E.B. Brik, I.I. Petrova:** Determination of the various forms of adsorbed water in porous titanium dioxide films *Sov. J. Opt. Technol.* 59 (1992) 54

185. a) **H.P. Boehm, M. Herrmann:** Bestimmung des aktiven Wasserstoffs, thermische Entwässerung und Rehydroxylierung *Z. anorg. allg. Chem.* 352 (1967) 156

b) **H.P. Boehm:** Acidic and basic properties of hydroxylated metal oxide surfaces *Disc. Faraday Soc.* 52 (1971) 264

186. a) **R.E. Day, G.D. Parfitt:** Characterisation of the surface of rutile by nitrogen and water adsorption *Trans. Faraday Soc.* 63 (1967) 708

b) **P. Jackson, G.D. Parfitt:** Infra-red study of the surface properties of rutile *Trans. Faraday Soc.* 67 (1971) 2469, 68 (1972) 896

c) **G.D. Parfitt:** The surface of titanium dioxide *Progr. Surf. Membr. Sci.* 11 (1976) 181

187. a) **G. Munuera, F. Moreno, F. Gonzalez:** A model for anatase TiO_2 surface, in *Reactivity of Solids*, J.S. Anderson, M.W. Roberts, F.S. Stone, eds., London 1972, p. 681

b) **G. Munuera, , V. Rives-Arnau, A. Saucedo:** Photo-adsorption and photo-desorption of oxygen on highly hydroxylated TiO_2 surfaces *J. Chem. Soc., Faraday Trans.* 1 75 (1979) 736

c) **P. Malet, G. Munuera:** Temperature-programmed desorption studies of activated chemisorption involving a precursor state: Desorption of water from TiO_2 *J. Chem. Soc., Faraday Trans.* 1 85 (1989) 4157

188 **P. Jones, J.A. Hockey:** Infra-red studies of rutile surfaces *Trans. Faraday Soc.* 67 (1971) 2669, 2679; 68 (1972) 907

189. **M. Primet, P. Pichat, M.-V. Mathieu:** Infrared study of the surface of titanium dioxides *J. Phys. Chem.* 75 (1971) 1216

190. **A. Córdoba, J.J. Lugne:** Mechanism of surface dehydration of anatase (TiO_2) *Phys. Rev.* B 31 (1985) 8111

191. a) **J.A.R. van Veen:** An enquiry into the surface dehydration of TiO_2 (anatase) *Z. Phys. Chem. N.F.* 162 (1989) 215

b) **J.A.R. van Veen, F.T.G. Veltmaat, G. Jonkers:** A method for the quantitative determination of the basic, acidic and total surface hydroxy content of TiO_2 *J. Chem. Soc., Chem. Commun.* 1985, 1656

192. **J. Augustynski:** Aspects of photo-electrochemical and surface behaviour of titanium (IV) oxide, in *Structure and Bonding* 69, Berlin 1988, p.1

193. **J.-L. Hébrard, P. Nortier, M. Pijolat, M. Soustelle:** Initial sintering of submicrometer titania anatase powder *J. Am. Ceram. Soc.* 73 (1990) 79

194. **M. Primet, J. Basset, M.V. Mathieu, M. Prettre:** Surface and bulk reations of carbon tetrachloride with titanium dioxide *J. Phys. Chem.* 74 (1970) 2868

195. **K.H. Yoon, J.S. Kim:** Photoelectric behaviour of sintered TiO_2 electrodes *J. Phys. Chem.* 90 (1986) 6488

196. **M. Grätzel, R.F. Howe:** Electron paramagnetic resonance studies of doped TiO_2 colloids *J. Phys. Chem.* 94 (1990) 2566

197. **T.R.N. Kutty, R. Vivekanandan, P. Murugaraj:** Preparation of rutile and anatase (TiO_2) fine powders and their conversion to $MTiO_3$ (M = Ba, Sr, Ca) by the hydrothermal method *Mat. Chem. Phys.* 19 (1988) 533

198. **M.K. Nazeeruddin, P. Liska, J. Moser, N. Vlachopoulos, M. Grätzel:** Conversion of light into electricity with trinuclear ruthenium complexes adsorbed on texured TiO_2 films *Helv. Chem. Acta* 73 (1990) 1788

199. **A. Mpandou, B. Siffert:** Sodium carboxylate adsorption on TiO_2 *J. Coll. Interf. Sci.* 102 (84) 138

200. **P.F. Rossi, G. Busca:** Microcalorimetric and FT-IR spectroscopic study of the adsorption of methanol on TiO_2 (anatase) *Coll. Surf.* 16 (1985) 95

201. **Y. Suda, T. Morimoto, M. Nagao:** Adsorption of alcohols on titanium dioxide (rutile) surface *Langmuir* 3 (1987) 99

202. **G. Ramis, G. Busca, V. Lorenzelli:** Structural effects on the adsorption of alcohols on titanium dioxides *J. Chem. Soc., Faraday Trans.* 1, 83 (1987) 1591

203. **M. Primet, P. Pichat, M.-V. Mathieu:** Infrared study of the surface of titanium dioxides *J. Phys. Chem.* 75 (1971) 1221

204. **T.W. Root, T.M. Duncan:** Formic acid on titania: Characterization of adsorbed structures with ^{13}C NMR spectroscopy *J. Catalysis* 101 (1986) 527

205. **W.J. Lo, Y.W. Chung, G.A. Somorjai:** Electron spectroscopy of the chemisorption of O_2, H_2 and H_2O on the TiO_2 (100) surfaces with varied stoichiometry *Surf. Sci.* 71 (1978) 199

206. **V.E. Henrich, R.L. Kuntz:** Surface electronic structure of TiO_2 *Phys. Rev. B* 23 (1981) 6280

207. **W. Göpel, G. Rocher, R. Feierabend:** Intrinsic defects of TiO_2 (110): Interaction with chemisorbed O_2, H_2, CO, and CO_2 *Phys. Rev. B* 28 (1983) 3247

208. **K. Sakamaki, K. Itoh, A. Fujishima, Y. Gohshi:** Surface density of states of TiO_2 (110) single crystal and adsorbed molecular observation by scanning tunneling microscopy and tunneling spectroscopy *J. Vac. Sci. Technol. A* 8 (1990) 614

209. **F.-R.F. Fan, A.J. Bard:** Scanning tunneling microscopy and tunneling spectroscopy of the n-TiO_2 (001) surface *J. Phys. Chem.* 94 (1990) 3761

210. **G.E. Poirier, B.K. Hance, J.M. White:** Identification of the facet planes of phase I TiO_2 (001) rutile by scanning tunneling microscopy and low energy electron diffraction *J. Vac. Sci. Technol. B* 10 (1992) 6

211. **G.S. Rohrer, V.E. Henrich, D.A. Bonnell:** A scanning tunneling microscopy and spectroscopy study of the TiO_{2-x} (110) surface *Surf. Sci.* 278 (1992) 146

212. **K. Ravindranathan Thampi, P. Ruterana, M. Grätzel:** Low-temperature thermal and photoactivation of TiO_2-supported Ru, Rh, and Cu catalysts for CO-NO reaction *J. Catalysis* 126 (1990) 572

213. **F. Izumi, Y. Fujiki:** The polymorphic crystallization of TiO_2 under hydrothermal conditions *Bull. Chem. Soc. Japan* 49 (1976) 709

214. **H. Berger, H. Tang, F. Lévy:** Growth and Raman spectroscopic characterization of TiO_2 anatase single crystals *J. Cryst. Growth* 130 (1993) 108

215. **P. Hartman:** Structure and morphology, in *Crystal growth*, P. Hartman, ed., Amsterdam 1973, p. 367

216. **Gmelin:** *Handbuch der anorganischen Chemie*, Vol.41, Ti, p. 238

217. **S. Jijima:** Electron microscopy of small particles *J. Electron Micros.* 34 (1985) 249

218. **V. Shklover:** to be published

219. **A. Clark:** *The Chemisorptive Bond*, Acad. Press, New York 1974, p. 179

220. **T. Wolfram, S. Ellialtioglu:** Concepts of surface states and chemisorption on *d*-band Perovskites, in *Theory of Chemisorption*, J.R. Smith, ed., Berlin 1980, p. 154

221. **O. Enea, J. Moser, M. Grätzel:** Achievement of incident photon to electric current conversion yields exceeding 80 % in the spectral sensitization of titanium dioxide by coumarin *J. Electroanal. Chem.* 259 (1989) 59

222. **T.K. Sham, M.S. Lazarus:** X-ray photoelectron spectroscopy (XPS) studies of clean and hydrated TiO_2 (rutile) surfaces *Chem. Phys. Lett.* 68 (1979) 426

223. **M.P. Dare-Edwards, J.B. Goodenough, A. Hamnett, K.R. Seddon, R.D. Wright:** Sensitization of semiconducting electrodes with ruthenium-based dyes *Faraday Discuss. Chem. Soc.* 70 (1980) 285

3. Dyes for spectral sensitization

3.1. General requirements for the sensitizer

The photosensitization by organic dyes has for a long time been employed in photography to extend the spectral response of silver halides to longer wavelengths or to make them sensitive for certain colors.[1] In contrast to solar cell applications the sensitizer in a photographic film needs to undergo a single turnover only, and may be irreversibly oxidized in this process. Silver chloride single crystals sensitized with rhodamin B or cyanine dyes have also been used in a photoelectrochemical cell to create a photocurrent.[2] However, the sensitization of semiconductor electrodes was more intensively studied with oxides, such as ZnO,[3-8] SnO_2,[9-14] ITO,[15] and TiO_2.[16-25] Taking into account these studies and the experience gathered in our lab we can specify the following requirements for a dye to be used as sensitizer in a solar cell:

1. The dye should have a broad absorption spectrum, in order to capture as much of the solar radiation as possible. Up to now, a single dye has usually been used for sensitization, since a combination of different dyes on the same semiconductor surface often involves complications, such as energy or electron transfer from one dye to the other. Fortunately, there are dyes, especially ruthenium complexes, that absorb throughout the visible spectrum. Since more than 50% of the solar energy is emitted in the region from 400 to 800 nm,[26] such a dye allows to capture most of the sunlight. In fact, a further shift of the absorption edge to longer wavelengths would cause a loss in photovoltage that is not fully compensated by the gain in photocurrent, so that the energy

conversion efficiency of the solar cell would decrease. It has been shown by purely thermodynamic arguments, that the theoretical efficiency of a single-band gap quantum converter under AM 1.2 solar radiation has a broad maximum for an absorption edge around $\lambda = 840$ nm.[26]

2. The extinction coefficient of the dye should be high over the whole absorption spectrum, to absorb most of the light with a minimum of dye. Although the optical density of the electrode could be enhanced by increasing its thickness, this would deteriorate the photovoltage by increasing the dark current and might cause diffusion problems in the electrolyte at high current densities. The extinction coefficient in the absorption maximum is less important than that in the weaker absorbing regions, since these limit the white light harvesting efficiency.

3. The excited state of the dye must energetically lie above the conduction band edge of the semiconductor, to guarantee fast electron injection. Unless extremely fast hot electron injection occurs, the energy of the injecting state is that of the lowest, vibrationally relaxed excited state. Its energy is given by the ground state oxidation potential plus the excitation energy, which is approximately obtained from the wavelength of luminescence onset. Dyes containing heavy metal centers like Ru^{2+} or paramagnetic metal ions like Cu^{2+} exhibit a very fast intersystem crossing and inject from the triplet state. This represents a loss of several 100 meV in excitation energy, that should better be avoided.

4. The excited state lifetime of the dye must be long enough for efficient electron injection. In general this seems not to be a limiting factor, since electron injection occurs on the subnanosecond timescale and thus can compete efficiently with other excited state decay processes, which, according to the emission lifetimes, take usually much longer. Only dyes with extremely short excited state lifetimes show decreased injection yields. For example certain Fe^{3+} complexes, such as the prosthetic group of hemoglobin (hemin or Fe^{3+}-protoporphyrin IX), exhibiting decay times in the femtosecond range, do not inject, while the free base analogs and even the nonfluorescent Cu^{2+} complexes give high photosensitization quantum yields (chapter 3.4).

5. The oxidized dye must have a more positive potential than the redox couple in the electrolyte. In order to prevent recombination of the injected electron with the oxidized dye, the latter has to be quickly regenerated by the

redox electrolyte, which requires a certain driving force. On the other hand, the redox potential of the electrolyte should be rather positive, since it determines the potential of the counter electrode and thus the photovoltage of the cell. However, the oxidation potential of the dye is restricted by the requirement of a high enough excited state potential (point 3), which again involves the cutoff wavelength of light absorption (point 1).

6. The dye needs attaching groups for adsorption on the semiconductor surface and possibly as bridges for electron injection. Since diffusional encounter is too slow compared to the excited state decay of most dyes, physi- or chemisorption on the semiconductor surface is necessary. Due to the strong distance dependence of electron transfer rates the electronically excited orbitals of the dye should be as close to the substrate as possible. Electron injection can be enhanced further by covalent bonds, especially by a π-system in conjugation with the chromophore.

7. The dye should be soluble in some solvent for adsorption on the electrode, and should not be desorbed by the electrolyte. Adsorption from solution is still the most practical way of dye application, since it does not require high temperatures (in contrast to evaporation) and normally gives just a monolayer. Coadsorbates can easily be added to decrease the coverage or insulate the space between dye molecules. However, solubility and strong adsorption are somewhat conflicting requirements and the solvent may itself undergo reactions with the activated semiconductor surface. The dye must of cause not be desorbed by the electrolyte, which in most cases excludes the use of highly eluotropic solvents like water.

8. The dye has to be stable on a long term. This is a very demanding quality, since a minimum lifetime of 20 years, as required for solar cells in power applications, implies enormous turnover numbers, which the dye must undergo without decomposition. For example, a dye with an average extinction coefficient of $\varepsilon = 5000\ M^{-1}cm^{-1}$ in its visible absorption spectrum has a light capture cross section of $\sigma = \varepsilon/N_A = 8 \cdot 10^{-22}\ m^2$. In full sunlight of 1000 W/m^2 there are about $1.5 \cdot 10^{21}$ photons/s·m^2 in the visible range. Hence a dye molecule in the top layer of the solar cell absorbs approximately one photon each second. The total annual sunlight in Europe amounts to around 900 kWh/year·m^2 (Figure 1), half of which is in the visible region and can be absorbed by the dye. This corresponds to ca. $5 \cdot 10^{27}$ photons/year·m^2 and means, that a dye molecule in the topmost layer of the solar cell has to undergo some 10^8

turnovers in 20 years. If the dye is to survive this time, all side reactions leading to the irreversible destruction of the dye must have a quantum yield below 10^{-8}. Up to now only ruthenium complexes have proved such an exceptional stability.[19] o This is in part due to the presence of ruthenium as internal redox couple, changing its oxidation state from Ru^{2+} to Ru^{3+} on electron injection. Most other dyes are oxidized to a π-radical, which is in general highly reactive, especially towards proton acceptors or oxygen. In this case, the long term stability of the sensitizer depends critically on the purity of the electrolyte and the hermetic sealing of the cell.

9. The price of the dye it is not expected to be a limiting factor, since only about one gram is needed per square meter of solar cell. For example, if 90% of the light is to be absorbed (equivalent to an optical density of A = 1) with a dye of decadic extinction coefficient $\varepsilon = 10^4\ M^{-1}cm^{-1}$ (which is asking a lot for spectral regions outside the absorption maximum), the loading must be $\Gamma = A/\varepsilon = 10^{-3}\ mol/m^2$. For a typical ruthenium dye of molecular mass $m \approx 1000$ g/mol this corresponds to 1 g/m^2. Even the precious metal ($m \approx 100$ g/mol or 0.1 g/cm^2) would not represent a significant contribution to the overall costs of the solar cell. The amount of dye needed for efficient light harvesting can be minimized further by increasing the effective optical thickness of the dye coated layer taking advantage of multiple light scattering in combination with a reflecting counter electrode.

A completely different approach is the use of a second semiconductor with narrow bandgap for sensitization of the TiO_2. This resembles a classical heterogeneous p-n-junction, although an electric field for charge separation cannot build up on the nanometer scale of the colloidal particles. For example, nanoporous TiO_2 films have been sensitized with pyrite (FeS_2), which has a very high extinction coefficient and injects up to 900 nm, although with rather low quantum efficiency.[27] Semiconductors having a too positive conduction band edge to inject into TiO_2, such as PbS, often become sensitizers in the form of quantum size particles, exhibiting a wider band gap than in the bulk state.[28] They are intermediate between molecular dyes with absorption bands due to HOMO (highest occupied molecular orbital) - LUMO (lowest unoccupied molecular orbital) excitation and bulk semiconductors with an absorption edge due to valence band - conduction band excitation. From this point of view there is no fundamental difference between a dye molecule and a semiconductor cluster, and the requirements listed above are still applicable.

A p-type semiconductor as sensitizer might be advantageous if it could be used as solid hole conductor at the same time, replacing the redox electrolyte. However, this would require filling of the pores of the TiO_2 film above the percolation limit and an ohmic back contact with the narrow band gap semiconductor only. The situation would still be different from classical heterogeneous p-n-junctions, such as in the Cu_2S/CdS cell, due to the much higher interfacial surface area and the virtual absence of band bending in the nanometer size particles. The practical realizability of such an interpenetrating p-n-junction and its possible advantages remain to be scrutinized..

Instead of passing from bulk inorganic semiconductors to Q-particles and clusters one can also proceed from single dye molecules to organic polymers with semiconductor properties.[29-31] Organic photoconductors are already widely employed in photocopying machines based on the Xerox process. It would be interesting to use the organic semiconductors as both sensitizer and hole conductor in an all solid state solar cell. The polymer may be grown *in situ*, e.g. electrochemically from the SnO_2 substrate through the porous TiO_2 film to the surface. However, the electrical contact with the conducting glass substrate would have to be broken afterwards, because it represents a short circuit. Another ohmic contact with the polymer only has to be made on the other side, e.g. by evaporation of a metal. This poses practical problems, since any pinhole in the coating would cause short circuiting of the solar cell.

Some conducting polymers like polyaniline are soluble in the presence of suitable counterions and might as such penetrate into the pores of the TiO_2 film. Preliminary experiments with polyaniline solubilized by camphor-10-sulfonic acid in chloroform [32] yielded in fact green electrodes and photocurrent efficiencies of IPCE $\approx$ 5% at 470 nm with I^-/I_3^- as redox couple. The photovoltage was close to zero, indicating an internal short circuit. It is difficult to imagine that a long chain polymer threads into the tortuous nanopores of the TiO_2 layer. Presumably the coloration was rather due to aniline oligomers present in the solution. Still, this result shows that sensitization with organic semiconductors is possible and may be worthwhile to be studied more systematically.

3.2. Experimental set-up for the acquisition of photocurrent action spectra

For the characterization of a new dye as sensitizer its photocurrent action spectrum is most revealing, since it represents the incident photon to current conversion efficiency (IPCE) as a function of wavelength. By convolution with the emission spectrum of a polychromatic source like the sun the total expected photocurrent can be calculated. This avoids the uncertainty due to the spectral distribution of a white light source, such as a Xenon lamp, which depends on so many parameters and is difficult to standardize. Still, the performance of the complete cell has to be tested under full white light illumination with a solar simulator to evaluate its energy conversion efficiency.

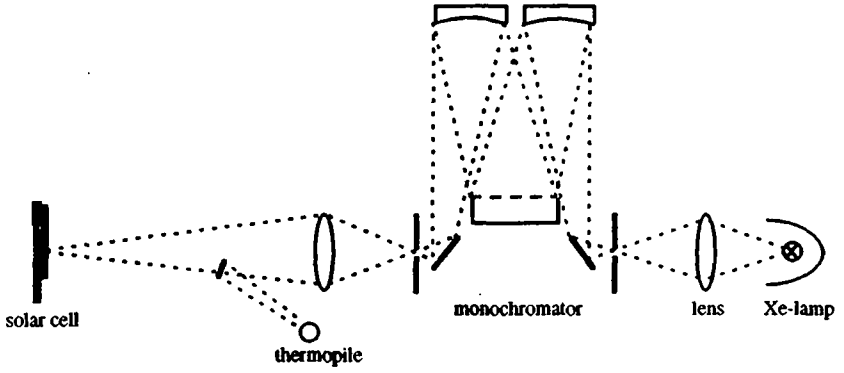

Figure 30: Illumination system for the measurement of photocurrent action spectra

The measurement of photocurrent action spectra requires a monochromatic light source illuminating uniformly the photoelectrode. In our set-up (figure 30) we use a Xenon lamp with ellipsoidal reflector (Cermax 300 W), which is focused onto the entrance slit of a high intensity monochromator (Kratos GM 252, blaze wavelength 300 nm, spectral bandwidth $\Delta\lambda$ = 10 nm). An enlarged image of the exit slit is projected onto the photoelectrode, which is wetted with electrolyte and clamped against a reflecting platinum foil counter electrode. The back contact with the SnO_2 substrate is made by a second platinum foil in plane with the first one. Part of the light beam is reflected by a surface mirror onto a fast thermopile (model 2M with quartz window of Laser Components GmbH, Germany), in order to measure the light intensity. Its signal is amplified by a chopper stabilized operational amplifier and fed together with the short-circuit

photocurrent of the electrode to be tested into an analog divider. A potentiometer attached to the monochromator gives a voltage proportional to the wavelength and is also connected to the analog divider, so that its output is directly proportional to the number of electrons divided by the number of incident photons:

$$\mathrm{IPCE} = \frac{n_{\mathrm{electrons}}}{n_{\mathrm{photons}}} = \frac{I/e}{P/h\nu} = \frac{I}{P} \cdot \frac{hc}{e\lambda} = \frac{I}{P} \cdot \frac{1240}{\lambda[\mathrm{nm}]} \quad \text{with} \quad \begin{array}{l} I = \text{photocurrent in A/m}^2 \\ P = \text{light power in W/m}^2 \end{array}$$

The absolute ICPE is obtained by measuring the light intensity with a calibrated radiometer (YSI model 65 A). During scanning of the monochromator with a motor the IPCE is registrated on the Y-scale of an X-Y-recorder, while the potentiometer attached to the monochromator gives the wavelength for the X-axis. The thus obtained action spectra exhibit artificial peaks around 470 nm, due to peaks in the xenon lamp spectrum, and at 680 nm, due to a sudden change in the monochromator efficiency (Wood's anomaly). They were taken into account by measuring the action spectrum of 1 cm^2 single crystalline silicon photodiode (no. 303-674 of RS Components, England) under the same conditions.

Photocurrent / voltage curves were obtained with the same illumination set-up, but the voltage of the photoelectrode was scanned with respect to the platinum counter electrode with a potentiostat in a two electrode configuration (Thompson precision potentiostat 251). For white light illumination the monochromator was turned into the zero diffraction order. Light below 360 nm and above 760 nm was removed by a bandpass filter (Schott type 113). This results only in a very crude simulation of sunlight, because the monochromator, even in its zero order, still changes the spectrum of the xenon lamp. The conversion efficiency was therefore determined with a solar simulator (Oriel model 81172), corresponding to AM 1.5 global solar radiation.

3.3. Ruthenium complexes as sensitizers

Transition metal charge transfer complexes have for a long time been investigated as sensitizers, especially for the photodecomposition of water into hydrogen and oxygen. Some of the most successful dyes are tris(2,2'-bipyridine)ruthenium(II) [$Ru(bpy)_3^{2+}$] and its derivatives.[33] They exhibit strong metal to ligand charge transfer (MLCT) bands in the visible spectrum. The singlet excited state undergoes rapid ($\tau << 1$ ns) deactivation to the lowest excited state of triplet character, due to the presence of the heavy Ru atom. The excited dye is both a stronger oxidant and reductant than in the ground state and usually sufficiently long lived to undergo electron transfer reactions even in homogeneous solution. Ru(II) bipyridine complexes have also been used for the sensitization of semiconductor electrodes, such as SnO_2[9b,11] and TiO_2,[16,18,20] as well as colloidal particles.[19b,d,22] However, significant solar energy conversion efficiencies were first achieved with the advent of polycrystalline TiO_2 films of high surface area.[19e-h,k,l,n,o,22-25]

The very first sensitizer for nanoporous TiO_2 electrodes was the carboxylated $Ru(bpy)_3^{2+}$ analog tris(2,2'-bipyridyl-4,4'-dicarboxylate)ruthenium(II) dichloride (furtheron called RuL_3), which, contrary to $Ru(bpy)_3^{2+}$, adsorbs strongly on the TiO_2 surface and shows more than ten times higher electron injection efficiency.[19e,h,l,23] The dye was adsorbed from slightly acidic water ($2 \leq pH \leq 5$), resulting in electrostatic attachment of its deprotonated carboxyl groups to the protonated hydroxyl groups on the TiO_2 surface. With 0.1 M KI in aqueous 1 mM $HClO_4$ (pH 3) as redox electrolyte $IPCE_{470nm}$ = 73% was reported.[19h] We have repeated the experiment with P 25 electrodes and nonaqueous electrolyte, in order to compare the photocurrent action spectrum of RuL_3 with other Ru(II)bipyridine derivatives (Figure 31b).

RuL_3 exhibits a maximum IPCE = 68% around 470 nm. The response below λ = 420 nm is due to band gap excitation of the TiO_2 itself (P 25 contains 30% rutile with E_g = 3.0 eV), as seen by comparison with the non sensitized electrode (Figure 31a). Although a tail of the dye spectrum extents beyond 700 nm, the light harvesting efficiency drops quickly above 500 nm, resulting in low white light conversion efficiencies. This situation was improved by replacing one of the bipyridine ligands with water, yielding *cis*-diaquabis(2,2'-bipyridyl-4,4'-dicarboxylate)-ruthenium(II) [$RuL_2(H_2O)_2$].[19g]

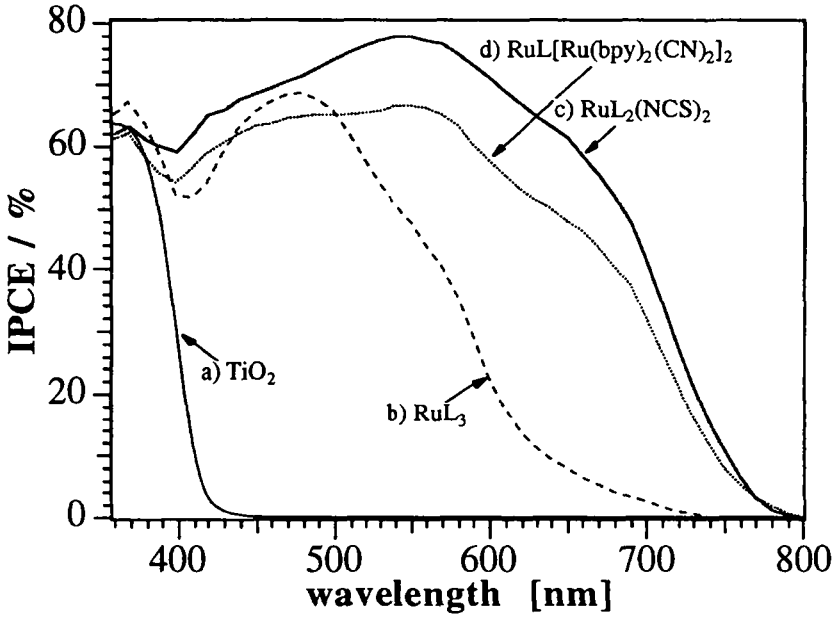

Figure 31: Photocurrent action spectra of TiO_2 electrodes (12 µm P 25) sensitized with different Ru(II) bipyridine complexes, electrolyte: 80% ethylene carbonate, 20% propylene carbonate, 0.5 M KI, 40 mM I_2, **a)** bare TiO_2 electrode, **b)** RuL_3 (L = 2,2'-bipyridine-4,4'-dicarboxylate) adsorbed from water, pH 4.8, **c)** $RuL_2(NCS)_2$ and **d)** $RuL_2[Ru(bpy)_2(CN)_2]_2$ adsorbed from ethanol

A further drastic improvement was achieved by replacing the water ligands with thiocyanate to give *cis*-di(thiocyanato)bis(2,2'-bipyridyl-4,4'-dicarboxylate)-ruthenium(II) $[RuL_2(NCS)_2]$.[19] The maximum of the photocurrent action spectrum is red shifted to 540 nm and a strong shoulder extends up to 800 nm (Figure 31c). While the dyes mentioned before are not soluble in ethanol and had to be adsorbed from water at pH 3-5, resulting in rehydroxylation of the TiO_2 surface and purely electrostatic attachment of the dye, $RuL_2(NCS)_2$ can be adsorbed from ethanol. This is supposed to result in covalent binding of the carboxyl groups to coordinatively unsaturated Ti^{4+} centers on the TiO_2 (chapter 2.4.5) and seems to contribute to the higher electron injection efficiencies. Also the photovoltage is higher after adsorption from neutral ethanol (U_{oc} = 500 mV) than from water of pH 4.8 (U_{oc} = 430 mV), due to the positive shift of the

semiconductor conduction band edge by surface protonation in the presence of acid.

Another reason for the high efficiency of this dye may be the presence of the pseudohalogenide ligand NCS^- as internal redox couple, which may transfer negative charge to the Ru^{3+} center resulting from electron injection. The consequent reduction by iodide is expected to be faster than with other ligands, because the NCS-ligand may act as a bridge for electron transfer. At least it does not hinder the approach of the rather large I^- ion to Ru^{3+} as much as bipyridine does. Since the charge separation efficiency depends on the competition between reduction of the oxidized dye by iodide and its recombination with the injected electron fast reduction is crucial for obtaining high efficiency.

The extinction coefficient of the dye can be increased and its absorption spectrum broadened by a peripheral antenna unit which absorbs at short wavelengths and transfers its energy to the central unit absorbing at longer wavelength. This is easily achieved by linking different Ru(II)bipyridine complexes with bridging ligands, such as a cyano group. Figure 31d shows the action spectrum of the trinuclear ruthenium complex $RuL_2[\mu\text{-}(CN)Ru(CN)L'_2]_2$ (L = 2,2'-bipyridine-4,4'-dicarboxylic acid, L' = 2,2'-bipyridine) on TiO_2.[19k,24] The spectrum resembles that of $RuL_2(NCS)_2$ (Figure 31e), although the maximum efficiency is somewhat lower ($IPCE_{540}$ = 67% compared to 78%). This is partially compensated by a higher open circuit voltage (U_{oc} = 530 mV compared to 500 mV).

We conclude, that nothing has been gained by the antenna units having their absorption maximum at λ = 478 nm in ethanol,[19k] since even the mononuclear dye has a sufficiently high extinction coefficient in this region to absorb nearly all of the incident light. As discussed in chapter 3.1 (requirement 2) it is rather the extinction coefficient in the weakly absorbing region which determines the overall light harvesting efficiency. Figure 31c indicates that a further increase in photocurrent may be achieved by improving the light absorption above λ = 650 nm. However, this requires a dye with lower excitation energy and would either result in lower electron injection efficiency or smaller photovoltage. Hence, with regards to its action spectrum the sensitizer $RuL_2(NCS)_2$ seems to be pretty well optimized. Only a combination of different dyes on separate electrodes would open new frontiers, but such a multiple bandgap device is beyond the scope of the present work.

Numerous other ruthenium (II) complexes have been synthesized and tested. Usually carboxyl groups served for attachment on the TiO_2 surface, but they are easily displaced by water. The more strongly binding phosphonate group has only recently been introduced. In this case a single attachment group is sufficient for adsorption on TiO_2. The sensitization efficiencies with non-aqueous electrolyte are quite promising, however they diminish again drastically in the presence of water. Since the titanium chelating phosphonate group is not expected to be displaced by water other factors, such as the creation of new surface states on TiO_2, a change in the reorganization energy of dye and redox couple or the protonation equilibrium of the phosphonate group may be responsible for the decreased electron injection yield.

In general there are many factors which determine the performance of the dye sensitized solar cell and the optimum conditions established for one dye are not necessarily the same for another dye. Moreover, impurities in the dye solution can strongly impair the sensitization efficiency. For example, we observed very poor sensitization with dye solutions made with ethanol that had been stored in a polyethylene bottle. By UV-spectroscopy and thin layer chromatography we found that an antioxidant present in polyethylene had been leached out by the ethanol. These antioxidants are sterically hindered phenols like 2,6-di-tert-butyl-4-methylphenol (BHT),[34] which react with oxygen under formation of peroxides:

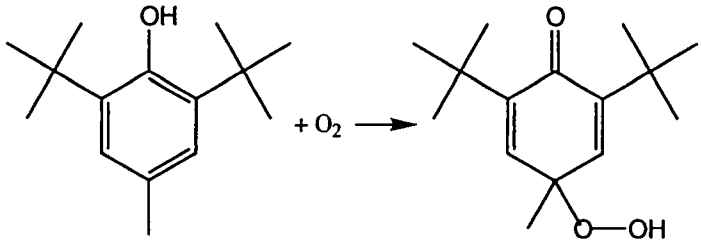

The peroxy group may adsorb on TiO_2 and in fact a colloidal TiO_2 electrode dipped into ethanol which had been stored in a polyethylene bottle developed a yellow color. The benzochinone adsorbed next to the dye molecule may either quench the excited sensitizer or recombine with the injected electron, which is a possible explanation for the decreased sensitization efficiency. Since the dye concentration is less than 1 mM small amounts of impurities in the solvent or on the glass ware may have a detrimental effect. However, the main source of impurities is probably the dye preparation itself, and it may well be that some dyes were judged inefficient just because of these impurities.

3.4. Chlorophyll derivatives and related natural porphyrins

3.4.1. Introduction

Chlorophyll is the oldest and most important photosensitizer on earth, since it constitutes the basis of natural photosynthesis. By converting sunlight into chemical energy photosynthesis provides the ultimate source of energy for nearly all forms of life. Even the fossil fuels coal, oil and gas, which we are about to consume within just a few decades, are the result of photosynthetic activity several 100 million years ago. The high efficiency of charge separation in the photosynthetic reaction center is still intriguing and an example for any artificial solar energy converter. In view of the great importance of chlorophyll it was obvious to test this natural dye also as a sensitizer for nanoporous TiO_2 electrodes.[35]

The sensitization of TiO_2 electrodes with Zn-tetracarboxyphenylporphyrin has already been reported.[23,36] The photosensitization of a wide bandgap semiconductor (ZnO) by chlorophylls was first investigated by Tributsch and Calvin.[37] Although quantum efficiencies of up to 0.125 electrons per absorbed photon were achieved in the presence of phenylhydrazine as sacrificial electron donor, the measured photocurrents were extremely small ($5 \cdot 10^{-6} A/cm^2$ under monochromatic illumination of unspecified intensity) due to the small light harvesting efficiency of a dye monolayer on the semiconductor crystal. Chlorophyll monolayers were also deposited on SnO_2 optically transparent electrodes by means of the Langmuir-Blodgett technique and the effect of different metal centers investigated.[38] Quantum efficiencies of up to 0.3 were reported. Much lower efficiencies result by simply dipping a SnO_2 electrode into a metallochlorophyll containing electrolyte solution.[39] The photosensitization of colloidal TiO_2 by copper chlorophyllin has been analyzed using fluorescence quenching, flash photolysis and microwave absorption by Kamat et al.[40] Their results will be compared with our experiments on fluorescence and transient absorption of Cu-chlorophyllin sensitized TiO_2 electrodes in chapter 3.5. Recently photosystem II particles were immobilized on a ruthenium dye sensitized TiO_2 electrode in order to transfer electrons from water to the oxidized dye.[41]

3.4.2. Experimental

Preparation of TiO_2 electrodes. Nanostructured TiO_2 films were prepared by spreading a colloidal TiO_2 (P 25) dispersion on SnO_2 conductive glass as described in chapter 2.3.13. Thus obtained films of 12 μm thickness are only translucent and scatter light strongly especially at short wavelengths. Therefore transparent films of 7 μm thickness were prepared [19n] for optical studies and treated with aqueous $TiCl_4$ solution as described in chapter 2.4.3.

Chlorophyll derivatives. Chlorophyll *a* was obtained from Sigma. A mixture of chlorophylls *a* and *b* was extracted from spinach with methanol and partially purified by precipitation with dioxane/water.[42] Treatment of a diethyl ether solution of the mixture with dilute HCl gave the magnesium-free pheophytins. The hydrolysis of the phytyl ester bond with HCl gave pheophorbides *a* and *b*, which were separated by extraction with diethyl ether at their respective HCl numbers.[43] Mg-chlorin e_6 was prepared by saponification of chlorophyll.[44] Chlorin e_6 trimethylester was obtained by transesterification of pheophytin *a* with $NaOCH_3$ in THF.[45] Copper was introduced into the ester in diethyl ether solution by addition of cupric acetate saturated acetic acid. Saponification of the trimethylesters with hot KOH in methanol gave free base and Cu-chlorin e_6. Cu-2-α-oxymesoisochlorin e_4 was isolated from commercial Cu-chlorophyllin (Merck, K&K or Sigma) by extraction of an aqueous solution with 1-butanol and column chromatography on silica gel with toluene/acetic acid (10:1).

Porphyrins. Mesoporphyrin IX dimethylester was obtained from Sigma. Copper was inserted in benzene solution from cupric acetate saturated acetic acid (several days at room temperature).[46] Zinc was introduced in acetone solution from zinc acetate saturated methanol (2 minutes under reflux). The esters were hydrolyzed in acetone with KOH/methanol under reflux.

The purity of all dyes was checked by thin layer chromatography on silica gel with water/1-butanol/acetic acid (50:50:1, upper phase) as eluent.

Dye adsorption and cell assemblage. The TiO_2 electrodes (1 cm^2 active surface area) were fired 30 minutes at 550°C in air and dipped still hot (≈ 80°C) in 1 ml of an ethanolic solution of the dye (≈ $5 \cdot 10^{-5}$ M) and any coadsorbate. After at least 5 hours of soaking the electrode was dried in a stream of dry air, wetted immediately with electrolyte (0.5 M KI, 40 mM I_2 in 80% ethylene carbonate, 20% propylene carbonate) and pressed against a platinum foil counter electrode.

3.4.3. Photocurrent action spectra

Chlorophyll. Chlorophyll *a* (Figure 32a) does not adsorb efficiently on TiO_2 from solvents like ethanol, acetone, THF or pyridine, due to the weak interaction of its ester and keto carbonyl groups with the hydrophilic oxide surface. However it does adsorb from less polar solvents like diethyl ether or hexane. The photocurrent action spectrum (Figure 32a) shows peaks corresponding to the absorption spectrum in solution, but the photocurrent rises earlier below 500 nm. The Q_y band, which corresponds to the lowest excited singlet state, is strongly broadened and red shifted. This may be caused by interaction with the polar TiO_2 surface as well as by aggregation of the chlorophyll [47] due to its high concentration on the electrode. The sharp rise below 400 nm is due to band gap excitation of the TiO_2 itself, as seen by comparison with an unsensitized electrode (Figure 32a).

The photocurrent efficiency is low, e.g. $IPCE_{670} = 3.5\%$ in spite of an optical density $A_{670} = 0.3$ for the electrode of Figure 32a. Since the transmitted light is reflected by the platinum counter electrode and traverses the electrode a second time, the effective absorbance is $A_{670} = 0.6$, corresponding to 75% light absorption in the red peak. Without addition of pyridine to the chlorophyll *a* solution in ether the IPCE is even lower, possibly due to enhanced dye aggregation, which can be reduced by an axial magnesium ligand like pyridine.[48]

Pheophytin, the free base of chlorophyll, shows similar low adsorption and photosensitization behavior on TiO_2.

Pheophorbide. Hydrolysis of the phytyl ester bond of pheophytin results in a free carboxyl group (Figure 32b) and thus in a much stronger adsorption on TiO_2 allowing adsorption from ethanol. The photocurrent action spectrum of pheophorbide *a* corresponds to its absorption spectrum in solution, which resembles the spectrum of pheophytin *a*, but the peaks are red shifted by about 10 nm. The optical density of the electrode in the Q_y band was $A_{675} = 0.7$ corresponding to 96% light absorption in the red peak, including the effect of the reflecting counter electrode. At $\lambda = 630$ nm the electrode had an absorbance of $A_{630} = 0.21$ resulting in still 62% light harvesting at this wavelength. This explains the reduced peak ratio in the action spectrum as compared to the absorption spectrum. Without addition of deoxycholic acid to the dye solution the coloration was even stronger, however, the photocurrent efficiency was actually smaller.

In spite of 96% light absorption only 25% of the incident red photons produce an electron flowing in the external circuit. The quantum efficiency (electrons per

absorbed photon) is slightly higher, since some of the incident light is already lost by reflection from the electrode surface. It reaches the highest value reported so far for the sensitization of a semiconductor by a chlorophyll derivative,[38] yet is far behind the nearly unity efficiency of primary charge separation in natural photosynthesis. It may be argued that the propionic acid side chain of pheophorbide is not a useful group for attachment on TiO_2, since it presents an insulating barrier for electron injection from the excited dye molecule into the conduction band of TiO_2. We therefore investigated chlorophyll derivatives which have a carboxyl group in conjugation with the π electron system of the tetrapyrrole macrocycle.

Chlorophyllin. Alkaline hydrolysis of chlorophyll not only saponifies the phytyl ester bond but also opens the cyclopentanone ring with formation of two additional carboxyl groups (Figure 32c). Chlorophyllin *a*, which is the Mg-complex of chlorin e_6, therefore adsorbs well on TiO_2. The absorption spectrum in ethanol depends strongly on the pH of the solution. As prepared the three carboxyl groups are dissociated and the absorption maxima lie at 418, 522, 602 and 645 nm. In contrast to chlorophyll, the Q_y band is much weaker than the Soret band, due to opening of the cyclopentanone ring. The fluorescence is strong with maxima at 654 and 705 nm. Protonation of the carboxyl groups with excess acetic acid or deoxycholic acid results in a shift of the Q_y band to 657 nm, while the other bands are only weakly red shifted (422, 528, 570 and 610 nm). However, the spectrum changes further with time, giving rise to a 688 nm peak, a Soret band shifted to 428 nm with a shoulder at 382 nm and new peaks at 586 and 644 nm. The fluorescence is about half as strong and shifted to 702 and 758 nm. Addition of base reverts the spectrum to that of the starting salt within a few minutes. This behavior has been ascribed to dimerization of the unionized chlorophyllin causing a bathochromic shift of the Q_y band by exciton interactions,[44,49] although this explanation has been called in question by others.[50] A chlorophyll dimer with red shifted Q_y band also constitutes the special pair in the reaction center of photosynthetic bacteria and green plants.

The highest photosensitization efficiencies are obtained after adsorption from a solution containing 20 mM deoxycholic acid (Figure 32c). The action spectrum shows contributions from all spectral forms of chlorophyllin *a* (the shoulder at 450 nm is due to chlorophyllin *b*). The efficiency at 688 nm is low, although this is the main solution species in the presence of acid.
Without deoxycholic acid the electrode is much more strongly colored and the action spectrum corresponds to the deprotonated species, but the efficiency is poor (7% at 648 nm). Addition of pyridine in order to prevent aggregation of the

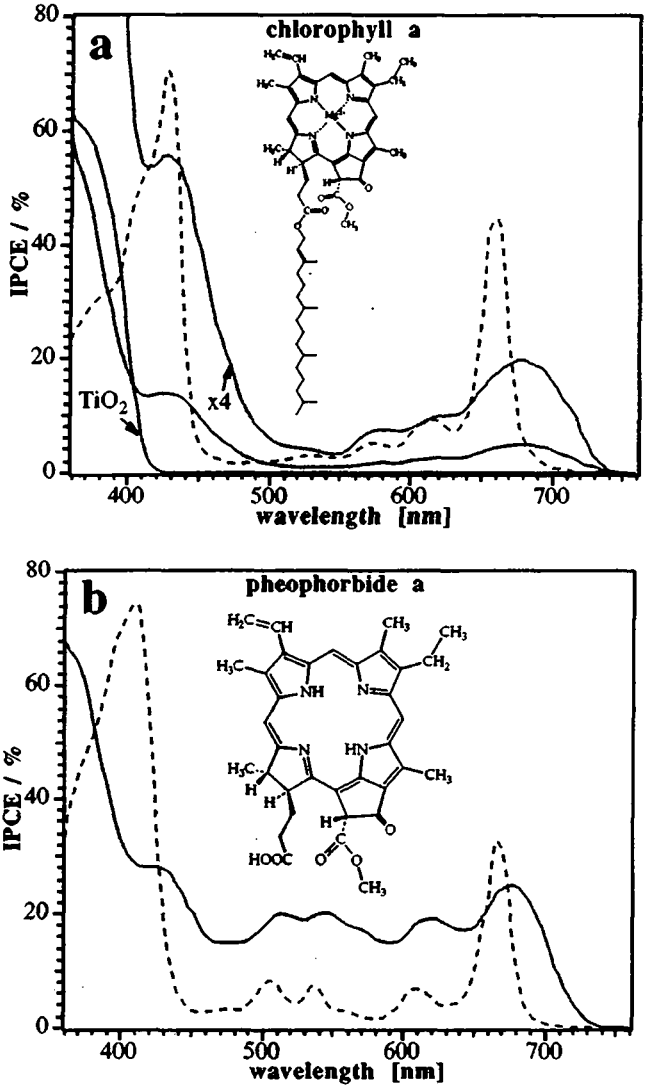

Figure 32: Photocurrent action spectra of TiO_2 (12 µm P25) electrodes sensitized with chlorophyll derivatives (solid lines) and absorption spectra of the dyes in solution (dashed lines); IPCE = incident photon to current efficiency

a) chlorophyll *a* adsorbed from diethyl ether containing 0.1 M pyridine; upper curve enlarged 4 times; curve on the left: photoresponse of the TiO_2 electrode without sensitizer

b) pheophorbide *a* / ethanol + 2 mM deoxycholic acid

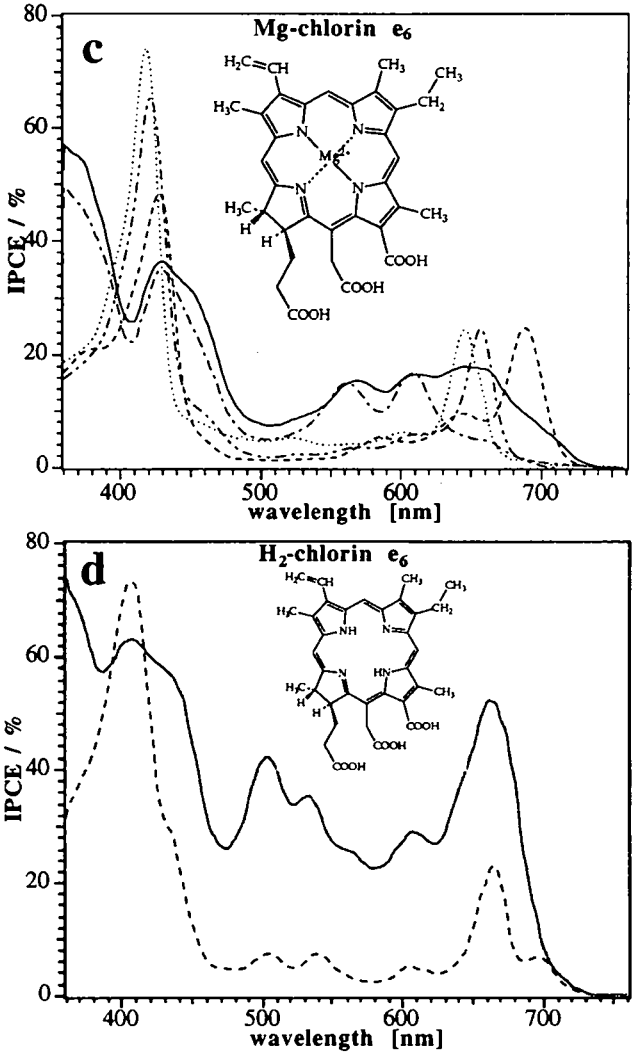

c) Mg-chlorin e_6; absorption spectra in ethanol: (·····) deprotonated form, (— - - —) immediately after addition of 5 mM acetic acid, (- - - - -) after 24 hours; action spectra after adsorption from ethanol containing 20 mM (———) and 100 mM (— - —) deoxycholic acid, respectively.

d) H_2-chlorin e_6 / ethanol + 20 mM deoxycholic acid

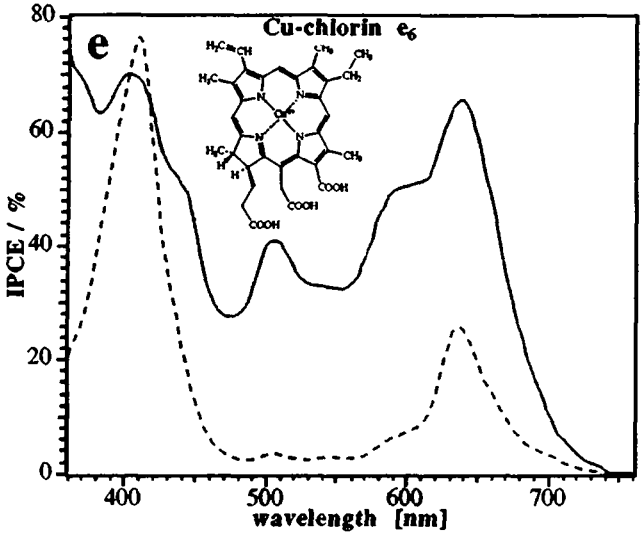

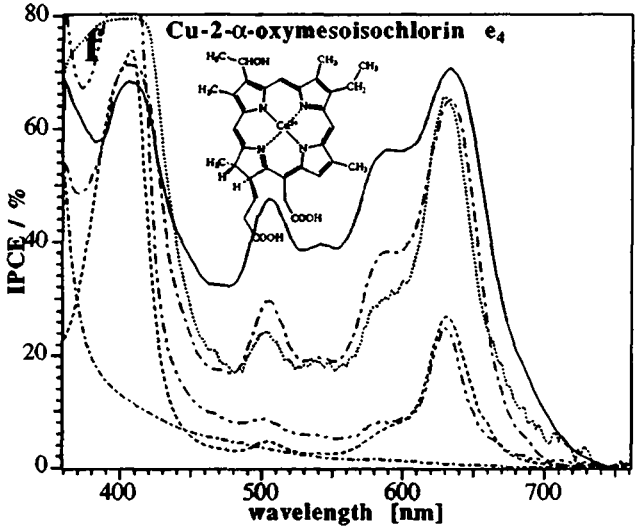

e) H_2, Cu-chlorin e_6 / ethanol + 20 mM deoxycholic acid

f) Cu-2-α-oxymesoisochlorin e_4 / ethanol + 100 mM deoxycholic acid; absorption spectra: (- - - - -) in ethanol, (— - - —) on a transparent TiO_2 electrode (thickness 7 µm, A_{630} = 0.91), (- · - · -) same electrode without sensitizer; (·····) percentage of light absorbed by the dye on the transparent TiO_2 electrode (vertical scale 0 to 100 %); (— - —) action spectrum of this electrode, (——) action spectrum on a light scattering TiO_2 electrode (12 µm P25).

dye has no effect. On increasing the deoxycholic acid concentration to 100 mM, the efficiency in the Q_y band region drops below 10% while the other bands are barely affected (Figure 32c). The depression of the red peak is also apparent in the absorption spectrum of the electrode, but is completely reversible on desorption of the dye from TiO_2 with 0.2 M acetic acid in ethanol. Probably the Q_y band is further red shifted and broadened by interaction with the polar, high refractive index TiO_2.

H_2-chlorin e_6. After removal of the central Mg^{2+} the solution spectrum of chlorophyllin shows only a weak red shifted peak at 697 nm in the presence of deoxycholic acid (Figure 32d). This peak does not appear in the photocurrent action spectrum, which otherwise compares well with the absorption spectrum in solution. The shoulder at 435 nm is again due to the chlorophyllin *b* derivative. The efficiency is quite high even in the green part of the spectrum, where the extinction coefficient of H_2-chlorin e_6 is small. This demonstrates the high light harvesting efficiency on the colloidal TiO_2 film.

Cu-chlorin e_6. Copper chlorophyllin is produced on a large scale as a water soluble dye for application in food coloring, cosmetics and medicine.[51] Copper is introduced to make the dye more stable against photooxidation by reducing its excited state lifetime (cf. chapter 3.5.3) However, commercial Cu-chlorophyllin is a mixture of several degradation products, almost all of which are lacking the carboxyl group in conjugation with the π electron system. To avoid decarboxylation reactions all three carboxyl groups have to be protected by esterification before Cu^{2+} insertion and only be saponified afterwards.[52b] Cu-chlorin e_6 prepared in this way, although not fluorescent, is an excellent photosensitizer for TiO_2 (Figure 32e). Up to 70% of the incident photons are converted into electrons which can be measured as current in the external circuit.

Cu-2-α-oxymesoisochlorin e_4. The commercial Cu-chlorophyllin is made by hot saponification of raw chlorophyll in the presence of a copper salt. One of the major products is Cu-2-α-oxymesoisochlorin e_4, which lacks the ring carboxyl group and has a hydrated vinyl group.[52] It can be separated from the other saponification products by chromatography. In spite of its weaker adsorption on silica gel and TiO_2, due to the lack of one carboxyl group, its photosensitization efficiency is as high as that of Cu-chlorin e_6 (Figure 32f solid curve). Thus the carboxyl group in conjugation with the π electron system of the tetrapyrrole macrocycle is not necessary for good electron injection. The action spectrum

again compares well with the solution spectrum. The shoulder at 440 nm is absent due to removal of the chlorophyllin *b* analog by chromatography.

Figure 32f also shows the absorption spectrum on a transparent TiO_2 electrode (cf. chapter 3.4.2). It corresponds to the solution spectrum except for the residual scattering background from the TiO_2 substrate. The action spectrum reflects the percentage of light absorbed by the sensitizer, as calculated from the absorption spectrum of bare and dye coated electrode. The photocurrent efficiency is higher with the nontransparent (P25) TiO_2 electrode in low absorption regions of the dye due to its increased layer thickness (12 µm compared to 7 µm) and the additional increase in effective optical thickness due to light scattering.[19i]

H_2, Zn, Cu-mesoporphyrin IX. Porphyrins are distinguished from chlorins by an additional double bond in one of the pyrrole rings, which is the reason for their red color. Protoporphyrin IX is the precursor in the biosynthesis of chlorophyll. Its Fe^{2+}-complex forms the oxygen binding prosthetic group of hemoglobin. Its derivatives also occur in redox active cytochromes and enzymes. Oddly enough nature does not employ red porphyrins as photosynthetic pigments.

Protoporphyrin IX has two propionic acid groups and adsorbs well on TiO_2. Here we report only the very similar results obtained with its hydrogenated derivative mesoporphyrin IX, in order to avoid complications arising from the reactive vinyl groups. The free base has a moderately high photocurrent efficiency with peaks corresponding to the solution spectrum (Figure 33a). The spectral response is very broad and extends to 680 nm. Insertion of Zn^{2+} increases the peak IPCE to nearly 80% (Figure 33b), however, the cutoff occurs already at 630 nm. The Cu^{2+}-complex, if adsorbed from THF, has an even higher IPCE of 83% in the Soret peak (Figure 33c), which corresponds to nearly unity quantum efficiency (electrons per *absorbed* photon) if reflection losses are taken into account. This confirms the observation that conjugation of the attaching carboxyl groups with the π electron system of the chromophore is not necessary for efficient electron injection. Adsorption of Cu-mesoporphyrin IX from ethanol gives a maximum IPCE of only 70%, but a higher open circuit photovoltage (490 mV) than from THF (350 mV). In both cases deoxycholic acid was present as coadsorbate, causing a positive shift of the conduction band edge of TiO_2 by protonation of the semiconductor surface. This shift seems to be more pronounced in THF, resulting in a larger driving force for electron injection from the excited dye yet a lower photovoltage.

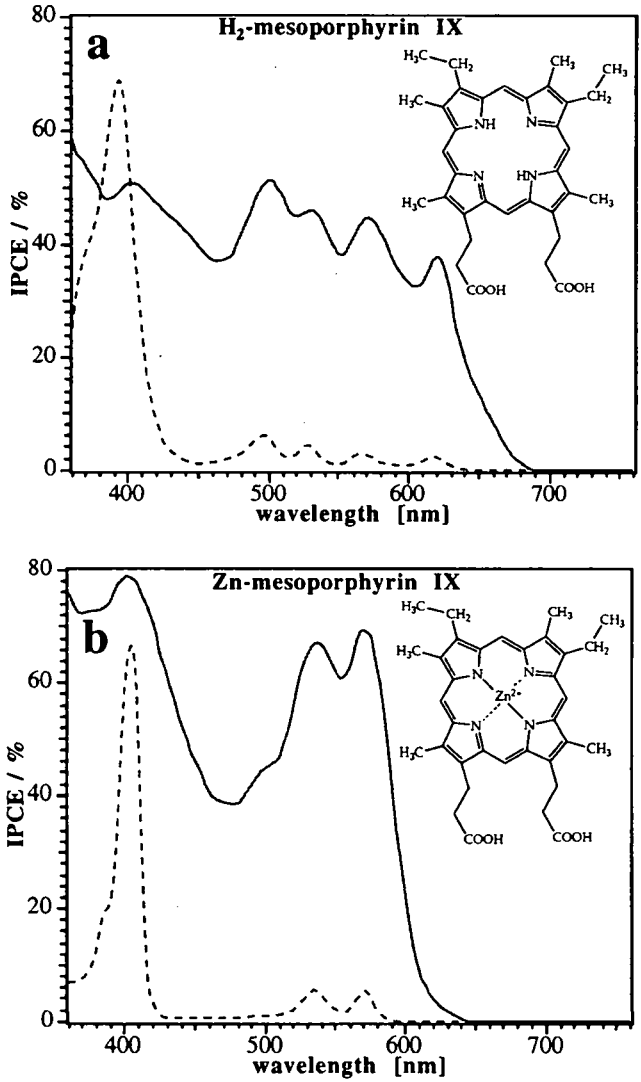

Figure 33: Photocurrent action spectra of TiO_2 electrodes sensitized with porphyrin derivatives (solid lines) and absorption spectra of the dyes in solution (dashed lines)

a) H_2-mesoporphyrin IX / ethanol + 20 mM deoxycholic acid

b) Zn-mesoporphyrin IX / ethanol + 20 mM deoxycholic acid

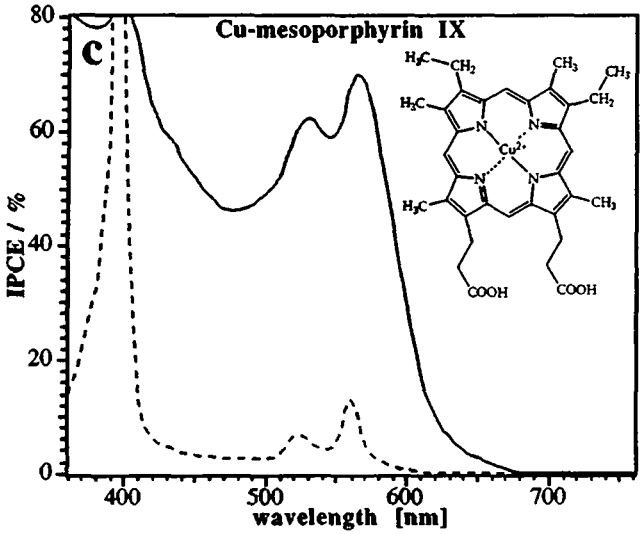

c) Cu-mesoporphyrin IX / THF + 20 mM deoxycholic acid

3.4.4. Photocurrent/voltage curves

While the photocurrent efficiency gives an indication of the quantum efficiency of the charge separation step it does not contain any information on the energy conversion efficiency. For this the electrical power output given by the product of photocurrent and photovoltage has to be compared with the light power input. The photocurrent/voltage curve of a Cu-2-α-oxymesoisochlorin e_4 electrode under monochromatic illumination ($\lambda = 630$ nm, $P = 0.75$ mW/cm^2) is shown in Figure 34a. At the maximum power point the electrical output is P_{max} = 0.23 mA/cm^2 · 0.34 V = 0.078 mW/cm^2 corresponding to an energy conversion of 10.4% in the red peak. The relatively low efficiency is mainly due to the low photovoltage of 0.42 V at open circuit, compared to a photon energy of 1.97 eV at 630 nm. The discrepancy is even larger for shorter wavelength light. This is one reason for the still lower total energy conversion efficiency of 2.6% under simulated sunlight illumination (Figure 34c). In addition the high current density of up to 9.4 mA/cm^2 results in ohmic losses, due to the series resistance

of the solar cell. At 10% white light intensity the energy conversion efficiency therefore improves to 3.1% (Figure 34b). Coadsorption of Cu-mesoporphyrin IX does not enhance the polychromatic efficiency of the electrode by improving green light absorption, which is already quite good with Cu-2-α-oxymesoisochlorin e_4 alone. Still the overlap of the photocurrent action spectrum with the solar emission spectrum is more complete with the Ru-complex $RuL_2(NCS)_2$ (cf. chapter 3.3.) exhibiting 60 to 80% photocurrent efficiency over the whole visible spectrum, with a tail extending up to 800 nm.

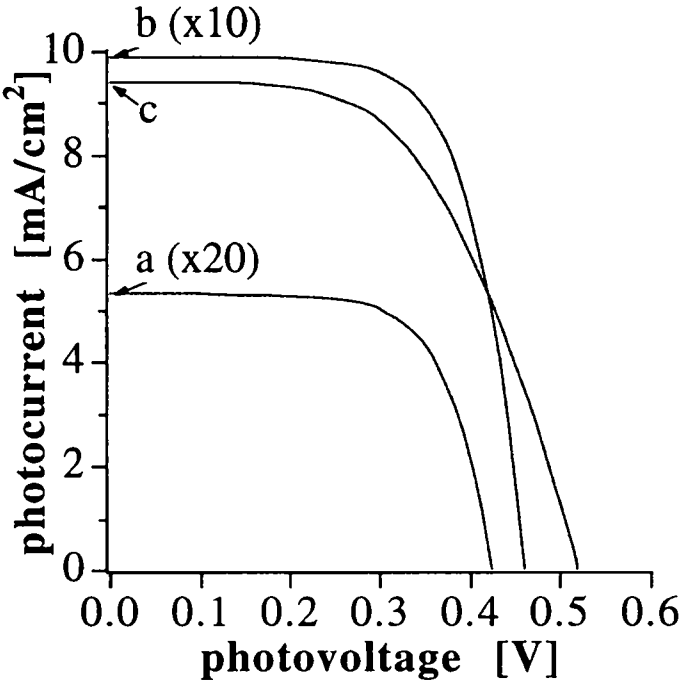

Figure 34: Photocurrent/voltage curve of a TiO_2 electrode (0.5 cm^2 active surface area) sensitized with Cu-2-α-oxymesoisochlorin e_4 (adsorbed from ethanol containing 20 mM chenodeoxycholic acid), electrolyte: 50% ethylene carbonate, 50% acetonitrile, 0.5 M tetrapropylammonium iodide, 40 mM iodine

a) under monochromatic illumination (λ = 630 nm, P = 0.75 mW/cm^2)

b, c) under white light illumination of 10 and 100 mW/cm^2, respectively

3.4.5. The effect of coadsorbates

Adsorption of a limited amount of Cu-2-α-oxymesoisochlorin e_4 from pure ethanol (50 nmol in 1 ml) onto 1 cm^2 of TiO_2 results in complete uptake of the dye by the outer part of the TiO_2 layer, while its inner part remains uncolored. The photocurrent efficiency is very low since the inner TiO_2 layer, facing the SnO_2 conducting substrate, remains insulating in the absence of electron injection from an adsorbed dye. Only after addition of another 50 nmol of dye does the electrode become homogeneously colored, yet the efficiency is still rather low (Table 8 d).

The dye concentration on the TiO_2 electrode, as calculated from the absorbance change of the dipping solution ($\varepsilon_{630} = 3.7 \cdot 10^4$ 1 mol^{-1} cm^{-1}) is 96 $nmol/cm^2$. The TiO_2 powder used for electrode preparation (Degussa P 25) has a primary particle size around 25 nm and a specific surface area of 55 m^2/g, giving a roughness factor of 1100 for a coating of 2 mg TiO_2/cm^2. Thus the real surface concentration of the dye is 87 $pmol/cm^2$, corresponding to a surface area of 1.9 nm^2 per molecule. Since the chromophore has a diameter of roughly 1 nm there should be enough surface area available even for a flat adsorption of the tetrapyrrole macrocycle on TiO_2. Hence the low efficiency is probably not due to multilayer formation. Also absorption and action spectra of the electrode show no indication of chlorophyllin aggregation in the pores of the electrode. This is in accordance with the observation that, contrary to the coordinatively unsaturated magnesium complexes, copper chlorophylls do not tend to coordinative aggregation.[53]

Adsorption from the more polar methanol results in homogenous coloration even with only 50 nmol of dye per cm^2 of TiO_2 yet the efficiency is still low (Table 8 b). Less polar solvents, like acetone, propylene carbonate, dioxane, pyridine or THF (Table 8 a,c) give inhomogenous coloration and even lower efficiencies than ethanol.

Both photocurrent and voltage can be improved appreciably by addition of cholanic acids to the ethanolic dye solution (Table 8 e-m). The effect also occurs on preadsorption of cholanic acids, while postadsorption on an already colored electrode is less effective. The common feature of these bile acids are a steroid skeleton with a flexible carboxylic acid side chain and one to three hydroxyl groups on one side of the steroid backbone (Figure 35a). This makes them chiral amphiphilic molecules with a hydrophobic and a hydrophilic side. They form chiral micelles in aqueous solution and channel type inclusion compounds with many guest molecules in the solid state.[54] Cholanic acids are expected to adsorb on the TiO_2 surface with their carboxyl and hydroxyl functions (Figure 36).

Table 8: Effect of coadsorbates on the dye coverage and photoelectrochemical properties of TiO_2-Cu-2-α-oxymesoisochlorin e_4 solar cells

	solvent/coadsorbate[a]	Γ[b] [nmol/cm^2]	IPCE$_{630}$[c] [%]	I_{sc}[d] [μA/cm^2]	V_{oc}[e] [mV]
a	pyridine	42	7	100	490
b	methanol	51	30	370	380
c	tetrahydrofurane	100	14	190	440
d	ethanol	96	25	330	430
e	40 mM cholic acid	45	49	740	460
f	5 mM deoxycholic acid	47	56	700	430
g	20 mM deoxycholic acid	43	58	820	440
h	100 mM deoxycholic acid	19	68	840	490
i	20 mM chenodeoxycholic acid	25	68	940	480
k	20 mM lithocholic acid	9	57	740	490
l	100 mM ursodeoxycholic acid	13	59	690	490
m	10 mM dehydrocholic acid	12	53	670	490
n	500 mM Triton X-100	31	35	390	490
o	100 mM acetic acid	25	45	670	400
p	1 M glycerol	25	33	300	530
q	10 mM sorbitol	42	27	320	520
r	5 mM D(+)-glucose	45	38	410	520
s	100 mM cyclohexanecarboxylic acid	21	49	620	360
t	100 mM 1-adamantaneacetic acid	28	51	650	380
u	5 mM R(-)-cyclohexylhydroxyacetic acid	19	39	480	360
v	1 mM D(-)-quinic acid	16	44	580	400

[a] the electrodes were dipped in 1 ml solvent (ethanol for e-v) containing 50 nmol (100 nmol for c and d) Cu-2-α-oxymesoisochlorin e_4

[b] dye surface concentration on the electrode

[c] photocurrent efficiency in the Q_y-band at 630 nm

[d,e] short circuit photocurrent and open circuit photovoltage under white light illumination of 10 mW/cm^2 (approx. 10% of full sunlight)

However, rather high concentrations are necessary to compete with the adsorption of Cu-2-α-oxymesoisochlorin e_4 (at 50 μM), which has two carboxyl groups (Table 8 e-m).

The decrease in surface concentration of the dye by the "spacer effect" of cholanic acids is not sufficient for enhanced photosensitization efficiency since other surfactants known to prevent chlorophyll aggregation, like Triton X-100 (Figure 35b), although decreasing the dye coverage, barely improve the electrode performance (Table 8 n). The same observation has been made with Langmuir-Blodgett films of Cu-chlorophyll on SnO_2 electrodes, where the photosensi-tization efficiency is not enhanced by two-dimensional dilution with lipids.[38e] The higher photocurrent can rather be explained by a positive shift of the conduction band edge of TiO_2 in the presence of acid, resulting in a larger driving force for electron injection from the excited dye. In fact, the addition of acetic acid to the ethanolic dye solution also increases the photocurrent, yet slightly decreases the open circuit voltage (Table 8 o). On the other hand, addition of base or even short exposure of the electrode to ammonia vapor drastically decrease the injection efficiency. The effect is most prominent in case of Cu-2-α-oxymesoisochlorin e_4, since its excited state oxidation potential lies just above the conduction band edge of TiO_2, so that small changes in the position of the latter strongly affect the injection efficiency (cf. chapter 3.5.6). In addition the excited state potential of chlorophyllin might be influenced by interaction of its hydrophobic tetrapyrrole macrocycle with the nonpolar backside of the adsorbed cholanic acid molecule. Tuning of the redox potential of chlorophyll is in fact very important in natural photosynthesis, where shifts of several hundreds of millivolts are effected by the surrounding protein matrix.[55]

The photovoltage is limited by the dark current, caused by reduction of iodine on the electrode at negative potentials, and can therefore be enhanced by adsorption of molecules which render the approach of iodine to the TiO_2 surface more difficult. The higher photovoltage in the presence of coadsorbed polyhydroxyl compounds like glycerol, sorbitol or glucose (Table 8 p-r and Figure 35 d-f) can be rationalized by this insulation mechanism (Figure 36). With cholanic acids, the photovoltage gain is less pronounced due to the counteracting conduction band shift in the presence of acid. Cyclohexanetriol (Figure 35 g) shows no effect, probably because its adsorption is restricted by the fixed distance of the hydroxyl groups, while glucose may adsorb in its flexible acyclic form (Figure 35 *f*).

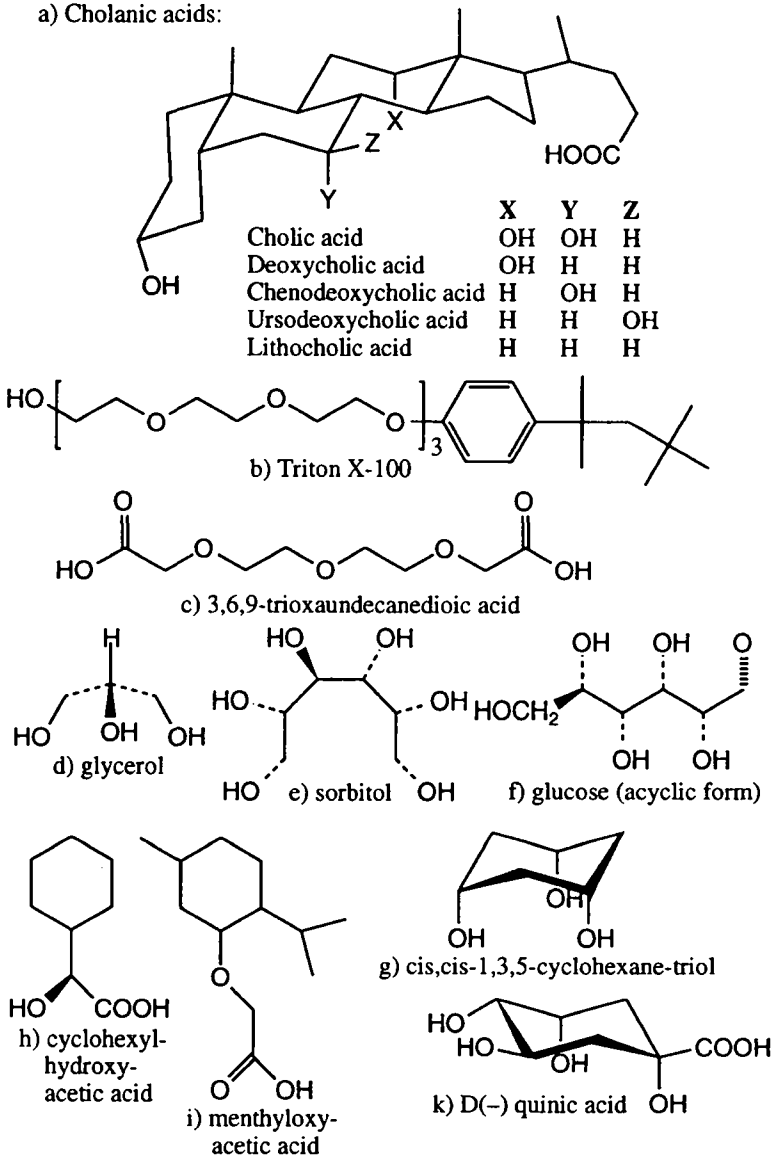

Figure 35: Molecular structures of some coadsorbates

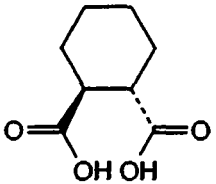

l) trans-cyclohexane-1,2-dicarboxylic acid

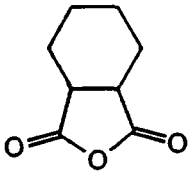

m) cis-cyclohexane-1,2-dicarboxylic acid anhydride

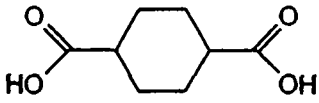

n) trans-cyclohexane-1,4-dicarboxylic acid

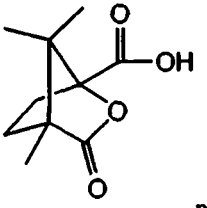

o) (–) camphanic acid

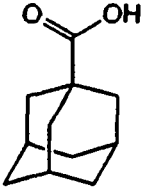

p) 1-adamantane-acetic acid

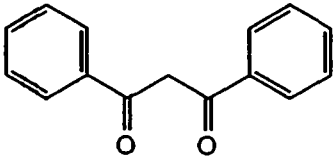

q) dibenzoylmethane

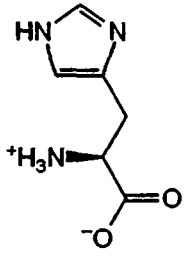

r) L-histidine

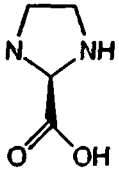

s) L-prolin

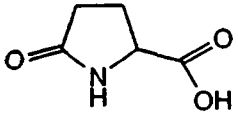

t) pyroglutamic acid

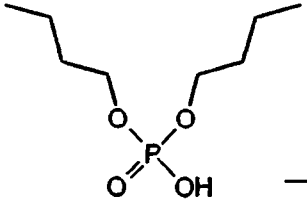

u) dibutyl-phosphate

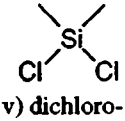

v) dichloro-dimethyl-silane

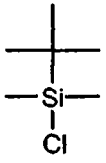

w) chloro-dimethyl-tert-butyl-silane

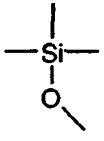

x) methoxy-trimethyl-silane

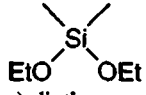

y) diethoxy-dimethyl-silane

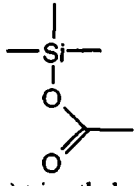

z) trimethyl-silyl-acetate

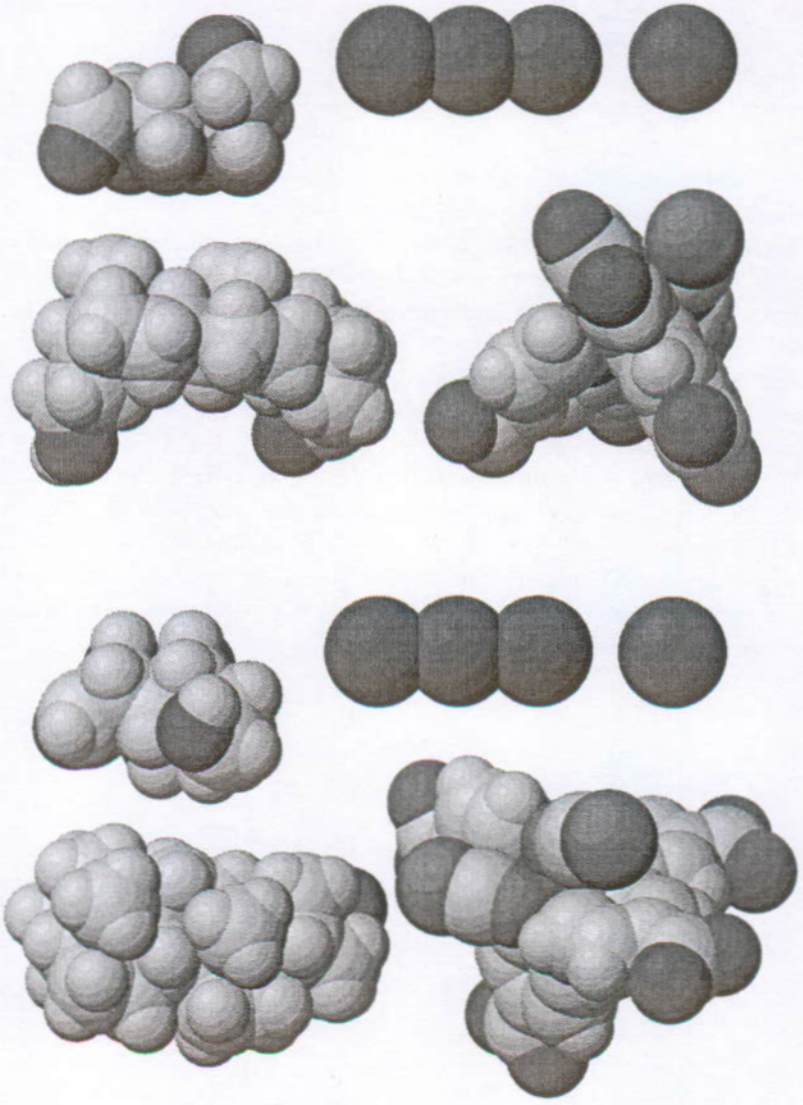

Figure 36: Side and top view of adsorbed glucose, lithocholic acid and $RuL_2(NCS)_2$ in comparison to I_3^- and I^-

Carboxylic acids with bulky hydrocarbon skeletons (Figure 35 h-p) only increase the photocurrent efficiency but not the voltage (Table 8 s-u). This also holds for quinic acid (Figure 35 k), which competes with chlorophyllin adsorption even at low concentration (Table 8 v).

Further investigated coadsorbates are water, urea, EDTA, paraldehyde, myristic, oleic, β-hydroxystearic and 5,5-diethylbarbituric acids, dibenzoylmethane, amino acids and dibutylphosphate (Figure 35 q-u): none of them improves both photovoltage and current as cholanic acids do.

Similar effects of coadsorbates are observed with the ruthenium complexes $RuL_2(NCS)_2$ and $RuL_2[Ru(bpy)_2(CN)_2]_2$ (L = 2,2'-bipyridine-4,4'-dicarboxylate). In particular glucose and cholanic acids improve photocurrent and voltage. The size of these coadsorbates is compared to that of the ruthenium dye and the redox species I^- and I_3^- in Figure 36. Both glucose and lithocholic acid are expected to adsorb on TiO_2 with their oxygen functionalities and may block the access for the large I_3^- ion. This reduces the dark current and increases the photovoltage of the solar cell.

We also attempted to insulate the TiO_2 surface between the dye molecules by silylation. The colored electrodes were dipped for one hour in 2% $Si(CH_3)_2Cl_2$ in CH_3CCl_3 or 10 mM $Si(t\text{-butyl})(CH_3)_2Cl$ in pyridin (Figure 35 v,w). Hydrolyzable organosilanes (Figure 35 x-z) were added in a concentration of 5% to the dye solution one hour before removal of the electrode. In no case a significant improvement was observed.

3.4.6. Conclusion

The photosensitization of colloidal TiO_2 electrodes by chlorophyll derivatives has been shown to give high photocurrent quantum yields, approaching the unity efficiency of primary charge separation in natural photosynthesis. Also the efficient light harvesting in plants was successfully imitated by adsorbing monolayers of the chlorophyll derivatives on nanostructured TiO_2 films.

Contrary to natural photosynthesis, where most chlorophyll molecules act as antennae and transfer the excitation energy to a small number of reaction centers, each molecule on the TiO_2 electrode can be photoelectrochemically active. Therefore photosensitization is possible even with the nonfluorescent Cu-chlorophyllin, which cannot undergo energy transfer. Mechanistic aspects of the sensitization process shall be investigated in chapter 3.5.

The practical usefulness of the chlorophyll solar cell is limited at present by the rather low energy conversion efficiency in sunlight. Ruthenium dyes are more promising in this regard, due to their better light harvesting properties, especially in the green spectral region (chapter 3.3). They are also preferred in view of long term stability: electron injection into the semiconductor only changes the oxidation state of the ruthenium center, while chlorophyll is oxidized to a cation radical (chapter 3.5), which is susceptible to side reactions before being rereduced. Contrary to chlorophyll in plants, which is renewed each springtime and even undergoes continuous turnover during the vegetation period, a photosensitizer for solar cells has to be stable for many years. Nevertheless, a Cu-2-α-oxymesoisochlorin e_4 sensitized TiO_2 electrode delivered an electrical charge of 200 C/cm^2 in 18 hours of illumination, corresponding to 10^5 turnovers per dye molecule. The photocurrent dropped to half of the initial value during this time while the edges of the electrode turned gray, probably due to the intrusion of oxygen into the not perfectly sealed cell.

3.5. The mechanism of photosensitization

3.5.1. Introduction

The general mechanism of dye sensitization has been reviewed by Gerischer, Willig and Spitler.[56] The sensitization of nanoporous TiO_2 electrodes has been studied by laser flash photolysis, revealing the charge injection and recombination kinetics.[19k] In particular electric field effects on the dynamics of light induced charge separation have been studied in detail.[19 l] Fast electron injection from the excited ruthenium complex into the conduction band of the TiO_2 electrode has been deduced from picosecond fluorescence decay measurements by Willig et al.[57] The photosensitization of colloidal TiO_2 with copper chlorophyllin has been analyzed by fluorescence quenching, laser flash photolysis, and microwave absorption by Kamat et al.[40]

We have investigated the mechanism of photosensitization of transparent TiO_2 electrodes with chlorophyll derivatives.[58] We compare the light emission properties of free base and copper chlorophyllin in solution and on non-quenching ZrO_2 films with those on the TiO_2 electrode and relate rate and extent of quenching to electron injection rate and efficiency. Results from electrochemical studies of dissolved and adsorbed dyes as well as of the TiO_2 electrode itself can be rationalized by an energy level diagram with two possible sensitization mechanisms. Laser flash photolysis experiments remove this uncertainty and provide insight into the charge recombination kinetics in the absence as well as presence of a reducing agent.

3.5.2. Experimental section

Materials . Chlorin e_6 was obtained from Porphyrin Products and its purity checked by thin layer chromatography. Cu-2α-oxymesoisochlorin e_4 was isolated from Cu-chlorophyllin (Merck) by column chromatography on silica gel with toluene + 10% acetic acid as eluent.

Nanoporous transparent TiO_2 films of 7 μm thickness were prepared from colloidal TiO_2 after autoclavation at 200°C as described in the literature.[19n] Analogous ZrO_2 films of 5 μm thickness served as non-quenching reference adsorbent. They were prepared form ZrO_2 powder (Degussa E8, BET surface

are 62 m^2/g) in the same way as TiO_2 electrodes from P 25 powder (chapter 2.3.13). Nanoporous transparent SnO_2 electrodes of about 1 μm thickness for spectroelectrochemical studies of the adsorbed dyes were prepared on SnO_2 conducting glass substrate from colloidal SnO_2[59] analogously to the TiO_2 electrodes.

The freshly fired TiO_2 or ZrO_2 films (1 cm^2) were dipped overnight in 1 mL of a 5 x 10^{-5} M solution of the chlorophyll derivative in ethanol containing 10 mM lithocholic acid as coadsorbate (chapter 3.4.5). To prevent adsorption of atmospheric water vapor, the dried films were wetted with high purity propylene carbonate (Burdick & Jackson, dried over molecular sieves) and protected with a microscope cover glass.

Methods. Absorption spectra were recorded with a Hewlett Packard (HP 8452A) or a Cary 5 spectrophotometer. Emission spectra were measured on a Spex Fluorolog II with a 450 W Xenon lamp as excitation source. A cooled Hamamatsu R 2658 photomultiplier used as detector allowed measurements up to 1000 nm. The photometric correction of the spectra was achieved using a National Bureau of Standards lamp as calibrated light source.

The luminescence in solution was measured at right angle, with chlorophyll *a* in ether as reference for quantum yield determinations (Φ_f = 0,32 [60]). The emission in the adsorbed state was measured in the front face configuration, due to the high optical density of the dye coated films. Chlorophyll *a* solution in ether of comparable optical density in a 1 mm cuvette served as quantum yield standard in this case.

Emission decay curves were recorded after excitation with a mode locked frequency doubled Nd-YAG laser (0.1 ns pulses at 4 Hz of 2 mJ/cm^2 at 532 nm). The emitted light was detected at right angle with a fast silicon photodiode connected to a transient digitizer after removal of laser stray light with suitable filters. Transient absorption spectra on TiO_2 were obtained under the same conditions with analyzing light from a 150 W xenon lamp passed through a monochromator (bandpass 10 nm) and traversing the electrode perpendicular to the laser beam.

To study the decay kinetics of the transient absorption the dye coated electrode was excited with single 532 nm laser pulses (duration 10 ns, fluence 2 mJ/cm^2). Light from a stabilized halogen lamp was filtered with cut-off and interference filters in order to avoid exposing the electrode to actinic light. The transmitted light was detected by a fast photodiode after removal of laser stray light and fluorescence from the electrode with an interference filter of the desired wavelength (half width 10 nm).

For the acquisition of photocurrent and photovoltage transients the electrodes were wetted with redox electrolyte (0.5 M KI, 40 mM I_2 in 80% ethylene carbonate, 20% propylene carbonate), pressed against a platinum foil counter electrode and excited with a single 10 ns laser pulse of 2 mJ/cm^2 at 532 nm. The photocurrent was recorded as a voltage drop over a 10 Ω resistor, while the photovoltage was measured directly into the 1 MΩ input of the transient digitizer.

Electrochemical studies of the dyes were carried out in propylene carbonate containing 0.1 M tetrabutylammoniumtetrafluoroborate ($TBABF_4$, Fluka, electrochemical grade) as supporting electrolyte. This solution was treated with neutral alumina (ICN, dried at 150°C under vacuum) to remove electrophilic impurities.[61] Cyclic voltammograms were measured under nitrogen on a BAS 100 electrochemical analyzer with a glassy carbon working electrode and an aqueous saturated calomel electrode reference (the ferrocene/ferrocenium couple had a midpoint potential of +0.38 V under these conditions).

3.5.3. Absorption and emission properties of dissolved and adsorbed dyes

Light absorption and emission properties of chlorin *e*$_6$ and Cu-2α-oxymeso–isochlorin *e*$_4$ in solution and on porous ZrO_2 and TiO_2 films are reported in Figure 37 and Table 9. ZrO_2 was chosen as non-quenching reference adsorbent, because its conduction band edge lies about 1 eV more negative than that of TiO_2,[62,63] thus precluding electron injection from the excited dye. On the other hand, its surface properties, especially the acid/base behavior of the surface hydroxyl groups, are comparable to TiO_2 (point of zero zeta potential pzzp(TiO_2, anatase) = 5.8, pzzp(ZrO_2) = 6.7), while SiO_2 or Al_2O_3 are more acidic or basic, respectively (pzzp(SiO_2) = 2.0, pzzp(Al_2O_3) = 9.2).[63] Also the refractive index, which influences fluorescence quantum yield measurements and natural radiative lifetimes, is closer to that of TiO_2 (anatase n = 2.5) for ZrO_2 (n = 2.2), than for SiO_2 (n = 1.5) or Al_2O_3 (n = 1.7).

Chlorin *e*$_6$. In ethanol chlorin *e*$_6$ fluoresces strongly with a quantum yield of 16%, which is comparable to Φ_{EtOH} = 23% [60] for its parent compound chlorophyll *a* . The Stokes shift with respect to the Q_y absorption band is also very small. However, the shoulder is not the mirror image of the vibronic overtone at 606 nm as in case of chlorophyll *a*,[64] but is rather composed of two contributions around 702 and 733 nm (Figure 37b). Adsorption on ZrO_2 or TiO_2 results in a red shift of both absorption and emission spectra as discussed in

chapter 3.4.3. The fluorescence quantum yield was corrected for the high refractive index of the porous, propylene carbonate wetted oxide film:[65]

$\Phi_{corr} = \Phi_{app} \cdot n^2_{film} / n^2_{ref}$ with $n(ZrO_2) = 2.0$, $n(TiO_2) = 2.1$, n(ether) = 1.35.

The refractive index correction amounts to more than 100%, which stresses the importance of the ZrO_2 film as reference with similar optical parameters as the TiO_2 film. The fluorescence quantum yield on ZrO_2 (Φ_f = 20%) is higher than in solution, due to the increased radiative rate constant in a medium of high refractive index.[66] The shoulder in the emission spectrum gains in intensity at the expense of the main peak at 674 nm and is better resolved into individual peaks at 720 and 740 nm (Figure 37c). The excitation spectra of all three fluorescence peaks correspond to the absorption spectrum of the adsorbed dye, which shows no peaks beyond the Q_y band that could be ascribed to dimerization or aggregation, as Mg-chlorin e_6 does (chapter 3.4.3). We found all three fluorescence peaks to be strongly polarized on excitation in the Q_y band (*P* close to 40 %), indicating immobilization of the dye on the ZrO_2 surface and negligible energy transfer to neighboring molecules.[67] Thus the three peaks probably arise from the same lowest excited singlet state of the chlorin e_6 monomer, decaying to three vibrational levels of the ground state. The change in intensity and position of the vibrational bands as compared to the emission from solution may be attributed to the adsorption on the ZrO_2 surface with at least two of the carboxyl groups.

Adsorption on TiO_2 quenches the emission by 70% in accordance with an electron injection efficiency of more than 63% (chapter 3.4.3). The remaining fluorescence from the non-injecting dye has a main peak at 676 nm, as on ZrO_2, but exhibits a stronger shoulder at 710 nm (Figure 37d).

The fluorescence decay on ZrO_2 is multiexponential, as has been observed before with dyes adsorbed on oxides, and ascribed to different adsorption sites.[68] A reasonably good fit of our data is already obtained with two exponentials (Table 9), although a distribution of many lifetimes cannot be excluded. The shorter component (0.4 ns) is probably due to electron transfer from the excited dye to surface states below the inaccessible conduction band of ZrO_2. Energy transfer quenching, although insignificant according to the strong polarization of the steady state fluorescence, may still be involved in the fast decay, which contributes only 10% to the overall fluorescence. Förster-type energy transfer may occur at a surface coverage approaching 1/10 of a monolayer, as calculated from absorbance and roughness factor of the ZrO_2 film.[69] However,

quenching still requires the presence of a trap for the excitation energy, such as a dye molecule adsorbed next to an electron accepting surface state. This is analogous to the energy transfer from antenna chlorophylls to reaction center chlorophylls in natural photosynthesis. Even the second fluorescence component on ZrO_2 (3.4 ns) decays faster than the fluorescence in solution (5.3 ns), in spite of the higher quantum yield. This is explained by a decrease of the natural radiative lifetime $\tau_0 = \tau_f / \Phi_f$ (Table 9) in a medium of high refractive index.[66]

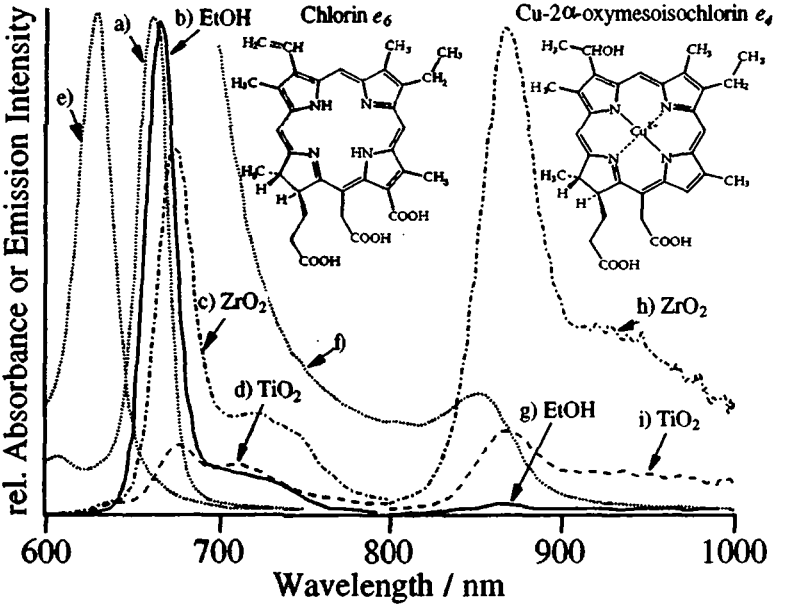

Figure 37: Absorption and emission spectra of dissolved and adsorbed dyes. **Chlorin e_6: (a)** absorbance and **(b)** emission in ethanol (excitation at 404 nm); **(c)** emission on ZrO_2 and **(d)** on TiO_2 (excitation at 408 nm); **Cu-2α-oxymesoisochlorin e_4: (e,f)** absorbance and **(g)** emission in ethanol; **(h)** emission on ZrO_2 and **(i)** on TiO_2 (excitation at 633 nm). The emission spectra are corrected for the absorbance at the excitation wavelength and the refractive index of the medium and thus represent true quantum yields.

On the TiO_2 electrode, 80% of the fluorescence decays with τ_f = 0.4 ns, indicating fast electron transfer to the conduction band from most chlorin e_6 molecules. The second component (1.4 ns) may be attributed to another adsorption site exhibiting slower electron injection. However, our data can also be interpreted by a distribution of many lifetimes, as mentioned before. This would correspond to a distribution of electron transfer times. The rate constant of electron transfer (k_{et}) can be calculated from the fluorescence lifetimes in presence (τ_s) and absence (τ_i) of electron transfer:[68a]

$$k_{et} = 1/\tau_s - 1/\tau_i$$

Taking the slow component on ZrO_2 as the fluorescence lifetime of the adsorbed chlorin e_6 in absence of electron transfer (τ_i = 3.4 ns), the fast component on TiO_2 (τ_s = 0.4 ns) gives an electron injection rate constant of k_{et} = 2.2 x 10^9 s^{-1} for 80% of the sensitizer molecules. This compares well with the value of k_{et} = 1.6 x 10^9 s^{-1} estimated by Watanabe et al.[69a] for injection from the singlet excited state of Pd-chlorophyll a into the conduction band of SnO_2. Kamat et al.[40a] obtained k_{et} = 4.2 x 10^9 s^{-1} from the fluorescence lifetime of copper chlorophyllin on TiO_2. However, the fluorescence observed by these authors is in fact due to free base impurities present in the commercial copper chlorophyllin, as discussed in the following section.

Table 9: Absorption and Emission Properties of Dissolved and Adsorbed Dyes

dye	in/on	λ_{max}^{abs} / nm	λ_{max}^{em} / nm	Φ_f[a]	τ_f[b] / ns	τ_0[c] / ns
Chlorin e_6	EtOH	404, 662	668, 702, 733	0.16	5.3	33
	ZrO_2	408, 666	674, 720, 740	0.20	0.4 (50%) 3.4	9.5
	TiO_2	410, 668	676, 710	0.06	0.4 (80%) 1.4	10
Cu-2α-oxy-mesoiso-chlorin e_4	EtOH	409, 628	869	$2.7x10^{-5}$	5.6	$2.1x10^5$
	ZrO_2	412, 633	869	$1.1x10^{-3}$	27 (57%) 110	$5.7x10^4$
	TiO_2	412, 633	869	$2.2x10^{-4}$	3 (45%) 16	$4.6x10^4$

a) quantum yield for excitation in the Soret peak
b) luminescence emission lifetimes for laser flash excitation at 532 nm; for biexponential fits the percentage of the shorter component is given in brackets
c) natural radiative lifetime $\tau_0 = \tau_f / \Phi_f$

Cu-2α-oxymesoisochlorin e_4. Commercial copper chlorophyllin shows a weak fluorescence at 670 nm in ethanolic solution. However, the excitation spectrum with its peak at 664 nm does not correspond to the absorption of the Cu-complex (Q_y band at 628 nm), but rather to that of free base chlorophyllin. The quantum yield of 0.3% indicates the presence of 2% free base impurity having 16% fluorescence efficiency. Chromatographically isolated Cu-2α-oxymesoisochlorin e_4, the main component of commercial copper chlorophyllin, still contains 0.1% fluorescing free base, due to its very similar chromatographic retention. Only remetallization of Cu-chlorophyllin with copper acetate in acetic acid followed by chromatography yields Cu-2α-oxymesoisochlorin e_4 which is nearly free of fluorescing impurities. Selective excitation of the copper complex at 580 nm, where the extinction coefficient of the free base is minimal, gives $\Phi_f < 10^{-6}$ for the fluorescence efficiency of Cu-2α-oxymesoisochlorin e_4, essentially limited by the background due to Raman scattering of the solvent.

A fluorescence quantum yield of 0.1% was reported [40a] for commercial copper chlorophyll in solution which was quenched by adsorption on colloidal TiO_2. This fluorescence must be attributed to the presence of free base impurities. The quenching of the fluorescence of chlorophyll derivatives and porphyrins by the insertion of copper is well established [70] and is due to the rapid decay of the singdoublet to the tripdoublet excited state in presence of the paramagnetic Cu^{2+} center.[71] This is also the reason for insertion of copper in chlorophyllin for dye applications, since the excited state becomes too short-lived to produce singlet oxygen, which would destroy the dye. In the case of copper porphyrin the singlet excited state is so short-lived, that the quasi-line spectra in Shpolskii matrices are broadened due to the uncertainty principle, indicating a lifetime of only 24 fs.[72] For Cu-2α-oxymesoisochlorin e_4 the Strickler-Berg relationship [73] gives a natural radiative lifetime of $\tau_0 = 22$ ns for emission at 640 nm and with the measured fluorescence quantum yield ($\Phi_f < 10^{-6}$) a fluorescence lifetime of $\tau_f = \tau_0 \cdot \Phi_f < 22$ fs.

The almost instantaneous and efficient population of the tripdoublet excited state gives rise to a rather strong phosphorescence of copper chlorins and porphyrins.[70,71] Cu-2α-oxymesoisochlorin e_4 emits in ethanolic solution at room temperature at around 869 nm with a quantum yield of 2.7×10^{-5} (Figure 37g). In a glassy matrix of 80% ethanol / 20% methanol at 77 K the peak shifts to 850 nm and the emission intensity increases by a factor of 100. The emission is mirror symmetrical to a weak ($\varepsilon \approx 50\ M^{-1}cm^{-1}$) absorption peak at 850 nm (Figure 37f). This peak may be ascribed to the $^2S_0 \rightarrow {}^2T_1$ transition, which gains in intensity by spin orbit coupling of the unpaired copper *d* electron with the chlorin π system.[71] Cu-2α-oxymesoisochlorin e_4 adsorbed on ZrO_2 emits

40 times stronger than in solution (Figure 37h), as generally observed for the phosphorescence of dyes immobilized by adsorption, due to slower internal conversion.[74] On TiO_2 the emission is quenched by 80% (Figure 37i), in accordance with an electron injection efficiency of at least 70% (chapter 3.4.3).

The phosphorescence decay on ZrO_2 can be described by two exponentials of comparable intensity, although a multiexponential decay cannot be excluded on the basis of our data. This is probably due to at least two adsorption sites, which immobilize the dye to different extents (Table 9). The average lifetime is much longer than in ethanol, but the natural radiative lifetime τ_0 is shorter, which can again be attributed to the high refractive index of the ZrO_2 film. On TiO_2 the phosphorescence decay can also be fitted by two exponentials of similar contribution (Table 9). The shorter component (τ_s = 3 ns) indicates electron injection with $k_{et} = 3 \times 10^8\ s^{-1}$, if the smaller lifetime on ZrO_2 is taken as reference in the absence of electron transfer (τ_i = 27 ns).

3.5.4. Electrochemical characterization of the dyes

The cyclic voltammograms of Cu-2α-oxymesoisochlorin e_4 and chlorin e_6 are shown in Figure 38a,b. Both exhibit a redox behavior similar to that of chlorophyll *a*.[61] The reversibility of the waves is somewhat reduced, probably due to the presence of free carboxyl groups, which may preferentially deprotonate in the cation radical state and protonate the π system of the anion radical. It is known that traces of proton donors affect the reversibility of chlorophyll reduction.[61] A new oxidation wave appears in Figure 38 at 0.2 and 0.3 V_{SCE}, respectively, after scanning through the reduction waves, which may be due to the protonation product.

The measured reduction midpoint potentials of chlorin e_6 (–0.98 and –1.25 V_{SCE}) are nearly the same as those reported for its trimethylester (–1.02 and –1.32 V_{SCE} in DMF [75a]). The redox potentials of chlorin e_6 are slightly more negative than the values reported for its parent compound pheophytin *a*.[75] Cu-2α-oxymesoisochlorin e_4 is more easily oxidized than the free base chlorin e_6, in accordance with the behavior of Cu-chlorophyll *a*.[69a] Its reversible oxidation at 0.55 V_{SCE} is also observed after adsorption on porous, transparent SnO_2 electrodes, allowing spectroelectrochemical characterization of the adsorbed dye. The difference spectrum after oxidation at 0.6 V_{SCE} is shown in Figure 40a. The same spectrum is obtained after chemical oxidation of the dye dissolved in propylene carbonate by iodine, which is reversible on addition of excess iodide. Attempts to obtain similar spectra for the cation radical of

chlorin e_6 by oxidation on porous SnO_2 electrodes or with bromine failed due to its short lifetime.

The primary redox potential difference $E^1_{ox} - E^1_{red} = \Delta E$ compares for both dyes well with their singlet excitation energy ε_S[75c] (chlorin e_6: ΔE = 1.78 V, ε_S = 1.86 eV; Cu-2α-oxymesoisochlorin e_4: ΔE = 1.93 V, ε_S = 1.97 eV). With the electrochemical data and the excited state energies for the 0-0 transitions estimated from the emission spectra of Figure 37 a redox potential diagram of the dyes in ground and excited states can be calculated [75b,c] (Figure 39).

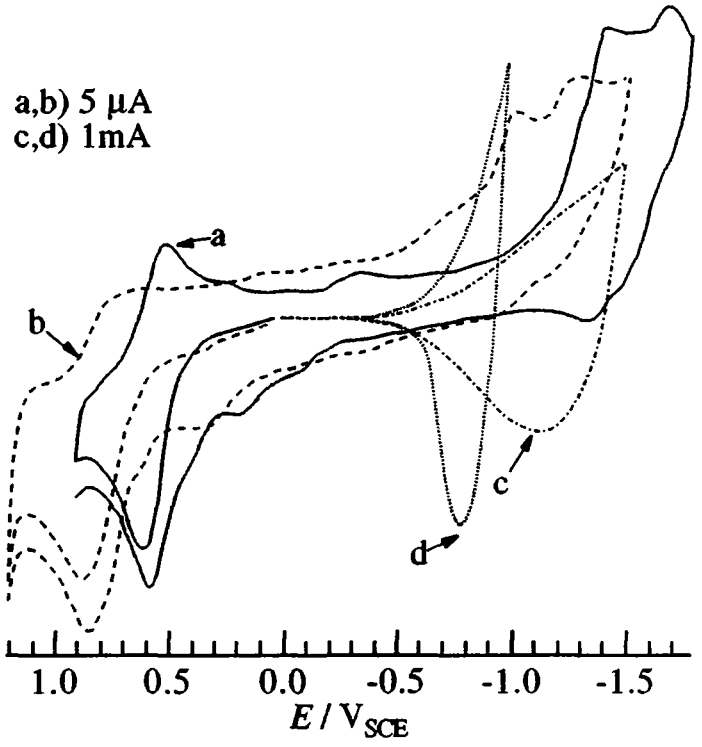

Figure 38: Cyclic voltammograms in 0.1 M $TBABF_4$/PC:
(a) 1 mM Cu-2α-oxymesoiso-chlorin e_4; **(b)** 1 mM chlorin e_6;
(c) TiO_2 electrode; **(d)** TiO_2 electrode in 1 M $LiClO_4$/PC;
scan rates: (a,c,d) 100 mV/s, (b) 200 mV/s

3.5.6. Cyclic voltammetry of bare nanocrystalline TiO_2 electrodes

In order to determine the density of acceptor states in the TiO_2 as a function of potential we measured the cyclic voltammogram of the bare electrode. Negative polarization in deaerated propylene carbonate containing $TBABF_4$ or $LiClO_4$ supporting electrolyte results in the capacitive currents shown in Figure 38c,d. The classical equations for the space charge capacity of a bulk semiconductor electrode [76] are not applicable in our case, due to the small size of the nanocrystalline TiO_2 particles compared to the extension of the space charge layer. Hence, as has been discussed before [19 1] and confirmed by others,[77] an appreciable electric field cannot build up in the colloidal film. The applied potential will rather drop in the Helmholtz double layer at the semiconductor–electrolyte interface, as in the case of a metal electrode. A similar situation arises for bulk semiconductors if the surface state capacity becomes large compared to the space charge capacity, resulting in Fermi level pinning.[78]

Contrary to a metal an ideal n-type semiconductor without surface states has electron acceptor states only above the conduction band edge and a sudden onset of the charging current would be expected as the Fermi level reaches this edge. By contrast the very smooth onset in Figure 38 c,d indicates a tail of surface states below the bulk conduction band edge, which are filled first. Such a band tail of localized states is generally observed in disordered or amorphous materials, so that it is more appropriate to talk about a mobility edge rather than a conduction band edge.[79] The surface states can be ascribed to coordinatively unsaturated Ti^{4+} centers on the colloidal TiO_2 particles.[80] Their reduction to Ti^{3+} gives rise to a broad absorption spectrum with a maximum around 800 nm (Figure 40b).[81] From the absorbance change and the number of electrons injected into the 1 cm^2 electrode we calculate a decadic extinction coefficient of $\varepsilon_{800} = 1300\ M^{-1}cm^{-1}$ for the trapped electrons.

The negative charge in the surface states ($Ti^{4+} + e^- \rightarrow Ti^{3+}$) is compensated by counterions in the outer Helmholtz layer, creating a potential drop that depends on the size of the cations.[78b] It is larger for the bulky TBA^+ ion than for Li^+, which is so small that it even can intercalate into the TiO_2 lattice. This is why the current rises much steeper in presence of Li^+ (Figure 38d). The wave during the reverse cyclic voltammetric scan (Figure 38c,d) shows a nearly complete recovery of the injected negative charge, indicating that most surface states are emptied on the time scale of the scan (seconds).

The energetic distribution of acceptor states in the TiO_2 electrode is directly given by the cyclic voltammogram, since the current (I) in a linear sweep (dV/dt = const.) is proportional to the differential capacity (C) at the respective potential against the reference electrode in solution:

$$I = \frac{dQ}{dt} = C\frac{dV}{dt}$$

In accordance with this equation, the current was found to be proportional to the sweep rate dV/dt. The total injected charge obtained by integration of the current in Figure 38 c,d up to $E = -0.8$ V_{SCE} for $LiClO_4$ and $E = -1.0$ V_{SCE} for $TBABF_4$ is $Q = 1.6$ mC. For a 1 cm^2 electrode of roughness factor 1000 ($A = 0.1$ m^2) this corresponds to an acceptor state density $n = Q/e{\cdot}A = 10^{17}m^{-2}$. This is about 1% of the surface titanium atoms on TiO_2 and seems to be a reasonable density for surface states on a nanocrystalline particle with many surface defects, such as steps and kinks. Due to the high surface to volume ratio of these small particles the border between surface states and bulk states is ill defined and we cannot give a definite potential for the conduction band or mobility edge. However, steady photocurrents are obtained already after injection of less than 20 μC, which is small compared to the quoted charge of $Q = 1.6$ mC, indicating that electron transport may occur by hopping between surface states.

As already discussed the energetic distribution of acceptor states given by the cyclic voltammogram is measured with respect to the reference electrode in solution and depends on the potential drop in the Helmholtz double layer. The adsorbed chlorophyll molecule with a diameter of about 1 nm is at least partially inside the Helmholtz layer, which has a thickness of several 0.1 nm, depending on the size of the counterion.[78a,b] We can therefore give only a relative distribution of the states seen by the sensitizer (DOS in Figure 39). Still, we can say that there are plenty of acceptor states below the excited state levels of the sensitizers.

According to this energy diagram chlorin e_6 can inject an electron into TiO_2 from its singlet excited state. The cation radical produced could be reduced by a redox couple in the electrolyte, like I^-/I_3^-. However, it is also conceivable that the singlet excited dye is first reduced by the redox couple to the anion radical, which then injects an electron into the semiconductor. From a kinetic point of view, though, this mechanism seems less probable, since it requires the encounter of an iodide ion within the very short lifetime of the excited dye.

In the case of Cu-2α-oxymesoisochlorin e_4 the singlet excited state is presumed to be too short-lived ($\tau < 22$ fs according to the fluorescence quantum yield measurements) to be involved in the sensitization process. While the triplet excited state is still able to inject into TiO_2 and the resulting cation radical able to oxidize I^-, the reduction of the triplet excited dye to the anion radical is energetically unfavorable (Figure 39). In order to clarify the sensitization mechanism, we have investigated the charge separation process by laser flash photolysis.

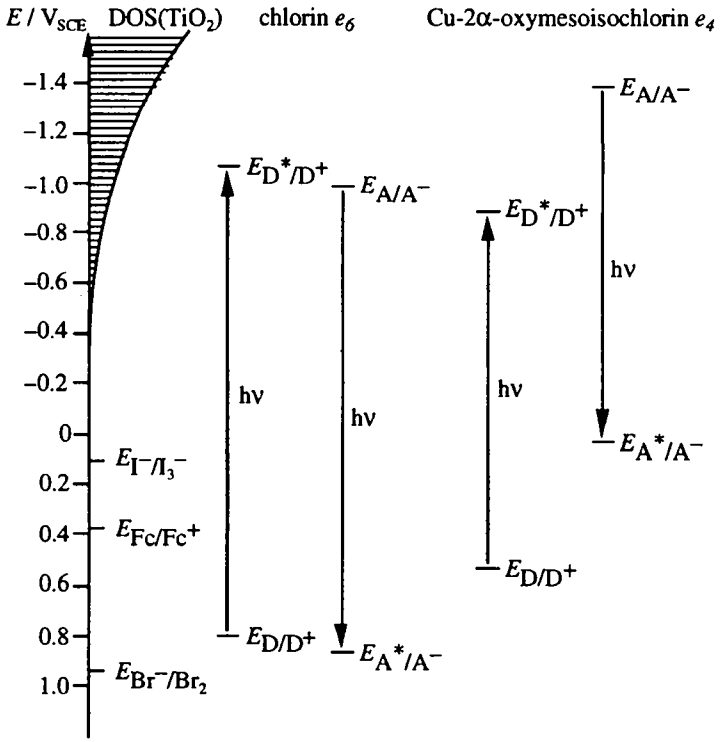

Figure 39: Energy levels at the semiconductor-adsorbed dye-electrolyte interface

E = midpoint redox potentials from cyclic voltammetry in propylene carbonate; E_{D/D^+} and E_{A/A^-} are the oxidation and reduction potential of the dye in the ground state; E_{D^*/D^+} and E_{A^*/A^-} are the respective potentials in the excited state (singlet for chlorin e_6, triplet for Cu-2α-oxymesoiso-chlorin e_4);
$DOS(TiO_2)$ = density of acceptor states in the TiO_2 electrode; **Fc** = ferrocene

3.5.7. Transient absorption spectra

The transient difference absorption spectrum of a Cu-2α-oxymesoisochlorin e_4 sensitized TiO_2 electrode measured 1 μs after laser flash excitation at 532 nm is shown in Figure 40c. The spectrum follows closely the sum of the difference spectra for the dye cation radical (Figure 40a, $\Delta\varepsilon_{633} = 3.7 \times 10^4\ M^{-1}cm^{-1}$) and the same amount of electrons in TiO_2 (Figure 40b, $\varepsilon_{800} = 1300\ M^{-1}cm^{-1}$). This is in accordance with the sensitization mechanism expected from the energy diagram (Figure 39), where an electron is injected into the semiconductor from the triplet excited dye, leaving the cation radical behind.

Since no reducing agent like I^- was present in this experiment, the alternative mechanism of reduction of the excited dye to the anion radical followed by electron injection can be excluded. Even addition of iodide (0.5 M NaI) does not change the transient spectrum taken 1 μs after the laser pulse (compare also Figure 41a). In particular, there is no absorption peak at 765 nm, as found spectroelectrochemically for the anion radical by polarizing a Cu-2α-oxymesoisochlorin e_4 sensitized TiO_2 electrode to −1.4 V_{SCE}, were electron transfer from the conduction band to the adsorbed dye takes place. The intermediate I^- oxidation product I_2^- also absorbs in the range 700-800 nm ($\varepsilon_{750} = 2800\ M^{-1}cm^{-1}$ in water) and can be observed with dye sensitized colloidal TiO_2 in solution.[82] However, due to the high initial I_2^- concentration in the small pore volume of the TiO_2 electrode most of it decays within 1 μs by the close to diffusion controlled disproportionation to $I_3^- + I^-$ and thus does not contribute to our transients.

We cannot exclude the photogeneration of a small amount of dye anion radicals, which decay very quickly after the laser pulse by electron injection into the semiconductor and escape our detection system. This would give rise to a transient absorption due to the injected electrons only. However, the equivalence of electrons injected and dye cation radicals created indicates that electron transfer from the neutral excited dye must be the predominant sensitization mechanism also in the presence of iodide.

The transient difference absorption spectrum of chlorin e_6 on TiO_2 (Figure 40d) shows again the bleaching of the Q_y band at 668 nm and an infrared tail due to the injected electrons. The spectrum of the cation radical could not be determined by electrochemical or chemical oxidation in this case, because of its short lifetime. However, a broad peak at 760 nm has been reported [83] for the cation radical of the related pheophorbide *a* and is also present in Figure 40d. The formation of a significant quantity of the triplet state can be excluded in

view of the fast and efficient quenching of the singlet state, which is seen in the fluorescence decays. This leads us to the conclusion, that sensitization of TiO_2 with chlorin e_6 occurs by the same mechanism as with the copper complex, only that the injecting dye is in the singlet excited state now.

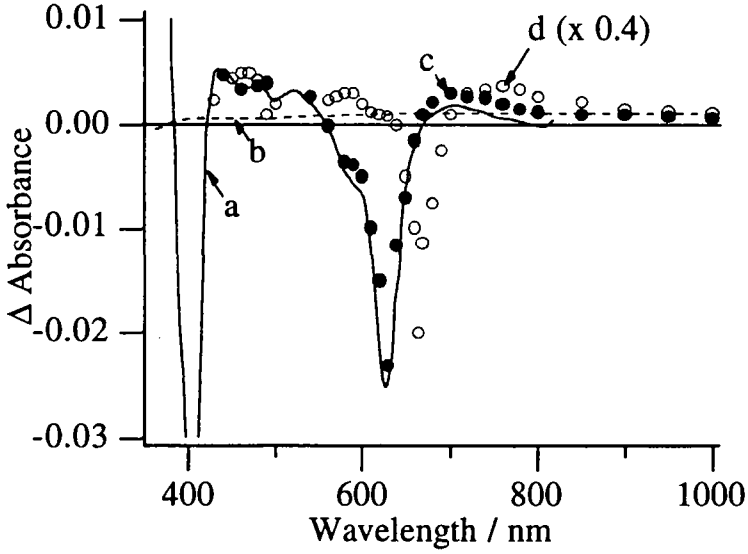

Figure 40: Difference absorption spectra of chlorophyllin cation radical and injected electrons in comparison to the transient difference absorption spectrum of the sensitized TiO_2 electrode.
(a) Cu-2α-oxymesoisochlorin e_4 on a porous SnO_2 electrode in 0.1 M $TBABF_4$ /PC at +0.6 V_{SCE}; **(b)** TiO_2 electrode in 0.1 M $TBABF_4$/PC at –0.5 V_{SCE}; **(c)** Cu-2α-oxymesoisochlorin e_4 and **(d)** chlorin e_6 sensitized TiO_2 electrode 1 μs after laser flash excitation with 2 mJ/cm^2 at 532 nm

3.5.8. Decay kinetics of the transient absorption

The time resolved absorption transients for the three wavelengths characteristic of Q_y band, cation radical and injected electron are reported in Figure 41. The time scale starts at 1 μs, since fluorescence from the glass substrate and also from the chlorin e_6 itself obscures the weak absorption changes at shorter times. With Cu-2α-oxymesoisochlorin e_4 (Figure 41a) in absence of a reducing agent the recovery of the bleaching in the Q_y band at 633 nm parallels the decay of the cation radical absorption at 720 nm and the electron absorption at 1000 nm, indicating recombination of the injected electrons with the oxidized dye molecules.

The absorbance change at 633 nm turns positive after 5 ms, which is in part explained by the reduction of some dye cations by impurities, so that only the broad absorption of the electrons is left behind. However, the absorbance at 633 and 720 nm at times longer than 5 ms is larger than the contribution of the electrons expected from their absorption at 1000 nm, so that further side reactions seem to be involved.

Addition of 0.5 M NaI (Figure 41a) leads to a much faster decay for dye recovery and cation radical absorption due to reduction of the oxidized dye by iodide within 100 μs. The electron absorption at 1000 nm stays constant after this time, since recombination with the dye cation is no longer possible. The broad absorption of the electron is responsible for the residual absorption at 633 and 720 nm. It decays at times longer than 100 ms, probably by reaction with the produced iodine or traces of oxygen.

With chlorin e_6 (Figure 41b) the same general behavior is observed, but recombination in the absence of iodide starts already on the μs time scale and reduction in presence of iodide is so fast, that most of the decay has already taken place after 1 μs. Both observations can be rationalized by the more positive oxidation potential of the chlorin e_6 cation in comparison to that of the copper complex (Figure 38).

The recombination process without iodide is for both dyes approximately linear on a logarithmic time scale, as observed before with a ruthenium dye on TiO_2 electrodes.[19 1] This has been ascribed to recombination of trapped electrons with the oxidized dye by tunneling and is consistent with our finding of a strong band tail due to surface states (Figure 38c,d). Interestingly, the charge recombination in photosynthetic reaction centers shows logarithmic kinetics as well, which again has been explained by electron tunneling from the reduced acceptor to the oxidized chlorophyll molecule.[84]

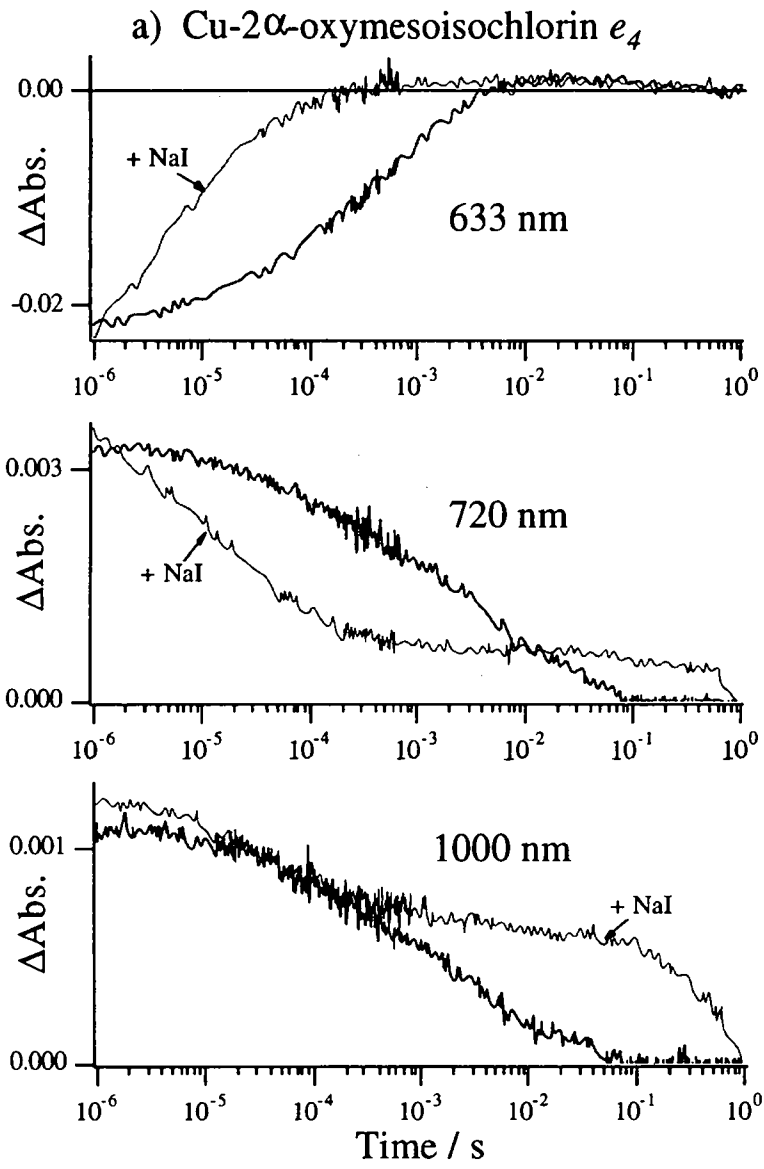

Figure 41: Decay kinetics of the transient absorbance change of chlorophyllin sensitized TiO_2 electrodes due to dye bleaching, cation radical and injected electron absorption. The propylene carbonate wetted TiO_2 electrodes were

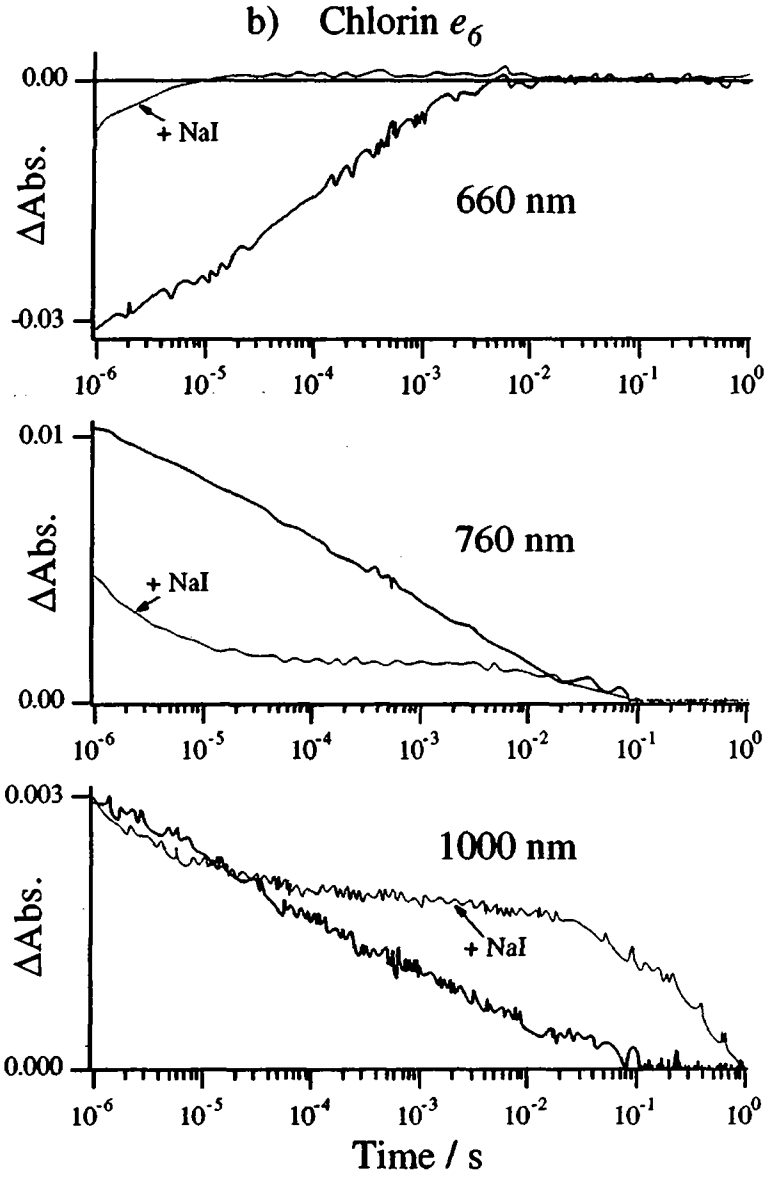

excited with a single laser pulse of 2 mJ/cm^2 at 532 nm. The decays marked "+NaI" were measured after addition of 0.5 M NaI/PC as reducing agent.

3.5.9. Photocurrent / voltage transients

The photocurrent and voltage transients of chlorophyllin sensitized TiO_2 electrodes after laser excitation are shown in Figure 42. We interpret the transients as follows: Electron injection takes place on the nanosecond scale and results in charging of the adsorbed dye – semiconductor interface. However, few electrons can be drawn off at these short times, since the positively charged dye adsorbed on the TiO_2 particles has to be compensated by a nearby electron. Only reduction of the dye by iodide charges the electrode with respect to the bulk electrolyte and hence the counter electrode. According to the transient absorption decays reduction of the dye cation is complete after about 100 µs for Cu-2α-oxymesoisochlorin e_4 and 10 µs for chlorin e_6 (Figure 41 a,b). The photovoltage and the thereby induced photocurrent through the external load reach their maximum at this moment of complete charging of the semiconductor–electrolyte interface (Figure 42).

The subsequent decline of the photocurrent depends on the size of the ohmic load (in this case 10 Ω external + 10 Ω from the SnO_2 substrate). The decay is linear in a double logarithmic plot, as typical for dispersive transport, due to the multiple trapping and release of the injected electrons by surface states.[85] The photovoltage (measured into 1 MΩ) decays more slowly by recombination of the trapped electrons with traces of oxygen and the iodine added to the electrolyte, which gives rise to the dark current of the solar cell and represents an internal load. Since the Fermi level in the TiO_2 depends in a non-linear fashion on the electron concentration a direct comparison of photovoltage and the transient absorption decay at 1000 nm is not possible.

3.5.10. Charge separation efficiencies from laser experiments

Integration of the photocurrent transients of Figure 42 yields an electrical charge of Q = 61 µC for chlorin e_6 as sensitizer and Q = 25 µC for Cu-2α-oxymesoisochlorin e_4. With a laser pulse energy of 2 mJ at 532 nm this corresponds to an incident photon to current efficiency of IPCE = 6.8% and 2.8%, respectively. Under continuos illumination IPCE = 13% and 10% were measured at 532 nm, where only 12% and 8% of the light are absorbed by the electrode in one pass, with the same platinum counter electrode, which reflects most of the transmitted light to pass the electrode a second time.

The lower IPCE under pulsed illumination can in part be attributed to the much higher recombination rate at the very high cation radical and trapped electron concentration created by the intense laser flash. This is reflected in

Figure 41, where an appreciable portion of the initial electron absorption at 1000 nm decays within a short time even in presence of iodide. In addition, for Cu-2α-oxymesoisochlorin e_4 the initial absorbance at 1000 nm is much lower than for chlorin e_6, which is only in part explained by the lower light absorption of the electrode at the laser wavelength (8% compared to 12%). One rather has to consider that the strong electron injection after high power laser excitation

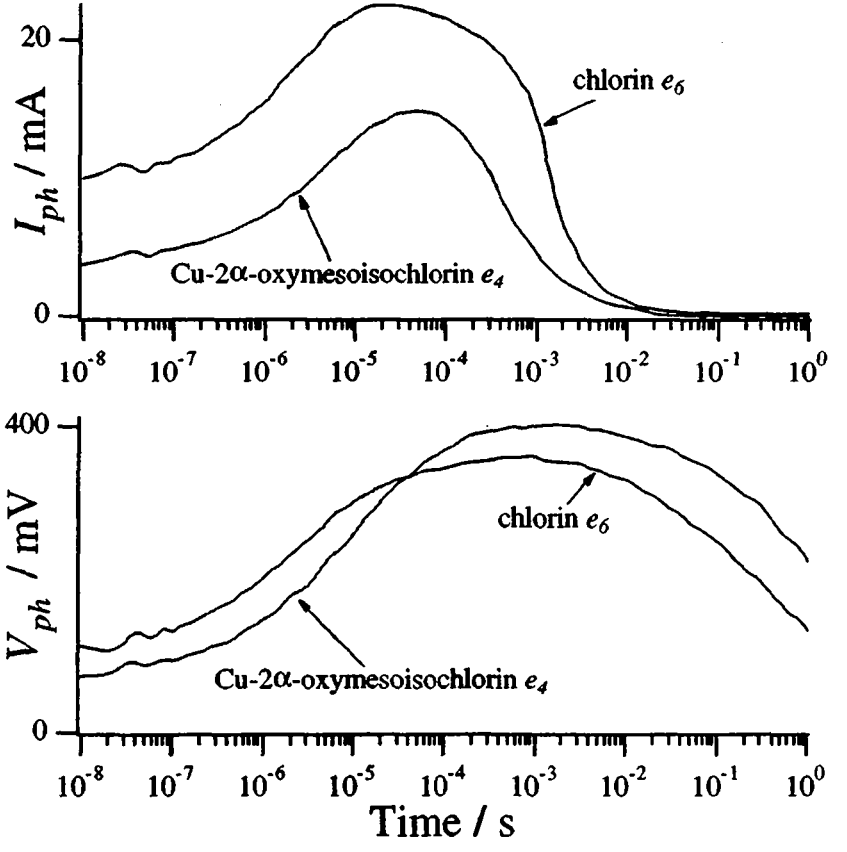

Figure 42: Photocurrent and photovoltage transients of chlorophyllin sensitized TiO_2 electrodes. The electrodes were wetted with electrolyte (0.5 M KI, 40 mM I_2 in 80% ethylene carbonate, 20% propylene carbonate), pressed against a platinum foil counter electrode and excited with a single 10 ns laser pulse of 2 mJ/cm^2 at 532 nm.

causes a negative shift of the quasi Fermi level in the semiconductor. Even with an external load of only 10 Ω (plus 10 Ω from the SnO_2) this shift amounts to several hundred millivolts, as can be inferred from Figure 42. Therefore, injection from Cu-2α-oxymesoisochlorin e_4 will soon cease, as the quasi Fermi level approaches the relatively low excited state level of this sensitizer (Figure 39). This is another reason for the low IPCE of 2.8% under laser flash excitation compared to 10% under continuos illumination.

3.5.11. Conclusions

The photosensitization of colloidal TiO_2 electrodes by chlorin e_6 and copper chlorophyllin has been shown to occur by electron injection from the neutral excited dye, leaving the cation radical behind, which is then reduced by iodide. The fluorescent chlorin e_6 injects from the singlet excited state with a rate constant of $k_{et} = 2.2 \times 10^9\ s^{-1}$, which competes efficiently with other decay processes. The non-fluorescent Cu-2α-oxymesoisochlorin e_4 injects from the triplet excited state with a smaller rate constant of $k_{et} = 3 \times 10^8\ s^{-1}$. This is still sufficient for a high electron injection yield, since the triplet lifetime increases in the adsorbed state due to slower internal conversion of the immobilized dye.

The electron transfer rate depends on the overlap of the donor states of the excited sensitizer with the acceptor states in the semiconductor.[56,86] The distribution function of donor states in the excited dye has a maximum at $E_{D^*/D^+} - \lambda$, the reorganization energy λ being in the order of 0.4 eV for a large rigid molecule like chlorophyllin in a polar solvent, although it may be lowered by hydrophobic interaction with the coadsorbed lithocholic acid.[1] According to the energy level diagram of Figure 39 the maximum lies at $E_{D^*/D^+} - \lambda = -0.7\ V_{SCE}$ for chlorin e_6 and at $-0.5\ V_{SCE}$ for Cu-2α-oxymesoisochlorin e_4, resulting in an optimal overlap with the lowest acceptor states of TiO_2 only. This is responsible for the slower electron injection from the copper complex and its lower injection efficiency under strong laser flash excitation, due to filling of the lowest acceptor states.

Recombination of the injected electron with the oxidized sensitizer follows approximately logarithmic kinetics from the microsecond range up to 100 ms. This can be ascribed to trapping of the electron in surface states with a distribution of depths and distances, from were back electron transfer to the chlorophyll cation occurs by tunneling.[84] Reduction of the oxidized dye by iodide can compete efficiently with this rather slow recombination process and results in a high charge separation yield. In contrast, the usual mechanism of charge separation by the electric field in the space charge region of the

semiconductor seems not to be operative in our case, due to negligible band bending in the nanoparticles of the colloidal electrode.[19,1,77] The purely kinetic charge separation mechanism in our artificial photosynthetic system is rather comparable to that of natural photosynthesis, were an electron is rapidly transferred from the excited reaction center chlorophyll to a distant acceptor of lower energy (the trap), thus preventing recombination before reduction of the chlorophyll cation by an electron donor has taken place. Obviously, the photosynthetic reaction center with its exactly defined geometry and well tuned donor–acceptor potentials is much more sophisticated than a semiconductor full of traps having chlorophyll molecules attached to it. In this respect the photocurrent quantum yields and energy conversion efficiencies obtained with such a system are even more remarkable.

3.6. Other sensitizers

Hundreds of other dyes have been tested as sensitizers for nanocrystalline TiO_2 electrodes, and we can only mention a few of them. The most simple class of sensitizers are compounds which develop a color only by reaction with the surface titanium atom. For example $Fe(CN)_6^{4-}$ forms an orange charge transfer complex with Ti^{4+}, which sensitizes the TiO_2 up to about 650 nm.[87] Also numerous Ti^{4+} complexing indicator dyes have been shown to sensitize TiO_2, e.g. 8-hydroxyquinoline,[19a] alizarin, gallein, morin, quercetin, coumarin [19i] and phenylfluorone.[19m]

In connection with our study on chlorophyll derivatives and related natural porphyrins (chapter 3.4) we tested further dyes of this class, such as H_2- and Zn-protoporphyrin IX, hematoporphyrin, uroporphyrin I, H_2- and Zn-tetra(4-carboxyphenyl)porphyrine. They show similar sensitization behavior as the mesoporphyrin IX complexes discussed in chapter 3.4.3. Only the iron complex heme and biliverdin, an open chain natural degradation product of heme, found in bile, showed no photosensitization at all, although the electrodes were nicely colored red and green, respectively:

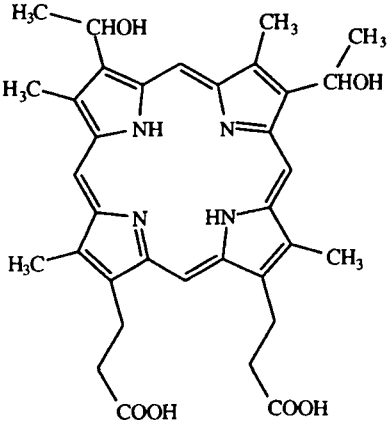

Hematoporphyrin

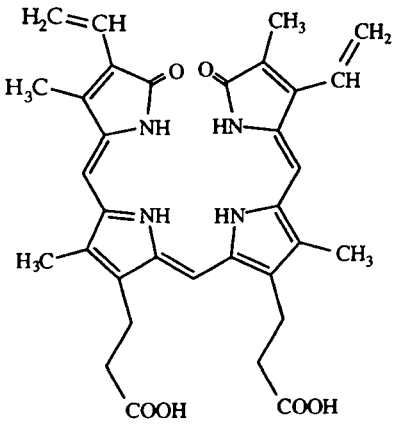

Biliverdin IX

Non-carboxylated phthalocyanines, such as aluminum phthalocyanine chloride (adsorbed from pyridine with blue color), gave no visible light photocurrent. Carboxylated phthalocyanines,[88] e.g. copper-tetracarboxyphthalocyanine, showed only poor sensitization in the red absorption bands (IPCE ≈ 15%).

Since carotenoids act as accessory pigments in natural photosynthesis we also tested β-apo-8'carotenoate, a carboxylated derivative of β-carotene,[89] as sensitizer for TiO_2. Absorption from ethanol results within only 30 minutes in a strong orange coloration of the electrode. The action spectrum is much broader than the absorption spectrum in solution and extents beyond 700 nm (Figure 43). The carotenoate molecules are supposed to form a closely packed monolayer on the TiO_2 surface, which may cause broadening of the absorption spectrum due to dipole-dipole interaction between the polyene chains. Interestingly, β-carotene exhibits semiconductor properties and photoconductivity in the solid state.[90] With iodine it forms a charge transfer complex which absorbs strongly around 1000 nm ($\varepsilon > 2 \cdot 10^5\ M^{-1}cm^{-1}$).[91] This is probably not formed in our case due to the presence of excess iodide. In view of the surprising photosensitization behavior of carotenoate it may be worth-while to investigate other monolayer forming dyes, such as oligothiophenes,[92-94] which exhibit electric conductivity as well.

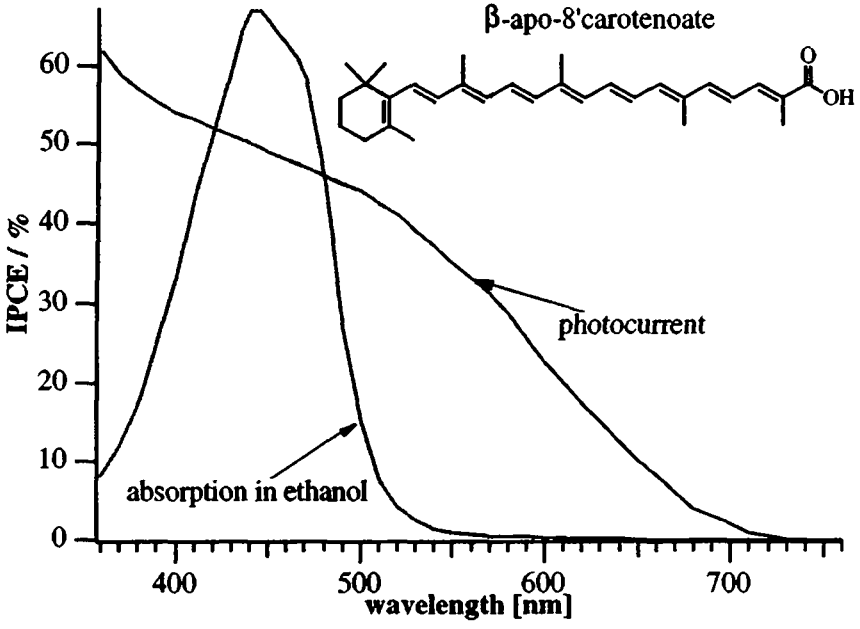

Figure 43: Absorption spectrum in solution and photocurrent action spectrum of an β-apo-8'carotenoate sensitized TiO_2 electrode (P 25, electrolyte: 80% ethylene carbonate, 20% propylene carbonate, 0.5 M KI, 40 mM I_2)

Also merocyanine dyes form monolayers with defined aggregate structures and semiconductor properties.[90] They have been used in solid state organic solar cell with sunlight efficiencies in excess of 1%.[95-97] Also sandwich cells with a TiO_2 single crystal anode have been reported.[98] A carboxylated merocyanine [95a] was introduced by J. Moser in our group and turned out to be an excellent sensitizer for nanocrystalline TiO_2 electrodes as well. Adsorption from ethanol resulted in the photocurrent action spectrum shown in Figure 44. The action spectrum corresponds to that reported for a solid state solar cell with a 260 nm thick film of the same merocyanine,[95a] but extends 100 nm further into the red than the absorption spectrum in solution. This has also been observed in the sensitization of ZnO by pseudoisocyanins [3d] and is due to the formation of J-aggregates in the closely packed dye monolayer.[99]

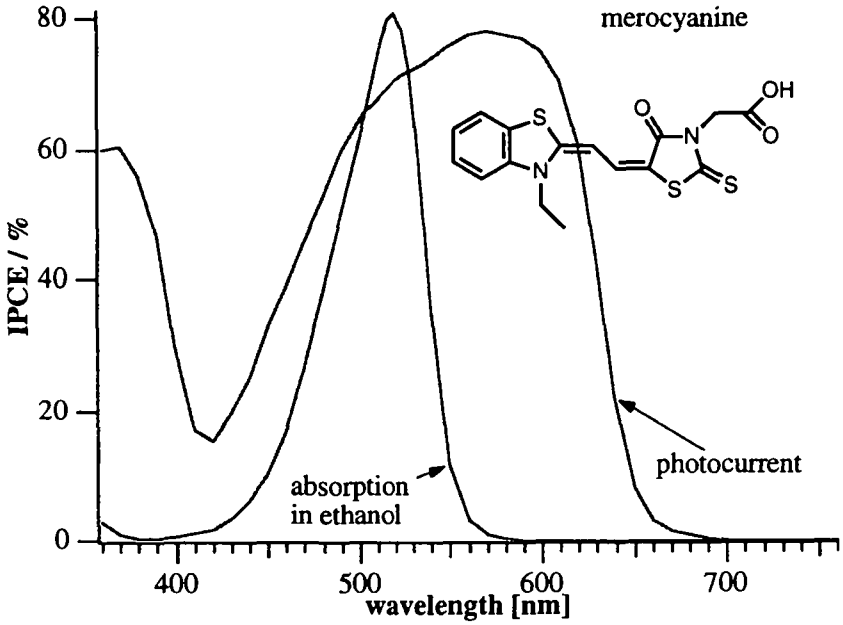

Figure 44: Absorption spectrum in solution and photocurrent action spectrum of a merocyanine sensitized TiO_2 electrode (P 25, dye adsorbed from ethanol containing 10 mM lithocholic acid, electrolyte: 80% ethylene carbonate, 20% propylene carbonate, 0.5 M KI, 40 mM I_2)

Interestingly, the merocyanine can also be applied by vacuum sublimation at about 250°C.[95] For this purpose we applied a thin layer of dye powder between a SnO_2 conducting glass electrode and the porous TiO_2 electrode and heated the SnO_2 electrode by an alternating current in vacuum ($1.5 \cdot 10^{-3}$ Pa) until sublimation and penetration of the dye into the TiO_2 film occurred. Although the electrode was very inhomogeneously colored, probably due to temperature gradients during sublimation, an IPCE of 53% was obtained. The open circuit photovoltage was also lower (0.30 V compared to 0.49 V after adsorption from ethanol), possibly due to some decomposition of the dye at the high temperature on the catalytic TiO_2 surface.

While a liquid I^-/I_3^- redox electrolyte was still used in this experiment to provide contact with the counter electrode, some conduction must have occurred through the solid merocyanine filling the pores of the TiO_2 film. It is known that solid merocyanines are p-type conductors [90] and exhibit hole conductivity, which can be increased by iodine doping.[98] The rather poor current/voltage characteristics with fill factors below 0.3 obtained with even very thin (100 nm) merocyanine films between two metal electrodes were attributed to the field dependence of exciton dissociation rather than to the ohmic resistance of the solid dye layer.[95] With our much thicker (≈10 μm) merocyanine filled TiO_2 films fill factors of 0.5 were obtained at current densities of 2 mA/cm^2. If this current was really carried by the solid merocyanine in the pores, this would indeed indicate a very high hole conductivity, possibly enhanced by photo-doping due to electron injection into TiO_2.

It would be interesting to build an all solid state solar cell by contacting the merocyanine directly, e.g. with an evaporated metal film. A thin merocyanine layer on top of the porous TiO_2 film would be required to prevent a short circuit between the metal and TiO_2. Preliminary experiments with a graphite tip contacting the merocyanine showed indeed a photoresponse without any electrolyte, although it was small, as expected form the small contact area.

References to chapter 3

1. **W. Jaenicke:** Electrochemical aspects of the photographic processes, in *Advances in Electrochemistry and Electrochemical Engineering,* H. Gerischer, C.W. Tobias, eds., Wiley, New York 1977, Vol.10, p. 91
2. **H. Gerischer, B. Bressel:** Photoelectrochemical studies of dye sensitization at silver chloride single crystals *Ber. Bunsenges. Phys. Chem.* 89 (1985) 1083
3. a) **H. Gerischer, H. Tributsch:** Elektrochemische Untersuchungen zur spektralen Sensibilisierung von ZnO-Einkristallen *Ber. Bunsenges. Phys. Chem.* 72 (1968) 437

   b) **H. Gerischer, M.E. Michel-Beyerle, F. Rebentrost, H. Tributsch:** Sensitization of charge injection into semiconductors with large band gap *Electrochim. Acta* 13 (1968) 1509

   c) **H.Tributsch, H.Gerischer:** Electrochemische Untersuchungen über den Mechanismus der Sensibilisierung und Übersensibilisierung an ZnO-Einkristallen *Ber. Bunsenges. Phys. Chem.* 73 (1969) 251

   d) **H. Tributsch:** Elektrochemische Untersuchungen über die Sensibilisierungseigenschaften und das photochemische Verhalten von Pseudoisocyanin-Farbstoffaggregaten an ZnO-Elektroden *Ber. Bunsenges. Phys. Chem.* 73 (1969) 582
4. **R. Brändli, P. Rys, H. Zollinger, H.R. Oswald, F. Schweizer:** Über die spektrale Sensibilisierung von Zinkoxid: I. Sorptionsverhalten von o,o'-Dihydroxyazofarbstoffen *Helv. Chim. Acta* 53 (1970) 1133
5. a) **H.J. Danzmann, K. Hauffe:** Spektrale Sensibilisierung von Zinkoxid durch chelatbildende Farbstoffe *Ber. Bunsenges. Phys. Chem.* 79 (1975) 438

   b) **U. Bode, K. Hauffe:** On the influence of sensitization of the electron transfer through the interface zinc oxide / electrolyte by salt addition *J. Electrochem. Soc.* 125 (1978) 51
6. **T.Yamase, H. Gerischer, M. Lübke, B. Pettinger:** Involvement of surface states in the spectral sensitization of zinc oxide electrodes *Ber. Bunsenges. Phys. Chem.* 82 (1978) 1041
7. a) **M. Matsumura, Y. Nomura, H. Tsubomura:** Effect of etching on intrinsic and dye-sensitized photocurrents in zinc-oxide electrodes *Bull. Chem. Soc. Japan* 52 (1979) 1559

   b) **M. Matsumura, S. Matsudaira, H. Tsubomura, M. Takata, H. Yanaigida:** Dye sensitization and surface structure of semiconductor electrodes *Ind. Eng. Chem. Prod. Res. Dev.* 19 (1980) 415
8. a) **C. Kavassalis, M.T. Spitler:** Photooxidation of thiacyanine dyes at ZnO single-crystal electrodes *J. Phys. Chem.* 87 (1983) 3166

   b) **M.T. Spitler:** Quenching of dye-sensitized photocurrents at ZnO semiconductor electrodes *J. Phys. Chem.* 90 (1986) 2156
9. a) **R. Memming:** Photochemical processes in monomolecular dye layers on SnO_2 *Faraday Disc. Chem. Soc.* 58 (1974) 261

   b) **R. Memming:** Electron transfer reactions of excited ruthenium(II) complexes at semiconductor electrodes *Surf. Sci.* 101 (1980) 551

10. a) **T. Osa, M. Fujihira:** Photocell using covalently-bond dyes on semiconductor surfaces *Nature* 264 (1976) 349, 268 (1977) 226

b) **M. Fujihira, T. Osa, D. Hursh, T. Kuwana:** Analysis of covalently bond rhodamin B photoelectrode *J. Electroanal. Chem.* 88 (1978) 285

11. **P.K. Ghosh, T.G. Spiro:** Photoelectrochemistry of tris(bipyridyl)ruthenium(II) covalently attached to n-type SnO_2 *J. Am. Chem. Soc.* 102 (1980) 5543

12. **M. Nakao, K. Itoh, T. Watanabe, K. Honda:** Mechanism of electrochemical dye sensitization *Ber. Bunsenges. Phys. Chem.* 89 (1985) 134

13. **I.R. Harrison, T.I. Quickenden:** Effect of electrodic dye layers on electron transfer and power conversion efficiency in rhodamine photoelectrochemical cells *J. Phys. Chem.* 91 (1987) 1481

14. **H. Sato, M. Kawasaki, K. Kasatuni, Y. Higuchi, T. Azuma, Y. Nishiyama:** Light-harvesting effect in photoelectric conversion with dye multilayers on a semiconductor electrode *J. Phys. Chem.* 92 (1988) 754

15. a) **W. Arden. P. Fromherz:** Sensitized photocurrent through a semiconductor electrode by consecutive energy and electron transfer in dye monolayers *Ber. Bunsenges. Phys. Chem.* 82 (1978) 868

b) **W. Arden. P. Fromherz:** Photosensitization of semiconductor electrode by cyanine dye in lipid bilayer *J. Electrochem. Soc.* 127 (1980) 370

16. **W.D.K. Clark, N. Sutin:** Spectral sensitization of n-type TiO_2 electrodes by polypyridine ruthenium(II) complexes *J. Am. Chem. Soc.* 99 (1977) 4676

17. **P.D. Fleischauer, J.K. Allen:** Photochemical hydrogen formation by the use of titanium dioxide thin-film electrodes with visible-light excitation *J. Phys. Chem.* 83 (1978) 432

18. a) **A. Hamnett, M.P. Dare-Edwards, R.D. Wright, K.R. Seddon, J.B. Goodenough:** Photosensitization of titanium(IV)oxide with tris(2,2'bipyridine)ruthenium(II)chloride *J. Phys. Chem.* 83 (1979) 3280

b) **S. Anderson, E.C. Constable, M.P. Dare-Edwards, J.B. Goodenough, A. Hamnett, K.R. Seddon, R.D. Wright:** Chemical modification of a titanium(IV)oxide electrode to give stable dye sensitization without supersensitization *Nature* 280 (1979) 571

c) **M.P. Dare-Edwards, J.B. Goodenough, A. Hamnett, K.R. Seddon, R.D. Wright:** Sensitization of semiconductor electrodes with ruthenium-based dyes *J. Chem. Soc., Faraday Disc.* 70 (1980) 285

19 a) **V.H. Houlding, M. Grätzel:** Photochemical H_2 generation by visible light. Sensitization of TiO_2 particles by surface complexation with 8-Hydroxyquinoline *J. Am. Chem. Soc.* 105 (1983) 5695

b) **D. Duonghong, N. Serpone, M. Grätzel:** Sensitization of TiO_2 particles by surface derivatization with ruthenium complexes *Sci. Papers Inst. Phys. Chem. Res.* 78 (1984) 232

c) **J. Moser, M. Grätzel:** Photosensitized electron injection in colloidal semiconductor *J. Am. Chem. Soc.* 106 (1984) 6557

d) **T. Nakahira, M. Grätzel:** Visible light sensitization of platinized TiO_2 photocatalyst by surface-adsorbed poly(4-vinylpyridine) derivatized with ruthenium trisbipyridyl complex *Makromol. Chem., Rapid Commun.* 6 (1985) 341

e) **J. Desilvestro, M. Grätzel, L. Kavan, J. Moser:** Highly efficient sensitization of titanium dioxide *J. Am. Chem. Soc.* 107 (1985) 2988

f) **N. Vlachopoulos, P. Liska, A.J. McEvoy, M. Grätzel:** Efficient spectral sensitization of polycrystalline titanium dioxide photoelectrodes *Surf. Sci.* 189/190 (1987) 823

g) **P. Liska, N. Vlachopoulos, M.K. Nazeeruddin, P. Compte, M. Grätzel:** *cis*-Diaquabis(2,2'-bipyridyl-4,4'-dicarboxylate)-ruthenium(II) sensitizes wide band gap oxide semiconductors very efficiently over a broad spectral range in the visible *J. Am. Chem. Soc.* 110 (1988) 3686

h) **N. Vlachopoulos, P. Liska, J. Augustynski, M. Grätzel:** Very efficient light energy harvesting and conversion by spectral sensitization of high surface area polycrystalline titanium dioxide films *J. Am. Chem. Soc.* 110 (1988) 1216

i) **O. Enea, J. Moser, M. Grätzel:** Achievement of incident photon to electric current conversion yields exceeding 80% in the spectral sensitization of titanium dioxide by coumarin *J. Electroanal. Chem.* 259 (1989) 59

k) **M.K. Nazeeruddin, P. Liska, J. Moser, N. Vlachopoulos, M. Grätzel:** Conversion of light into electricity with trinuclear ruthenium complexes adsorbed on textured TiO_2 films *Helv. Chim. Acta* 73 (1990) 1788

l) **B. O'Regan, J. Moser, M. Andersson, M. Grätzel:** Vectorial electron injection into transparent semiconductor membranes and electric field effects on the dynamics of light -induced charge separation *J. Phys. Chem.* 94 (1990) 8720

m) **H. Frei, D.J. Fitzmaurice, M. Grätzel:** Surface chelation of semiconductors and interfacial electron transfer *Langmuir* 6 (1990) 198

n) **B. O'Regan, M. Grätzel:** A low-cost, high efficiency solar cell based on dye-sensitized colloidal TiO_2 films *Nature* 353 (1991) 737

o) **M.K. Nazeeruddin, A. Kay, I. Rodicio, R. Humphry-Baker, E. Müller, P. Liska, N. Vlachopoulos, M. Grätzel:** Conversion of light into electricity by *cis*-X_2Bis(2,2'-bipyridyl-4,4'-dicarboxylate)-ruthenium(II) charge transfer sensitzers (X = Cl^-, Br^-, I^-, CN^- and SCN^-) on nanocrystalline TiO_2 electrodes *J. Am. Chem. Soc.* 115 (1993) 6382

20. **D.A. Gulino, H.G. Drickammer:** High-pressure studie of the dye-sensitzed photocurrent spectrum of titanium dioxide *J. Phys. Chem.* 88 (1984) 1173
21. **L.P. Sonntag, M.T. Spitler:** Examination of the energetic threshold for dye-sensitized photocurrent at $SrTiO_3$ electrodes *J. Phys. Chem.* 89 (1985) 1453
22. **D.N. Furlong, D.Wells, W.H.F. Sasse:** Colloid semiconductors in systems for the sacrificial photolysis of water: Sensitization of TiO_2 by adsorption of ruthenium complexes *J. Phys. Chem.* 90 (1986) 1107
23. **R. Dabestani, A.J. Bard, A. Campion, M.A. Fox, M.E. Mallouk, S.E. Webber, J.M. White:** Sensitization of titanium dioxide and strontium

titanate electrodes by ruthenium(II)tris(2,2'-bipyridine-4,4'-carboxylic acid) and zinc tetrakis(4-carboxyphenyl)porphyrin *J. Phys. Chem.* 92 (1988) 1872

24. **R. Amadelli, R. Argazzi, C.A. Bignozzi, F. Scandola:** Design of antenna-sensitizer polynuclear complexes. Sensitization of titanium dioxide with $[Ru(bpy)_2(CN)_2]_2Ru(bpy)(COO)_2)_2^{2-}$ *J. Am. Chem. Soc.* 112 (1990) 7099
25. a) **R. Knödler, J. Sopka, F. Harbach, H.W Grünling:** Photoelectrochemical cell based on dye sensitized colloidal TiO_2 layers *Sol. Energy Mater.* 30 (1993) 277

    b) **A. Hagfeldt, B.Didriksson, T.Palmquist, H. Lindström, S. Södergren, H. Rensmo, S.E. Lindquist:** *Sol. Energy Mater.* 31 (1994) 481
26. **J.R. Bolton:** Solar fuels, *Science* 202 (1978) 705
27. **A. Ennaoui, S. Fiechter, C.H. Pettenkofer, N. Alonso-Vante, K. Büker, M. Bronold, Ch. Höpfner, H. Tributsch:** Iron disulfide for solar energy conversion *Sol. Energy Mat. Sol. Cells* 29 (1993) 289
28. **H. Weller:** Colloidal semiconductor Q-particles *Angew. Chem. Int. Ed. Engl.* 32 (1993) 41
29. **J. Simon, J.-J. André:** *Molecular Semiconductors*, Berlin 1985
30. **M. Kaneko, A. Yamada:** Solar energy conversion by functional polymers *Adv. Polymer Sci.* 55 (1984) 1
31. **A.O. Patil, A.J. Heeger, F. Wudl:** Optical properties of conducting polymers *Chem. Rev.* 88 (1988) 183
32. a) **Y. Cao, G.M. Treacy, P. Smith, A.J. Heeger:** Solution-cast films of polyaniline *Appl. Phys. Lett.* 60 (1992) 2711

    b) **Y. Cao, P. Smith, A.J. Heeger:** Counter-ion induced processibility of conducting polyaniline *Synth. Metals* 48 (1992) 91
33. a) **A. Juris, V. Balzani, F. Barigelletti, S. Campagna, P. Belser, A. von Zelewsky:** Ru(II)polypyridine complexes *Coord. Chem. Rev.* 84 (1988) 85

    b) **K. Kalyanasundaram:** Photochemistry of polypyridine and porphyrin complexes, Acad. Pr., London 1992
34. **Kirk-Othmer:** *Encyclopedia of Chemical Technology*, 3rd edition, Wiley, New York 1978, Vol. 3, p. 130
35. **A. Kay, M. Grätzel:** Artificial Photosynthesis. 1. Photosensitization of TiO_2 solar cells with chlorophyll derivatives and related natural porphyrins *J. Phys. Chem.* 97 (1993) 6272
36. **K. Kalyanasundaram, N. Vlachopoulos, V. Krishnan, A. Monnier, M. Grätzel:** Sensitization of TiO_2 in the visible light region using zinc porphyrin *J. Phys. Chem.* 91 (1987) 2342
37. a) **H. Tributsch, M. Calvin:** Electrochemistry of excited molecules: Photoelectrochemical reactions of chlorophylls *Photochem. Photobiol.* 14 (1971) 95

    b) **H. Tributsch:** Reaction of excited chlorophyll molecules at electrodes and in photosynthesis *Photochem. Photobiol.* 16 (1972) 261
38. a) **T. Miyasaka, T. Watanabe, A. Fujishima, K. Honda:** Light energy conversion with chlorophyll monolayer electrodes *J. Am. Chem. Soc.* 100 (1978) 6657

b) **T. Miyasaka, T. Watanabe, A. Fujishima, K. Honda:** Highly efficient quantum conversion at chlorophyll a - lecithin mixed monolayer coated electrodes *Nature* 277 (1979) 638

c) **T. Miyasaka, T. Watanabe, A. Fujishima, K. Honda:** Photoelectrochemical study of chlorophyll-a multilayers on SnO_2 electrode *Photochem. Photobiol.* 32 (1980) 217

d) **T. Watanabe, A. Fujishima, K. Honda:** Photoelectrolysis of water and sensitization of semiconductors, in *Energy Resources through Photochemistry and Catalysis*, M.Grätzel, Ed., Acad. Press, New York, 1983, p. 359

e) **T. Watanabe, K. Machida, H. Suzuki, M. Kobayashi, K. Honda:** Photoelectrochemistry of metallochlorophylls *Coord. Chem. Rev.* 64 (1985) 207

39. **K. Takehara, H. Imai, Y. Ide:** Characteristics of dye-sensitized photocurrent by metallochlorophylls *Mem. Fac. Sci., Kyushu Univ. Ser. C* 16 (1987) 1

40. (a) **P.V. Kamat, J.-P. Chauvet, R.W. Fessenden:** Photosensitization of a TiO_2 semiconductor with a chlorophyll analogue *J. Phys. Chem.* 90 (1986) 1389

    (b) **P.V. Kamat, J.-P. Chauvet:** Photoelectrochemical sensitization and spectroscopic properties of reduced and oxidized forms of chlorophyll analogue *Radiat. Phys. Chem.* 37 (1991) 705

41. **K.K. Rao, D.O. Hall, N. Vlachopoulos, M. Grätzel, M.C.W. Evans, M. Seibert:** Photoelectrochemical responses of photosystem II particles immobilized on dye derivatized TiO_2 films *J. Photochem. Photobiol. B* 5 (1990) 379

42. **K. Iriyama, N. Ogara, A. Takamiya:** A simple method for extraction and partial purification of chlorophyll from plant material, using dioxane *J. Biochem.* 76 (1974) 901

43. **H. Fischer, A. Stern:** *Die Chemie des Pyrrols*, Vol. 2, Part 2, Leipzig 1940

44. **G. Oster, S.B. Broyde, J.S. Bellin:** Spectral properties of chlorophyll a *J. Am. Chem. Soc.* 86 (1964) 1309 & 1313

45. **J.-H. Fuhrhop, K.M. Smith:** in *Porphyrins and Metalloporphyrins*, Smith, K.M., Ed., Elsevier, Amsterdam 1975, p.777

46. **A.L. Verma, R. Mendelsohn, H.J. Bernstein:** Resonance Raman spectra of the nickel, cobalt and copper chelates of mesoporphyrin IX dimethyl ester *J. Chem. Phys.* 61 (1974) 383

47. (a) **J.C. Goedheer:** Visible absorption and fluorescence of chlorophyll and its aggregates in solution, in *The Chlorophylls*, L.P. Vernon. ; G.R. Seely, Eds., Acad. Press, New York 1966, p. 147

    (b) **J.J. Katz, M.K. Bowman, T.J. Michalski, D.L. Worcester:** Chlorophyll aggregation, in *Chlorophylls*, H. Scheer, Ed., CRC, Boca Raton 1991, p. 211

48. **J.J. Katz, L. Shipman, T.M. Cotton, T.R. Janson:** Chlorophyll aggregation, in *The Porphyrins*, Vol. 5, Dolphin, D., Ed., Acad. Press, New York 1978, p.401

49. **R.R. Bucks, S.G. Boxer:** Synthesis and spectroscopic properties of a novel cofacial chlorophyll-based dimer *J. Am. Chem. Soc.* 104 (1982) 340

50. **R.C. Davis, R.M. Pearlstein:** Chlorophyllin-apomyoglobin complexes *Nature* 280 (1979) 413

51. **J.C. Kephart:** Chlorophyll derivatives - Their chemistry, commercial preparation and uses *Econ. Bot.* 9 (1955) 3

52. (a) **M.Strell, A. Kalojanoff, F. Zuther:** Zur Analytik von Chlorophyll-Präparaten *Arzneimittel-Forsch.* 5 (1955) 640; 6 (1956) 8

(b) **F. Zuther:** *Neue Reaktionen in der Chlorophyllchemie*, Dissertation, München 1955

53. **L.J. Boucher, J.J. Katz:** Aggregation of metallochlorophyllin *J. Am. Chem. Soc.* 89 (1967) 4703

54. **W.C. Herndon:** The structure of choleic acids *J. Chem. Educ.* 44 (1967) 724

55. **T. Watanabe, M. Kobayashi:** Electrochemistry of chlorophylls in *Chlorophylls*, Scheer, H., Ed., CRC, Boca Raton 1991, p.287

56. a) **H. Gerischer, F. Willig:** Reaction of excited dye molecules at electrodes, in *Physical and Chemical Applications of Dyestuffs, Topics in Current Chemistry* 61, Berlin 1976, p. 31

b) **H. Gerischer, M.T. Spitler, F. Willig:** Electrode reactions of excited molecules, in *Proc. 3rd Symp. Electr. Proc.* (Boston 1979), S. Bruckenstein, ed., Princeton 1980

57. a) **R. Eichberger, F. Willig:** Ultrafast electron injection from excited dye molecules into semiconductor electrodes *Chem. Phys.* 141 (1990) 159

b) **F. Willig, R. Kietzmann, K. Schwarzburg:** Time-resolved luminescence, photo-current and simple reaction scheme for a folded ultra-thin-layer solar cell, in *Proc. Int. Symp. Opt. Mat. Technol. for Energy Efficiency and Solar Energy*, Toulouse, May 1992, SPIE Publication

58. **A. Kay, R. Humphry-Baker, M. Grätzel:** Artificial Photosynthesis. 2. Investigations on the mechanism of photosensitization of nanocrystalline TiO_2 solar cells by chlorophyll derivatives, *J. Phys. Chem.* in print

59. **M. Ocaña, E. Matijevic:** Well-defined colloidal tin(IV)oxide particles *J. Mater. Res.* 5 (1990) 1083

60. **G. Weber, F.W.J. Teale:** Determination of the absolute quantum yield of fluorescent solutions *Trans. Faraday Soc.* 53 (1957) 646

61. **T. Saji, A.J. Bard:** Electrogenerated luminescence. 29. The electrochemisty and chemi-luminescence of chlorophyll a in N,N-Dimethylformamide solution *J. Am. Chem. Soc.* 99 (1977) 2235

62. **H.H. Kung, H.S. Jarrett, A.W. Sleight, A. Ferretti:** Semiconducting oxide anodes in photoassisted electrolysis of water *J. Appl. Phys.* 48 (1977) 2463

63. **M.A. Butler, D.S. Ginley:** Prediction of flatband potentials at semiconductor-electrolyte interfaces from atomic electron-negativities *J. Electrochem. Soc.* 125 (1978) 228

64. **J.C. Goedheer:** Visible absorption and fluorescence of chlorophyll and its aggregates in solution, in *The Chlorophylls*, L.P. Vernon.; G.R. Seely, Eds., Acad. Press, New York 1966, p.147

65. a) **J.C. Demas, G.A. Crosby:** The measurement of photoluminescence quantum yields *J. Phys. Chem.* 75 (1971) 991

b) The refractive index of the porous, propylene carbonate filled oxide films was calculated from the interference maxima in the transmission spectrum [**Chopra, K.L.**: *Thin Film Phenomena*, McGraw-Hill, New York 1969, p. 102], while the thickness of the film was measured with a mechanical stylus (Tencor instruments: alpha-step).

66. a) **S. Hirayama, D. Phillips:** Correction for refractive index in the comparison of radiative lifetimes in vapor and solution phases *J Photochem.* 12 (1980) 139

b) **S. Hirayama, Y. Iuchi, F. Tanaka, K. Shobatake:** Natural lifetimes of anthracene derivatives and their dependence on refractive index *Chem. Phys.* 144 (1990) 401

c) **W. Lukosz:** Theory of optical-environment-dependent spontanous-emission rates for emitters in thin layers *Phys. Rev. B* 22 (1980) 3030

67. a) **A.A. Frolov, E.J. Zenkevich, G.P. Gurinovich, G.A. Kochubeyev:** Chlorin e_6-liposome interactions. Investigation by the methods of fluorescence spectroscopy and inductive energy transfer *J. Photochem. Photobiol. B* 7 (1990) 43

b) **S.S. Dvornikov, V.N. Knyukshto, K.N. Solovev:** Spectral-polarization study of the luminescence of mesopheophytin a, chlorin e_6, and their metal complexes *Opt. Spectrosc.* 51 (1981) 155

68. a) **K. Hashimoto, M. Hiramoto, T. Sakata:** Photo-induced electron transfer from adsorbed rhodamin B to oxide semiconductor substrates in vacuo *Chem. Phys. Lett.* 148 (1988) 215

b) **K. Hashimoto, M. Hiramoto, A.B.P. Lever, T. Sakata:** Luminescence decay of ruthenium (II) complexes adsorbed on metaloxide powders in vacuo *J. Phys. Chem.* 92 (1988) 1016

c) **Y. Liang, A.M. Ponte Goncalves:** Time-resolved measurements of the fluorescence of rhodamin B on semiconductor and glass surfaces *J. Phys. Chem.* 89 (1985) 3290

d) **A.M. Ponte Goncalves:** Fluorescence of dye molecules adsorbed on semiconductor surfaces, in *Photochemistry on Solid Surfaces*, M. Anpo, T. Matsuura, Eds.; Elsevier: Amsterdam 1989, p. 403

69. a) **T. Watanabe, K. Machida, H. Suzuki, M. Kobayashi, K. Honda:** Photoelectrochemistry of metallochlorophylls *Coord. Chem. Rev.* 64 (1985) 207

b) **K. Itoh, Y. Chiyokawa, M. Nakao, K. Honda:** Fluorescence quenching processes of rhodamin B on oxide semiconductors and light-harvesting action of its dimers *J. Am. Chem. Soc.* 106 (1984) 1620

70. **J. Fernandez, R.S. Becker:** Unique luminescence of dry chlorophylls *J. Chem. Phys.* 31 (1959) 467

71. a) **M.Gouterman:** Optical spectra and electronic structure of porphyrins and related rings, In *The Porphyrins*; Dolphin, D., Ed.; Academic Press: New York 1978, Vol. III, p. 79

b) **A. Harriman:** Luminescence of porphyrins and metalloporphyrins *J. Chem. Soc., Faraday Trans. 1* 77 (1981) 369

c) **M. Asano, Y. Kaizu, H. Kobayashi:** The lowest excited states of copper porphyrins *J. Chem. Phys.* 89 (1988) 6567

72. **Y.J. Aronowitz, M. Gouterman:** Effect of metal and substituents on the quasi-line spectra of some metalloporphyrins *J. Mol. Spectr.* 64 (1977) 267

73. **S.J. Strickler, R.A. Berg:** Relationship between absorption intensity and fluorescence lifetime of molecules *J. Chem. Phys.* 37 (1962) 814

74. **E.M. Schulman, C. Walling:** Triplet-state phosphorescence of adsorbed ionic organic molecules at room temperature *J. Phys. Chem.* 77 (1973) 902

75. a) **R.H. Felton:** Primary redox reactions of metalloporphyrins, In *The Porphyrins*, D. Dolphin, Ed.; Academic Press: New York 1978, Vol. V, p. 97

b) **G.R. Seely:** The energetics of electron-transfer reactions of chlorophyll and other compounds *Photochem. Photobiol.* 27 (1978) 639

c) **T. Watanabe, M. Kobayashi:** Electrochemistry of chlorophylls in *Chlorophylls*, Scheer, H., Ed., CRC, Boca Raton 1991, p.287

76. **S.R. Morrison:** *Electrochemistry at Semiconductor and Oxidized Metal Electrodes*; Plenum Press: New York 1980, p. 127

77. a) **A. Hagfeldt, U. Björkstén, S.-E. Lindquist:** Photoelectrochemical studies of colloidal TiO_2-film *Sol. Energy Mater. Sol. Cells* 27 (1992) 293

b) **G. Hodes, I.D.J. Howell, L.M. Peter:** Nanocrystalline photoelectrochemical cells *J. Electrochem. Soc.* 139 (1992) 3136

78. a) **M. Green:** Electrochemistry of the semiconductor-electrolyte electrode. I. The electrical double layer *J. Chem. Phys.* 31 (1959) 200

b) **H. Gerischer:** Semiconductor electrochemistry, In *Physical Chemistry - An Advanced Treatise*, Eyring, H.; Henderson, D.; Jost, W., Eds.; Academic Press: New York, 1970; Vol. IX A, pp. 467-477

c) **A.J. Bard, A.B. Bocarsly, F.F. Fan, E.G. Walton, M.S. Wrighton:** The concept of Fermi level pinning at semiconductor / liquid junctions *J. Am. Chem. Soc.* 102 (1980) 3671

79. a) **N.F. Mott:** *Conduction in Non-Crystalline Materials*, Oxford 1987

b) **N.F. Mott, E.A. Davis:** *Electronic processes in Non-Crystalline Materials*, Oxford 1979

80. **J. Moser, S. Punchihewa, P.P. Infelta, M. Grätzel:** Surface complexation of colloidal semiconductors strongly enhances interfacial electron-transfer rates *Langmuir* 7 (1991) 3012

81. **G. Rothenberger, D. Fitzmaurice, M. Grätzel:** Spectroscopy of conduction band electrons in transparent metal oxide semiconductor films *J. Phys. Chem.* 96 (1992) 5983

82. **D.J. Fitzmaurice, H. Frei:** Transient near-infrared spectroscopy of visible light sensitized oxidation of I^- at colloidal TiO_2 *Langmuir* 7 (1991) 1129

83. **J.-P.Chauvet, R. Viovy, R. Santus, E.J. Land:** One-electron oxidation of photosynthetic pigments in micelles *J. Phys. Chem.* 85 (1981) 3449

84. **B. Ke, S. Demeter, K.I. Zamaraev, R.F. Khairutdinov:** Charge recombination in photosystem I at low temperatures. Kinetics of electron tunneling *Biochim. Biophys. Acta* 545 (1979) 265

85. a) **K. Schwarzburg, F. Willig:** Influence of trap filling on photocurrent transients of polycrystalline TiO_2 *Appl. Phys. Lett.* 58 (1991) 2520

    b) **R. Könenkamp, R. Henninger, P. Hoyer:** Photocarrier transport in colloidal TiO_2 films *J. Phys. Chem.* 97 (1993) 7328

86. a) **F. Willig, R. Eichberger, N.S. Sundaresan, B.A. Parkinson:** Experimental time scale of Gerischer's distribution curves for electron-transfer reactions at semiconductor electrodes *J. Am. Chem. Soc.* 112 (1990) 2702

    b) **T. Sakata, K. Hashimoto, M. Hiramoto:** New aspects of electron transfer on semiconductor surface: Dye-sensitized systems *J. Phys. Chem.* 94 (1990) 3040

87. a) **E.Vrachnou, N. Vlachopoulos, M. Grätzel:** Efficient visible light sensitization of TiO_2 by surface complexation with $Fe(CN)_6^{4-}$ *J. Chem. Soc. Chem. Commun.* (1987) 868

    b) **J. Desilvestro, S. Pons, E. Vrachnou, M. Grätzel:** Electrochemistry and FTIR spectroscopic characterization of ferrocyanide-modified TiO_2 electrodes designed for efficient photosensitization *J. Electroanal. Chem.* 246 (1988) 411

    c) **E. Vrachnou, M. Grätzel, A.J. Mc Evoy:** Efficient visible light photoresponse following surface complexation of titanium dioxide with transition metal cyanides *J. Eletroanal. Chem.* 258 (1989) 193

88. The carboxylated phthalocyanines were a gift of Prof. D. Woehrle, University of Bremen, Germany

89. **F. Kienzle, O. Isler:** Synthetic carotenoids as colarants for food and feed, in *The chemistry of synthetic dyes*, K. Venkataraman, ed., Akad. Pr., New York 1978, Vol. 8, p. 38

90. a) **H. Meier:** Organic Semiconductors, Weinheim 1974

    b) **H. Meier:** Application of the semiconductor properties of dyes, in *Physical and Chemical Applications of Dyestuffs, Topics in Current Chemistry* 61, Berlin 1976, p. 85

91. **J.H. Lupinski:** The charge transfer complex between β-carotene and iodine *J. Phys. Chem.* 67 (1963) 2725

92. **U. Schoeler, K.H. Tews, H. Kuhn:** Potential model of dye molecule from measurements of the photocurrent in monolayer assemblies *J. Chem. Phys.* 61 (1974) 5009

93. **H. Nakahara, J. Nakayama, M. Hoshino, K. Fukuda:** Langmuir-Blodgett films of oligo- and polythiophenes with well-defined structure *Thin Solid Films* 160 (1988) 87

94. **P. Garcia, J. M. Pernant, P. Hapiot, V. Wintgens, P. Valat, F. Garnier, D. Delabouglise:** Effect of endsubstitution on electrochemical and optical properties of oligothiophenes, *J. Phys. Chem.* 97 (1993) 513

95. a) **A.K. Ghosh, T. Feng:** Merocyanine organic solar cells *J. Appl. Phys.* 49 (1978) 5982

b) **D.L. Morel, A.K. Ghosh, T. Feng, E.L. Stogryn, P.E. Purwin, R.F. Shaw, L. Fishman:** High-efficiency organic solar cells *Appl. Phys. Lett.* 32 (1978) 445

c) **D.L. Morel:** Some aspects of the role of solid state chemistry in the performance of organic solar cells *Mol. Cryst. Liq. Cryst.* 50 (1979) 127

96. a) **G.A. Chamberlain, R.E. Malpas:** Solid-state and liquid-junction photovoltaic properties of some polar dyes *Faraday Disc. Chem. Soc.* 70 (1980) 299

b) **G.A. Chamberlain, P.J. Cooney, S. Dennison:** Photovoltaic properties of merocyanine solid-state photocells *Nature* 289 (1981) 45

97. **T. Moriizumi, K. Kudo:** Merocyanine-dye photovoltaic cell on a plastic film *Appl. Phys. Lett.* 38 (1981) 85

98. **T. Skotheim, J.M. Yang, J. Otvos, M.P. Klein:** Photovoltaic properties of Au-Merocyanine-TiO_2 sandwich cells *J. Chem. Phys.* 77 (1982) 6144, 6151

99. **G.Scheibe:** Wechselseitige Bindung und Energieübertragung in Molekeln in flüssiger Phase *Zeitschrift für Elektrochemie* 52 (1948) 283

4. The Redox-Electrolyte

4.1 General requirements for the electrolyte

The redox-electrolyte serves to regenerate the dye which has been oxidized by electron injection into the semiconductor, and to transfer the positive charge to the counter electrode, where the redox-couple itself is regenerated by an electron flowing back through the external circuit. The following requirements must be fulfilled by the redox-electrolyte:

1. The redox-couple must have a more negative electrochemical potential than the oxidized dye, so that reduction can take place. A certain driving force is necessary to guarantee fast reduction of the dye cation before recombination with the injected electron occurs.

2. On the other hand, **the redox-potential should be as positive as possible,** since the open circuit voltage depends on the potential of the counter electrode and thus the electrolyte.

3. The redox-couple must be reversible at the counter electrode but should not react on the TiO_2 electrode. The overvoltage for reduction at the counter electrode should be small at current densities up to 20 mA/cm^2, since it represents a loss in the photovoltage of the cell. By contrast, the overvoltage at the dye coated TiO_2 electrode should be as high as possible, since the dark current caused by back transfer of the injected electrons to the electrolyte diminishes the available photocurrent. The blocking character of the TiO_2

electrode can be improved by coadsorbates which insulate the space between the dye molecules (chapter 3.4.5). Unfortunately, the dye itself often catalyses the electron transfer to the electrolyte and thereby contributes to the dark current.

4. The electrolyte must not absorb strongly in the visible spectrum. Although the electrolyte layer is very thin (about 20 μm), the concentration of the redox couple is rather high (e.g. 0.5 M for the reduced, and 50 mM for the oxidized form). Hence, the extinction coefficient should not exceed $\varepsilon = 1000\ M^{-1}cm^{-1}$ in the reduced state, if light losses of more than 10% are to be avoided. Light absorption is less important if the solar cell is illuminated from the TiO_2 side, since only the electrolyte in the pores of the TiO_2 film intercepts the light in this case. However, a reflecting counter electrode is only effective if the light is not much affected by traversing the total electrolyte layer even two times.

5. The electrolyte should not quench the excited state of the sensitizer. In particular the oxidized form of the redox couple may quench the excited dye by energy or electron transfer. This quenching should be slow compared to electron injection into the semiconductor, which is only the case, if the oxidized species does not form a complex with the dye and if its concentration is not too high.

6. The electrolyte must be able to carry a current of up to 20 mA/cm^2 without diffusion limitation or significant ohmic losses. While the ohmic resistivity of the thin electrolyte layer is usually small enough at the salt concentrations used, the diffusion limit demands a minimum concentration of both redox species. Under the simplifying assumption of constant diffusivity over the whole electrolyte including the porous TiO_2 film, the limiting current density is given by

$$I_{lim} = \frac{2nFDc_0}{d}$$

The limiting current depends on the thickness of the electrolyte (d), the concentration (c_0) and the diffusion coefficient (D) of the limiting redox species, as well as the number of charges (n) carried by it. The thickness is limited by the porous TiO_2 film itself ($d \approx 10$ μm), which certainly represents the most important diffusion resistance, but also by the flatness of photo- and counter-electrode. The concentration of the oxidized form is limited by requirements 3 to 5. We are left with the diffusion coefficient, which may be increased by using a redox couple of small hydrodynamic radius and a solvent of low viscosity.

The number of transported charges is usually n =1, but in the case of I^-/I_3^- two positive charges are carried by the triiodide ion, which doubles the limiting current density. However, a two-electron transfer reaction is expected to be more complicated, involving intermediate species of high energy, and may therefore be slower or require a higher driving force.

7. To be practical, the redox-electrolyte must be stable on a long term, retain its properties over a fairly wide range of temperatures, be non-toxic, non-volatile and cheap. With regards to stability simple couples like I^-/I_3^- are certainly advantageous. However, the very reactive intermediate I-atom and I_2^--ion [1] are suspicious to undergo side reactions with the dye or the solvent. Also light absorption by I_3^- may give rise to reactive species. Low viscosity even at low temperatures requires a solvent of low melting point, while a low vapor pressure is demanded for small volatility. These properties can often only be combined by employing binary or even ternary mixtures of solvents, as they are known from battery applications.

4.2 The iodide / triiodide redox couple

Redox electrolytes based on the I^-/I_3^- couple have up to now mostly been employed in dye sensitized solar cells. It has a suitable redox potential ($E(I^-/I_3^-)$ = 0.1 - 0.3V_{SCE} depending on the solvent) and a still acceptable light absorption in the visible (I_3^- in propylene carbonate: $\varepsilon_{462\ nm}$ = 1053 M^{-1} cm^{-1}).[2,3] The I^-/I_3^- couple has the great advantage of showing a high overvoltage for reduction on SnO_2 or TiO_2, which may be attributed to the complicated two electron transfer mechanism. Still it exhibits large exchange current densities on catalytic surfaces like platinum and carbon,[4] as required for low overvoltage at the counter electrode (chapter 5).

Originally aqueous solutions were used in dye sensitized nanocrystalline TiO_2 cells. They had to be acidified to pH 3-4 in order to prevent desorption of the dye, which was only electrostatically attached to the protonated hydroxyl groups on the TiO_2 surface. As discussed in chapter 2.4.4 dehydroxylation of the TiO_2 surface improves the electron injection efficiency, but requires nonaqueous electrolytes to prevent rehydroxylation. Ethanol was employed in the beginning and was later replaced by less volatile solvents of high dielectric constant. Especially ethylene carbonate / propylene carbonate mixtures, known from battery applications, have proved successful. These and other solvents as well as ternary mixtures have been compared by Y. Athanassov in our lab.[5]

The iodide salt concentration must be rather high (about 0.5 M) to insure rapid reduction of the dye cation and good conductivity of the electrolyte film. The triiodide concentration must suffice to carry the diffusion limited current (chapter 4.1 point 6). On the other hand, it should not be too high, since I_3^- absorbs light around 460 nm, quenches the excited dye and increases the dark current due to its reduction at the photoelectrode. A concentration of about 50 mM I_3^- is usually a good compromise.

The counterion of iodide is also of considerable importance. Although it does not participate in charge transfer in the steady state (contrary to battery applications, where the cation is generally the electroactive species), the counterion has an appreciable influence on photocurrent and voltage of the solar cell. The highest electron injection yields but lowest photovoltages are observed with Li^+, while the reverse holds for large cations, such as tetrapropylammonium (TPA^+). As discussed in chapter 3.5.6 the voltage drop in the Helmholtz layer at the TiO_2 electrode - electrolyte interface depends on the size of the cation. The small Li^+ ion can adsorb on the TiO_2 surface, if not even intercalate into the TiO_2 lattice, and thus causes a positive shift of the energy levels in TiO_2 with respect to the solution. This is analogous to the well known flatband potential

shift of oxide semiconductors in the presence of acids due to protonation of the surface hydroxyl groups. The compared to Li^+ large dye molecule therefore "sees" more positive acceptor levels in TiO_2, which increases the electron injection efficiency. However, the photovoltage is reduced due to the more positive potential of the TiO_2 electrode. By contrast, bulky cations like TPA^+ cannot approach the TiO_2 surface so closely and hence give higher photovoltages, but usually lower currents, because the driving force for electron injection is smaller.

Besides this cation effect the common pH-effect is also operative. Traces of acid or base in the dye solution or electrolyte and even short exposure of the electrode to ammonia vapor can influence the photocurrent / voltage characteristics drastically. Theoretically a change in the surface pH of hydroxylated TiO_2 by one unit causes a flatband potential shift of 59 mV. Since neither dye solution nor electrolyte are buffered shifts of several pH units are easily produced, especially in the neutral pH region, and may cause photovoltage changes well beyond 100 mV.

The stability of the redox couple I^-/I_3^- itself is beyond question, however, a loss of I_3^- may occur if species other than I^- are oxidized. Even traces of reducing impurities in the cell may result in a slow disappearance of the small amount of I_3^- present (for a 20 µm thick film of electrolyte containing 50 mM I_3: 10^{-7} mol/cm^2, which is comparable to the amount of dye on the electrode, as calculated in chapter 3.1, point 9). Since a dye molecule has to undergo some 10^8 turnovers in 20 years (chapter 3.1, point 8) reduction of the strongly oxidizing dye cation by other species than I^- with a quantum efficiency above 10^{-8} would limit the lifetime of the solar cell due to consumption of the available I_3^-. Also the highly reactive intermediate I-atom and I_2^--ion [1] created by oxidation of I^- may undergo side reactions instead of regenerating I_3^-:

$$I^- \rightarrow I + e^-$$
$$I + I^- \rightarrow I_2^-$$
$$2\,I_2^- \rightarrow I_3^- + I^-$$

Finally light absorption by I_3^- around 460 nm creates electronically excited species of higher oxidation potential which may react with the solvent and lead to a loss of triiodide. Although the I_3^- supply may be replenished by an electrolyte reservoir or by periodic replacement of the electrolyte, this would significantly complicate construction or maintenance of the solar cell.

4.3. Other redox couples

Hydroquinone has often been used as electron donor in dye sensitized photoelectrochemical cells, but requires water as proton acceptor and is not photostable in the oxidized state.[6] The ferro/ferricyanide couple has been reported to stabilize CdSe photoanodes in nonaqueous solvents, however, the cyanide itself is photolytically unstable.[7] The same problem arises with other metalcyanides.[8] Bromide has been employed as donor for the sufficiently oxidizing RuL_3 cation (L = 2,2'-bipyridyl-4,4'-carboxylate) and yields photovoltages close to 1 V.[9] However, the strongly oxidizing Br_2 is too reactive to be used in an organic solar cell. The ferricenium / ferrocene couple and its derivatives give high efficiencies in silicon photoelectrochemical cells.[3a,10,11] Yet they absorb strongly below 660 nm, and are therefore not suited for dye sensitized cells supposed to utilize just this light.

A number of macrocylic transition metal complexes, e.g. the copper-thiaether complexes found in the blue copper proteins,[12,13] as well as Cu, Ni and Co-ions complexed by polyaza ligands exhibit suitable redox potentials and good reversibility. However, they are often highly colored, have too small diffusion coefficients because of their large size, or they are not soluble to the extent required for high current densities. Moreover, they may easily be reduced at the SnO_2 conducting glass substrate and thus demand a blocking underlayer below the porous TiO_2 film to limit the dark current (cf. chapter 2.2). Finally their complex structure is expected to make them more susceptible to decomposition, especially under light. In view of these complications it is not astonishing that a good alternative to the I^-/I_3^- couple has not yet been found.

4.4. Solid electrolytes

A liquid electrolyte has the advantage of high mobility of the electroactive species and thus high conductivity. It also penetrates easily into the nanopores of the TiO_2 film and fills the space between photo- and counter electrode by capillary action. However, it requires hermetic sealing of the cell and holding the electrodes together at the edges to keep the electrolyte layer as thin as possible. For large cells the spacing is limited by the flatness of the electrode substrates (e.g. SnO_2 conducting glass). In order to keep the separation minimal over the whole surface of the cell it would be nice to have an electrolyte that acts at the same time as glue. There are different approaches to achieve this.

4.4.1. Gel electrolytes

A conventional liquid electrolyte can be incorporated into a solid, porous matrix, such as a silica gel, without affecting much the diffusion coefficient of the dissolved species. The TiO_2 film is in fact such a matrix and it would only have to be extended by an insulator to the counter electrode. This approach is used in lead acid batteries, where the sulfuric acid electrolyte is gelatinized by SiO_2. The gelation would have to take place *in situ* in the electrolyte between photo- and counter electrode. This limits the reaction temperature as well as the choice of the reactants, which must be compatible with the components of the cell and not leave any reactive byproducts. For example the acid or base catalyzed condensation employed in the preparation of silica gel or the radical initialized polymerization of polyacrylamide gel are not suitable.

The best choice would in fact be a pressure-sensitive glue, well known from self-adhesive tapes, which connects the electrodes upon simple lamination.[14] The liquid electrolyte containing some dissolved or dispersed polymer would be applied as thin layer ($\approx$ 10 µm) onto the counter electrode. Upon contact with the photoelectrode only the electrolyte would be sucked up by the nanoporous TiO_2 film, leaving the large polymer molecules in a very thin, more concentrated and therefore more sticky film behind. Adhesion would thus result from solvent removal by absorption in the pores of the TiO_2 layer instead of the more common drying of glues by evaporation.

Instead of an organic polymer colloidal silica or alumina may be added to the electrolyte to form a porous network similar to the TiO_2 film. For example Aerosil, a nanosized SiO_2 powder prepared by flame hydrolysis in the same way as P-25 (chapter 2.3.12), forms a gel with most liquids due to hydrogen bonding

between the surface hydroxyl groups of the particles.[15,16] In fact, addition of 0.1 g Aerosil 200 to 1 ml electrolyte (80% ethylene carbonate, 20% propylene carbonate, 0.5 M KI, 40 mM I_2) yields a transparent gel, which becomes liquid again, if a shear force is applied. Although photo- and counter electrode are already hold together by adhesion and cohesion of the thin electrolyte layer itself, a further reinforcement by the gel matrix is required to prevent formation of bubbles due to flow of the electrolyte. The gel itself can be strengthened by binding the colloidal particles covalently together. This may be achieved by addition of crosslinking agents, such as tetraethoxysilane or tetraacetoxysilane, which are also used in the vulcanization of silicone rubber.[17]

While the gel matrix does not much influence the diffusivity of ions in the electrolyte it also does not prevent its evaporation.[15] (p.313) Therefore a hermetic sealing of the cell edges is still necessary. But since an adhesive electrolyte keeps the electrode separation minimal even for cells of large surface area the length of the edges becomes relatively less important.

4.4.2. Solid polymer electrolytes

A different approach to achieve cohesion between photo- and counter electrode is the use of a solid polymer electrolyte. For battery applications solid solutions of alkali metal salts in polyethylene oxide (PEO) have found some interest, due to the mobility of the cation in the helical chains of the polymer. Solid PEO / KI / I_2 electrolytes have also been used in photoelectrochemical cells with silicon photoanode.[18] The transference number of iodide, which is the electroactive species in this case, has been measured to be in the range 0.2-0.4. Unfortunately, the conductivity is only in the order of $10^{-6}\ \Omega^{-1}cm^{-1}$ at room temperature, and increases to $10^{-4}\ \Omega^{-1}cm^{-1}$ only at 50-80°C. For a 10 µm thick electrolyte layer the conductivity has to be at least $10^{-4}\ \Omega^{-1}cm^{-1}$ to keep the resistance for a 1 cm^2 electrode below 10 Ω, a value that would already cause a voltage loss of 100 mV at a current density of 10 mA/cm^2.

Anyway, the PEO used by the cited authors [18] had a molecular mass of 600000 g/mol, which corresponds to a molecule diameter of many nanometers and certainly excludes penetration into the nanoporous TiO_2 film. We therefore prepared a solution of 0.1 mol LiI and 0.01 mol I_2 in 1 mol of Carbowax 1540, a polyethylene glycol with a molecular mass of only 1300-1600 g/mol. The polymer is liquid at 100°C and penetrates into the pores of the TiO_2 electrode. At room temperature it is semi-solid and acts as adhesive between counter- and photoelectrode. However, the current/voltage characteristics indicated a series

resistance of several 100 Ω per cm^2, as expected from the cited conductivity values.

More recently, the room temperature conductivities of PEO based solid electrolytes have been greatly enhanced by the addition of plasticizing solvents, such as ethylene carbonate and propylene carbonate. This leads back to the idea of adding a polymer to the liquid electrolyte, in order to provide adhesion between the electrodes (chapter 4.4.1). Higher conductivities have also been reported for rubbery polymer-in-salt solutions, e.g. PEO in different lithium salts.[19] While crystalline Li-salts exhibit very low cation conductivity, these amorphous solid solutions have similar high conductivities as molten salts. The same effect is in fact observed after the uptake of water by the highly hygroscopic Li-salts. Thus, a dye sensitized TiO_2 cell containing 0.5 M LiI + 50 mM I_2 in acetone as electrolyte remains functioning after evaporation of the acetone, provided the salt left behind is sufficient to fill the space between photo- and counter electrode. An increase of the ionic conductivity of salts by orders of magnitude also occurs on the addition of submicrometer insulating particles, such as Al_2O_3, SiO_2 and TiO_2,[20] which may contribute to the high conductivity of the LiI salt in the pores of the nanocrystalline TiO_2 layer. However adhesion to the counter electrode still requires the addition of a sticky polymer.

While a high cation conductivity is demanded for solid polymers in battery applications, iodide and triiodide transport is required in the solar cell, where the positive counterion only serves for charge compensation but does not migrate in the steady state. Solutions of iodide salts in molten iodine have for a long time been known to be highly conductive (e.g. 10^{-1} $\Omega^{-1}cm^{-1}$ for 29 wt% LiI in I_2 at 130°C).[21] This has been attributed to iodide hopping between polyiodide chains, which is also observed in solid polyiodide solutions in PEO and polypropylene oxide (PPO).[12] This results in an electron (or hole) transport without a net diffusion of ions, similar to the Grotthus mechanism of proton transport in water. The room temperature conductivity of PPO-polyiodide complexes reaches values above 10^{-3} $\Omega^{-1}cm^{-1}$ at high polyiodide concentration (>50wt%). However, the high iodine content of these polymer electrolytes renders them strongly light absorbing and probably less suitable for solar cell applications. Still, the idea of replacing the ionic conductor by an electron or hole conductor is very attractive and shall be resumed in the following two chapters.

4.4.3. Mixed-valence compounds and redox polymers

The mixed-valence compound insoluble Prussian blue, $Fe_4[Fe(CN)_6]_3$, has for some time been known to exhibit electron conductivity, due to electron hopping (electron self-exchange) between reduced and oxidized Fe sites (redox conduc-tivity).[23-26] Unfortunately, the electron diffusion coefficient of dry and wet Prussian blue films is only in the order of 10^{-9} cm^2/s, resulting in conductivities below 10^{-5} $\Omega^{-1}cm^{-1}$. Prussian blue is reversibly reduced to the transparent Everitt's salt at 0.2 V_{SCE}:[25]

$$\underset{\text{Prussian blue}}{Fe_4^{+3}[Fe^{+2}(CN)_6]_3} + 4\,K^+ + 4\,e^- \rightleftarrows \underset{\text{Everitt's salt}}{K_4Fe_4^{+2}[Fe^{+2}(CN)_6]_3} \quad E = 0.2\ V_{SCE}$$

The redox potential is appropriate for dye-sensitized solar cell applications, but an excess of the reduced form is demanded, which would presumably result in even lower conductivity.

Many other redox conductors based on mixed-valence redox ion sites have been studied in recent years.[27-28] In particular redox polymers with Fe, Ru and Os polypyridine complexes attached to a polymer backbone have found great interest.[29] But in spite of the high concentration of redox active sites ($\approx$ 1.5 M), which corresponds to a separation of about 1 nm and renders these polymers highly colored, the electron diffusion coefficients are still in the range of 10^{-9} to 10^{-7} cm^2/s only, resulting in a conductivity of $1.5 \cdot 10^{-4}\Omega^{-1}cm^{-1}$ in the best case.[29b] These studies are nevertheless interesting for us, since they reveal electron hopping between Ru-bipyridine complexes at distances typical for closely packed sensitizer molecules on the TiO_2 surface (chapter 2.4.5). Thus, the hole on the ruthenium dye created by electron injection into TiO_2 might in principle be transported by electron hopping within the dye monolayer, rendering the redox electrolyte superfluous. A dye coated porous layer of an insulator, such as Al_2O_3 or SiO_2 had to prolong the electron transfer chain up to the counter electrode (Figure 45).

Unfortunately, this two dimensional conductivity would be even lower than in the three dimensional redox polymer. Moreover, it would lead to a significant build-up of the amount of oxidized dye, entailing increased recombination with the injected electrons. The electron exchange rate between the dye molecules may be enhanced by covalent bridges, as known from polynuclear ruthenium complexes (chapter 3.3). However, this is restricted by the sterical arrangement

of the dye molecules adsorbed on the semiconductor surface. The stronger interaction is also expected to enhance energy or electron transfer quenching of the excited sensitizer by the neighboring dye molecules, which competes with electron injection into TiO_2.

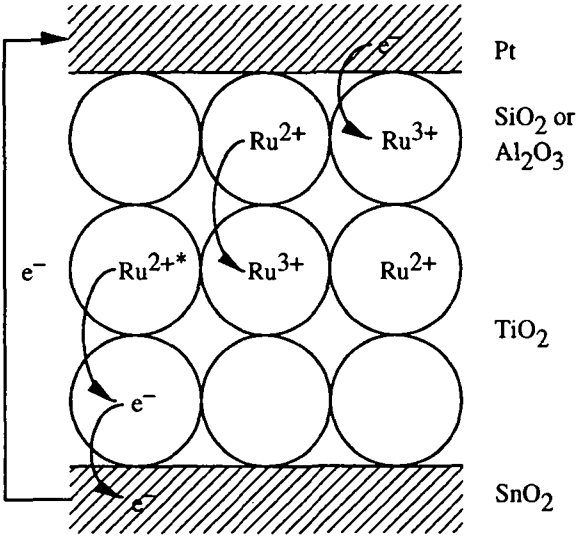

Figure 45: Electron transport within the dye layer by hopping between ruthenium centers

4.4.4. Conducting polymers and organic semiconductors

Conducting polymers exhibit high electronic conductivities, often approaching those of metals.[30] However, a metal-like behavior with electron conduction over a wide potential range would result in electron injection from TiO_2 and cause a short circuit in the solar cell. We rather need a material that is redox active in the range were reduction of the oxidized dye occurs ($\approx$ 0.3 V_{SCE}). Some conducting polymers,such as polyaniline[31] and poly-3-methylthiophene[32] fulfill this condition, while polypyrrole is redox active at –0.3 V_{SCE},[32] which is much too positive for our purposes. Unfortunately, these polymers are strongly colored and would interfere with light absorption by the sensitizer. Recently conducting polymers with small band gap, absorbing in the infrared but transparent in the visible have been described. For example poly(isothianaphthene) with a band gap of 1 eV is transparent yellow in the doped, oxidized and conducting state.[33] Oxidation occurs at 0.6 V_{SCE}, but reduction only at 0 V_{SCE}, which might give rise to a high dark current due to electron injection from TiO_2.

The conducting polymer had to be polymerized *in situ*, in the pores of the nanocrystalline TiO_2 layer, e.g. by electropolymerization on the SnO_2 substrate. However, this would result in an ohmic contact with the photoelectrode, which had to be broken somehow, to prevent short-circuiting of the cell. It is also questionable that the polymer chains threading through the tortuous pore structure of the TiO_2 film over a thickness of 10 μm still exhibit the high conductivity of bulk material, which usually consists of microfibrils of aligned polymer chains. In fact, a simple kink in the polymer chain can break the charge delocalization and impede electronic conduction. Also electron transfer between the chains by hopping depends on their parallel alignment and is expected to be hampered in the disordered material filling the pores of the TiO_2 electrode.

In view of these problems it seems to be more promising to employ molecular semiconductors of low molecular mass as conductors or even as sensitizers at the same time.[34] We have already mentioned this approach at the end of chapter 3.1 and 3.6 and reported some preliminary experiments with oligoaniline and merocyanine. There are many other organic compounds exhibiting semiconductor properties in the solid state, and some of them are also possible sensitizers. For example certain planar aromatic derivatives, metal complexes and charge-transfer complexes form columnar stacks exhibiting one-dimensional conduction.[34,35] In particular oxygen bridged Si-phthalocyanine shows this effect.[34] But even simple sublimation of phthalocyanines [36] and porphyrins [37] yields films with semiconductor properties. Together with merocyanines and oligothiophenes (chapter 3.6) these dyes are candidates for a solid state solar cell with heterogeneous p-n-junction between the p-type organic dye and the n-type TiO_2.

References to chapter 4

1. **D.J. Fitzmaurice, H. Frei:** Transient near-infrared spectroscopy of visible light sensitized oxidation of I^- at colloidal TiO_2 *Langmuir* 7 (1991) 1129
2. **K.J. Hanson, Ch.W. Tobias:** Electrochemistry of iodide in propylene carbonate *J. Electrochem. Soc.* 134 (1987) 2204, 2210
3. a) **M.E. Langmiur, P. Hoenig, R.D. Rauh:** Electrochemical photovoltaic cells base on n-GaAs in propylene carbonate *J. Electrochem. Soc.* 128 (1981) 2357

   b) **M.E. Langmuir, M.A. Parker, R.D. Rauh:** Electrochemical photovoltaic cells based on n-GaAs and the triiodide/iodide redox couple in acetonitril *J. Electrochem. Soc.* 129 (1982) 1705
4. **J.F. Coetzee, C.W. Gardner:** Exchange current densities and other properties of reference electrodes based on the triiodide-iodide and silver(I)ion-silver couples in organic solvents *Anal. Chem.* 54 (1982) 2530
5. **Y. Athanassov:** Utilisation de melanges ternaires comme solvants d'electrolyte dans les cellules photoelectrochimiques regeneratrices, Travail de diplome, Lausanne 1993
6. **R. Dabestani, A.J. Bard, A. Campion, M.A. Fox, M.E. Mallouk, S.E. Webber, J.M. White:** Sensitization of titanium dioxide and strontium titanate electrodes by ruthenium(II)tris(2,2'-bipyridine-4,4'-carboxylic acid) and zinc tetrakis(4-carboxyphenyl)porphyrin *J. Phys. Chem.* 92 (1988) 1872
7. a) **R. Noufi, D. Teuch, L.F. Warren:** Stabilization of n-CdSe photoanodes in nonaqueous $Fe(CN)_6^{3-/4-}$, electrolytes *J. Electrochem. Soc.* 127 (1980) 2709

   b) **R. Noufi, D. Teuch, L.F. Warren:** Photoelectrochemical evaluation of the n-CdSe / methanol / ferro-ferricyanide system *J. Electrochem. Soc.* 128 (1981) 2363
8. **N. Oyama, T. Ohsaka, N. Yamamoto, J. Matsui, O. Hatozaki:** Determination of heterogeneous electron-transfer rate constants for the redox couples $Mo(CN)_8^{4-/3-}$, $W(CN)_8^{4-/3-}$, $Fe(CN)_6^{4-/3-}$, $Os(CN)_6^{4-/3-}$ and $IrCl_6^{3-/2-}$ using fast sweep cyclic voltammetry at carbon fibre electrodes *J. Electroanal. Chem.* 265 (1989) 297
9. **N. Vlachopoulos, P. Liska, J. Augustynski, M. Grätzel:** Very efficient light energy harvesting and conversion by spectral sensitization of high surface area polycrystalline titanium dioxide films *J. Am. Chem. Soc.* 110 (1988) 1216
10. **K.D. Legg, A.B. Ellis, J.M. Bolts, M.S. Wrighton:** n-type Si-based photoelectrochemical cell: New liquid junction photocell using a nonaqueous ferricenium / ferrocene electrolyte *Proc. Natl. Acad. Sci. USA* 74 (1977) 4116
11. a) **C.M. Gronet, N.S. Lewis, G. Cogan, J. Gibbons:** n-type silicon photoelectrochemistry in methanol *Proc. Natl. Acad. Sci. USA* 80 (1983) 1152

b) **J.F. Gibbons, G.W. Cogan, C.M. Gronet, N.S. Lewis:** A 14% efficient nonaqueous semiconductor / liquid junction solar cell *Appl. Phys. Lett.* 45 (1984) 1095

12. **Th.E. Jones, D.B. Rorabacher, L.A. Ochrymowycz:** Simple models for "blue" copper proteins, The copper-thiaether complexes *J. Am. Chem. Soc.* 97 (1975) 7485, 7163; 98 (1976) 4322
13. **J.R. Hartman, S.R. Cooper:** Crown thioether chemistry *J. Am. Chem. Soc.* 108 (1986) 1202, 1208
14. **D. Satas,** ed.: *Handbook of pressure sensitive adhesive technology*, New York 1989
15. **C.J. Brinker, G.W. Scherer:** *Sol-Gel Science*, Acad. Press, New York 1990, p. 292
16. **F. Ehrburger, V. Guerin, J. Lahaye:** Phenomenological study of gelification of liquids by pyrogenic silica *Coll. Surf.* 9 (1984) 371
17. **K.J. Saunders:** *Organic Polymer Chemistry*, London 1973, p. 360
18. a) **T. Skotheim, I. Lundström:** Solid polymer electrolyte photovoltaic cell *J. Electrochem. Soc.* 129 (1982) 894

    b) **T.A. Skotheim, O. Inganans:** Polymer solid electrolyte photoelectrochemical cells with n-Si-polypyrrole photoelectrodes *J. Electrochem. Soc.* 132 (1985) 2116
19. **C.A. Angell, C. Lin, E. Sanchez:** Rubbery solid elelctrolytes with dominant cationic transport and high ambient conductivity *Nature* 362 (1992) 137
20. **A. Kumar, K. Shahi:** Enhanced ionic conduction in PbI_2-Al_2O_3 composite solid electrolytes *J. Mater. Sci.* 28 (1992) 1257
21. **Gmelins** *Handbuch der anorganischen Chemie*, Lithium, Ergänzungsband, Weinheim 1960, p. 469
22. a) **L.Ch. Hardy, D.F. Shriver:** Poly(ethylene oxide)-sodium polyiodide conductors *J. Am. Chem. Soc.* 108 (1986) 2887

    b) **H.-C. zur Loye, B.J. Heyen, H.O. Marcy, D.C. De Groot, C.R. Kannewurf, D.F. Shriver:** Dielectric response and conductivity of poly(propylene oxide) sodium polyiodide complexes. Discussion of charge transfer by an ion relay mechanism *Chem. Mater.* 2 (1990) 603

    c) **M. Forsyth, D.F. Shriver, M.A. Ratner, D.C. de Groot, C.R. Kannewurf:** Conductivity percolation in polyiodide / polymer complexes *Chem. Mater.* 5 (1993) 1073
23. **H. Inoue, S. Yanagisawa:** Bonding nature and semicondutivity of Prussian blue and related compounds *J. inorg. nucl. Chem.* 36 (1974) 1409
24. a) **D. Ellis, M. Eckhoff, V.D. Neff:** Electrochromism in the mixed-valence hexacyanides. 1. Voltammetric and spectral studies of the oxidation and reduction of thin films of Prussian blue *J. Phys. Chem.* 85 (1981) 1225

    b) **J.W. McCargar, V.D. Neff:** Thermodynamics of mixed-valence intercalation reactions: The electorchemical reduction of Prussian blue *J Phys. Chem.* 92 (1988) 3598

25. **A. Viehbeck, D.W. De Berry:** Electrochemistry of Prussian blue films on metal and semiconductor electrodes *J. Electrochem. Soc.* 132 (1985) 1369
26. **B.J. Feldman, R.W. Murray:** Electron diffusiton in wet and dry Prussion blue films on interdigitated array electrodes *Inorg. Chem.* 26 (1987) 1702
27. **R.P. Buck:** Electron hopping in one dimension: mixed conductor membranes *J. Phys. Chem.* 92 (1988) 4196
28. **J.M. Savéant:** Electron hopping between fixed sites *J. Electroanal. Chem.* 242 (1988) 1
29. a) **P.G. Pickup, R.W. Murray:** Redox conduction in mixed-valent polymers *J. Am. Chem. Soc.* 105 (1983) 4510

    b) **P.G. Pickup, W. Kutner, C.R. Leidner, R.W. Murray:** Redox conduction in single and bilayer films of redox polymer *J. Am. Chem. Soc.* 106 (1984) 1991

    c) **Ch.E.D. Chidsey, R.W. Murray:** Redox capacity and direct current electron conductivity in electroactive materials *J. Phys. Chem.* 90 (1986) 1479
30. **M.G. Kanatzidis:** Conductive polymers *Chem. Eng. News* Dec.3, 1990, p. 36
31. **E.M. Geniès, M. Lapkowski, C.Tsintavis:** La polyaniline: préparations, propriétés et applications *New J. Chem.* 12 (1988) 181
32. **T. Hirai, S. Kuwabata, H. Yoneyama:** Electrochemical behaviors of polypyrrole, poly-3-methylthiophene, and polyaniline deposited on Nafion-coated electrodes *J. Electrochem. Soc.* 135 (1988) 1132
33. a) **M. Kobayashi, N. Colaneri, M. Boysel, F. Wudl, A.J. Heeger:** The electronic and electrochemical properties of poly(isothianaphthene) *J. Chem. Phys.* 82 (1985) 5717

    b) **A.O. Patil, A.J. Heeger, F. Wudl:** Optical properties of conducting polymers *Chem. Rev.* 88 (1988) 183
34. **J. Simon, J.-J. André:** *Molecular Semiconductors*, Berlin 1985
35. **A.F. Underhill:** Compounds exhibiting unusual electric properties, in *Comprehensive Coordination Chemistry*, Wilkinson et al., eds., Oxford 1987, Vol. 6, p. 133
36. **T. Shichiri, M. Suezaki, T. Inoue:** Three-layer organic solar cell, *Chem. Lett.* 1992, 1717
37. **K. Yamashita, Y. Harima, T. Matsubayashi:** Conductance control of porphyrin solids by molecular design and doping *J. Phys. Chem.* 93 (1989) 5311

5. The counter electrode

The function of the electrode is to transfer the electrons arriving from the external circuit back to the redox electrolyte. Hence it must be well conducting and exhibit a low overvoltage for reduction of the redox couple. In addition, it may serve as mirror, reflecting the light transmitted by the photoelectrode to traverse it a second time, thus enhancing light absorption with a given amount of dye. In other cases, e.g. in a series connection of cells (cf. Figure 10), half of which are illuminated from the front, the other half from the back side, or in a tandem cell with two different dyes on separate electrodes the counter electrode has to be transparent.

The two electron redox couple iodide / triiodide requires a catalytically active counter electrode to keep the overvoltage for reduction low at current densities up to 20 mA/cm^2. In particular platinum exhibits a very high standard exchange current density (0.4 A/cm^2 for I^-/I_3^- in water at pH 0) and the reaction mechanism has been studied in detail.[1] However, the exchange current density depends strongly on the solvent (for 0.1 M NaI / 50 mM I_2 in propylene carbonate: $9 \cdot 10^{-5}$ A/cm^2, in acetonitrile: $3.5 \cdot 10^{-4}$ A/cm^2, in water: $3.2 \cdot 10^{-4}$A/cm^2).[2,3] The platinum electrode was found to be covered with a monolayer of atomic iodine, which renders triiodide reduction more difficult.[3,4]

Evaporated platinum films have a moderately high reflectance of 66-78% between 400 and 800 nm (polished or electroplated platinum has a lower reflectance)[5] and can thus be used as mirror at the same time. However, a film thickness of about 50 nm is needed for reflectance and electrical conductivity, corresponding to 1 g of platinum per square meter, which would render the coating rather expensive. At least the costly vacuum evaporation could be replaced by pyrolytic decomposition of platinum salts or chemical vapor deposition.[6]

Transparent counter electrodes can be made by deposition of small amounts of platinum on SnO_2 conducting glass. The transmission of even 50 nm thick platinum films remains high (>90%), if the particles constituting the film are small relative to the wavelength of light and if they are not electronically well connected.[7] Such films can be prepared by electrodeposition from dilute

platinum salt solution (e.g. $5 \cdot 10^{-4}$ M H_2PtCl_6) on SnO_2 as cathode with a platinum anode.[7,8] The catalytic activity of the platinized SnO_2 is favored by short electrodeposition at high overvoltage, resulting in nucleation of platinum islands distributed over the whole SnO_2 surface instead of the growth of a few platinum dendrites. With a loading of only 0.1 g Pt/cm^2 and without loosing much of its transparency a such treated SnO_2 electrode becomes as active for triiodide reduction as a pure platinum electrode.

The electrodeposited platinum was found to appear mainly as Pt^0 with a small amount of $Pt(OH)_2$.[9] Platinization of SnO_2 has also been carried out by simple chemisorption,[10] radiolytic grafting,[11] and photodeposition.[12] Platinization by thermal decomposition of a thin platinum salt layer, a method commonly used in the metal catalyst impregnation of oxide powders, was investigated by N. Papas in our lab and found to give counter electrodes with superior long term stability. It is well known that catalysts are easily poisoned, usually due to formation of an inactive adsorbate monolayer. The activity of the platinum counter electrode for triiodide reduction is for example affected by dipping into the dye solution, presumably due to adsorption of the dye on the platinum surface. A slow migration of the dye from the photoelectrode to the counter electrode may also occur in the solar cell, because of its finite solubility in the electrolyte. The electrodeposited platinum exhibits better long term stability after firing as well. This may be due to removal of surface hydroxy groups, acting as adsorption sites for the dye and hindering the electron transfer to triiodide.

Other platinum group metals, such as iridium, ruthenium, rhenium [11] and palladium [8] have been deposited on SnO_2 as catalysts for triiodide reduction, and iridium was found to be even more active than platinum. Rhodium may be interesting for a reflecting counter electrode, since it has a higher reflectance in the visible than platinum.[5] However, in view of the high price of platinum metals it is probable more economical to use a small loading on the SnO_2 side of the conducting glass substrate as transparent counter electrode, and to apply an electroless silver coating to the back side, which is the usual method for fabricating mirrors.

The only other material that exhibits corrosion stability and low overvoltage for triiodide reduction is to our knowledge carbon. The mechanism of the electrode reaction has been studied for graphite.[13] Transparent amorphous carbon films made by sputtering and electron beam evaporation on silicon were reported to exhibit an anodic overvoltage of only 50 mV at a current density of 20 mA/cm^2 in 1 M HI + 0.28 M I_2 combined with good long term stability.[14] Carbon therefore represents an interesting alternative for platinum as catalyst for a transparent counter electrode.

References to chapter 5

1. **L.M. Dané, L.J.J. Janssen, J.G. Hoogland:** The iodine/iodide redox couple at a platinum electrode *Electrochim. Acta* 13 (1968) 507
2. **J.F. Coetzee, C.W. Gardner:** Exchange current densities and other properties of reference electrodes based on the triiodide-iodide and silver(I)ion-silver couples in organic solvents *Anal. Chem.* 54 (1982) 2530
3. **K.J. Hanson, Ch.W. Tobias:** Electrochemistry of iodide in propylene carbonate *J. Electrochem. Soc.* 134 (1987) 2204, 2210
4. a) **B.G. Bravo, Th. Mebrahtu, J.F. Rodriguez, M.P. Soriaga:** Electroactivity of strongly-adsorbed redox centers: Reduction of iodine chemisorbed on platinum in aprotic solvents *J. Electroanal. Chem.* 221 (1987) 281

   b) **B.G. Bravo, J.F. Rodriguez, Th. Mebrahtu, M.P. Soriaga:** Reductive desorption of iodine from platinum electrodes. A comparison in protic and aprotic solvents *J. Phys. Chem.* 91 (1987) 5660

   c) **G.M. Berry, M.E. Bothwell, B.G. Bravo, G.J. Cali, J.E. Harris, Th. Mebrahtu, S.L. Michelhaugh, J.F. Rodriguez, M.P. Soriaga:** Spectroscopic and electrochemical studies of iodine coordinated to noble-metal electrode surfaces *Langmuir* 5 (1989) 707
5. **G. Hass:** Mirror coatings, in *Applied Optics and Optical Engeneering*, R. Kingslake (ed.) New York 1966, Vol.3, p. 309
6. a) **Gmelins** *Handbuch der anorganischen Chemie*, Platin, Teil A: Spiegel und Häutchen aus Platinmetallen, Weinheim 1939, p. 402

   b) **Gmelin** *Handbook of inorganic chemistry*, Platinum, Suppl. A1: Thin films of high purity platinum-group metals, Berlin 1986, p. 43
7. a) **A. Heller, D.E. Aspnes, J.D. Porter, T.T. Sheng, R.G. Vadminsky:** "Transparent" metals: preparation and characterization of light-transmitting platinum films *J. Phys. Chem.* 89 (1985) 4444

   b) **J.D. Porter, A. Heller, D.E. Aspnes:** Experiment and theory of 'transparent' metal films *Nature* 331 (1985) 664
8. **R. Tenne, M. Peisach, C.A. Rabe, C.A. Pineda, A. Wold:** Catalytic effect of heavy metal ions on the SnO_2/aqueous polyiodide interface and its application to photoelectrochemical cells *J. Electroanal. Chem.* 269 (1989) 389
9. **G.B. Hoflund, D.F. Cox, H.A. Laitinen:** Preparation and surface characteristics of platinized antimony-doped tinoxide films *Thin Solid Films* 83 (1981) 261
10. **M Watanabe, S. Venkatesau, H.A. Laitinen:** Preparation of dispersed platinum on conductive tin oxide and its catalytic activity for oxygen reduction *J. Electrochem. Soc.* 130 (1983) 59
11. a) **J. Bruneaux, H. Cachet, M. Froment, J. Amblard, J. Belloni, M. Mostafavi:** Improvement of charge transfer kinetics at transparent SnO_2

counterelectrodes by means of a radiolytic grafting of metallic nanoaggregates *Electrochim. Acta* 32 (1987) 1533

b) **J. Bruneaux, H. Cachet, M. Froment, J. Amblard, M. Mostafavi:** Electrochemical behavior of transparent heavily doped SnO_2 electrodes. Effect of radiolytic grafting of iridium nanoaggregate *J. Electroanal. Chem.* 269 (1989) 375

12. **H. Cachet, M. Froment, A. Messad:** Photoinduced metal deposition on sprayed SnO_2 films *J. Electroanal. Chem.* 284 (1990) 263
13. **H.S. Wroblowa, A. Saunders:** Flow-through electrodes. II. The I_3^-/I^- redox couple *Electroanal. Chem. Interf. Electrochem.* 42 (1973) 329
14. **A.T. Howe:** Electrocatalytic properties of amorphous carbon thin films and their use as coatings for photoelectrodes *J. Electrochem. Soc.* 134 (1987) 2470

6. Conclusion

We have presented a new type of solar cell based on dye-sensitized nanocrystalline TiO_2 electrodes. Several methods for the preparation of such electrodes have been investigated and shown to result in high charge separation efficiencies even with cheap starting materials and simple nonvacuum coating techniques. The energy conversion efficiency of 10% under AM 1.5 solar radiation is already competitive with amorphous silicon cells. A further improvement should be possible, since the open circuit voltage of $U_{oc} = 0.72$ V obtained with $RuL_2(SCN)_2$ as sensitizer is still small compared to the excited state energy of $E_{0\text{-}0} = 1.55$ eV.[1] Thus more than 0.8 V are lost in the sensitization process.

The voltage loss is mainly due to the non-optimized I^-/I_3^- redox electrolyte with its low potential of $E = 0.15\ V_{SCE}$ in comparison to a standard potential of $E^0 = 0.85\ V_{SCE}$ for the oxidized dye.[1] The large driving force of 0.7 V may be necessary in this case, since oxidation of iodide proceeds via intermediate I atoms and I_2^- radicals (cf. chapter 4.2) with very positive standard potentials ($E^0(I/I^-) = 1.1\ V_{SCE}$ and $E^0(I_2^-/I^-) = 0.80\ V_{SCE}$ in aqueous solution).[2] One electron redox couples are expected to require less overvoltage for fast enough regeneration of the oxidized dye to prevent recombination with the injected electron. According to Marcus theory, fastest electron transfer occurs if the driving force $-\Delta G$ and the reorganization energy λ are matched. The reorganization energy amounts to several hundred millivolts in a polar solvent, so that a solid electrolyte that excludes dipole reorientation may be advantageous in this respect.[3]

However, the photovoltage of the solar cell is also limited by the dark current arising from reduction of the redox electrolyte at the semiconductor electrode. While the overvoltage is high for triiodide reduction, the photoelectrode is less blocking for one electron redox couples. The cited photovoltage of $U_{oc} = 0.72$ V was in fact obtained after treating the dye-covered electrode with 4-tert-butylpyridine, while only $U_{oc} = 0.38$ V were measured before.[1] This points to the importance of surface states on the nanocrystalline TiO_2 particles in trapping the injected electrons, lowering their quasi-Fermi level and mediating their transfer

to triiodide. The potential of the coordinatively unsaturated Ti^{4+} centers responsible for these surface states can be negatively displaced by adsorption of a Lewis base, such as a pyridine derivative. In fact, we found that the tail of surface states indicated by cyclic voltammetry (cf. Figure 38) shows a dip around –0.7 V_{SCE} after treatment with 4-tert-butylpyridine. Obviously, the geometric as well as electronic structure of the nanocrystalline semiconductor / sensitizer / electrolyte interface is crucial for photoinduced charge separation and needs further scrutiny to enhance the energy conversion efficiency of this new type of solar cell.

Already today the "artificial leaf" exhibits light harvesting and charge separation efficiencies comparable to those of natural photosynthesis. An important step in the further evolution of this leaf to larger surfaces will be the incorporation of "veins" to draw off the photogenerated current:

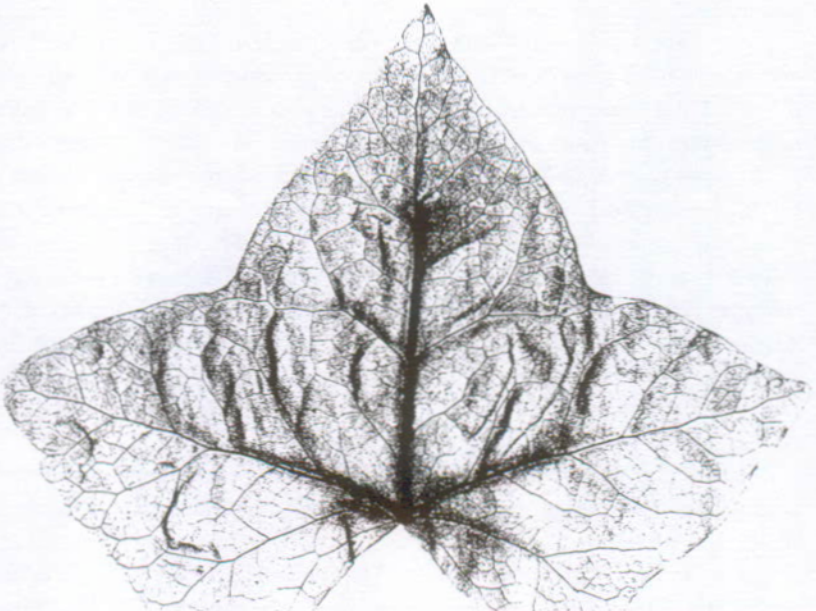

References to chapter 6

1. **M.K. Nazeeruddin, A. Kay, I. Rodicio, R. Humphry-Baker, E. Müller, P. Liska, N. Vlachopoulos, M. Grätzel:** Conversion of light into electricity by *cis*-X_2Bis(2,2'-bipyridyl-4,4'-dicarboxylate)-ruthenium(II) charge transfer sensitzers (X = Cl^-, Br^-, I^-, CN^- and SCN^-) on nanocrystalline TiO_2 electrodes *J. Am. Chem. Soc.* 115 (1993) 6382
2. a) **D.J. Fitzmaurice, H. Frei:** Transient near-infrared spectroscopy of visible light sensitized oxidation of I^- at colloidal TiO_2 *Langmuir* 7 (1991) 1129

   b) **D.J. Fitzmaurice, M. Eschle, H. Frei, J. Moser:** Time-resolved rise of I_2^- upon oxidation of iodide at aqueous TiO_2 colloid *J. Phys. Chem.* 97 (1993) 3806
3. **F. Willig, R. Kietzmann, K. Schwarzburg:** Time-resolved luminescence, photo-current and simple reaction scheme for a folded ultra-thin-layer solar cell, in *Proc. Int. Symp. Opt. Mat. Technol. for Energy Efficiency and Solar Energy*, Toulouse, May 1992, SPIE Publication

Acknowledgments

First of all, I would like to thank my adviser Professor Michael Grätzel for having given me the opportunity to work on his "artificial leaf". I acknowledge in particular the great liberty he allowed me in pursuing my sometimes unconventional ideas and his patience if positive results were long in coming.

I am very grateful to all my colleagues of the institute for their help and cooperation as well as for the relaxed atmosphere they provided at work.

Special thanks are due to Robin Humphry-Baker for his help and advice on many occasions, and to Brian O'Regan for numerous stimulating discussions and his initiation to cross-country skiing.

Curriculum vitae

Andreas Kay, born on January 30, 1963 in Cologne, Germany

1973-1982	Gymnasium in Cologne, final examination: "Abitur"
1982-1984	Student in natural sciences at the University of Cologne, "Vordiplom" in biology
1984-1986	Civil service in a laboratory for environmental analysis
1986-1988	Student in biology at the University of Cologne, diploma examens in biochemistry, genetics and physical chemistry
1988-1989	Diploma thesis under the direction of Prof. L. Jaenicke at the Biochemical Institute of Cologne on "Light Induced Charge Separation and Hydrogen Evolution at Precipitation Membranes."
1989-1993	Ph. D. student and assistant under the direction of Prof. M. Grätzel at the Institute of Physical Chemistry, Swiss Federal Institute of Technology Lausanne